Numerical solution of coupled flow in plain and porous media

Vsevolod Laptev

2

Vsevolod Laptev

Abteilung Strömungen und komplexe Strukturen

Fraunhofer-Institut für Techno- und Wirtschaftsmathematik (ITWM)

Europaallee 10 (PRE-PARK) 67657 Kaiserslautern, Germany.

laptev@itwm.fraunhofer.de

http://www.itwm.fhg.de

Acknowledgement

I would like to express my deep gratitude to PD.Dr. O. Iliev for his supervision and support during the preparation of this dissertation. I am very thankful to Prof.Dr. H. Neunzert, for giving me the opportunity to continue my study in the Ph.D program, and helpful criticism.

I would like to thank Dipl.-Math. S. Rief and Dr. D. Stoyanov for calculating some cell problems for me, all members of the SKS department in ITWM for the friendly atmosphere and especially Dr. K. Steiner. Without his patience I would not have been able to finish this thesis.

I am deeply indebted to Prof.Dr. Ph. Angot, Prof.Dr. R. Lazarov, Prof.Dr. A. Mikelić for the fruitful discussions related to my research.

The financial support from the Graduiertenkolleg "Mathematik und Praxis" (DFG) and Fraunhofer Institute for Industrial Mathematics (ITWM) is highly appreciated.

Contents

Introduction

The main objects considered in this thesis are the fluids and the porous medium. In [43, p.1], the porous medium is defined as "*a material consisting of a solid matrix with an interconnected void. ... The interconnectedness of the void (the pores) allows the flow of one or more fluids through the material*". Examples of porous media are (see, e.g. [5, p.4]): soil, sand, fissured rock, cemented sandstone, Karstic limestone, ceramics, foam rubber, bread, lungs, textile, paper, etc.

Typically, the solid matrix has a very complicated structure (see Fig.1). The geometry of the solid structure significantly changes on a distance $\bar{\varepsilon}$, which is much smaller than the characteristic size L of the porous media in the whole problem, and this motivates the usage of the term *microstructure* for denoting the solid matrix of the porous medium. $\bar{\varepsilon}$ can be also used to denote a typical pore size. We don't have a precise definition for $\bar{\varepsilon}$ in the general case, but for the case of periodic porous media it can be defined as the (smallest) period of the solid microstructure. If we consider a characteristic function, taking values one at the void points, and zero at the solid points, then this function rapidly oscillates in the porous media.

In this thesis we will deal with saturated porous media only. It means that the void space is occupied by a single fluid, which we suppose to be incompressible, Newtonian with dynamical viscosity μ. Moreover, we restrict our considerations to steady-state, isothermal flows. Unsteady problems, having as a limit steady-state solution, can be considered as well at time moments far enough from the initial stage.

In many cases, the porous medium is surrounded completely or partially by a region, occupied purely by a fluid. We will use the terms "plain media", "free fluid" or "pure fluid" to denote such a region. We suppose that its size is comparable with the size of the porous medium. Coupled flows in the plain and in the porous media are the main subject of investigation in the thesis. Some examples of coupled considerations are:

- coupling of the surface flow with the groundwater flow (what is very important for studying contaminant transport, for predicting flooding, etc.);

- coupling of the water waves with the flow through porous breakwaters;

- coupled flows through certain heat exchangers or mixers which are based on porous medium mixing;

- coupling the flow between the porous tows with the flow within them during resin transfer moulding;

- coupled flows through industrial and others filters, etc.

The flows through oil filters are of special interest for us, therefore we will explain this case in more details. The oil filter consists of a filter box and a porous filtering medium, which completely separates the inlet of the filter box from the outlet. The purpose of these filters is to catch inside the filtering medium (small) dirt particles coming with the oil flow from inlet. What

is the motivation for simulating the flow through filters? Usually, a designer uses a CAD system to create a geometry for a new filter box with the filtering medium inside. The designing process and the further modifications often take days. After the design, next stage is to manufacture a prototype and to perform experiments, determining properties of the designed filter. In fact, many of these properties (e.g., pressure drop - flow rate ratio, uniformity of the loading of the filtering media, etc.) are governed by the coupled flow within pure liquid subregions of the box, and the flow within the filtering porous medium. Altogether, manufacturing the prototype and performing experiments takes a couple of weeks or more. Based on the obtained experimental results, a decision is taken whether the properties of the new filter are appropriate, or the filter needs further improvements. Often, several steps of improvements need to be performed. The overall designing process can be significantly optimized: the manufacturing of a prototype and the performance of experiments can be replaced (at least partially) by numerical simulations. The CAD data with the filter's geometry can be directly used to construct the computational domain and to perform computer simulations. This allows significantly to shorten the time for the design of a new filter, at the same time preserving the needed accuracy.

The above examples demonstrate the practical importance of studying such coupled flows. The problem, however, is very attractive also from the mathematical point of view. There are several challenges in mathematical modeling of these coupled flows:

- the choice of the model for the plain and for the porous media, and what is even more important, formulation of proper interface (i.e., transmission) conditions on the interface between the plain and the porous media;

- analysis of the formulated mathematical problem: under which conditions it is a well posed one;

- developing efficient numerical algorithms for this kind of coupled problem;

These three topics, as well as the closely related problems for the validation of the models and the algorithms, and for the application of the developed algorithms in simulation of real industrial problems, are a subject of investigation in this thesis. The main purpose of the thesis is to investigate from theoretical and numerical point of view the Brinkman model in porous media, coupled to the free fluid part with the help of the recently suggested by Whitaker and Ochoa-Tapia interface conditions. We will focus on solvability of the problem and the uniqueness of the solution, on comparison with the well studied channel problem (including the disputable question concerning the pressure continuity through the interface), on the numerical algorithm for the model, on some aspects of the model verification and determination of the tensor coefficient $\mathcal{M}$, and on 3D simulations of coupled flows through a real filter.

We will proceed as follows. In Chapter 1 we present the problem and make an overview of known models and approaches related to the problem. Also, we describe there the mathematical model, recently proposed by J.A. Ochoa-Tapia and S. Whitaker in [44], which is the main subject of investigation in the following chapters. In Chapter 2 we consider flow over a porous block in a channel. We compare the asymptotical behaviour for the solution of the above mentioned model (based on Brinkman equation and on Ochoa-Tapia&Whitaker interface conditions), with what was analytically found by W. Jäger, A. Mikelić, N. Neuss [24]-[25] (they use a model based on Darcy law and on Beavers-Joseph interface conditions). Also, we introduce in this Chapter the notion of a generalized solution for the model in the linear case, and study the existence and the uniqueness of the generalized solution. In Chapter 3 we propose a numerical algorithm for the considered model for coupled flows, and make some tests to validate the algorithm and its implementation. Chapter 4 is devoted to validation of the selected model on the base of

direct numerical simulation: we design model problems where the microscopical solid structure of the porous media can be resolved by the computational grid. The numerical (micro-)solutions for such geometries are compared with the numerical solutions of the macro-model, where the porous medium is treated as a homogeneous medium without complicated microstructures. Also, we investigate the pressure jump effect, predicted in [23],[25]. In the Chapter 5, the results from numerical simulation of a 3D industrial problem, concerning coupled flow through a car oil filter, are presented and compared with measurements. This Chapter contains also some other 2D and 3D calculations related to the filtration problem which is one of the most important applications for the problem of coupled flow in free fluid and in porous media. Chapter 6 is left for conclusions and open problems.
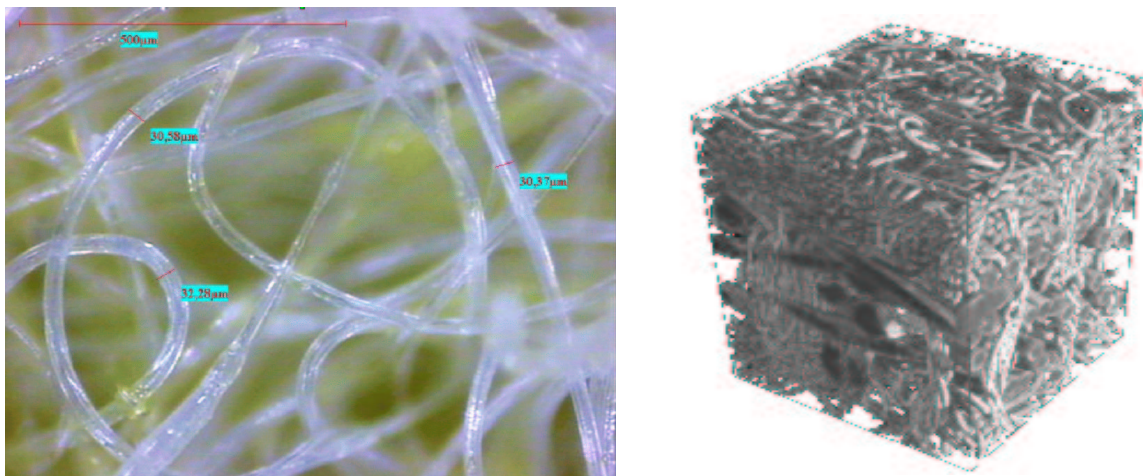

Figure 1: Large magnification of fiber materials

Chapter 1

Mathematical models for the coupled flow in free fluid and in porous media

1.1 Preliminaries. Models in the free fluid domains and in the solid part.

Let Ω be a connected bounded domain in $\mathbb{R}^d$, $d = 2$ (2D) or $d = 3$ (3D). Points in Ω are denoted by $\mathbf{x}$, $\mathbf{x} = (x^1, \dots, x^d)$. We assume that Ω is subdivided into three subdomains: pure fluid part Ω_f, saturated porous media Ω_p and pure solid part Ω_s ($\overline{\Omega} = \overline{\Omega_f} \cup \overline{\Omega_p} \cup \overline{\Omega_s}$). The partition is appropriate for macroscopic descriptions of the problem. For microscopical descriptions one needs additionally internal structure of Ω_p given by its subdivision into the solid matrix Ω_{ps}, and the pore space Ω_{pf} which is completely occupied by the fluid ("ps", "pf" mean porous–solid, porous–fluid). The total fluid part $\overline{\Omega_f \cup \Omega_{pf}}$ should be connected (if there is a void space in the porous media which is surrounded by solid so that there is no connection to Ω_f then we can assume that this void space belongs to the solid phase). From a microscopic point of view, the macroscopic interface $\Sigma = \partial\Omega_p \cap \partial\Omega_f$, is an imaginary interface and therefore there is a freedom in choosing its exact position within a layer with typical pore size thickness.

The flow is characterized by velocity $\mathbf{u} \in \mathbb{R}^d$ and pressure $p \in \mathbb{R}$, which are functions of spatial coordinates only (we have already mentioned that we restrict ourselves to stationary flow and all variables as well as the subdomains of Ω are time independent). The exact domain of definition of $(\mathbf{u}, p)$ is different for macro and micro formulation:

- $(\mathbf{u}, p)(\mathbf{x})$: $\overline{\Omega \setminus \Omega_s} \to (\mathbb{R}^d, \mathbb{R})$ (macro formulation);

- $(\mathbf{u}, p)(\mathbf{x})$: $\overline{\Omega_f \cup \Omega_{pf}} \to (\mathbb{R}^d, \mathbb{R})$ (micro formulation);

Also, the meaning of the macroscopic velocity is different in the free fluid region and in the porous media

The velocity defined at some $\mathbf{x} \in \Omega$ is $\mathbf{u} = (u^1, \dots, u^d)$. We will also use index-free notation: $\mathbf{x} = (x, y, z)$, $\mathbf{u} = (u, v, w)$ in 3D and $\mathbf{x} = (x, y)$, $\mathbf{u} = (u, v)$ in 2D.

The geometry of the problem is schematically drawn in Fig.1.1. The solid phase is shown with black color. On the left one can see the geometry on a macroscale, as it is treated in the macroscopic formulation. But in fact, the macroscopic formulation hides small heterogeneities which are important for microscopical formulation. They are drawn in the right subfigure as a high magnification of a small part of the left subfigure (see also Fig.1). The dashed line on the
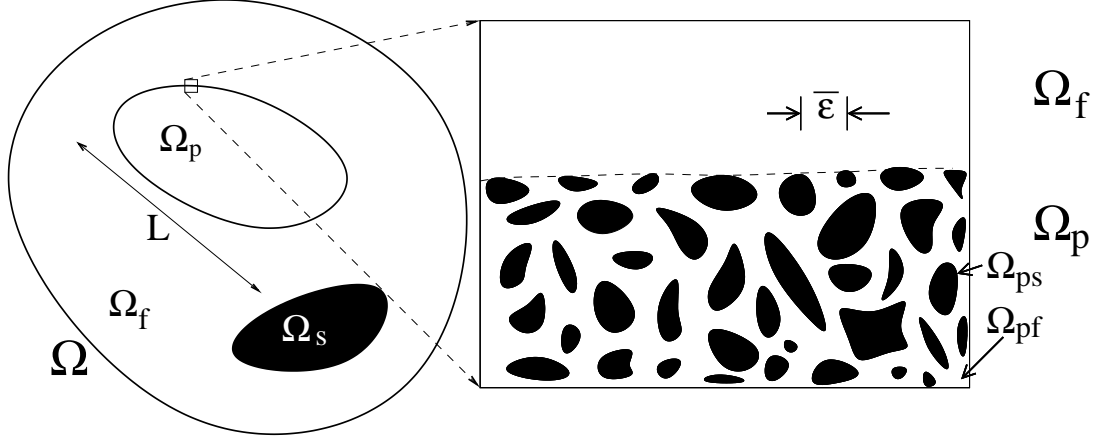
Figure 1.1: Domain Ω, pure fluid part Ω_f, porous part $\Omega_p = \Omega_{ps} \cup \Omega_{pf}$, pure solid part Ω_s

right subfigure shows one possible location for the interface. L is a characteristic length for the macroscale, while $\bar{\varepsilon}$ is the one for the microscale. It is clear, that $\bar{\varepsilon} \ll L$.

Now let us consider each of the subdomains Ω_f, Ω_s, Ω_p separately, in order to fix the mathematical models that can be used there. The mathematical model in the fluid region Ω_f is based on laminar, incompressible, isothermal stationary Navier-Stokes equations (see, e.g. [16]):

$$-\mu \triangle \mathbf{u} + (\rho \mathbf{u} \cdot \nabla)\mathbf{u} + \nabla p = \mathbf{f},$$
$$\nabla \cdot \mathbf{u} = 0 \tag{1.1}$$

We will also use the linearized version for creeping flows:

$$-\mu \triangle \mathbf{u} + \nabla p = \mathbf{f},$$
$$\nabla \cdot \mathbf{u} = 0. \tag{1.2}$$

One usually neglects the convective term when the Reynolds number $Re = \rho U L / \mu$, calculated with respect to the macro distance L and characteristic velocity U, is small for the flow in Ω_f.

We may exclude Ω_s from consideration since there is no flow there, and the flow variables $(\mathbf{u}, p)$ need not be defined there: $\Omega^{new} := \Omega \setminus \overline{\Omega_s}$. One can set the Dirichlet boundary condition $\mathbf{u} = \mathbf{0}$ on the fluid–solid boundary $\partial\Omega_f \cap \partial\Omega_s$. Either $\mathbf{u} = \mathbf{0}$, or only no-penetration condition $\mathbf{u} \cdot \mathbf{n}_s = 0$ can be set on the porous–solid boundary $\partial\Omega_p \cap \partial\Omega_s$, depending on the model in Ω_p (here $\mathbf{n}_s$ is an outer normal to Ω_s). On the other hand, it might be more convenient (for example when $\Omega \setminus \overline{\Omega_s}$ becomes a complicated domain) to use fictitious domain method (see [37],[35],[3],[4]) and to consider in Ω_s a kind of (Navier–) Stokes system, penalized by the zero order velocity term $B\mathbf{u}$, where B is a large number. An additional penalization can be done by choosing also a large viscosity μ_s:

$$-\nabla \cdot (\mu_s \nabla \mathbf{u}) + (\rho \mathbf{u} \cdot \nabla)\mathbf{u} + B\mathbf{u} + \nabla p = \mathbf{f},$$
$$\nabla \cdot \mathbf{u} = 0 \tag{1.3}$$

The flow in Ω_s is not forbidden in this case, but the large coefficients B and μ_s force it to be almost negligible there.

1.2 Models in the porous media Ω_p

We have described the models in domains consisting of only one phase: either fluid Ω_f or solid Ω_s. The porous media is then an intermediate case. There are two possibilities to deal with such

heterogeneous media. The first possibility is to consider the equations on a microlevel (pore level), this is the so-called microscopical model. Second possibility is to try to substitute the heterogeneous medium by an imaginary homogeneous medium and to consider macroscopic (effective) equations there for macroscopic unknowns, this is the so-called macroscopic model. The effective equations can be completely different from the equations on a microlevel. The information about the heterogeneities is usually contained in effective parameters of the macroscopic model. The macroscopic unknowns may have a quite complicated relation with the microscopic unknowns, but often the macroscopic unknowns have a meaning of spatially averaged microscopic unknowns as it happens in our case with velocity and pressure $(\mathbf{u}, p)$.

1.2.1 Microscopical model

The porous media is represented as a connected domain of pore space filled with the fluid and the flow there is governed by the Stokes (1.2) or the Navier–Stokes (1.1) equations. No-penetration and no-slip boundary conditions on the solid boundary (which has a very complex geometrical structure) are prescribed. The pore space domain Ω_{pf} can be readily added to the free flow region Ω_f to have the same system of equations (Navier–Stokes or Stokes) in the whole fluid domain $\Omega_f \cup \Omega_{pf} \cup \Sigma$. The model approximates the physical problem with a good precision, but it seems to be inappropriate for applications with real porous media since it needs unrealistic amount of CPU time/memory resources. Additional difficulty is that the internal geometry of the solid matrix can be even unknown (although it is possible nowadays to look inside some particular porous medium without destroying it by using X-ray microtomography with resolution up to one micrometer).

The information, contained in the microsolution is superfluous for most purposes. It often needs further processing in order to obtain a smooth, large scale (averaged) data, which are much more appropriate for qualitative conclusions, compared to the rapidly oscillated functions on a pore level.

However, the micromodel is useful for theoretical purposes, such as deriving macroscopic models for porous media (some overview is given below) and for direct numerical simulations (when possible) of fluid flows in porous media (see also the Chapter 4).

1.2.2 Macroscopic models in the porous media

Many macroscopic models for different physical processes in heterogeneous media were obtained empirically, without considering the equations on a microscale as a starting point. One successful example is the famous Darcy law, discovered in 1856. Nowadays much effort is made to establish a relation between micro and macro formulations. Some reasons are: to justify the macroscopic model, to get its precise form, checking that there are no missing or excessive terms, to determine assumptions and restrictions for the model, as well as to obtain (if possible) macroscopic parameters needed in macro formulation. The idea in the last case is, that calculations (based on available microparameters and microgeometry), can (partially) replace the experiments, needed for determining macroparameters.

Of course, all derivations have some assumptions and restrictions. But the model may also work reasonably in a significantly larger area as it was assumed in the derivation. We also believe that rigorous derivation is desirable, but not necessary for a model. Validation via a comparison with experiments, is also a reason to use a model, even if no rigorous derivation is known.

To sketch ideas of two upscaling techniques we assume that we have to solve (approximately) a microscopical problem (for example the microproblem discussed above, but restricted to Ω_p

since in this subsection we don't discuss difficulties coming from the interfaces). Denote it by $\mathcal{P}$. We assume that $\mathcal{P}$ is a well posed problem and there is enough information to determine its solution. The only difficulty is that an accurate numerical solution is extremely resource-extensive.

1.2.3 Local volume averaging

Let us assume that the micro solution of $\mathcal{P}$ is known. Then an averaged solution at some point $\mathbf{x}$ can be introduced as a spatially averaged value of the micro variables taken over the so-called Representative Elementary Volume (REV), denote it by $V(\mathbf{x})$. The REV $V(\mathbf{x})$ is a neighbourhood of the point $\mathbf{x}$, having the same form and size for all $\mathbf{x}$. It can be, for example, an open ball with the centre at $\mathbf{x}$. The size should be small compared with L, but not too small: it should contain enough pores and solid structures to justify the word "representative" in its name (see also [5, Sec. 1.2.3]). Some microscopical variables are defined only in one phase (like pressure in the fluid part Ω_{pf}). Then one can define the fluid component of REV: $V_f(\mathbf{x}) = V(\mathbf{x}) \cap \Omega_{pf}$, and the surface where the microscopic boundary conditions are imposed: $A_{sf}(\mathbf{x}) = V(\mathbf{x}) \cap \partial\Omega_{ps}$. The averaged variables $(\overline{\mathbf{u}}, \overline{p})$ can be calculated from the microscopical variables:

$$\overline{\mathbf{u}}(\mathbf{x}) = \frac{1}{|V(\mathbf{x})|} \int_{V_f(\mathbf{x})} \mathbf{u}(\mathbf{y})\,d\mathbf{y}, \qquad \overline{p}(\mathbf{x}) = \frac{1}{|V_f(\mathbf{x})|} \int_{V_f(\mathbf{x})} p(\mathbf{y})\,d\mathbf{y} \qquad (1.4)$$

We note, that $\overline{\mathbf{u}}$, $\overline{p}$ are defined up to the choice of size and form of V and there is uncertainty near the boundaries since the microvariables are not necessary defined outside the domain.

But the microscopical solution is not known and it is not the purpose here to obtain it. Nevertheless, using the fact that it satisfies the equations on a micro level (in our case (1.2) or (1.1)), one can integrate them over REV and apply the so-called averaging theorems [26, p. 54],[22] like

$$\overline{\nabla\psi} = \nabla\overline{\psi} + \frac{1}{|V(\mathbf{x})|} \int_{A_{sf}(\mathbf{x})} \psi\mathbf{n}\,d\sigma \qquad \overline{\nabla\cdot\mathbf{b}} = \nabla\cdot\overline{\mathbf{b}} + \frac{1}{|V(\mathbf{x})|} \int_{A_{sf}(\mathbf{x})} \mathbf{b}\cdot\mathbf{n}\,d\sigma. \qquad (1.5)$$

The purpose is to exclude all micro unknowns and to have at the end a closed system containing the averaged variables as unknowns and material parameters, assumed to be known properties independent of micro unknowns. Thus, the system for the averaged unknowns (macroscopic model) can be solved without knowledge of the microsolution. Unfortunately it is not always possible to exclude micro unknowns from all their entries in averaged microscopic equations using rigorous or formal techniques, and therefore additional unknowns are introduced which require experimental verifications.

The volume averaging of the Stokes equation (1.2) in the porous media ([44]) leads to the stationary Brinkman system of equations (see [44]):

$$-\frac{\mu}{\phi}\triangle\overline{\mathbf{u}} + \mu\mathbf{K}^{-1}\overline{\mathbf{u}} + \nabla\overline{p} = \mathbf{f} \quad \text{in } \Omega_p,$$
$$\nabla\cdot\overline{\mathbf{u}} = 0$$

where ϕ is the porosity of the porous media. The averaged unknowns $(\overline{\mathbf{u}}, \overline{p})$ are in fact the main unknowns $(\mathbf{u}, p)$ in the macro formulation

$$-\nabla\cdot(\mu_{eff}\nabla\mathbf{u}) + \mu\mathbf{K}^{-1}\mathbf{u} + \nabla p = \mathbf{f} \quad \text{in } \Omega_p, \qquad (1.6)$$
$$\nabla\cdot\mathbf{u} = 0$$

where $\mu_{eff} = \mu/\phi$. $\mathbf{u}$, p have no *bar* any more, but they have different meaning comparing with the micro formulation.

1.2.4   Homogenization

Describing homogenization of some problem one usually starts with a sequence of problems depending on a parameter ε. The main purpose is to obtain the so-called limit problem when $\varepsilon \to 0$. Here our priorities will be somewhat different: the main purpose is to approximate the solution of $\mathcal{P}$. The sequence of problems and the limit problem are just a way to reach it. More precisely, under a deterministic homogenization of the microscopical problem $\mathcal{P}$ in heterogeneous media, we will understand a method of constructing a sequence of imaginary problems $\{\mathcal{P}^\varepsilon\}$, such that one of them $\mathcal{P}^{\bar\varepsilon}$ coincides with $\mathcal{P}$. The positive numbers ε, and in particular $\bar\varepsilon$, are members of some sequence $\{\varepsilon_n\}_{n=0}^\infty \to 0$. When dealing with spatial heterogeneities we will treat $\bar\varepsilon$ as a typical size of heterogeneities in the problem $\mathcal{P}^{\bar\varepsilon}$ (in this case $\bar\varepsilon$ is small in comparison with L, but it is not correct to say that $\bar\varepsilon$ is small itself). If we choose L as a unit length, and measure everything in L, then ε is the same as it is usually used as a dimensionless small parameter equal to the ratio between the typical lengths in micro and macro scales.

If the sequence is convergent in some sense to some limit problem $\mathcal{P}^0$ which can be approximately solved with moderate requirement on resources (comparing to what is necessary for $\mathcal{P}^\varepsilon$), then the solution of $\mathcal{P}^0$ can be used in approximating (in some sense) the solutions of $\mathcal{P}^\varepsilon$, and in particular, of $\mathcal{P}^{\bar\varepsilon}$ (it is exactly our purpose claimed above). The "convergence of problems" is, of course, related to convergence of their solutions, but it is too restrictive to say something more precise: for example it can be weak or strong convergence in some norm of solutions itself, or multiplied by some degree of ε (examples and references are given below in homogenization of our microproblem). Also, the "limit problem" can be in fact not a single problem, but a series of problems for determining terms in some asymptotic expansion (see [9, p.12],[48, p.48],[21, p.9],[13, p.128]) for the solution of $\mathcal{P}^\varepsilon$. The "approximation" of $\mathcal{P}^{\bar\varepsilon}$ using the solution(s) of $\mathcal{P}^0$ depends on the "convergence".

$$\mathcal{P}^{\varepsilon_0}, \quad \ldots \quad, \mathcal{P}^{\varepsilon_{n-1}}, \quad \mathcal{P}^{\bar\varepsilon}, \quad \mathcal{P}^{\varepsilon_{n+1}}, \quad \ldots \quad, \mathcal{P}^\varepsilon, \quad \ldots \qquad \dashrightarrow \quad \mathcal{P}^0.$$
$$\parallel$$
$$\mathcal{P}$$

Some additional restrictions on the sequence $\{\mathcal{P}^\varepsilon\}$ are that the problem $\mathcal{P}^{\bar\varepsilon}$ should be a "natural" member of the sequence, and other problems there should also be well-posed. The first restriction is important since a convergent sequence will still be convergent if we substitute one of its elements by some arbitrary element that has nothing to do with the sequence, but then the limit of the sequence will be a bad approximation for this particular element.

The convergence of $\{\mathcal{P}^\varepsilon\}$ alone cannot guarantee that the approximation is good enough even in the same sense as we understand the convergence, since $\bar\varepsilon$ cannot be made smaller, and $\mathcal{P}^\varepsilon$ for small enough ε is of no practical interest. The ideal case is when the speed of convergence (in some norm) can be estimated as some function $E(\varepsilon)$, tending to zero as $\varepsilon \to 0$. Then we have a number $E(\bar\varepsilon)$ that estimates the particular error of approximation for our problem $\mathcal{P}$. And for any admissible error we can find from the function how small the microstructure should be to obtain an admissible approximation for the microsolution by the limit problem $\mathcal{P}^0$. Unfortunately there are no simple ways to improve the approximation. One possibility is to try to construct another sequence $\{\tilde{\mathcal{P}}^\varepsilon\}$ with other limit problem $\tilde{\mathcal{P}}^0$ which may give better approximation. Another is to use the same sequence $\{\mathcal{P}^\varepsilon\}$, but to generalize $\mathcal{P}^0$ by adding more terms in the asymptotic expansion.

The construction of such a sequence is not an easy task. One well adopted for theoretical investigations case, often resulting in a cheap and accurate macroscopic model, is the case of periodic micro geometry in $\mathcal{P}$. If inhomogeneity of $\mathcal{P}$ has periodic microstructure with period $\bar\varepsilon$

in some domain D, and can be described in a fixed coordinate system with axes parallel to the directions of periodicity by some $\bar{\varepsilon}$-periodic function

$$\chi(\mathbf{x}) : \mathbb{R}^d \to \mathbb{R}, \qquad \chi(\mathbf{x} + \bar{\varepsilon}\mathbf{e}_i) = \chi(\mathbf{x}), \qquad \forall \mathbf{x} \in \mathbb{R}^d, \quad i \in \{1, \dots, d\},$$

then one well-known way to create heterogeneous micro-structure for the problem $\mathcal{P}^{\varepsilon}$ is to use the ε-periodic functions $\chi^{\varepsilon}(\mathbf{x}) = \chi(\bar{\varepsilon}\mathbf{x}/\varepsilon)$, restricted to D. When $\varepsilon = \bar{\varepsilon}$ then the microstructure in D is exactly the same as for the problem $\mathcal{P}$: $\chi^{\bar{\varepsilon}}(\mathbf{x}) = \chi(\mathbf{x})$.

With the help of this approach it is quite often possible to construct a sequence $\{\mathcal{P}^{\varepsilon}\}$, whose solutions converge in some sense when $\varepsilon \to 0$. An overview of mathematical techniques used to obtain the limit problem $\mathcal{P}^0$, and to show the convergence to the solution of $\mathcal{P}^0$, can be found for example in [21, p.225-247]. Examples of different sequences and limit problems can be found, among others, in [9],[48].

On derivation of the Darcy law

In particular, dealing with periodic porous media, the function $\chi(\mathbf{x})$ in Ω_p is a characteristic function of the fluid part: for $\mathbf{x} \in \Omega_p$, $\chi(\mathbf{x}) = 1$ if and only if $\mathbf{x} \in \Omega_{pf}$. Since at the moment we are interested in macroscopic model describing the flow in Ω_p only, it is reasonable not to consider the microscopical problem in the whole Ω, but to consider it in some domain $D \subseteq \Omega_p$ with boundary conditions on ∂D (we exclude pure fluid and solid parts since they destroy periodicity and make the problem much more complicated and irrelevant to deriving macroscopic model in Ω_p). The microscopical problem $\mathcal{P}$, based on Stokes system can be written as:

$$\mathcal{P} : \begin{cases} -\mu \triangle \mathbf{u} + \nabla p = \mathbf{f} & \text{in } \Omega_{pf} \cap D \\ \nabla \cdot \mathbf{u} = 0 & \text{in } \Omega_{pf} \cap D \\ \mathbf{u} = 0 & \text{on } \partial\Omega_{pf} \cap D \\ \text{boundary conditions} & \text{on } \partial D \end{cases} \tag{1.7}$$

The right hand side $\mathbf{f} \in [L^2(D)]^d$. The porous media structure for the problem $\mathcal{P}^{\varepsilon}$ depends on ε and is described with the help of χ^{ε}:

$$\Omega_{pf}^{\varepsilon} = \{\mathbf{x} \in \Omega_p \mid \chi^{\varepsilon}(\mathbf{x}) = 1\} \qquad \Omega_{ps}^{\varepsilon} = \{\mathbf{x} \in \Omega_p \mid \chi^{\varepsilon}(\mathbf{x}) = 0\}$$

An important role is played by a microgeometry of one period magnified so that it becomes a cube $Y = (0,1)^d$, namely

$$Y_f = \{\mathbf{y} \in Y \mid \chi(\bar{\varepsilon}\mathbf{y}) = 1\}, \qquad Y_s = \{\mathbf{y} \in Y \mid \chi(\bar{\varepsilon}\mathbf{y}) = 0\}.$$

The function χ is not arbitrary. One have to check that the resulting $\Omega_{pf}^{\varepsilon}$ are connected, Y_f, Y_s have positive measures, and smooth enough boundaries. A discussion on admissible geometries can be found in [1].

The governing system in $\Omega_{pf}^{\varepsilon}$, determining the problem $\mathcal{P}^{\varepsilon}$ is (see [21, p.46])

$$\mathcal{P}^{\varepsilon} : \begin{cases} -\eta\varepsilon^2 \triangle \mathbf{v}^{\varepsilon} + \nabla p^{\varepsilon} = \mathbf{f} & \text{in } \Omega_{pf}^{\varepsilon} \cap D \\ \nabla \cdot \mathbf{v}^{\varepsilon} = 0 & \text{in } \Omega_{pf}^{\varepsilon} \cap D \\ \mathbf{v}^{\varepsilon} = 0 & \text{on } \partial\Omega_{pf}^{\varepsilon} \cap D \\ \text{boundary conditions} & \text{on } \partial D \end{cases} \tag{1.8}$$

Existence and uniqueness of the solutions for (1.7), (1.8) come from correspondent results for the Stokes system. In the problems $\mathcal{P}^{\varepsilon}$, not only the perforated domain $\Omega_{pf}^{\varepsilon}$ depends on ε, but also the viscosities $\eta\varepsilon^2$ become smaller together with the microstructures. To satisfy the condition $\mathcal{P}^{\bar{\varepsilon}} = \mathcal{P}$ we should set $\eta := \mu/\bar{\varepsilon}^2$.

Remark 1 *An alternative way to construct the sequence $\mathcal{P}^\varepsilon$ is given in [1],[13, p.131]:*

$$\mathcal{P}^\varepsilon : \begin{cases} -\mu \triangle \mathbf{u}^\varepsilon + \nabla p^\varepsilon = \mathbf{f} & \text{in } \Omega^\varepsilon_{pf} \cap D \\ \nabla \cdot \mathbf{u}^\varepsilon = 0 & \text{in } \Omega^\varepsilon_{pf} \cap D \\ \mathbf{u}^\varepsilon = 0 & \text{on } \partial\Omega^\varepsilon_{pf} \cap D \\ boundary\ conditions & \text{on } \partial D \end{cases} \tag{1.9}$$

These two sequences (1.8), (1.9) are equivalent since $\mathbf{u}^\varepsilon = \varepsilon^2 \mathbf{v}^\varepsilon$. The sequence of solutions $\{\mathbf{u}^\varepsilon\}$ and also $\{\mathbf{u}^\varepsilon/\varepsilon\}$ tend to zero as $\varepsilon \to 0$. The first non-zero term in the asymptotic expansion of $\mathbf{u}^\varepsilon$ has a magnitude of ε^2. This can be justified by a priory estimates (see [13]).

For the case of homogeneous Dirichlet boundary conditions on ∂D: $\mathbf{v}^\varepsilon = \mathbf{0}$ in (1.7) and (1.8), the result concerning the limit problem and the convergence is given in [21, p.46]:

Proposition 1 *There exists an extension $(\tilde{\mathbf{v}}^\varepsilon, \tilde{p}^\varepsilon)$ of the solution $(\mathbf{v}^\varepsilon, p^\varepsilon)$ of (1.8) from $\Omega^\varepsilon_{pf} \cap D$ to D such that the velocity $\tilde{\mathbf{v}}^\varepsilon$ converges weakly in $[L^2(D)]^d$ to $\mathbf{v}^0$, and the pressure $\tilde{p}^\varepsilon$ converges strongly in $L^2(D) \setminus \mathbb{R}$ to p^0. Here $(\mathbf{v}^0, p^0)$ is the unique solution of the homogenized problem, the Darcy law (the problem $\mathcal{P}^0$):*

$$Limit\ Problem\ \mathcal{P}^0 : \begin{cases} \mathbf{v}^0 = \frac{1}{\eta}\mathcal{K}(\mathbf{f} - \nabla p^0) & \text{in } D \\ \nabla \cdot \mathbf{v}^0 = 0 & \text{in } D \\ \mathbf{v}^0 \cdot \mathbf{n} = 0 & \text{on } \partial D \end{cases} \tag{1.10}$$

The symmetric positive definite dimensionless permeability tensor $\mathcal{K}$ can be calculated as

$$\mathcal{K}_{ij} = \int_{Y_f} w_i^j(\mathbf{y})\, d\mathbf{y}$$

where $(\mathbf{w}_i, \pi_i)$, $i = 1, \ldots, d$ are unique Y-periodic solutions of the so-called cell problems:

$$Cell\ Problems\ : \begin{cases} -\triangle_{\mathbf{y}} \mathbf{w}_i(\mathbf{y}) + \nabla_{\mathbf{y}} \pi_i(\mathbf{y}) = \mathbf{e}_i, & \text{in } Y_f \\ \nabla_{\mathbf{y}} \cdot \mathbf{w}_i(\mathbf{y}) = 0, & \text{in } Y_f; \\ \mathbf{w}_i = 0 \text{ on } \partial Y_s, \\ \int_{Y_f} \pi_i(\mathbf{y})\, d\mathbf{y} = 0, \end{cases} \tag{1.11}$$

where Y-periodic function $f(\mathbf{y})$ means that it is defined in $\mathbb{R}^d$ and $f(\mathbf{y} + \mathbf{e}_i) = f(\mathbf{y})$ for any $\mathbf{y} \in \mathbb{R}^d$, $i \in \{1, \ldots, d\}$, .

Remark 2 *In [13, Sec.1] similar result (Darcy law) is obtained for periodic boundary conditions when D is a square.*

Remark 3 *The extensions $\tilde{\mathbf{v}}^\varepsilon$, $\tilde{p}^\varepsilon$ are given explicitly in [1],[21, p.52]. The velocity $\mathbf{v}^\varepsilon$ is extended by $\mathbf{0}$ to the solid part. The pressure in each periodicity cell $Y_{\mathbf{i}}^\varepsilon \subset D$ (with microgeometry like in Y):*

$Y_{\mathbf{i}}^\varepsilon = \{\mathbf{y} \in D \mid \varepsilon i^k < y^k < \varepsilon(i^k+1), \mathbf{i} = (i^1, \ldots, i^d) \in \mathbb{Z}^d\}$, $Y_{s,\mathbf{i}}^\varepsilon = Y_{\mathbf{i}}^\varepsilon \cap \Omega^\varepsilon_{ps}$, $Y_{f,\mathbf{i}}^\varepsilon = Y_{\mathbf{i}}^\varepsilon \cap \Omega^\varepsilon_{pf}$,

is extended to the solid part $Y_{s,\mathbf{i}}^\varepsilon$ by the constant

$$\tilde{p}_{\mathbf{i}}^\varepsilon = \frac{1}{|Y_{f,\mathbf{i}}^\varepsilon|} \int_{Y_{f,\mathbf{i}}^\varepsilon} p^\varepsilon\, d\mathbf{y}. \tag{1.12}$$

Next we need to understand in which sense $\mathbf{v}^0$, p^0 approximates the microsolutions $\mathbf{v}^\varepsilon$, p^ε. The convergence of $\tilde{\mathbf{v}}^\varepsilon$ to $\mathbf{v}^0$ is weak in $[L^2(D)]^d$, meaning that for any $\mathbf{h} \in [L^2(D)]^d$: $\int_D \tilde{\mathbf{v}}^\varepsilon \mathbf{h} \, d\mathbf{y} \to \int_D \mathbf{v}^0 \mathbf{h} \, d\mathbf{y}$. Let us consider a REV $V(\mathbf{x}) \subset D$ from Sec. 1.2.3 and its characteristic function $\chi_V(\mathbf{y}) \in L^2(D)$: $\chi_V(\mathbf{y}) = 1$ when $\mathbf{y} \in V(\mathbf{x})$ and 0 otherwise. The left integral tested with $\mathbf{h} = \mathbf{e}_k \chi_V / |V(\mathbf{x})|$ according to the zero extension in the solid part, gives the k-th component of the vector $\overline{\mathbf{v}^\varepsilon}(\mathbf{x})$ (see the expression (1.4) for averaged velocities). If $\mathbf{v}^0$ changes slowly on a microscale then the right integral is approximately the k-th component of the vector $\mathbf{v}^0(\mathbf{x})$. We write it roughly as $\overline{\mathbf{v}^\varepsilon} \simeq \mathbf{v}^0(\mathbf{x})$.

Now we compare average values of micro and macro pressures over some measurable set $\mathcal{V}$. For small enough ε, the averages are close enough to each other:

$$\left| \frac{1}{|\mathcal{V}|} \int_\mathcal{V} \tilde{p}^\varepsilon \, d\mathbf{y} - \frac{1}{|\mathcal{V}|} \int_\mathcal{V} p^0 \, d\mathbf{y} \right| \leq \frac{1}{|\mathcal{V}|} \int_\mathcal{V} |\tilde{p}^\varepsilon - p^0| \cdot 1 \, d\mathbf{y} \leq \frac{\|\tilde{p}^\varepsilon - p^0\|_{L^2(\mathcal{V})}}{|\mathcal{V}|} \sqrt{\int_\mathcal{V} 1^2 \, d\mathbf{y}} \leq \frac{\|\tilde{p}^\varepsilon - p^0\|_{L^2(D)}}{\sqrt{|\mathcal{V}|}}$$

due to convergence of $\tilde{p}^\varepsilon$ to p^0 in $L^2(D) \setminus \mathbb{R}$. If we choose $\mathcal{V} = V(\mathbf{x})$, consisting of entire $Y_\mathbf{i}^\varepsilon$ only: $V(\mathbf{x}) = \bigcup_{\mathbf{i} \in J^\varepsilon [V(\mathbf{x})]} Y_\mathbf{i}^\varepsilon$ then using the extension (1.12) we obtain a connection to (1.4):

$$\frac{1}{|\mathcal{V}|} \int_\mathcal{V} \tilde{p}^\varepsilon \, d\mathbf{y} = \frac{1}{|V(\mathbf{x})|} \sum_{I \in J^\varepsilon} \left(1 + \frac{|Y_{s,\mathbf{i}}^\varepsilon|}{|Y_{f,\mathbf{i}}^\varepsilon|} \right) \int_{Y_{f,\mathbf{i}}^\varepsilon} p^\varepsilon \, d\mathbf{y} = \frac{1}{|V_f^\varepsilon(\mathbf{x})|} \int_{V_f^\varepsilon(\mathbf{x})} p^\varepsilon \, d\mathbf{y} = \overline{p^\varepsilon}(\mathbf{x})$$

where $V_f^\varepsilon(\mathbf{x}) = V(\mathbf{x}) \cap \Omega_{pf}^\varepsilon$ since $|V(\mathbf{x})|/|V_f^\varepsilon(\mathbf{x})| = |Y_\mathbf{i}^\varepsilon|/|Y_{f,\mathbf{i}}^\varepsilon| = 1 + |Y_{s,\mathbf{i}}^\varepsilon|/|Y_{f,\mathbf{i}}^\varepsilon|$ for such $V(\mathbf{x})$. Another choice leading to the same result $\overline{p^\varepsilon}(\mathbf{x})$ without additional assumptions is $\mathcal{V} = V_f^\varepsilon(\mathbf{x})$.

The mean value of p^0 over $\mathcal{V}$ is approximately $p^0(\mathbf{x})$ if the macroscopic pressure changes slowly on a microscale, and if $\mathcal{V} \subseteq V(\mathbf{x})$ ($V(\mathbf{x})$ is a small neighbourhood of D). The assumption that $\mathbf{v}^0$, p^0 change slowly on a microscale is reasonable since there is no microscale in the limit problem: the resulting $\mathcal{K}$ is a constant matrix.

So (roughly speaking), the macroscopic variables $\mathbf{v}^0$, p^0 have a meaning of spatially averaged microscopical variables $\mathbf{v}^\varepsilon$, p^ε similar to (1.4): $\mathbf{v}^0(\mathbf{x}) \simeq \overline{\mathbf{v}^\varepsilon}(\mathbf{x})$, $p^0(\mathbf{x}) \simeq \overline{p^\varepsilon}(\mathbf{x})$.

Last but not the least, we should return to the problem $\mathcal{P} = \mathcal{P}^{\bar{\varepsilon}}$. This equality needs $\eta = \mu/\bar{\varepsilon}^2$. Plugging it into the Darcy law (1.10) we obtain the Darcy law for $\mathcal{P}$:

$$\begin{aligned} \mathbf{v}^0 &= \tfrac{1}{\mu} \mathbf{K}(\mathbf{f} - \nabla p^0) \\ \nabla \cdot \mathbf{v}^0 &= 0 \end{aligned} \qquad \text{in } D \qquad (1.13)$$

The permeability tensor of our $\bar{\varepsilon}$-periodic media Ω_p is

$$\mathbf{K} := \bar{\varepsilon}^2 \mathcal{K}. \qquad (1.14)$$

with relation between microvariables $\mathbf{u} = \mathbf{v}^{\bar{\varepsilon}}$, $p = p^{\bar{\varepsilon}}$ and macrovariables $\mathbf{v}^0$, p^0 discussed above.

Remark 4 *For the alternative sequence (1.9), $\tilde{\mathbf{u}}^\varepsilon/\varepsilon^2$ weakly converges to $\mathbf{v}^0$ in $[L^2(D)]^d$, $\tilde{p}^\varepsilon$ converges strongly in $L^2(D) \setminus \mathbb{R}$ to p^0, $(\mathbf{v}^0, p^0)$ satisfies (1.10) with $\eta = \mu$. $\mathbf{u}^\varepsilon$ is approximated by $\varepsilon^2 \mathbf{v}^0$ in the same sense as $\mathbf{v}^\varepsilon$ was approximated by $\mathbf{v}^0$. In particular, $\mathbf{u} = \mathbf{u}^{\bar{\varepsilon}}$ is approximated by $\mathbf{u}^0 = \bar{\varepsilon}^2 \mathbf{v}^0$. If we multiply all equations in (1.10) by $\bar{\varepsilon}^2$, then we obtain again (1.13), but with $\mathbf{u}^0$ instead of $\mathbf{v}^0$. $\mathbf{u}^0$, p^0 have a meaning of spatially averaged solution $\mathbf{u}$, p of $\mathcal{P}$. The permeability is also given by (1.14).*

The system (1.13) describes the behaviour of flows in porous media: plugging the first equation into the second, one obtains a well studied second order elliptic equation with respect to a single unknown p^0:

$$\nabla \cdot \left(\mathbf{K} \nabla p^0 \right) = \nabla \cdot \left(\mathbf{K} \mathbf{f} \right). \qquad (1.15)$$

For known p^0, $\mathbf{v}^0$ can be calculated using the first expression in (1.13).

    Besides zero normal flux condition like in (1.10), another classical boundary conditions for (1.15) are Dirichlet for pressure: $p^0 = g_1$ on ∂D, or

$$\mathbf{v}^0 \cdot \mathbf{n} = g_2 \quad \text{on } \partial D, \qquad \int_{\partial D} g_2 \, d\sigma = 0 \quad \text{(compatibility condition)}$$

(pressure in (1.13) will be defined up to a constant).

    For numerical experiments in Chapter 4, we will need permeability of two types of periodic microstructures: see Fig. 1.2 for $Y = Y_f \cup Y_s$ in cases CG I and CG II. The permeability tensors
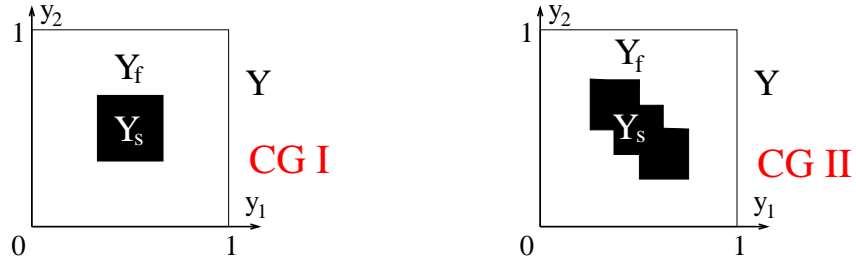

Figure 1.2: Cell Geometries: CG I (left) and CG II (right).

$\mathcal{K}_I$ and $\mathcal{K}_{II}$ were calculated in [47] and [52], respectively:

$$\mathcal{K}_I = \begin{pmatrix} 0.034 & 0 \\ 0 & 0.034 \end{pmatrix}, \quad \mathcal{K}_{II} = \begin{pmatrix} 0.0194 & -0.004 \\ -0.004 & 0.0194 \end{pmatrix} \tag{1.16}$$

The geometry CG I leads to isotropic macroscopic medium. For the second case, the matrix $\mathcal{K}_{II}$ has two different eigenvalues: $\lambda_1 = 0.0154$, $\lambda_2 = 0.0234$ resulting in anisotropic macroscopic medium.

On derivation of the Brinkman system

Nothing prevents $\mathcal{P}$ to be a member of another sequence of problems $\{\tilde{\mathcal{P}}^\varepsilon\}$, the latter converging (in some sense) to another limit problem $\tilde{\mathcal{P}}^0$, when $\varepsilon \to 0$ (see Fig.1.3). The solutions of the
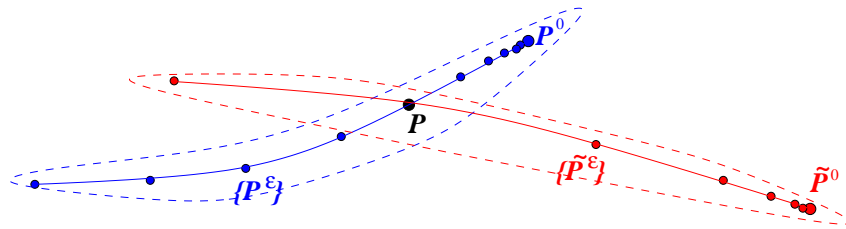
Figure 1.3: Two different sequences $\{\mathcal{P}^\varepsilon\}$, $\{\tilde{\mathcal{P}}^\varepsilon\}$ passing through $\mathcal{P}$.

limit problems $\mathcal{P}^0$ and $\tilde{\mathcal{P}}^0$ have also no reason to be the same, or even similar to each other, since the ways to construct approximations for the solution of $\mathcal{P}$ can be different. However, if two approximations for the solution of $\mathcal{P}$, obtained from $\mathcal{P}^0$ and $\tilde{\mathcal{P}}^0$ are quite different from each other, then at least one of them gives a bad approximation.

    Construction of another sequence for our problem $\mathcal{P}$ for the case when the porous media is a periodic distribution of solid obstacles, (e.g., when Ω_p contains blocks drawn in Fig.1.2) is given in [2]. The geometries of $\tilde{\mathcal{P}}^\varepsilon$ are again periodic, with period ε. The obstacles building up

$\Omega_{ps}^{\varepsilon}$ have the same shape, but their size a_{ε} tends to zero much quicker than ε: $\lim_{\varepsilon \to 0} a_{\varepsilon}/\varepsilon = 0$. The equations are the same as for $\mathcal{P}$, only the domain $\Omega_{pf}^{\varepsilon} = \Omega_p \setminus \Omega_{ps}^{\varepsilon}$ depends on ε:

$$\tilde{\mathcal{P}}^{\varepsilon} : \begin{cases} -\mu \triangle \mathbf{v}^{\varepsilon} + \nabla p^{\varepsilon} = \mathbf{f} & \text{in } \Omega_{pf}^{\varepsilon} \cap D \\ \nabla \cdot \mathbf{v}^{\varepsilon} = 0 & \text{in } \Omega_{pf}^{\varepsilon} \cap D \\ \mathbf{v}^{\varepsilon} = \mathbf{0} & \text{on } \partial \Omega_{ps}^{\varepsilon} \cap D \\ \mathbf{v}^{\varepsilon} = \mathbf{0} & \text{on } \partial D \end{cases} \tag{1.17}$$

In [2], it was found that depending on the behavior of a_{ε} (more precise σ_{ε}, see below) the sequence $\{\tilde{\mathcal{P}}^{\varepsilon}\}$ may have different limit problems. According to the asymptotical behaviour of the sequence of positive numbers $\{\sigma_{\varepsilon}\}$:

$$\sigma_{\varepsilon} = \begin{cases} \left(\frac{\varepsilon^d}{a_{\varepsilon}^{d-2}}\right)^{1/2} & d \geq 3 \\ \varepsilon |ln(\frac{a_{\varepsilon}}{\varepsilon})|^{1/2} & d = 2 \end{cases}$$

three cases were distinguished:

- $\lim_{\varepsilon \to 0} \sigma_{\varepsilon} = 0$: the limit system is again the Darcy law (1.13) with the permeability tensor $\mathbf{K} = \sigma_{\varepsilon}^2 \tilde{\mathcal{K}}$. σ_{ε}^2 makes this tensor small for small ε like it was in (1.14))

- $\lim_{\varepsilon \to 0} \sigma_{\varepsilon} = \sigma > 0$: the limit system is the Brinkman law (1.6) with the permeability tensor $\mathbf{K} = \sigma^2 \tilde{\mathcal{K}}$, $\mu_{eff} = \mu$.

- $\lim_{\varepsilon \to 0} \sigma_{\varepsilon} = +\infty$: the limit system is the Stokes equations with absence of the solid obstacles.

The exact statement is given in [2, p.266-273] or in a compact form in [21, p.63]. The tensor $\tilde{\mathcal{K}}$ is calculated from cell problems which are different from (1.11).

Of course, for the given problem $\mathcal{P}$ with period $\bar{\varepsilon}$ and the size of the obstacle $\bar{a}$ ($\bar{a} < \bar{\varepsilon}$, but not necessary $\bar{a} \ll \bar{\varepsilon}$) it is possible to choose a function $a(\varepsilon)$ ($d \geq 3$):

$$a(\varepsilon) = \left[\frac{\bar{a}}{\bar{\varepsilon}^{\gamma}}\right] \varepsilon^{\gamma}, \qquad \text{for arbitrary } \gamma > 1, \qquad \sigma_{\varepsilon} = \left[\frac{\bar{\varepsilon}^{\gamma}}{\bar{a}}\right]^{(d-2)/2} \varepsilon^{[d-\gamma(d-2)]/2}$$

which suggests sizes of obstacles for the problems $\{\tilde{\mathcal{P}}^{\varepsilon}\}$. The sequence $\{\tilde{\mathcal{P}}^{\varepsilon}\}$ constructed in this way satisfies the condition $\{\tilde{\mathcal{P}}^{\bar{\varepsilon}}\} = \mathcal{P}$ since $a(\bar{\varepsilon}) = \bar{a}$. We can control the limit problem by choosing γ: the first, second or third limit cases appear when $1 < \gamma < d/(d-2)$, $\gamma = d/(d-2)$ or $\gamma > d/(d-2)$, respectively. For example, choosing in 3D $\gamma = 3$, one obtains a sequence with the Brinkman system with permeability $\tilde{\mathcal{K}}\bar{\varepsilon}^3/\bar{a}$ as a macroscopic model. Another γ or another $a(\varepsilon)$ will lead to another sequence $\{\tilde{\mathcal{P}}^{\varepsilon}\}$, another limit problem and another approximation for the solution of $\mathcal{P}$. If the solution of $\mathcal{P}$ can be calculated directly, then it is possible to check whether the approximations are good and which one is better than others. Otherwise, it might be a difficult task to choose a macroscopic model for $\mathcal{P}$ if more than one candidate is known. A possible situation is schematically drawn in Fig.1.3 where the sequence $\tilde{\mathcal{P}}^{\varepsilon}$ going through $\mathcal{P}$ converges, but the limit $\tilde{\mathcal{P}}^0$ is still "far away" from $\mathcal{P}$, meaning that the approximations for microscopical solutions work well for $\tilde{\mathcal{P}}^{\varepsilon}$ with ε much smaller than $\bar{\varepsilon}$. Therefore it seems reasonable to apply the Brinkman model (and also other models in this paragraph derived under the assumption $\lim_{\varepsilon \to 0} a_{\varepsilon}/\varepsilon = 0$) only if $\bar{a} \ll \bar{\varepsilon}$ for $\mathcal{P}$, otherwise the approximation can be too rough. But in this case such porous media are idealizations, hardly applicable for real cases: the obstacles in 3D are disconnected but assumed to be rigid, motionless; porosity

should be extremely close to 1. Also, for numerical experiments which we perform in 2D for periodic geometries from Fig.1.2, these assumptions seem to be inappropriate. First, the solid obstacles are not small in comparison with the size of the unit cells Y. Second, it was obtained [2, p.232] that in 2D case the (Brinkman) permeability is a scalar which is even independent on the obstacle's shape. Our numerical experiments done for example in Section 4.1 show the importance of the shape of the obstacles. Therefore it is questionable whether these macroscopic models are able to give reasonable approximations to microsolutions in our cases.

The Brinkman model can be rehabilitated as an approximation to the Darcy model if we use the same permeability as for the Darcy law : $\mathbf{K}$ from (1.14) is very small since $\bar{\varepsilon}$ is a small distance (with respect to L), and one can expect that the term $\mu \mathbf{K}^{-1}\mathbf{u}$ dominates over the viscosity term $\mu \triangle \mathbf{u}$ in internal part of the porous media where the macro velocity $\mathbf{u}$ is typically smooth (see also the dimensionless form: (1.43) in Sec.1.4.1). The deviations from the solution of the Darcy system are expected near the boundary of Ω_p due to variations in velocity, but the assumptions needed to derive the Darcy law also breaks down there.

One can also start from the microscopical problem $\mathcal{P}$, where the flow is governed by the Navier-Stokes equations (1.1) instead of the Stokes equations in (1.7). An important role in classifying such flows is played by the local Reynolds number $Re_p^{loc} = \rho U_p \bar{\varepsilon}/\mu$, based on a typical pore size $\bar{\varepsilon}$, and on typical flow velocity in the porous media U_p. The only case we consider here is the flow in porous media with small Re_p^{loc}: the convective term is much smaller than the viscous term, and the Navier-Stokes equations are a small perturbation of the Stokes equations. The corresponding sequence $\{\mathcal{P}^\varepsilon\}$ converges again to the Darcy law (see [40]). When the local Reynolds number increases, the convective terms start to play an important role and the so-called two-pressure Navier-Stokes system gives a better approximation for the flow (see [13, p.168]). We will not consider this case.

It is also possible to consider $\tilde{\mathcal{P}}^\varepsilon$ like above, but based on Navier–Stokes equations [21, p.65]. The limit problem for the case $\lim_{\varepsilon\to 0} \sigma_\varepsilon = \sigma > 0$ is a Navier–Stokes–Brinkman system:

$$-\nabla \cdot (\mu_{eff}\nabla\mathbf{u}) + (\rho\mathbf{u} \cdot \nabla)\mathbf{u} + \mu\mathbf{K}^{-1}\mathbf{u} + \nabla p = \mathbf{f} \quad \text{in } \Omega_p$$
$$\nabla \cdot \mathbf{u} = 0 \qquad\qquad\qquad\qquad (1.18)$$

with $\mu_{eff} = \mu$ and $\mathbf{K} = \sigma^2 \tilde{\mathcal{K}}$ (one can divide everything by ρ in (1.18) and rescale $\mu, p, \mathbf{f}$ to obtain exactly the same equations like in [21]).

If we use in (1.18) the Darcy permeability (1.14), then (1.18) is again an approximation to the Darcy law (1.13), provided that additionally $\mu\mathbf{K}^{-1}\mathbf{u}$ dominates over the convective term $(\rho\mathbf{u} \cdot \nabla)\mathbf{u}$ (see a dimensionless form (1.38): the product of Reynolds and Darcy numbers $ReDa$ should be small).

1.3 Interface conditions

Up to this point our purpose was to obtain macroscopic models for the flow in the porous media only. We fence ourselves off from fluid part Ω_f by restricting consideration to D, $D \subseteq \Omega_p$, and setting boundary condition on ∂D. But in our original problem the boundary conditions are given on $\partial\Omega$, and $\Sigma = \partial\Omega_p \cap \partial\Omega_f$ is an interface inside Ω. In this section we discuss some known approaches to treat the coupled problem between Ω_f and Ω_p, when Darcy or Brinkman macroscopic models are considered in the porous media. The microscopical model doesn't need any special interface conditions (see Sec.1.2.1).

It is important to note that if we deal with a macroscopic model in the porous media then the velocity and pressure variables have different meanings in Ω_p and Ω_f, although we will use the same notation for both: $\mathbf{u}$, p (to distinguish them one have just to check where the variables

are defined: in Ω_p or in Ω_f, and whether microscopical or macroscopic model is used). In Ω_f they are usual fluid velocity and pressure, but in the porous media Ω_p $\mathbf{u}$, p have the meaning of spatially averaged microscopical variables like $\overline{\mathbf{u}}, \overline{p}$ from (1.4) (see Sec.1.2.3, 1.2.4). The velocity there has also other names: seepage velocity, filtration velocity, volumetric flux density (see, e.g., [43, p.5]).

Concerning the values on the interface Σ. We will distinguish the interface "seen" from the porous part Σ_p, and the interface "seen" from the fluid part Σ_f (Of course $\Sigma = \Sigma_p = \Sigma_f$, but if some value ϕ is discontinuous through Σ, we can write that the jump $[\phi]|_\Sigma := \phi|_{\Sigma_f} - \phi|_{\Sigma_p} \neq 0$). Depending on the macroscopic model for the porous media flow, different interface conditions have to be specified on the interface Σ.

1.3.1   Interface conditions between Ω_f and Ω_p(Darcy)

First of all, we consider the (Navier–)Stokes equations (1.2),(1.1) in Ω_f, and Darcy system (1.13) in Ω_p. These are different order systems of PDEs, and they need different number of conditions on Σ. If Σ was not an interface but a boundary, then a reasonable choice would be a given velocity vector (d conditions) for the system in Ω_f and a given normal mass flux/given pressure (1 condition) for the system in Ω_p.

One condition comes from the mass flux continuity through the interface,

$$\mathbf{u} \cdot \mathbf{n}_p|_{\Sigma_f} - \mathbf{u} \cdot \mathbf{n}_p|_{\Sigma_p} = 0, \qquad (1.19)$$

where $\mathbf{n}_p$ is an outer normal vector to Ω_p. Recall, that $\mathbf{u}$ has a different meaning in Ω_f and Ω_p. This condition is not enough even to determine the flow in Ω_p since the flux is still unknown.

One usually needs the microscopical model or experimental results to make conclusions on further macroscopic interface conditions. The sequence of microscopical problems $\{\mathcal{P}^\varepsilon\}$ with ε-periodic solid matrix in Ω_p constructed as before with the help of characteristic functions $\chi^\varepsilon(\mathbf{x})$, and ε-independent fluid part Ω_f, was considered in [12],[32],[48, p.147],[23],[24],[25]. Since the sequence of problems $\{\mathcal{P}^\varepsilon\}$ is fixed, there is no reason to mark out one of them $(\mathcal{P}^{\bar\varepsilon})$ as the "main" problem. From now any ε from $\{\varepsilon_n\}$ can be consider as $\bar\varepsilon$, all problems $\mathcal{P}^\varepsilon$ are "equal in rights" and the main purpose is to approximate solutions of $\mathcal{P}^\varepsilon$ by effective solutions constructed from $\mathcal{P}^0$ for small enough ε.

A condition, satisfied by effective solutions on the interface is a candidate to become a macroscopic interface condition. The crucial role is played by the fact that in the sequence $\mathcal{P}^\varepsilon$ the permeabilities for Ω_p $(\mathbf{K}^\varepsilon = \varepsilon^2 \mathcal{K})$ tend to zero when $\varepsilon \to 0$, roughly meaning that the same pressure gradient (or force $\mathbf{f}$) in Ω_f and Ω_p leads to much smaller mass flux in Ω_p than in Ω_f and also the same mass flux needs much higher pressure gradient (or $\mathbf{f}$) in Ω_p than in Ω_f. The words "much smaller" and "much higher" have a sense since instead of unique problem where such qualifications are relative, one deals with the sequence of problems where the qualifications become more and more evident as $\varepsilon \to 0$.

The Sanchez-Palencia, Ene, Levy conditions

In [12],[32] the authors H.I. Ene, E. Sanchez-Palencia, T. Levy distinguished two qualitatively different kinds of flow, according to the question whether the velocities or the pressure gradients are comparable in Ω_p and Ω_f:

Case A. The velocity in the free fluid part is much larger than the filtration velocity in the porous medium, the pressure gradients in both subregions have comparable magnitudes. With respect to the interface this case was called "near parallel flow" in [26, p. 68])

Case B. The velocities in both subregions have comparable magnitudes. The pressure gradient

in the porous media is much larger than in the free fluid part and is almost perpendicular to Σ_p. This case was called "near normal flow" in [26, p. 68]).

The classification is important since the conditions proposed in [12],[32] are different for *Case A* and *Case B*.

$$\text{Case A:} \quad \mathbf{u}|_{\Sigma_f} = \mathbf{0} \qquad p|_{\Sigma_p} = p|_{\Sigma_f} \tag{1.20}$$

The filtration velocity (in Ω_p), being negligible comparing with velocity in Ω_f, is approximated by $\mathbf{0}$. The first condition makes it possible to solve the flow in Ω_f (at least the interface creates no problems). The pressure field in Ω_p can be found by solving the elliptic equation (1.15) with the given pressure condition on Σ_p taken from the known pressure field in Ω_f due to the second condition in (1.20). In Ω_p one can use the velocity field obtained from the Darcy law instead of $\mathbf{0}$. It is small (of order ε^2 if we deal with the sequence of problems) and its normal component is small (but non-zero in general). This makes the condition (1.19) only approximately true.

The *Case B* was considered in [32], and the following conditions were proposed additional to (1.19):

$$\text{Case B:} \quad p|_{\Sigma_p} = C; \qquad \mathbf{u} \cdot \mathbf{t}_i|_{\Sigma_f} = 0 \quad i = 1, \dots, d-1. \tag{1.21}$$

Here C is an unknown constant, $\mathbf{t}_i$ is a tangential vector to the interface so that $\mathbf{n}$, $\mathbf{t}_1$, ..., $\mathbf{t}_{d-1}$ is an orthogonal basis. To have a comparable velocity field, the pressure gradient in Ω_p should be much larger than the one in Ω_f, so that although $p|_{\Sigma_p}$ is not a constant and depends on the flow in Ω_f, its variation is negligible in comparison with the pressure variation in Ω_p. Here it might be possible to solve the problem in Ω_p first, if, for example, the problem allows to choose the value for the constant pressure arbitrary (pressure is often defined up to a constant), or using additional information like the total mass flux through Ω_p. If the flow in Ω_p is known, then the Dirichlet condition for the velocity is given on Σ_f due to conditions for tangential velocity components (1.21) and the known normal flux from (1.19).

The flow type classification needs a qualitative information about the flow, but should be done before solving the problem, since the choice of interface conditions depend on the classification. If the flow is originated by the boundary conditions and not by the right hand side force $\mathbf{f}$, then the classification often can be guessed from the geometrical information (subdivision of Ω into Ω_p, Ω_f), and from the boundary conditions on $\partial\Omega$. In [48, p.147] two typical examples for both cases are presented: *Case A* – a porous body is embedded in a domain filled with fluid (the flow in the porous medium is a consequence of the flow in the free fluid region); or the opposite situation for the *Case B* – when the fluid region is surrounded by the porous medium (the flow in the cavity is a consequence of the flow in the porous medium).

In the Chapter 4 we will consider some flow problems where the boundary $\partial\Omega$ is solid (with no-slip boundary condition) except one connected part for "Inlet" boundary condition ($S_{in} \subset \partial\Omega_f$) and another connected part with "Outlet" condition ($S_{out} \subset \partial\Omega_f$). Each of Ω_f and Ω_p can be consisting of connected subdomains Ω_f^j, Ω_p^i, respectively. We will deal with at most two such subdomains for Ω_f, and Ω_p will be always a single connected subdomain. If Ω_f is connected, then we have *Case A*. If Ω_f is disconnected, and S_{in}, S_{out} belong to different $\overline{\Omega}_f^j$, then the porous media separates the Inlet from the Outlet, and this is a typical filtration problem corresponding to the *Case B*.

If we have several connected subdomains Ω_f^j, Ω_p^i, and several parts of the boundary (placed in different Ω_f^j) where the flow comes in and goes out, then the presented classification can become much more difficult, or even impossible.

The Beavers–Joseph condition

G.S. Beavers and D.D. Joseph [6] performed experiments with fluid flow in a channel over a porous media block (see Fig.2.1). A uniform pressure gradient was maintained in the longitudinal direction in Ω_f and Ω_p. They found out that the mass flux through Ω_f is larger than what could be predicted by the Poiseuille flow. The last corresponds to using no slip conditions on the channel boundaries. In our notations it would mean considering *Case A*, and posing conditions (1.20) on the interface. They explained this effect with appearance of a slip velocity on the interface, and have found an empirical condition which was in good correlation with the experimental results:

$$\frac{\partial u}{\partial y}(\cdot, 0) = \frac{\alpha_{BJ}}{\sqrt{K}}(u(\cdot, 0) - Q) \tag{1.22}$$

Here Ω_f is above ($0 < y < h$), and Ω_p is below the interface. The latter is located at $y = 0$. u is a horizontal velocity in Ω_f and Q is a (uniform) horizontal filtration velocity in Ω_p, K is a scalar permeability and α_{BJ} is a [6]:"*dimensionless quantity depending on the material parameters which characterize the structure of permeable material within the boundary region*".

The following table is presented in [6]. It contains the measured slip coefficients α_{BJ}, the scalar permeability K, and the estimation for the typical pore size $\bar{\varepsilon}$. We add the column with numbers $\mathcal{K} = K/\bar{\varepsilon}^2$ as a dimensionless permeability (the length was initially given in inches. 1 inch ≈ 0.0254 meter (m)):

Porous medium	α_{BJ}	$K(m^2)$	$\bar{\varepsilon}(m)$	$K/\bar{\varepsilon}^2$
Foametal A	0.78	$9.7 \cdot 10^{-9}$	0.0004	0.058
Foametal B	1.45	$3.9 \cdot 10^{-8}$	0.00084	0.053
Foametal C	4.0	$8.2 \cdot 10^{-8}$	0.0011	0.063
Aloxte	0.1	$6.5 \cdot 10^{-10}$	0.00033	0.0059
Aloxte	0.1	$1.6 \cdot 10^{-9}$	0.0007	0.0034

In [7] the condition was retested and laminar-turbulent translation was investigated, and in [8] it was verified for gas flows.

Saffman's modification of the Beavers–Joseph condition   The Beavers-Joseph condition establishes a connection between velocities in Ω_f and Ω_p. The systems in Ω_f and Ω_p should be solved simultaneously. In [49] P.G. Saffman proposed a modification of the Beavers–Joseph condition which contains only variables in Ω_f:

$$u(\cdot, 0) = \frac{\sqrt{K}}{\alpha_{BJ}}\frac{\partial u}{\partial y}(\cdot, 0) + O(K) \tag{1.23}$$

since the filtration velocity is much smaller than the slip velocity $u(0)$. In turn, the slip velocity can be small compared to the maximal velocity in Ω_p (for example when the channel's width is much larger than $\sqrt{K}$) then setting tangential velocity to zero like in (1.20) also gives a reasonable approximation.

On mathematical justification of interface conditions

In [23]-[25] W. Jäger, A. Mikelić, N. Neuss continued to investigate the interface problem from an asymptotical point of view, according to the sequence of problems $\mathcal{P}^{\mathcal{E}}$. The 2D geometry Ω was defined as $\Omega = (0, b) \times (y_{min}, y_{max})$, $\Omega_p = (0, b) \times (y_{min}, 0)$, $\Omega_p = (0, b) \times (0, y_{max})$. y_{min}, y_{max} are either infinite in [23] or finite in [24],[25]. The ε–periodicity assumption on the solid

microstructure breaks down near the interface $y = 0$, but the problem still has ε–periodicity in the direction OX.

Restricting themselves to this geometry, the authors treated the problem rigorously for both, *Case A* and *Case B*. Although the exact microsolutions $(\mathbf{u}^\varepsilon, p^\varepsilon)$ cannot be explicitly written, their approximate solutions were constructed with the help of several auxiliary problems. Each of them is either a macroscopic problem, or a cell problem (in Y), or a boundary layer problem (in Z; defined below). This approach needs much less computational resources, compared to solving the microproblem $\mathcal{P}^\varepsilon$ itself. The approximation errors were estimated as functions of ε, tending to zero when $\varepsilon \to 0$ (this makes possible to estimate the approximation error for $\mathcal{P}^\varepsilon$).

The boundary layer problems use the periodicity in the direction OX. The boundary layer $Z = (0,1) \times \mathbb{R}$ is subdivided into solid and fluid parts with the help of the $\bar{\varepsilon}$–periodic function $\chi(\mathbf{x})$:

$$Z_s = \{\mathbf{z} = (z^1, z^2) \in Z \mid z^2 < 0, \chi(\bar{\varepsilon}\mathbf{z}) = 0\}, \qquad Z_f = Z \setminus Z_s, \qquad S = [0,1] \times \{0\}.$$

In [23] the micromodel is based on the Stokes system. The flow regimes corresponding to *Cases A* and *B* were originated due to different choices of the right hand side $\mathbf{f}$ depending on ε.

For the *Case B*, the approximation satisfies continuity of the normal flux (1.19), and the first condition in (1.21) postulating a constant pressure along the interface. Instead of the second condition in (1.21), the approximation for the tangential velocity has a jump on the interface (see [23, p. 428,429])

The investigation of the *Case A* started in [23] was continued in [24],[25] for the parallel flow in a channel as it was in Beavers–Joseph experiments. The no-slip condition from (1.20) (which leads to the Poiseuille flow in Ω_f) was found to be a first order (in ε) approximation for the flow in Ω_f. This approximation can be further improved by a velocity field (effective velocity) which has a zero vertical velocity ($v = 0$) and a non-zero horizontal velocity (u) at the interface satisfying the Saffman's form of the Beavers–Joseph condition:

$$u(x, 0 + 0) = -\varepsilon C_1^{bl} \frac{\partial u}{\partial y}(x, 0 + 0) \tag{1.24}$$

To simplify notations, we refer to the following interface condition

$$u(x, 0 + 0) = \alpha \frac{\partial u}{\partial y}(x, 0 + 0) \tag{1.25}$$

as to Beavers–Joseph condition in a Saffman's form. The parameter α which is used in (1.25) is related to similar parameters α_{BJ} in (1.22),(1.23) and C_1^{bl} in (1.24): $\alpha = \frac{\sqrt{k}}{\alpha_{BJ}}$ and $\alpha = -\varepsilon C_1^{bl}$, respectively. In both cases α is $O(\varepsilon)$, if one estimates its dependence on the typical pore size.

The pressure field in Ω_f has a uniform gradient parallel to the interface. To obtain the pressure field in Ω_p, one should solve the elliptic equation (1.15). The pressure on the interface from the side of Ω_p (needed to pose the boundary conditions), can be found from the pressure jump condition:

$$p(x, 0 - 0) = p(x, 0 + 0) + \mu C_\omega^{bl} \frac{\partial u}{\partial y}(x, 0 + 0). \tag{1.26}$$

For more details see [25]. In order to obtain the constant coefficients C_1^{bl}, C_ω^{bl}, the following

boundary layer problem should be solved:

$$
\text{Boundary layer problem} \quad : \quad
\begin{cases}
- \triangle_{\mathbf{y}}\, \vec{\beta}_{bl} + \nabla_{\mathbf{y}} \omega_{bl} = 0 & \text{in } Z_f \\
\nabla_{\mathbf{y}} \cdot \vec{\beta}_{bl} = 0 & \text{in } Z_f \\
\vec{\beta}_{bl} = \mathbf{0} & \text{on } \partial Z_s \\
\left[\vec{\beta}_{bl} \right]_S (\cdot, 0) = \mathbf{0} & \text{on } S \\
\left[(\nabla_{\mathbf{y}}\vec{\beta}_{bl} - \omega_{bl}\mathbf{I})\mathbf{e}_2 \right]_S (\cdot, 0) = \mathbf{e}_1 & \text{on } S \\
\vec{\beta}_{bl},\ \omega_{bl} \text{ are 1-periodic in } y^1.
\end{cases}
\tag{1.27}
$$

where $[\phi]_S = \phi(\cdot, 0+0) - \phi(\cdot, 0-0)$. The coefficients can be calculated from the solution $(\vec{\beta}_{bl}, \omega_{bl})$ as follows:

$$
C_1^{bl} = \int_0^1 \beta_{bl}^1(y^1, 0)\, dy^1, \qquad C_\omega^{bl} = \int_0^1 \omega_{bl}(y^1, 0)\, dy^1.
\tag{1.28}
$$

Remark 5 *We note, that the constants C_1^{bl} and C_ω^{bl} will be used later in the Section 2.1 to determine coefficients in a stress jump condition for the Brinkman equations, when we consider another model for the coupled flow.*

To have the pressure continuity like it was proposed in (1.20), it is sufficient that the $\bar{\varepsilon}-$ periodic function $\chi(\mathbf{x})$ is symmetric with respect to some vertical line $x = x_*$: $\chi(x, y) = \chi(2x_* - x, y)$. In the general case $C_\omega^{bl} \neq 0$ (see Remark 3.9 in [25]). In the Chapter 4 we will perform direct numerical solutions for microproblems for geometries with symmetric and non-symmetric obstacles in artificial periodic porous media.

On solving practical problems

Practical applications need robust algorithms, working well for problems having complicated, possibly disconnected domains Ω_f, Ω_p, with curved boundaries and interfaces, where the flow classification (*Cases A,B*) can be either complicated or impossible. It often means that the interface conditions, derived or experimentally verified for model problems, should be generalized and modified in order to be applicable in a priory unknown situations. They should be valid for possibly large range of applications and (desirably) to lead to well-posed problems. Some recent works in this direction based on domain decomposition approach are [31],[10],[11].

1.3.2 Interface conditions between Ω_f and Ω_p(Brinkman)

The Brinkman system is often used as a flow model in the porous media. The main reason is that it has similar form with the equations, governing the flow in the free fluid part. If instead of porous part we have another fluid part, then the interface would be an imaginary line dividing the fluid into two subregions. The interface conditions in this case are the continuity of the velocity and continuity of the normal component of the stress tensor. The first one reads:

$$
\mathbf{u}\big|_{\Sigma_f} = \mathbf{u}\big|_{\Sigma_p}.
\tag{1.29}
$$

The total force on a small element of the interface, $\mathbf{ds} = \mathbf{n}ds$, from the side for which $\mathbf{n}$ is an external normal is given by [34, p.56]:

$$
d\mathbf{F} = [-\tilde{\mu}(\nabla\mathbf{u} + \nabla\mathbf{u}^T) + p\mathbf{I} + \rho\mathbf{u}\mathbf{u}^T]\mathbf{n}ds
$$

and the force balance for incompressible viscous Newtonian fluid together with (1.29) leads to continuity of the normal stress tensor through the interface:

$$\bar{\mathbf{T}}\mathbf{n}|_{\Sigma_f} = \bar{\mathbf{T}}\mathbf{n}|_{\Sigma_p}, \qquad \bar{\mathbf{T}} = \tilde{\mu}(\nabla\mathbf{u} + \nabla\mathbf{u}^T) - p\mathbf{I} \qquad (1.30)$$

or further to

$$\mathbf{T}\mathbf{n}|_{\Sigma_f} = \mathbf{T}\mathbf{n}|_{\Sigma_p}, \qquad \mathbf{T} = \tilde{\mu}\nabla\mathbf{u} - p\mathbf{I} \qquad (1.31)$$

if $\tilde{\mu}$ is continuous through the interface (see section. 2.2). With $\tilde{\mu}$ we denote a function defined in $\Omega_p \cup \Omega_f$

$$\tilde{\mu} = \begin{cases} \mu & \text{in } \Omega_f \\ \mu_{eff} & \text{in } \Omega_p \end{cases} \qquad (1.32)$$

The velocity continuity condition (1.29) is usually used as the first out of d conditions on the interface, when dealing with the Brinkman model in Ω_p and with (Navier–)Stokes in Ω_f. And it seems to be more adequate, compared to the jump conditions needed for the Darcy model. A reason is that the micro-velocity is continuous and its spatial average is also continuous, although jumps don't prevent appropriate approximations in integral norms (if the rapid velocity changes in a small boundary region are substituted by a jump).

But neither the stress tensor $\bar{\mathbf{T}}$ nor $\mathbf{T}$ has the same physical meaning for the Brinkman equations in Ω_p, as they have in Ω_f for (Navier–) Stokes equations. In the porous media the influence of the solid matrix is not taken into account by considering stress continuity. Also on the interface: the influence from the free fluid part is given by $\mathbf{T}\mathbf{n}$ to Ω_{pf} and Ω_{ps}, but it is unclear how to express the balance from the porous part in such situation (see also [43, p.17]). The conditions (1.30), (1.31) are therefore purely mathematical. Some articles using the conditions (1.29), (1.30) or (1.31) are [19],[51],[3],[39], [42],[38],[27].

An effective viscosity, μ_{eff}, can be introduced with twofold purposes. From one side, to improve the model in internal part of Ω_p, as it is proposed, for example, in [36] or [27]. From another side, to control the flow behaviour in the region near the interface (we have already mentioned that there the viscosity term plays an important role).

In [42], G. Neale, W. Nader considered a flow in a channel like in Beavers – Joseph experiments, but with Brinkman model instead of Darcy model in Ω_p. Using an exact solution to corresponding ODE equation, they found that the effective viscosity μ_{eff} can be found from the relation $\sqrt{\mu_{eff}/\mu} = \alpha_{BJ}$ to provide a good agreement with the Beavers–Joseph model based on Darcy law. It was noted in [26, p. 75] that $\sqrt{\mu_{eff}/\mu}$ is a parameter of the porous media itself (it is defined in Ω_p), and α_{BJ} depends on the microgeometry of the interfacial region (it is defined on Σ). Therefore the usage of this approach is quite limited.

In [38] the authors N. Martys, D.P. Bentz, E. Garboczi made numerical experiments with the 3D Stokes flow in the channel with randomly generated solid matrix in Ω_p. Then they fitted the Brinkman's 1D macrosolution for different μ_{eff} with the averaged Stokes microsolution to obtain a dependence of μ_{eff} on porosity. Good fitting was obtained for porosities between 0.5 and 0.8 (similar purposes we will have in the Chapter 4).

M. Sahraoui and M. Kaviany in [50] also did numerical experiments and comparison of the microsolution with the macrosolution with Brinkman model (the solid matrix in the porous medium was periodic and constructed from cylinders). They reported that for the choice of μ_{eff} proposed in [42], the macrosolution differs from the averaged microsolution in a small part of the porous region near the interface. They also considered models where the effective viscosity and permeability change near the interface.

Remark 6 *The effective viscosity terms that may appear in the Brinkman equation:* $\mu_{eff}\triangle\mathbf{u}$, $\nabla\cdot(\mu_{eff}\nabla\mathbf{u})$, $\nabla\cdot[\mu_{eff}(\nabla\mathbf{u} + \nabla\mathbf{u}^T)]$ *are the same if* μ_{eff} *is a constant in* Ω_p, *have different*

form otherwise: the k-th components of these vectors are respectively:

$$\mu_{eff}\triangle u^k, \qquad \mu_{eff}\triangle u^k + \nabla\mu_{eff}\cdot\nabla u^k, \qquad \mu_{eff}\triangle u^k + \nabla\mu_{eff}\cdot\nabla u^k + \nabla\mu_{eff}\cdot\left(\frac{\partial\mathbf{u}}{\partial x^k}\right) + \frac{\partial}{\partial x^k}\overbrace{(\nabla\cdot\mathbf{u})}^{=0}.$$

Ochoa-Tapia, Whitaker interface conditions: Based on the local volume averaging technique for Stokes system, J.A. Ochoa-Tapia, S. Whitaker [44], additionally to (1.29) proposed the so-called stress jump condition

$$\mathbf{n}_p\cdot(\mu\nabla\mathbf{u} - p\mathbf{I})\,|_{\Sigma_f} - \mathbf{n}_p\cdot(\mu_{eff}\nabla\mathbf{u} - p\mathbf{I})\,|_{\Sigma_p} = \mu\overline{\mathcal{M}}\mathbf{u}. \qquad (1.33)$$

Here $\mathbf{n}_p$ is the unit normal vector to the interface external to the porous part Ω_p, the second order tensor coefficient $\overline{\mathcal{M}}$ should be determined from experiments. $\overline{\mathcal{M}}$ was decomposed there into constitutive parts, but we will not use it since the problem of their experimental determination is more complicated than for $\overline{\mathcal{M}}$. The magnitude of $\overline{\mathcal{M}}$ was estimated as $1/\sqrt{K}$. A one dimensional investigation of the conditions (1.29),(1.33) were undertaken in [45] [28], [29] for the channel flow when the 1D solution can be constructed and compared with the results of the Beavers–Joseph experiment.

Further development is given in [46], where the Navier–Stokes equations are considered, and as a result the stress jump condition (1.33) is generalized by adding a term containing a fourth order tensor that should be experimentally determined. We will not deal here with this more complicated condition.

To simplify the notation, we include μ into $\mathbf{M}$: $\mathbf{M} = \mu\overline{\mathcal{M}}$. The condition (1.33) can be rewritten using the notation from (1.31) as

$$(\mathbf{T}|_{\Sigma_f} - \mathbf{T}|_{\Sigma_p})\mathbf{n}_p = \mathbf{M}\mathbf{u}. \qquad (1.34)$$

An alternative condition can be obtained if we substitute $\mathbf{T}$ by the stress tensor $\bar{\mathbf{T}}$:

$$(\bar{\mathbf{T}}|_{\Sigma_f} - \bar{\mathbf{T}}|_{\Sigma_p})\mathbf{n}_p = \mathbf{M}\mathbf{u} \qquad (1.35)$$

but we don't consider it here. Excepting some test examples for the algorithm in Chapter 3, we will use $\mu_{eff} = \mu$ in numerical simulations, and consequently the condition (1.34) is the same as (1.35) (see Section 2.2).

On solving practical problems The conditions mentioned here like (1.29), (1.30)/(1.31) can be used for quite general types of geometries without a priory classification. The numerical methods can be based on similar discretization in the whole domain but with some modifications specific for porous, fluid parts and interfacial region. In this thesis we propose a numerical method for the case with interface conditions (1.29), (1.34).

1.4   (Navier–)Stokes–Brinkman macroscopic model

Let us consider the so-called Navier–Stokes–Brinkman system of equations in $\Omega_f \cup \Omega_p$:

$$-\nabla\cdot(\tilde{\mu}\nabla\mathbf{u}) + (\rho\mathbf{u}\cdot\nabla)\mathbf{u} + \mu\mathbf{K}^{-1}\mathbf{u} + \nabla p = \mathbf{f},$$
$$\nabla\cdot\mathbf{u} = 0 \qquad (1.36)$$

where $\tilde{\mu}$ is defined in (1.32), $\mathbf{K}$ is the (Darcy) permeability tensor in Ω_p, and $\mathbf{K}^{-1} = \mathbf{0}$ in Ω_f. According to the fictitious domain method [3], it is also possible to consider (1.36) in Ω_s by

choosing a small number $\delta > 0$ and setting there either $\tilde{\mu} = \mu$, $\mathbf{K} = \delta\mathbf{I}$ or $\tilde{\mu} = \mu/\delta$, $\mathbf{K} = \delta\mathbf{I}$. We will often deal with the so-called Stokes–Brinkman system: (1.36) without the convective term $(\rho\mathbf{u} \cdot \nabla)\mathbf{u}$:

$$-\nabla \cdot (\tilde{\mu}\nabla\mathbf{u}) + \mu\mathbf{K}^{-1}\mathbf{u} + \nabla p = \mathbf{f}.$$
$$\nabla \cdot \mathbf{u} = 0$$
$$\tag{1.37}$$

The (Darcy) permeability $\mathbf{K}$ for the $\bar{\varepsilon}$-periodic porous media is symmetric and positive definite, and can be determined from (1.11), (1.14). $\mathbf{K}^{-1}$ is well defined. For the real porous media $\mathbf{K}$ is usually obtained experimentally. In the Table on p.24, the values of typical pore size $\bar{\varepsilon}$, permeability $\mathbf{K} = K\mathbf{I}$ and $K/\bar{\varepsilon}^2$ are presented for some real porous materials. One can check that the formula (1.14), separating the magnitude of the permeability $\bar{\varepsilon}^2$ from the geometrical properties $\mathcal{K}$ for periodic porous media, also has a meaning for the real porous materials. The existence of $\mathbf{K}^{-1}$ comes from the physically reasonable assumption that if we have a nonzero pressure gradient ∇p in the porous media then the resulting flux vector $\mathbf{u}$ should be non-zero (using the Darcy law: $\mathbf{u} = -\mathbf{K}\nabla p/\mu$). It is also reasonable that the angle between $\mathbf{u}$ and $-\nabla p$ should always be acute. This means that $\mathbf{K}$ is positive definite: $(\mathbf{K}\nabla p) \cdot \nabla p = \mu\mathbf{u} \cdot (-\nabla p) > 0$.

1.4.1 Dimensionless equations

Let us define a dimensionless coordinates $\mathbf{x}_*$ and variables $\mathbf{u}_*$, p_* (see [16, II,p.12]):

$$\mathbf{x} = L\mathbf{x}_*, \quad \mathbf{u}(\mathbf{x}) = U\mathbf{u}_*(\mathbf{x}_*), \quad p(\mathbf{x}) = \rho U^2 p_*(\mathbf{x}_*), \quad \tilde{\mu}(\mathbf{x}) = \mu\tilde{\mu}_*(\mathbf{x}_*), \quad \mathbf{f}(\mathbf{x}) = \rho g\mathbf{f}_*(\mathbf{x}_*),$$

where L is a characteristic length for the whole problem (see Fig.1.1), U is a characteristic velocity (for example the maximal Dirichlet velocity on S_{in}), g is the gravity acceleration.

The spatial derivatives changes in the following way for some function $\phi(\mathbf{x}) = \phi_*(\mathbf{x}_*)$:

$$\frac{\partial}{\partial x^i}\phi(\mathbf{x}) = \frac{\partial\phi_*}{\partial x^i}(\mathbf{x}_*(\mathbf{x})) = \sum_j \frac{\partial\phi_*}{\partial x_*^j}(\mathbf{x}_*(\mathbf{x}))\frac{\partial x_*^j}{\partial x^i} = \frac{1}{L}\frac{\partial}{\partial x_*^i}\phi_*(\mathbf{x}_*)$$

and formally $\nabla = L^{-1}\nabla_*$. If we change from $(\mathbf{u}, p)$ to $(\mathbf{u}_*, p_*)$ in (1.36) and multiply the resulting momentum equations by $L/\rho U^2$ in order to have 1 in front of the convective term we get:

$$-\tfrac{\mu}{\rho UL}\nabla_* \cdot (\tilde{\mu}_*\nabla_*\mathbf{u}_*) + (\mathbf{u}_* \cdot \nabla_*)\mathbf{u}_* + \tfrac{\mu L}{\rho U}\mathbf{K}^{-1}\mathbf{u}_* + \nabla_* p_* = \tfrac{Lg}{U^2}\mathbf{f}_*$$
$$\nabla_* \cdot \mathbf{u}_* = 0$$

$Re = \rho UL/\mu$ is a Reynolds number (corresponding to macro length L), $Fr = U/\sqrt{Lg}$ is a Froude number. $\mu L/(\rho U) = L^2/Re$, $\mathbf{K}^{-1} = \bar{\varepsilon}^{-2}\mathcal{K}^{-1}$. Hence it is convenient to define a Darcy number $Da = (\bar{\varepsilon}/L)^2$ to obtain a dimensionless system with three dimensionless parameters Re, Da, Fr. instead of (1.36) (we omit stars which denote the dimensionless variables):

$$-\tfrac{1}{Re}\nabla \cdot (\tfrac{\mu_{eff}}{\mu}\nabla\mathbf{u}) + (\mathbf{u} \cdot \nabla)\mathbf{u} + \tfrac{1}{ReDa}\mathcal{K}^{-1}\mathbf{u} + \nabla p = \tfrac{1}{Fr^2}\mathbf{f}$$
$$\nabla \cdot \mathbf{u} = 0$$
$$\tag{1.38}$$

in a porous part Ω_p for macro simulations and

$$-\tfrac{1}{Re}\triangle\mathbf{u} + (\mathbf{u} \cdot \nabla)\mathbf{u} + \nabla p = \tfrac{1}{Fr^2}\mathbf{f}$$
$$\nabla \cdot \mathbf{u} = 0$$
$$\tag{1.39}$$

in the fluid part Ω_f for macro simulations or in $\Omega_f \cup \Omega_{pf}$ for micro simulations. For practical problems the right hand side $\mathbf{f}$ is usually the density of the gravity force $\mathbf{f} = \rho g\mathbf{e}_g$, where

$\mathbf{e}_g$ is a unit vector in the direction of the gravity force. But the gravity force with variable direction enter an additional undesirable factor in the model. It is an advantage of computational experiment in comparison with physical experiment that we can easily turn it off and to consider $\mathbf{f} \equiv \mathbf{0}$ avoiding the uncertainty related to the choice of Fr and the direction $\mathbf{e}_g$. Formally this term can be neglected when the Froude number is large. In any case the external force can be included into the numerical algorithm without evident difficulties. But there can be another reason for non-zero right hand side: it is a usual approach in theoretical treatment to transform the problem with non-homogeneous boundary condition into similar problem with homogeneous boundary condition having an additional item in the right hand side.

Let us recall that on p.21, in order to justify the usage of the Brinkman equation for the same problems where the Darcy law is proved to be valid, we used the argument that the third term with permeability is much larger than the other velocity terms in the equation. Formally this needs that the Darcy number Da is small and the product of Reynolds and Darcy numbers $ReDa$ is small (1.38). Near the interface where high gradients may occur, the flow behaviour is determined mostly by the interface conditions. Using the dimensionless variables we obtain:

$$\mathbf{n}_p \cdot \left(\frac{\mu U}{L} \nabla_* \mathbf{u}_* - \rho U^2 p_* \mathbf{I} \right) |_{\Sigma_f} - \mathbf{n}_p \cdot \left(\frac{\mu_{eff}}{\mu} \frac{\mu U}{L} \nabla_* \mathbf{u}_* - \rho U^2 p_* \mathbf{I} \right) |_{\Sigma_p} = U \mathbf{M} \mathbf{u}_*$$

$$\mathbf{u}_* |_{\Sigma_p} - \mathbf{u}_* |_{\Sigma_f} = 0$$

We can scale $\overline{\mathcal{M}}$ as it was proposed in [45] but instead of $\sqrt{K}$ we can use $\bar{\varepsilon}$: $\overline{\mathcal{M}} = \mathcal{M}/\bar{\varepsilon}$ where $\mathcal{M}$ is dimensionless. If we multiply the first interface condition by $1/(\rho U^2)$ and use that $\mathbf{M} = \mu \overline{\mathcal{M}} = \mu \mathcal{M}/\bar{\varepsilon}$ then after omitting stars we will obtain the dimensionless interface stress jump condition:

$$\mathbf{n}_p \cdot \left(\frac{1}{Re} \nabla \mathbf{u} - p \mathbf{I} \right) |_{\Sigma_f} - \mathbf{n}_p \cdot \left(\frac{\mu_{eff}}{\mu} \frac{1}{Re} \nabla \mathbf{u} - p \mathbf{I} \right) |_{\Sigma_p} = \frac{\mathcal{M}}{Re\sqrt{Da}} \mathbf{u} \qquad (1.40)$$

or in particular ($\mathcal{M} = \mathbf{0}$) the continuous stress condition:

$$\mathbf{n}_p \cdot \left(\frac{1}{Re} \nabla \mathbf{u} - p \mathbf{I} \right) |_{\Sigma_f} - \mathbf{n}_p \cdot \left(\frac{\mu_{eff}}{\mu} \frac{1}{Re} \nabla \mathbf{u} - p \mathbf{I} \right) |_{\Sigma_p} = \mathbf{0} \qquad (1.41)$$

Also the dimensionless velocity is continuous on the interface:

$$\mathbf{u} |_{\Sigma_p} - \mathbf{u} |_{\Sigma_f} = 0 \qquad (1.42)$$

Most of our examples are based on the dimensional system (1.37) instead of (1.36). It leads to dimensionless systems (1.38), (1.39) where the term $(\mathbf{u} \cdot \nabla) \mathbf{u}$ is absent. In this case the Reynolds number loses its importance since we can multiply the first equation in (1.38), (1.39) by Re and renormalize pressure as $p_* = Re\, p$ to finish with

$$-\nabla \cdot \left(\frac{\mu_{eff}}{\mu} \nabla \mathbf{u} \right) + \frac{1}{Da} \mathcal{K}^{-1} \mathbf{u} + \nabla p = \mathbf{0} \qquad \text{in } \Omega_p \text{ (Macro problem)} \qquad (1.43)$$
$$\nabla \cdot \mathbf{u} = 0$$

$$-\triangle \mathbf{u} + \nabla p = \mathbf{0} \qquad \text{in } \Omega_f \text{ or in } \Omega_f \cup \Omega_{pf} \qquad (1.44)$$
$$\nabla \cdot \mathbf{u} = 0$$

where the star was again omitted from p_* and the interface conditions are

$$\mathbf{n}_p \cdot (\nabla \mathbf{u} - p \mathbf{I}) |_{\Sigma_f} - \mathbf{n}_p \cdot \left(\frac{\mu_{eff}}{\mu} \nabla \mathbf{u} - p \mathbf{I} \right) |_{\Sigma_p} = \frac{\mathcal{M}}{\sqrt{Da}} \mathbf{u}. \qquad (1.45)$$

In the particular case $\mathcal{M} = \mathbf{0}$, when the continuous stress condition is written as:

$$\mathbf{n}_p \cdot (\nabla \mathbf{u} - p\mathbf{I}) |_{\Sigma_f} - \mathbf{n}_p \cdot \left(\frac{\mu_{eff}}{\mu} \nabla \mathbf{u} - p\mathbf{I} \right) |_{\Sigma_p} = \mathbf{0} \tag{1.46}$$

The other interface condition is still (1.42).

The Darcy law is just the first equation in (1.36) without first two terms. We can scale it exactly as it was done above for Navier–Stokes–Brinkman system to have a dimensionless form

$$\frac{1}{ReDa} \mathcal{K}^{-1} \mathbf{u} + \nabla p = \mathbf{0}, \qquad \text{or further} \qquad \frac{1}{Da} \mathcal{K}^{-1} \mathbf{u} + \nabla p = \mathbf{0} \tag{1.47}$$

for Stokes–Brinkman system.

The dimensionless equations we will use for the numerical experiments in the Chapters 4 and 5.

Chapter 2

The Stokes–Brinkman model with stress jump condition

In this chapter we discuss some theoretical aspects related to the (Navier-)Stokes–Brinkman model accomplished with the interface conditions (1.29), (1.34), as proposed in [44].

In the Section 2.1 we consider the well investigated case of parallel flow in a channel over a porous medium (this problem has been studied both from experimental and theoretical point of view in [6]-[8],[49],[24]-[25]). Our purpose is to show that at least for the flow regime we consider, the solution, corresponding to the (Navier–) Stokes–Brinkman model is able to approximate the solution, corresponding to the (Navier–) Stokes–Darcy model which satisfies the Saffman's modification of the Beavers-Joseph condition [49] and the pressure jump condition, proposed by Jäger and Mikelić.

In more general situations, the stress jump coefficient $\mathbf{M}$ can be a matrix-valued function on a curvilinear interface. The vector condition (1.34), written in scalar equations may have a different form at different points. To simplify the analysis of the conditions at a particular point, to compare the conditions at different points, we introduce in Section 2.2 a notion of "laboratory system" for any point on the interface. In the "laboratory system" the conditions have a fixed form, similar to what was for the channel in the Section 2.1. We investigate how the coefficient $\mathbf{M}$ at a given point on the interface is related to $\mathbf{M}'$ in the "laboratory system". We also compare (1.34) with (1.35).

In the Section 2.3, we apply the concept of generalized solutions to the linearized version of our problem (Stokes–Brinkman). Although there is a class of $\mathbf{M}$ for which the problem has the unique solution, in general, the solvability is not obvious and can be related to a spectral problem. And we present a problem where for some $\mathbf{M}$ the uniqueness of the solution is violated.

2.1 Parallel flow (Beavers-Joseph experiment)

Let us consider a 2D channel, $(x, y) \in \Omega = (x_{-\infty}, x_{+\infty}) \times (-l, h)$, where l, h are positive constants, and $x_{-\infty}$, $x_{+\infty}$, $x_{-\infty} < x_{+\infty}$, are finite or infinite. The solution $(\mathbf{u}, p)$, $\mathbf{u} = \mathbf{u}(x, y) = (u(x, y), v(x, y))$, $p = p(x, y)$, satisfies (1.2) in Ω_f and (1.37) in Ω_p with $\mathbf{f} \equiv \mathbf{0}$, as well as conditions (1.29), (1.34) at the porous fluid interface $y = 0$, and the no-slip conditions $\mathbf{u} = \mathbf{0}$ on the lower boundary $y = -l$ and on the upper boundary $y = h$. We choose μ_{eff}, $\mathbf{K}$ to be constants in Ω_p. $\mathbf{K}$ does not necessarily correspond to an isotropic porous medium, and can be a tensor. We will not be interested in the solution in the whole channel Ω, but only in a part of it, $\Omega_{far} = (x_{min}, x_{max}) \times (-l, h)$, where $\Omega_p \cap \Omega_{far} = (x_{min}, x_{max}) \times (-l, 0)$, $\Omega_f \cap \Omega_{far} = (x_{min}, x_{max}) \times (0, h)$, (see Fig.2.1). The exact subdivision of Ω into Ω_p and Ω_f in the other part

of Ω can be unknown together with the left, right boundaries and boundary conditions there. This lack of information plays no role, since we will consider only a fully developed flow regime in Ω_{far} in the sense that $\frac{\partial u}{\partial x} = 0$ there. This rather strong restriction aims at obtaining an exact solution in Ω_{far}. The analytical solution can be used for several purposes:
• in the investigation of the solutions behaviour,
• in comparison with the Navier-Stokes-Darcy model and interface conditions proposed for this model,
• in determination of the coefficient $\mathbf{M}$,
• in testing of numerical algorithms, etc.
In practical cases, we expect that for long enough channels, in the regions far away from the entrance (we used the word "far" in Ω_{far}) this flow regime may approximately occur: $\frac{\partial u}{\partial x} \approx 0$. So let us suppose that $\frac{\partial u}{\partial x} = 0$ in Ω_{far}. Using the incompressibility condition

$$\frac{\partial u}{\partial x}(x,y) + \frac{\partial v}{\partial y}(x,y) = 0$$

in $\Omega_p \cap \Omega_{far}$ and $\Omega_f \cap \Omega_{far}$, we have $\frac{\partial v}{\partial y}(x,y) = 0$ there. If we take some line $x = x_0$ in Ω_{far}, we have

$$v(x_0,y) = v(x_0,-l) + \int_{-l}^{y} \frac{\partial v}{\partial y}(x_0,\xi)\,d\xi = 0 \qquad \text{in } \Omega_p \cap \Omega_{far},$$

$$v(x_0,y) = v(x_0,h) - \int_{y}^{h} \frac{\partial v}{\partial y}(x_0,\xi)\,d\xi = 0 \qquad \text{in } \Omega_f \cap \Omega_{far}.$$

Because of boundary conditions $v(x_0,-l) = v(x_0,h) = 0$, and accounting for $\frac{\partial v}{\partial y}(x,y) = 0$, we find that $v(x_0,y) = 0$, and therefore $v(x,y) \equiv 0$ in Ω_{far} since x_0 is an arbitrary point from (x_{min}, x_{max}). Additionally, $u(x,y) = u(y)$ there. The incompressibility condition has played its role and we can forget it since any vector function in a form $\mathbf{u}(x,y) = (u(y),0)$ satisfies it. The momentum equations now are:

$$\mu \frac{\partial^2 u}{\partial y^2}(y) = \frac{\partial p}{\partial x}(x,y) \tag{2.1}$$

$$\frac{\partial p}{\partial y}(x,y) = 0 \tag{2.2}$$

in $\Omega_f \cap \Omega_{far}$; and

$$\mu_{eff} \frac{\partial^2 u}{\partial y^2}(y) - \mu\kappa_{11}u(y) = \frac{\partial p}{\partial x}(x,y) \tag{2.3}$$

$$-\mu\kappa_{21}u(y) = \frac{\partial p}{\partial y}(x,y) \tag{2.4}$$

in $\Omega_p \cap \Omega_{far}$. We have used the fact that $\frac{\partial u}{\partial x} = 0$ in Ω_{far} implies $\frac{\partial^2 u}{\partial x^2} = 0$; $\{\kappa_{ij}\}$ are elements of $\mathbf{K}^{-1}$.

Remark 7 *It was also possible to consider the Navier–Stokes–Brinkman model in the channel: (1.1) in Ω_f and (1.36) in Ω_p, instead of (1.2) and (1.37). Anyway, $v \equiv 0$ and $\frac{\partial u}{\partial x} = 0$ implies that the convective terms*

$$\rho\left(u\frac{\partial u}{\partial x} + v\frac{\partial u}{\partial y}\right), \qquad \rho\left(u\frac{\partial v}{\partial x} + v\frac{\partial v}{\partial y}\right)$$

disappear, and the momentum equations will be exactly (2.1)-(2.4).

From (2.2) and (2.4), the pressure can be written as

$$p(x, y) = p(x) \qquad \text{in } \Omega_f \cap \Omega_{far}$$

$$p(x, y) = \tilde{p}(x) + \mu \kappa_{21} \int_y^0 u(\xi) \, d\xi \quad \text{in } \Omega_p \cap \Omega_{far},$$

where $\tilde{p}(x) = p(x, 0 - 0)$. $\frac{\partial p}{\partial x}(x, y) = \frac{\partial \tilde{p}}{\partial x}(x)$ doesn't depend on y in $\Omega_p \cap \Omega_{far}$. Hence, in (2.1) and in (2.3) the left hand sides depend on y and the right hand sides on x only. If $F(y) = G(x)$, then $F(y_1) = F(y_2) = G(x_1) = G(x_2) = const$ and the constant doesn't depend on x, y. Thus the momentum equations (2.1) - (2.4) can be rewritten as

$$\mu u''(y) = P_f, \quad p(x, y) = p(x) = p_f^0 + P_f x \qquad \text{in } \Omega_f \cap \Omega_{far}, \tag{2.5}$$

$$\mu_{eff} u''(y) - \mu \kappa_{11} u(y) = P_p, \quad p(x, y) = p_p^0 + P_p x + \mu \kappa_{21} \int_y^0 u(\xi) \, d\xi \qquad \text{in } \Omega_p \cap \Omega_{far}. \tag{2.6}$$

Here P_f, p_f^0, P_p, p_p^0 are some constants.

Now we consider the interface conditions. Continuity of the velocity implies $u(0 - 0) = u(0 + 0) \ =: u(0)$. We assume that the coefficient $\mathbf{M}$ is a constant matrix along the interface. The normal vector to the interface is $\mathbf{n} = (0, 1)^T$. The stress jump conditions (1.34) are:

$$\mu u'(0 + 0) - \mu_{eff} u'(0 - 0) = M_{11} u(0) \qquad - p(x, 0 + 0) + p(x, 0 - 0) = M_{21} u(0).$$

(it is a particular case of (2.45), when $v \equiv 0$). If we plug the expressions for pressure from (2.5), and (2.6) into the second interface condition, then we get

$$-p_f^0 + p_p^0 - P_f x + P_p x = M_{21} u(0)$$

and consequently $P_f = P_p$ and $-p_f^0 + p_p^0 = M_{21} u(0)$, since the right hand side doesn't depend on x. Thus, we can simplify the notation: $P := -P_f = -P_p$, $p^0 := p_f^0$. The constants P and p^0 can be considered as input parameters. Without loss of generality we can set $P > 0$ in order to have the flow in the positive direction. From the 2D problem we came to the boundary value problem for ordinary differential equations

$$u(-l) = 0, \tag{2.7}$$

$$-\mu_{eff} u''(y) + \mu \kappa_{11} u(y) = P, \qquad y \in (-l, 0), \tag{2.8}$$

$$u(0 - 0) = u(0 + 0), \tag{2.9}$$

$$\mu u'(0 + 0) - \mu_{eff} u'(0 - 0) = M_{11} u(0), \tag{2.10}$$

$$-\mu u''(y) = P, \qquad y \in (0, h) \tag{2.11}$$

$$u(h) = 0, \tag{2.12}$$

If $u(y)$ is known then the solution of the 2D problem can be calculated as $\mathbf{u}(x, y) = (u(y), 0)$ for the velocity field and

$$p(x, y) = p^0 - Px, \quad y \in (0, h); \tag{2.13}$$

$$p(x, y) = p^0 - Px + M_{21} u(0) + \mu \kappa_{21} \int_y^0 u(\xi) \, d\xi, \quad y \in (-l, 0) \tag{2.14}$$

for the pressure field. The general solution of (2.8),(2.11) is given by

$$u(y) = \frac{P}{B} + \tilde{C}_1 e^{-\lambda y} + \tilde{C}_2 e^{\lambda y} \qquad \text{in } (-l, 0) \tag{2.15}$$

$$u(y) = -\frac{Py^2}{2\mu} + C_1 y + C_2 \qquad \text{in } (0, h), \tag{2.16}$$

where $B = \mu\kappa_{11}$, $\lambda = \sqrt{B/\mu_{eff}}$. We note that $\kappa_{11} > 0$ since $\mathbf{K}^{-1}$ is positive definite. The constants C_1, C_2, $\tilde{C}_1$, $\tilde{C}_2$ are free parameters of the general solutions, they should be fixed from the interface and boundary conditions (2.7),(2.9),(2.10),(2.12). These constants will be determined later in (2.24)-(2.26).

2.1.1   Approximation of the Saffman's interface condition

The flow in the channel over a porous medium is well investigated (see Section 1.3.1). Instead of solving the problem with M_{11}, M_{21} considered as known parameters, we can try to determine them from the known behaviour of the flow. From the Beavers–Joseph condition in a Saffman form (1.25), we have

$$u_{eff}(0 + 0) = \alpha \frac{\partial u_{eff}}{\partial y}(0 + 0), \qquad \alpha > 0.$$

The effective flow, $\mathbf{u}_{eff} = (u_{eff}(y), 0)$ can be obtained in $\Omega_f \cap \Omega_{far}$ using no-slip condition at $y = h$, and Saffman condition at $y = 0$

$$u_{eff}(y) = -\frac{Py^2}{2\mu} + \underbrace{\frac{Ph^2}{2\mu(h + \alpha)}}_{C_1^*} y + \alpha \underbrace{\frac{Ph^2}{2\mu(h + \alpha)}}_{C_2^*}. \tag{2.17}$$

In this case the flow is independent from the flow in the porous media (the initial Beavers–Joseph interface condition (1.22) depends on the Darcy velocity in the porous media).

We search now M_{11}^*, such that the solution to (2.7-2.12) for $M_{11} = M_{11}^*$ satisfies $u(y) \equiv u_{eff}(y)$ for $y \in (0, h)$. The constants C_1, C_2 in (2.16) are already fixed by C_1^*, C_2^* from (2.17). The other two constants: $\tilde{C}_1$, $\tilde{C}_2$ in (2.15), which correspond to this situation we also mark with stars: $\tilde{C}_1^*$, $\tilde{C}_2^*$. The unknowns $\tilde{C}_1^*$, $\tilde{C}_2^*$, M_{11}^* should satisfy the system of linear equations

$$\begin{array}{ll} (2.7) \Rightarrow \\ (2.9) \Rightarrow \\ (2.10) \Rightarrow \end{array} \left\{ \begin{array}{c} P/B + \tilde{C}_1^* e_+ + \tilde{C}_2^* e_- = 0 \\ P/B + \tilde{C}_1^* + \tilde{C}_2^* = C_2^* \\ \mu C_1^* - \mu_{eff}\lambda(\tilde{C}_2^* - \tilde{C}_1^*) = M_{11}^* C_2^* \end{array} \right.$$

Some notations, which we often use in this section, are:

$$B = \mu\kappa_{11}, \quad \lambda = \sqrt{\frac{\mu}{\mu_{eff}}\kappa_{11}}, \quad e_\pm = \exp(\pm\lambda l), \quad E_\pm = e_+ \pm e_-. \tag{2.18}$$

From the first two equations above, we calculate $\tilde{C}_1^*$, $\tilde{C}_2^*$:

$$\tilde{C}_1^* = -\frac{(1 - e_-)P/B + C_2^* e_-}{E_-}, \quad \tilde{C}_2^* = \frac{(1 - e_+)P/B + C_2^* e_+}{E_-}. \tag{2.19}$$

The coefficient M_{11}^*, that we are interested in, is given by

$$M_{11}^* = \frac{\mu}{\alpha} - \mu_{eff}\lambda\frac{E_+}{E_-} + \frac{\mu_{eff}\lambda P}{C_2^* B}\frac{E_+ - 2}{E_-}. \tag{2.20}$$

It depends on C_2^*, E_+, E_-, and consequently on macroscopic geometry parameters h,l. This is not in accordance with the assumption, that M_{11}^* is a local characteristic of the porous media near the interface. At the same time, $\mathbf{u}_{eff}$ is not an exact microscopical solution in Ω_p, but only an approximation. Further, the Saffman's form of the Beavers–Joseph condition needs the assumption $h/\sqrt{K} \gg 1$ That's why we can try to simplify the expression (2.20), neglecting small terms. The aim is to obtain such M_{11}, which doesn't depend on macroscopic parameters, but still leads to a solution $u(y)$, which is close to $u_{eff}(y)$ in $(0,h)$. If we fix certain porous medium, then the parameters α, λ, B, $E_\pm$, C_2^* will be just numbers, and a decision, that some numbers are small or large enough comparing with others, is subjective. But if one considers a sequence of problems $\mathcal{P}^\varepsilon$ for ε-periodic porous media, as it was done in [24],[25] (see Section 1.3.1, p.25) then the parameters become ε-dependent and it is possible to compare them when $\varepsilon \to 0$. The effective solutions of macroscopic problems $\mathcal{P}^\varepsilon_{eff}$ were shown in [24],[25] to give an appropriate approximation to the microscopical solutions of $\mathcal{P}^\varepsilon$ for small enough ε. To compare the asymptotic behaviour of parameters and variables as $\varepsilon \to 0$ we use the following notation:

• $f(\varepsilon) = o(g(\varepsilon))$: $\lim_{\varepsilon \to 0} f(\varepsilon)/g(\varepsilon) = 0$;

• $f(\varepsilon) = O(g(\varepsilon))$: there are constants $C, \varepsilon_0 > 0$ such that $|f(\varepsilon)/g(\varepsilon)| \le C$ for $\varepsilon \in (0, \varepsilon_0)$.

• $f(\varepsilon) \sim g(\varepsilon)$: $f(\varepsilon) = O(g(\varepsilon))$, $g(\varepsilon) = O(f(\varepsilon))$. Some parameters appear in numerators as well as in denominators – they should be estimated from above together with their inverse.

We have two primary ε-dependent parameters: $\mathbf{K}$ and α. Others are either ε-independent or depend on it through $\mathbf{K}$ and α. The (Darcy) permeability of our ε–periodic porous depends on ε as $\mathbf{K} = \mathbf{K}(\varepsilon) = \varepsilon^2 \mathcal{K}$ (see (1.14)). $\mathcal{K}^{-1}$ is positive definite and therefore diagonal elements of $\mathcal{K}^{-1}$: $\varkappa_{ii}$ are strictly positive. $\mathbf{K}^{-1} = \varepsilon^{-2} \mathcal{K}^{-1}$ has elements $\kappa_{ij} = \kappa_{ij}(\varepsilon) = \varepsilon^{-2} \varkappa_{ij}$. Therefore

$$B \sim \varepsilon^{-2}, \qquad \lambda = \varepsilon^{-1} \sqrt{\frac{\mu}{\mu_{eff}} \varkappa_{11}} \sim \varepsilon^{-1}.$$

Consequently, $\lambda l \sim \varepsilon^{-1}$. Hence $e_+ = e^{\lambda l}$ tends to infinity quicker than ε^{-n}, and $e_- = e^{-\lambda l}$ tends to zero quicker than ε^n, for any $n \in \mathbb{N}$. For arbitrary $n \in \mathbb{N}$, $e_- = e_+^{-1} = o(\varepsilon^n)$.

$$\frac{E_+}{E_-} = 1 + \frac{2e_-}{e_+ - e_-} = 1 + o(\varepsilon^n), \qquad \frac{E_+ - 2}{E_-} = 1 + 2\frac{e_- - 1}{e_+ - e_-} = 1 + o(\varepsilon^n).$$

The coefficient α in (1.25) depends on ε as $\alpha = -\varepsilon C_1^{bl}$. $C_1^{bl} < 0$ can be calculated from (1.28) after solving the boundary layer problem (1.27). Therefore $C_2^* \sim \varepsilon$, and the terms in (2.20) have the following asymptotical behaviour:

$$\frac{\mu}{\alpha} \sim \varepsilon^{-1}, \quad \mu_{eff}\lambda \frac{E_+}{E_-} \sim \varepsilon^{-1}, \quad \frac{\mu_{eff}\lambda P}{C_2^* B} \frac{E_+ - 2}{E_-} \sim 1 \qquad (2.21)$$

The third term in (2.20) is small compared to others, and it can be neglected. So we simplify (2.20) up to

$$M_{11} := \frac{\mu}{\alpha} - \mu_{eff}\lambda, \qquad (2.22)$$

which is independent of the macro geometrical parameters. If we set this M_{11} into (2.7)-(2.12), the solution $u(y)$ for $y \in (0,h)$ will be of course different from $u_{eff}(y)$.

To estimate the difference between these two solutions, we will first obtain expressions for C_1, C_2, $\tilde{C}_1$, $\tilde{C}_2$, such that $u(y)$ from (2.15),(2.16) solves (2.7)-(2.12), provided M_{11} is known (for example from (2.22)). The linear system for unknowns C_1, C_2, $\tilde{C}_1$, $\tilde{C}_2$ is given by

$$
\begin{aligned}
(2.7) &\Rightarrow \\
(2.9) &\Rightarrow \\
(2.10) &\Rightarrow \\
(2.12) &\Rightarrow
\end{aligned}
\left\{
\begin{aligned}
P/B + \tilde{C}_1 e_+ + \tilde{C}_2 e_- &= 0 \\
P/B + \tilde{C}_1 + \tilde{C}_2 &= C_2 \\
\mu C_1 - \mu_{eff}\lambda(\tilde{C}_2 - \tilde{C}_1) &= M_{11} C_2 \\
-\frac{Ph^2}{2\mu} + C_1 h + C_2 &= 0
\end{aligned}
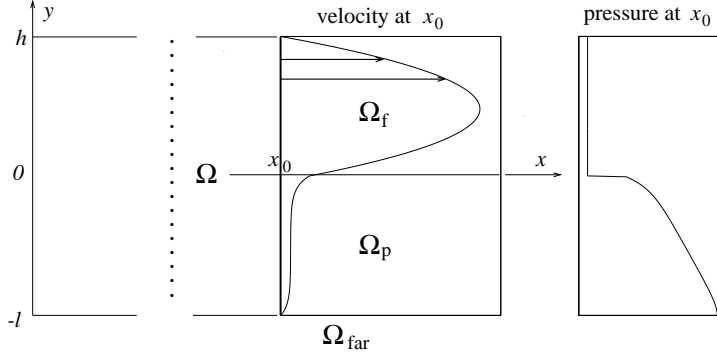\right.
\qquad (2.23)
$$

Figure 2.1: Geometry for the flow in a channel and typical solution of the Stokes–Brinkman equations (velocity and pressure profiles).

and the solution can be explicitly written starting from C_2:

$$C_2 = \left(\frac{Ph}{2} + \frac{\mu_{eff}\lambda P}{B} \frac{E_+ - 2}{E_-} \right) \Big/ \left(M_{11} + \mu_{eff}\lambda \frac{E_+}{E_-} + \frac{\mu}{h} \right) \qquad (2.24)$$

$$C_1 = \frac{Ph}{2\mu} - \frac{C_2}{h} \qquad (2.25)$$

$$\tilde{C}_1 = -\frac{(1 - e_-)P/B + C_2 e_-}{E_-}, \quad \tilde{C}_2 = \frac{(1 - e_+)P/B + C_2 e_+}{E_-} \qquad (2.26)$$

Remark 8 *In the Section 3.3 we will also use the solution (2.15),(2.16), (2.24)-(2.26) to compare this analytical solution with the numerical one.*

Remark 9 *The expression (2.24) has a zero denominator if*

$$M_{11} = M_{11}^\emptyset = -\mu_{eff}\lambda \frac{E_+}{E_-} - \frac{\mu}{h}. \qquad (2.27)$$

In this case the expressions (2.24)-(2.26) cannot be used. For M_{11} chosen in this way, the determinant of the matrix, corresponding to the linear system (2.23), is zero. $M_{11}^\emptyset$ is different from M_{11} in (2.22) since

$$0 > -\frac{\mu}{h} \neq \frac{\mu}{\alpha} + \mu_{eff}\lambda \frac{2e_-}{E_-} > 0.$$

Now, we assume M_{11} in (2.24)-(2.26) is given by (2.22). If in (2.24) we would have M_{11}^* instead of M_{11}, then C_1, C_2 would coincide with C_1^*, C_2^*. Let us approximate C_2 through C_2^*. From (2.21) we know that $M_{11} = M_{11}^* + O(1)$. The denominator in (2.24), multiplied by ε is given by

$$\varepsilon \left(M_{11} + \mu_{eff}\lambda \frac{E_+}{E_-} + \frac{\mu}{h} \right) = \underbrace{\varepsilon \left(M_{11}^* + \mu_{eff}\lambda \frac{E_+}{E_-} + \frac{\mu}{h} \right)}_{f(\varepsilon)} + O(\varepsilon). \qquad (2.28)$$

Using (2.20) and (2.21), the asymptotical behaviour of $f(\varepsilon)$ is estimated as

$$f(\varepsilon) = \varepsilon \left(\frac{\mu}{\alpha} + \frac{\mu_{eff}\lambda P}{C_2^* B} \frac{E_+ - 2}{E_-} + \frac{\mu}{h} \right) = \varepsilon \frac{\mu}{\alpha} + O(\varepsilon) \sim 1.$$

The last follows from (2.21). If $f(\varepsilon) \sim 1$ and $g(\varepsilon) = O(\varepsilon)$, then

$$\frac{1}{f(\varepsilon) + g(\varepsilon)} = \frac{1}{f(\varepsilon)} + O(\varepsilon).$$

Using $f(\varepsilon)$ from (2.28), we can apply it to (2.24), in order to estimate how C_2 approximates C_2^*:

$$C_2 = \varepsilon \left(\frac{Ph}{2} + \frac{\mu_{eff}\lambda P}{B}\frac{E_+ - 2}{E_-} \right) \bigg/ (f(\varepsilon) + O(\varepsilon)) = C_2^* + O(\varepsilon^2)$$

Consequently,

$$C_1 = \frac{Ph}{2\mu} - \frac{C_2}{h} = \frac{Ph}{2\mu} - \frac{C_2^*}{h} + O(\varepsilon^2) = C_1^* + O(\varepsilon^2).$$

C_2 and C_1 have the same orders of magnitude as C_2^* and C_1^*, namely $O(\varepsilon)$ and $O(1)$, respectively. We are ready to estimate the difference between u and u_{eff} in the free fluid part. First, the pointwise estimate reads

$$u(y) - u_{eff}(y) = \underbrace{(C_1 - C_1^*)}_{\Delta C_1}y + \underbrace{C_2 - C_2^*}_{\Delta C_2} = O(\varepsilon^2) \quad \text{uniformly in } y \in (0, h).$$

Next, the L^2 estimate is given by

$$\|u - u_{eff}\|^2_{L^2(0,h)} = \Delta C_1^2\frac{h^3}{3} + \Delta C_1\Delta C_2 h^2 + \Delta C_2^2 h = O(\varepsilon^4)$$

The Beavers–Joseph condition in a Saffman form (1.25) in this case can be written as

$$u(0+) - \alpha\frac{\partial u}{\partial y}(0+) = C_2 - \alpha C_1 = C_2^* + O(\varepsilon^2) - \alpha(C_1^* + O(\varepsilon^2)) = O(\varepsilon^2), \qquad (2.29)$$

since from (2.17) we have

$$u_{eff}(0+) - \alpha\frac{\partial u_{eff}}{\partial y}(0+) = C_2^* - \alpha C_1^* = 0.$$

$O(\varepsilon^2)$ is similar to $O(K)$ used in (1.25). The pressure $p(x, y)$ from (2.13) doesn't depend on ε – it is also an effective pressure in the free fluid part.

Thus, we have shown that the analytical solution of the (Navier-)Stokes–Brinkman model with Ochoa-Tapia, Whitaker condition satisfies the Beavers–Joseph condition in a Saffman form (2.29) when M_{11} is given by (2.22), and furthermore, it approximates the effective solution for the (Navier-)Stokes–Darcy model in the fluid part of the channel (Ω_f). In the next subsection we discuss the proximity of the solutions in the porous medium.

2.1.2 Approximation of the pressure jump condition

In the porous media the solution is determined by (2.14),(2.15),(2.26). As it was mentioned in the Section 1.3.1, Jäger and Mikelić proposed the jump condition (1.26) between the pressure in the free fluid part, given by (2.13), and the effective pressure in the porous media. The latter is a solution of an elliptic equation (1.15), corresponding to the Darcy law and the incompressibility condition. We use another macroscopic equation in the porous part, and it is interesting to check if its solution (with appropriate choice of M_{21}) is able to approximate the pressure jump condition on the interface, as well as the Darcy's relation between velocity and pressure in the porous part.

Velocity $u(y)$ and pressure $p(x, y)$ are given explicitly by (2.14),(2.15),(2.26) for $-l < y < 0$. Let us fix some $\hat{y}$, $-l < \hat{y} < 0$ and estimate $u(\hat{y})$ and $p(x, \hat{y})$ with respect to the small parameter ε. First of all,

$$\tilde{C}_1 = \frac{P + o(\varepsilon^n)}{BE_-} = o(\varepsilon^n), \qquad \tilde{C}_2 = C_2 - \frac{P}{B} + o(\varepsilon^n) = C_2 + O(\varepsilon^2), \qquad (2.30)$$

$$\frac{e^{-\lambda\hat{y}}}{E_-} = o(\varepsilon^n), \qquad e^{\lambda\hat{y}} = o(\varepsilon^n) \qquad \text{for any } n \in \mathbb{N}$$

For each $\hat{y}$, $(-l < \hat{y} < 0)$, we have

$$u(\hat{y}) = \frac{P}{B} + o(\varepsilon^n) \qquad \text{for any } n \in \mathbb{N}.,$$

Then, it is natural to define an effective velocity field for the internal part of $\Omega_p \cap \Omega_{far}$ as $\mathbf{u}_{eff} = (P/B, 0)$. At any point $(x, \hat{y}) \in \Omega_p \cap \Omega_{far}$, $\mathbf{u}(x, \hat{y}) = (u(\hat{y}), 0)$ tends to $\mathbf{u}_{eff}(x, \hat{y})$ when $\varepsilon \to 0$ quicker than $\mathbf{u}_{eff}(x, \hat{y})$ tends to $\mathbf{0}$.

Later we will see that the effective velocity corresponds to the Darcy's velocity, and it differs from $u(y)$ – velocity from the Brinkman equation mostly near the interface $y = 0$, and near the solid wall $y = -l$, where higher order derivatives play an important role. If we choose an interval (y_1, y_2), $(-l < y_1 \le y_2 < 0)$, strictly in $(-l, 0)$ in order to restrict our considerations to the internal part of the porous media only, then

$$\|u(y) - P/B\|^2_{L^2(y_1,y_2)} = \tilde{C}_1^2 \frac{e^{-2\lambda y_1} - e^{-2\lambda y_2}}{2\lambda} + \tilde{C}_2^2 \frac{e^{2\lambda y_2} - e^{2\lambda y_1}}{2\lambda} + 2\tilde{C}_1\tilde{C}_2(y_2 - y_1) = o(\varepsilon^n),$$

for each $n \in \mathbb{N}$. This follows from the fact, that for any fixed $\hat{y}$, $-l < \hat{y} < 0$, it holds:

$$e^{2\lambda\hat{y}} = o(\varepsilon^n), \qquad \frac{e^{-2\lambda\hat{y}}}{E_-^2} = o(\varepsilon^n).$$

When accounting for boundary points, $y = 0$ and $y = -l$, the estimation becomes worse:

$$\int_{-l}^0 \tilde{C}_1^2 e^{-2\lambda y}\, dy = \left(\frac{P + o(\varepsilon^n)}{BE_-}\right)^2 \frac{e_+^2 - 1}{2\lambda} = \frac{P^2}{2\lambda B^2} + o(\varepsilon^n) = O(\varepsilon^5), \qquad (2.31)$$

$$\int_{-l}^0 \tilde{C}_2^2 e^{2\lambda y}\, dy = (C_2 - \frac{P}{B} + o(\varepsilon^n))^2 \frac{1 - e_-^2}{2\lambda} = \frac{C_2^2}{2\lambda} + \frac{P^2}{2\lambda B^2} - \frac{C_2 P}{\lambda B} + o(\varepsilon^n) = O(\varepsilon^3), \qquad (2.32)$$

$$\|u(y) - P/B\|^2_{L^2(-l,0)} = O(\varepsilon^3)$$

$\|u(y) - P/B\|_{L^2(-l,0)}$ is not smaller than $O(\varepsilon^{3/2})$ since the largest term is $C_2^2/(2\lambda) \sim \varepsilon^3$. But $\|P/B\|_{L^2(-l,0)}$ is $O(\varepsilon^2)$ itself.

Now, let us seek for the effective pressure field in $\Omega_p \cap \Omega_{far}$. Of course, $p(x, y)$ from (2.13),(2.14) has a jump at $y = 0$ equal to $M_{21}u(0)$. The last integral in (2.14), being a smooth function in $(-l, 0)$, changes quickly in a negative neighbourhood of $y = 0$, so that there can be some kind of additional jump in the effective pressure. The integral can be explicitly calculated:

$$\int_y^0 u(\xi)\, d\xi = -\frac{P}{B}y - \frac{\tilde{C}_1}{\lambda}(1 - e^{-\lambda y}) + \frac{\tilde{C}_2}{\lambda}(1 - e^{\lambda y}), \quad y \in (-l, 0) \qquad (2.33)$$

To catch the additional jump, let us fix some $\hat{y}$, $-l < \hat{y} < 0$, and estimate $p(x, \hat{y})$ again with respect to the small parameter ε.

$$\int_{\hat{y}}^{0} u(\xi)\, d\xi = -\frac{P}{B}\hat{y} + \frac{C_2 + O(\varepsilon^2)}{\lambda} = -\frac{P}{B}\hat{y} + \frac{C_2}{\lambda} + O(\varepsilon^3)$$

$$p(x, \hat{y}) = p^0 - Px + M_{21}u(0) - \mu\kappa_{21}\frac{P}{B}\hat{y} + \mu\kappa_{21}\frac{C_2}{\lambda} + O(\varepsilon) \qquad (2.34)$$

According to (2.34), we can define an effective pressure field in the porous media as

$$p_{eff}(x, y) = p^0 - Px + M_{21}u(0) - \frac{\kappa_{21}}{\kappa_{11}}Py + \mu\kappa_{21}\frac{C_2}{\lambda}. \qquad (2.35)$$

The effective pressure field at any point $(x, \hat{y}) \in \Omega_p \cap \Omega_{far}$, is a limit of the $p(x, \hat{y})$ when $\varepsilon \to 0$. We note that $u(0) = C_2$. The pair $(\mathbf{u}_{eff}, p_{eff})$ satisfy the Darcy law:

$$\mu \mathbf{K}^{-1}\mathbf{u}_{eff} = \mu \begin{bmatrix} \kappa_{11} & \kappa_{12} \\ \kappa_{21} & \kappa_{22} \end{bmatrix} \begin{bmatrix} P/B \\ 0 \end{bmatrix} = \begin{bmatrix} P \\ \kappa_{21}P/\kappa_{11} \end{bmatrix} = -\nabla p_{eff}$$

The jump at $y = 0$, between the pressure in the free fluid (2.13) and the effective pressure in the porous media (2.35), is given by

$$p(x, 0+0) - p_{eff}(x, 0-0) = -M_{21}u(0) - \mu\kappa_{21}\frac{C_2}{\lambda} = -\left(M_{21} + \mu\frac{\kappa_{21}}{\lambda}\right)u(0+0)$$

since $C_2 = u(0) = u(0+0)$. If we use (2.29), then

$$p(x, 0+0) - p_{eff}(x, 0-0) = -\left(M_{21} + \mu\frac{\kappa_{21}}{\lambda}\right)\alpha\frac{\partial u}{\partial y}(0+0) + O(\varepsilon).$$

A comparison with (1.26) suggests that we have to choose

$$M_{21} := \mu\left(\frac{C_\omega^{bl}}{\alpha} - \frac{\kappa_{21}}{\lambda}\right) = -\mu\left(\frac{C_\omega^{bl}}{\varepsilon C_1^{bl}} + \frac{\kappa_{21}}{\lambda}\right) = O(\varepsilon^{-1}), \qquad (2.36)$$

if we want to have a similar pressure jump condition.

Now, recall, that in order to make expressions shorter we included μ into $\mathbf{M}$: $\mathbf{M} = \mu\overline{\mathcal{M}}$, where $\overline{\mathcal{M}}$ was originally used by J.A.Ochoa-Tapia and S. Whitaker in [44]; $\mathcal{M}$ we used as a dimensionless coefficient in the Section 1.4.1. The order of magnitude of $\overline{\mathcal{M}}$ was estimated as $O(K^{-1/2})$ (K is a scalar permeability). Putting (2.22), (2.36) together we obtain

$$\overline{\mathcal{M}} = \frac{1}{\mu}\begin{bmatrix} M_{11} & M_{12} \\ M_{21} & M_{22} \end{bmatrix} = \begin{bmatrix} \frac{1}{\alpha} - \frac{\kappa_{11}}{\lambda} & \cdot \\ \frac{C_\omega^{bl}}{\alpha} - \frac{\kappa_{21}}{\lambda} & \cdot \end{bmatrix} = \varepsilon^{-1}\begin{bmatrix} -\frac{1}{C_1^{bl}} - \sqrt{\frac{\mu_{eff}}{\mu\varkappa_{11}}}\varkappa_{11} & \cdot \\ -\frac{C_\omega^{bl}}{C_1^{bl}} - \sqrt{\frac{\mu_{eff}}{\mu\varkappa_{11}}}\varkappa_{21} & \cdot \end{bmatrix} = \varepsilon^{-1}\mathcal{M} \quad (2.37)$$

Two other elements, $\mathcal{M}_{12}$ and $\mathcal{M}_{22}$, play no role for the particular flow we are considering, and we leave them unknown or just give them zero values.

Let us estimate the difference between $p(x, y)$ from (2.14), and the effective pressure from (2.35) in L^2 norm:

$$\int_{-l}^{0} |p(x, y) - p_{eff}(x, y)|^2\, dy = \int_{-l}^{0}\left|\mu\kappa_{21}\int_{y}^{0} u(\xi)\, d\xi + \frac{\kappa_{21}}{\kappa_{11}}Py - \mu\kappa_{21}\frac{C_2}{\lambda}\right|^2 dy.$$

The internal integral was calculated in (2.33), so we obtain:

$$\int_{-l}^{0} |p(x,y) - p_{eff}(x,y)|^2 \, dy = \left(\frac{\mu\kappa_{21}}{\lambda}\right)^2 \int_{-l}^{0} [\tilde{C}_1 e^{-\lambda y} - \tilde{C}_2 e^{\lambda y} + \underbrace{(-\tilde{C}_1 + \tilde{C}_2 - C_2)}_{g(\varepsilon)}]^2 \, dy =$$

$$= \left(\frac{\mu\kappa_{21}}{\lambda}\right)^2 \int_{-l}^{0} \left(\tilde{C}_1^2 e^{-2\lambda y} + \tilde{C}_2^2 e^{2\lambda y} + g^2(\varepsilon) - 2\tilde{C}_1\tilde{C}_2 + 2g(\varepsilon)[\tilde{C}_1 e^{-\lambda y} - \tilde{C}_2 e^{\lambda y}]\right) \, dy$$

For the first two terms see (2.31) and (2.32). They are $O(\varepsilon^5)$ and $O(\varepsilon^3)$, respectively. The third, fifth and sixth terms need estimation for the function $g(\varepsilon)$, which doesn't depend on y:

$$g(\varepsilon) = -\frac{P}{B} + o(\varepsilon^n) = O(\varepsilon^2), \qquad g^2(\varepsilon) = O(\varepsilon^4).$$

$\tilde{C}_1$, $\tilde{C}_2$ were estimated in (2.30).

$$\int_{-l}^{0} (g^2(\varepsilon) - 2\tilde{C}_1\tilde{C}_2) \, dy = g^2(\varepsilon)l + o(\varepsilon^n) = O(\varepsilon^4)$$

The following two terms are multiplied by $2g(\varepsilon) = O(\varepsilon^2)$

$$\int_{-l}^{0} \tilde{C}_1 e^{-\lambda y} \, dy = \frac{P + o(\varepsilon^n)}{BE_-} \frac{e_+ - 1}{\lambda} = \frac{P}{\lambda B} + o(\varepsilon^n) = O(\varepsilon^3),$$

$$\int_{-l}^{0} \tilde{C}_2 e^{\lambda y} \, dy = (C_2 - \frac{P}{B} + o(\varepsilon^n))\frac{1 - e_-}{\lambda} = \frac{C_2}{\lambda} - \frac{P}{\lambda B} + o(\varepsilon^n) = O(\varepsilon^2).$$

The largest term again is $C_2^2/(2\lambda) \sim \varepsilon^3$ from (2.32). There is no other term it could cancel with. We return to our L^2 estimate for the pressure difference:

$$\|p - p_{eff}\|_{L^2(-l,0)}^2 = \left(\frac{\mu\kappa_{21}}{\lambda}\right)^2 O(\varepsilon^3) = O(\varepsilon) \quad \text{or} \quad \|p - p_{eff}\|_{L^2(-l,0)} = O(\sqrt{\varepsilon}).$$

We can summarize results in this section in the

Proposition 2 *If we consider a flow in a 2D channel Ω, governed by Stokes system (1.2) (or Navier-Stokes system (1.1)) in Ω_f, by Brinkman system (1.6) (or Brinkman system with convective term (1.18)) in Ω_p; completed with the interface conditions (1.29), (1.34), such that in the region Ω_{far} (described at the beginning of the section) $\mathbf{M}$ is a constant parameter along the interface, and the solution is fully developed in the sense that $\frac{\partial u}{\partial y}(x,y) = 0$ in Ω_{far}, then*

1. *if $M_{11} \neq -\mu/h - \mu_{eff}\lambda E_+/E_-$, then the solution $(\mathbf{u}, p)$ in Ω_{far}, $\mathbf{u} = (u(y), 0)$ is given by (2.15), (2.16),(2.13), (2.14) with constants defined in (2.24)-(2.26), and the expression for the integral in (2.14) is from (2.33);*

2. *if we consider a sequence of problems with small parameter $\varepsilon > 0$, such that some parameters depend on ε:*

$$\mathbf{K} = \varepsilon^2 \mathcal{K}, \qquad M_{11} = \frac{\mu}{\varepsilon}\left(-\frac{1}{C_1^{bl}} - \sqrt{\frac{\mu_{eff}}{\mu\varkappa_{11}}}\varkappa_{11}\right)$$

where $C_1^{bl} < 0$ is a known constant, then the horizontal component $u(y)$ of the solution satisfies the Beavers-Joseph condition in a Saffman's form:

$$u(0+0) = -\varepsilon C_1^{bl}\frac{\partial u}{\partial y}(0+0) + O(\varepsilon^2).$$

3. *further, there exists an effective velocity-pressure field* $(\mathbf{u}_{eff}, p_{eff})$ *in* $\Omega_p \cap \Omega_{far}$, *given by divergence-free effective velocity,* $\mathbf{u}_{eff} = (P/B, 0)$, *and by the pressure from (2.35), that satisfies the Darcy law:* $\mathbf{u}_{eff} = -\frac{1}{\mu}\mathbf{K}\nabla p_{eff}$ *there, and has a pressure jump on the interface between the free fluid part and the porous medium:*

$$p(x, 0+0) - p_{eff}(x, 0-0) = -\left(M_{21} + \mu\frac{\kappa_{21}}{\lambda}\right)u(0).$$

Further, if

$$M_{21} = \frac{\mu}{\varepsilon}\left(-\frac{C_\omega^{bl}}{C_1^{bl}} - \sqrt{\frac{\mu_{eff}}{\mu\varkappa_{11}}}\varkappa_{21}\right),$$

where C_ω^{bl} *is a known constant, then*

$$p(x, 0+0) - p_{eff}(x, 0-0) = -\mu C_\omega^{bl}\frac{\partial u}{\partial y}(0+0) + O(\varepsilon);$$

4. *the relation between* $(\mathbf{u}, p)$ *and* $(\mathbf{u}_{eff}, p_{eff})$ *is the following: for a given point* $(\hat{x}, \hat{y}) \in \Omega_p \cap \Omega_{far}$, *and for any* $n \in \mathbb{N}$,

$$\mathbf{u}(\hat{x}, \hat{y}) = \mathbf{u}_{eff}(\hat{x}, \hat{y}) + o(\varepsilon^n), \qquad p(\hat{x}, \hat{y}) = p_{eff}(\hat{x}, \hat{y}) + O(\varepsilon).$$

and for arbitrary $x \in (x_{min}, x_{max})$ *we have*

$$\|p(x, \cdot) - p_{eff}(x, \cdot)\|_{L^2(-l,0)} = O(\sqrt{\varepsilon}).$$

Remark 10 *The constants* C_1^{bl}, C_ω^{bl} *are defined in [25] where the solution to the Navier–Stokes–Darcy model was compared with the solution to the microscopical model based on periodic porous media. We should note that the results in [25] were formulated for the constant pressure boundary conditions given on the left and right boundaries of* Ω_{far} *and it is different from the situation we have when the pressure on the left and on the right boundaries depends on* y, *provided* $\kappa_{21} \neq 0$.

2.1.3 Some generalization of the analytical solution in the channel

Let us consider the system of equations (2.7)–(2.12) where the homogeneous Dirichlet conditions (2.7), (2.12) are substituted by the non-homogeneous conditions: $u(-l) = u_{-l}$, $u(h) = u_h$. In the section 3.1 we will use this case to interpolate velocity on the interface. The solution $u(y)$ is given by (2.15), (2.16). The difference is in C_1, C_2, $\tilde{C}_1$, $\tilde{C}_2$:

$$C_2 = \left(\frac{Ph}{2} + \frac{\mu_{eff}\lambda P}{B}\frac{E_+ - 2}{E_-} + \frac{\mu}{h}u_h + 2\frac{\mu_{eff}\lambda}{E_-}u_{-l}\right)\bigg/\left(M_{11} + \mu_{eff}\lambda\frac{E_+}{E_-} + \frac{\mu}{h}\right) \qquad (2.38)$$

$$C_1 = \frac{Ph}{2\mu} - \frac{C_2}{h} + \frac{u_h}{h} \qquad (2.39)$$

$$\tilde{C}_1 = -\frac{(1 - e_-)P/B + C_2 e_- - u_{-l}}{E_-}, \quad \tilde{C}_2 = \frac{(1 - e_+)P/B + C_2 e_+ - u_{-l}}{E_-} \qquad (2.40)$$

The velocity on the interface is C_2 and it depends on the (input) parameters P, u_h, u_{-l} as

$$C_2 = aP + bu_h + cu_{-l}, \qquad a, b, c \text{ are functions of } \mu, \mu_{eff}, l, h, \mathbf{M}, \mathbf{K}. \qquad (2.41)$$

2.2   The stress jump condition and basic properties of M.

From the particular case of the parallel flow in the channel we return to the case of general geometry. The system of equations (1.36) or (1.37) with interface conditions (1.29), (1.34) and appropriate boundary conditions are considered in some fixed orthogonal coordinate system $OX_1 \ldots X_d$. $\mathbf{M}$ is a given $d \times d$ matrix function on Σ. If we consider another orthogonal coordinate system $O'X_1' \ldots X_d'$ according to the transformation: $\mathbf{x}' = \mathbf{x}'(\mathbf{x}) = \mathbf{C}(\mathbf{x} - \mathbf{r}_{OO'})$, $\mathbf{C}^{-1} = \mathbf{C}^T$, $\mathbf{r}_{OO'}$ – coordinates of $\overrightarrow{OO'}$ in $OX_1 \ldots X_d$, then one can calculate values of the tensor fields in the new coordinates using:

$$s'(\mathbf{x}') = s(\mathbf{x}(\mathbf{x}')), \qquad \mathbf{v}'(\mathbf{x}') = \mathbf{C}\mathbf{v}(\mathbf{x}(\mathbf{x}')), \qquad \mathbf{B}'(\mathbf{x}') = \mathbf{C}\mathbf{B}(\mathbf{x}(\mathbf{x}'))\mathbf{C}^T$$

for scalars like p; for vectors like $\mathbf{u}$, $\mathbf{n}$; and for second order tensors like $\nabla\mathbf{u}$, $\nabla\mathbf{u}^T$, $p\mathbf{I}$, $\mathbf{K}$, $\mathbf{T}$, $\bar{\mathbf{T}}$, respectively. If we multiply the interface condition (1.34) by $\mathbf{C}$ from the left side then:

$$[\mathbf{T}]_\Sigma \, \mathbf{n} = \mathbf{M}\mathbf{u} \qquad \Rightarrow \qquad \mathbf{C}[\mathbf{T}]_\Sigma \mathbf{C}^T \mathbf{C}\mathbf{n} = \mathbf{C}\mathbf{M}\mathbf{C}^T\mathbf{C}\mathbf{u} \tag{2.42}$$

since $\mathbf{C}^T\mathbf{C} = \mathbf{I}$. Using values, calculated in the new coordinates, $\mathbf{n}' = \mathbf{C}\mathbf{n}$, $\mathbf{u}' = \mathbf{C}\mathbf{u}$, $\mathbf{T}' = \mathbf{C}\mathbf{T}\mathbf{C}^T$, the equality (2.42) leads to the following interface condition in the new coordinates

$$[\mathbf{T}']_{\Sigma'}\mathbf{n}' = \mathbf{C}\mathbf{M}\mathbf{C}^T\mathbf{u}' \quad = \mathbf{M}'\mathbf{u}'.$$

It has the same form as (1.34), and $\mathbf{M}$ in the old coordinates is related to $\mathbf{M}'$ in the new coordinates by

$$\mathbf{M} = \mathbf{C}^T\mathbf{M}'\mathbf{C}, \qquad \mathbf{M}' = \mathbf{C}\mathbf{M}\mathbf{C}^T. \tag{2.43}$$
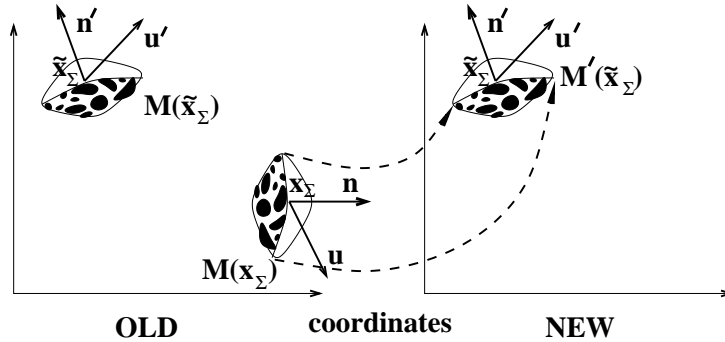

Figure 2.2: Two "equivalent" parts of the boundary.

Now we assume that there are two different points on the interface $\mathbf{x}_\Sigma$ and $\tilde{\mathbf{x}}_\Sigma$, such that (see Fig. 2.2, left) some neighbourhood of one of them can be obtained by rotation, reflection and translation from a neighbourhood of another by the formula

$$\mathbf{x}' = \mathbf{x}'(\mathbf{x}) = \tilde{\mathbf{x}}_\Sigma + \mathbf{C}(\mathbf{x} - \mathbf{x}_\Sigma) = \mathbf{C}\left(\mathbf{x} - (\mathbf{x}_\Sigma - \mathbf{C}^T\tilde{\mathbf{x}}_\Sigma)\right) \tag{2.44}$$

(if $\mathbf{x}$ from the neighbourhood of $\mathbf{x}_\Sigma$ belongs to some of the following sets: Ω_{ps}, Ω_{pf}, Ω_p, Ω_f, Σ then the same happens with the point $\mathbf{x}'(\mathbf{x})$). Although for real porous media such situation is purely hypothetical (something similar may occur but in statistical sense: a possible example is the constant α_{BJ} in the Beavers–Joseph condition) we will often have such situation in the Chapter 4 (see Fig. 4.1, 4.6, 4.13, 4.20).

If we use (2.44) to change coordinates in the whole space, then according to (2.43) we have $\mathbf{M}'(\tilde{\mathbf{x}}_\Sigma) = \mathbf{C}\mathbf{M}(\mathbf{x}_\Sigma)\mathbf{C}^T$. On the other hand, the neighbourhood of $\mathbf{x}_\Sigma$ in new coordinates coincides with the neighbourhood of $\tilde{\mathbf{x}}_\Sigma$ in the old coordinates (see Fig.2.2). We assume that $\mathbf{M}(\mathbf{x})$ is a local characteristic depending only on the microgeometry of the porous medium around the point $\mathbf{x}$ on the interface, and on the position of the interface. Then, one can imagine the same microflows in the neighbourhoods of $\tilde{\mathbf{x}}_\Sigma$ on the left subfigure as well as on the right subfigure of Fig. 2.2 leading to the same macroscopic quantities like $\mathbf{u}$, $\mathbf{T}$ (the coincident neighbourhoods shouldn't be too small). Therefore it seems reasonable to equate $\mathbf{M}(\tilde{\mathbf{x}}_\Sigma)$ with $\mathbf{M}'(\tilde{\mathbf{x}}_\Sigma)$ and consequently in such situations we will use the following relation between $\mathbf{M}(\mathbf{x}_\Sigma)$ and $\mathbf{M}(\tilde{\mathbf{x}}_\Sigma)$: $\mathbf{M}(\tilde{\mathbf{x}}_\Sigma) = \mathbf{C}\mathbf{M}(\mathbf{x}_\Sigma)\mathbf{C}^T$. The interface condition (1.34) has quite
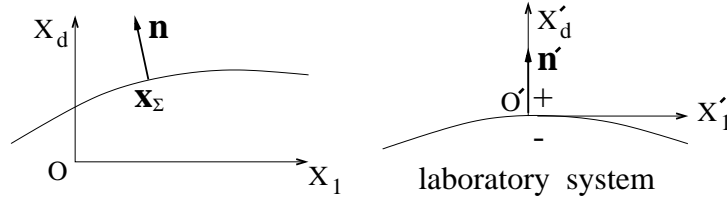

Figure 2.3: Laboratory coordinate system for $\mathbf{x}_\Sigma$.

different form for points on Σ having different normal vectors. That's why it is convenient to consider a "laboratory" system for each point $\mathbf{x}_\Sigma \in \Sigma$ with origin at $\mathbf{x}_\Sigma$ and coordinate axis $(O'X_1', \ldots, O'X_d')$ directed in such a way that one of them coincide with the normal vector (see Fig.2.3). To change coordinates we can use the transformation $\mathbf{x}' = \mathbf{x}'(\mathbf{x}) = \mathbf{C}(\mathbf{x} - \mathbf{x}_\Sigma)$ where $\mathbf{C}$ transforms $\mathbf{n}$ into $\mathbf{n}' = (0, \ldots, 0, 1)$. If we know $\mathbf{M}' = \mathbf{M}_{Lab}$ for the laboratory system then using (2.43) the real $\mathbf{M}$ for the boundary condition at $\mathbf{x}_\Sigma$ can be calculated. We will do this in Chapters 3 and 4. In the laboratory system, or for any interface point where the normal vector is co-directed with OX_d, the interface condition in 2D has a form ($\mathbf{u} = (u, v)^T$):

$$[\mathbf{T}]_\Sigma \mathbf{n} = \begin{bmatrix} \tilde{\mu}\frac{\partial u}{\partial x} - p & \tilde{\mu}\frac{\partial u}{\partial y} \\ \tilde{\mu}\frac{\partial v}{\partial x} & \tilde{\mu}\frac{\partial v}{\partial y} - p \end{bmatrix}_\Sigma \begin{pmatrix} 0 \\ 1 \end{pmatrix} = \begin{bmatrix} \tilde{\mu}\frac{\partial u}{\partial y} \\ \tilde{\mu}\frac{\partial v}{\partial y} - p \end{bmatrix}_\Sigma = \begin{pmatrix} M_{11}u + M_{12}v \\ M_{21}u + M_{22}v \end{pmatrix}$$

Different microstructures may lead to different values of the matrix $\mathbf{M}$. The form

$$
\begin{array}{rcl}
\mu\frac{\partial u}{\partial y}|_{\Sigma_f} - \mu_{eff}\frac{\partial u}{\partial y}|_{\Sigma_p} & = & M_{11}u + M_{12}v \\
\mu\frac{\partial v}{\partial y}|_{\Sigma_f} - \mu_{eff}\frac{\partial v}{\partial y}|_{\Sigma_p} - p|_{\Sigma_f} + p|_{\Sigma_p} & = & M_{21}u + M_{22}v
\end{array}
\tag{2.45}
$$

of the jump interface conditions is more suitable than (1.34) for interpretation and comparison with the Darcy case (Beavers–Joseph, pressure jump conditions).

If some quantity is continuous through a smooth interface (in our case the velocity components u^k are continuous) then derivatives of this quantity in the direction tangential to the interface can also be considered as continuous quantities through the interface. To justify this statement let us consider a point $\mathbf{x}_\Sigma$ on the interface Σ between two subdomains Ω_1 and Ω_2 and a function ϕ continuous at least in some neighbourhood O of $\mathbf{x}_\Sigma$. Here the interface is smooth (belongs to $\mathcal{C}^1$) and can be uniquely projected to the hyperplane which is perpendicular to the normal at $\mathbf{x}_\Sigma$. Additionally, $\nabla\phi$ is continuous up to the interface in each part $O_1 = \Omega_1 \cap O$ and $O_2 = \Omega_2 \cap O$ (see Fig.2.4, left): $\phi \in C(O)$, $\phi \in C^1(\overline{O}_1)$, $\phi \in C^1(\overline{O}_2)$. "Up to the interface" means that $\nabla\phi$ can be defined on the interface as a limit of gradients approaching the interface point from the internal part of either O_1 or O_2. The limits from both sides can be different. $|\nabla\phi|$ in $\overline{O}$ is bounded by $C_{\nabla\phi}$. Our purpose is to show that $\frac{\partial}{\partial \mathbf{t}}\phi = \mathbf{t} \cdot \nabla\phi$ (where $\mathbf{t}$ stands for the
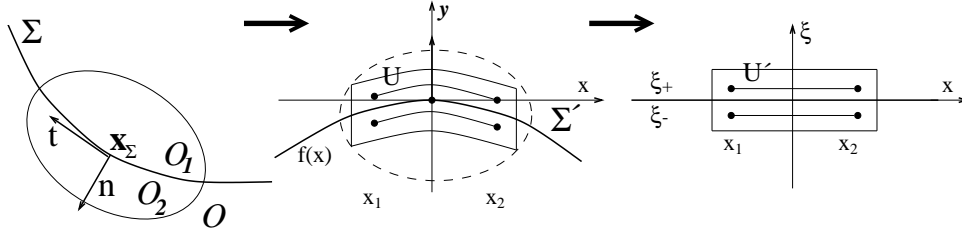
Figure 2.4: Continuity of tangential derivatives

tangential vector) has the same limit from both sides of the interface. To do it, let us assume the opposite: they are not equal and the absolute value of the jump is $C_{jump} > 0$.

First, we can change the coordinate system so that the new origin is at $\mathbf{x}_\Sigma$, $\mathbf{t}$ and $\mathbf{n}$ become $\mathbf{e}_1$ and $\mathbf{e}_d$ correspondingly, and the part of the interface in $\Sigma \cap O$ is described by the points $(x^1, \dots, x^{d-1}, f(x^1, \dots, x^{d-1}))$, e.g. the equation of the surface is $x^d = f(x^1, \dots, x^{d-1})$. Our orthogonal transformation doesn't change the bound for $|\nabla u|$. Without loss of generality we can reduce number of dimensions to 2: $OX \parallel \mathbf{e}_1$, $OY \parallel \mathbf{e}_d$ (see Fig.2.4, middle). The jump at $\mathbf{x}_\Sigma$ in the old coordinates is the same as the jump at $(0,0)$ in the new coordinates:

$$\left| \frac{\partial \phi}{\partial x}(0, 0+0) - \frac{\partial \phi}{\partial x}(0, 0-0) \right| = C_{jump}. \tag{2.46}$$

Due to the continuity of $\frac{\partial \phi}{\partial x}$ in $\overline{O_1}$ and $\overline{O_2}$ separately, there is a neighbourhood

$$U = \left\{ (x,y) \mid \quad x \in (-\delta_x, \delta_x), y \in (f(x) - \delta_y, f(x) + \delta_y) \right\}$$

divided by the interface $\Sigma' = \{(x,y) \in U \mid y = f(x)\}$ into two parts such that for $(x,y) \in U' \backslash \Sigma'$ we have

$$\begin{array}{ll} \text{either} & |\frac{\partial \phi}{\partial x}(x,y) - \frac{\partial \phi}{\partial x}(0, 0-0)| < C_{jump}/4, \quad \text{for } y < f(x) \\ \text{or} & |\frac{\partial \phi}{\partial x}(x,y) - \frac{\partial \phi}{\partial x}(0, 0+0)| < C_{jump}/4, \quad \text{for } y > f(x); \end{array} \tag{2.47}$$

and also for $x \in (-\delta_x, \delta_x)$ we have $|f'(x)| = |f'(x) - f'(0)| < C_{jump}/8C_{\nabla\phi}$ due to continuity of $f'(x)$, $f'(0) = 0$. Let us introduce a rectangular neighbourhood of $\mathbf{0}$

$$U' = \left\{ (x, \xi) \mid \quad (x, \xi + f(x)) \in U \right\} = \left\{ (x, \xi) \mid \quad x \in (-\delta_x, \delta_x), \quad \xi \in (-\delta_y, \delta_y) \right\}$$

(see Fig.2.4, right), and an auxiliary function $\psi(x, \xi)$ defined in U' by

$$\psi(x, \xi) = \phi\Big(x, f(x) + \xi\Big), \qquad \frac{\partial \psi}{\partial x}(x, \xi) = \frac{\partial \phi}{\partial x}\Big(x, f(x) + \xi\Big) + \frac{\partial \phi}{\partial y}\Big(x, f(x) + \xi\Big) f'(x)$$

From the properties of ϕ and smoothness of $f(x)$, we conclude that $\psi \in C^1(U' \backslash \{\xi = 0\})$, $\psi \in C(U')$.

For some points $\xi_+ > 0$, $\xi_- < 0$ which belong to a small neighbourhood of 0, and for some fixed points $x_1 < 0 < x_2$, we can integrate just below and above the interface:

$$\psi(x_2, \xi_+) = \psi(x_1, \xi_+) + \int_{x_1}^{x_2} \frac{\partial \phi}{\partial x}\Big(x, f(x) + \xi_+\Big) + \frac{\partial \phi}{\partial y}\Big(x, f(x) + \xi_+\Big) f'(x)\, dx$$

$$\psi(x_2, \xi_-) = \psi(x_1, \xi_-) + \int_{x_1}^{x_2} \frac{\partial \phi}{\partial x}\Big(x, f(x) + \xi_-\Big) + \frac{\partial \phi}{\partial y}\Big(x, f(x) + \xi_-\Big) f'(x)\, dx.$$

Let us subtract the second equation from the first one and put integrals of $\frac{\partial \phi}{\partial x}$ to the left hand side, other terms to the right hand side and let us take the absolute value from the result:

$$\left| \int_{x_1}^{x_2} \frac{\partial \phi}{\partial x}\left(x, f(x) + \xi_+\right) - \frac{\partial \phi}{\partial x}\left(x, f(x) + \xi_-\right) dx \right| \leq |\psi(x_2, \xi_+) - \psi(x_2, \xi_-)| + \qquad (2.48)$$

$$+ |\psi(x_1, \xi_+) - \psi(x_1, \xi_-)| + \int_{x_1}^{x_2} \left| \frac{\partial \phi}{\partial y}\left(x, f(x) + \xi_+\right) - \frac{\partial \phi}{\partial y}\left(x, f(x) + \xi_-\right) \right| |f'(x)| <$$

$$< 2\frac{C_{jump}}{8}(x_2 - x_1) + 2C_{\nabla\phi}\frac{C_{jump}}{8C_{\nabla\phi}}(x_2 - x_1) = \frac{C_{jump}}{2}(x_2 - x_1)$$

The terms $|\psi(x_2, \xi_+) - \psi(x_2, \xi_-)|$, $|\psi(x_1, \xi_+) - \psi(x_1, \xi_-)|$ can be made arbitrary small, for example, less than $\frac{C_{jump}}{8}(x_2 - x_1)$ for small enough $|\xi_+ - \xi_-|$ due to continuity of ψ through the interface $\xi = 0$. $\frac{\partial \phi}{\partial y}$ in the last integral are not necessarily small, but bounded in U by $C_{\nabla\phi}$. But this term is small enough due to $|f'(x)|$.

Now we estimate the left hand side of (2.48) from below. The integrand has the same sign for all $x \in [x_1, x_2]$ as $\frac{\partial \phi}{\partial x}(0, 0 + 0) - \frac{\partial \phi}{\partial x}(0, 0 - 0)$ due to (2.46), (2.47) leading to

$$\left| \int_{x_1}^{x_2} \frac{\partial \phi}{\partial x}\left(x, f(x) + \xi_+\right) - \frac{\partial \phi}{\partial x}\left(x, f(x) + \xi_-\right) dx \right| = \int_{x_1}^{x_2} \left| \frac{\partial \phi}{\partial x}\left(x, f(x) + \xi_+\right) - \frac{\partial \phi}{\partial x}\left(x, f(x) + \xi_-\right) \right| dx$$

The absolute value in the last integral is greater than $C_{jump}/2$ due to (2.46), (2.47). Hence, the whole integral is greater than $\frac{C_{jump}}{2}(x_2 - x_1)$. Here we have a contradiction with the estimation of the left hand side of (2.48) from above. We can summarize the above results in

Proposition 3 *Let O be a neighbourhood of some point $\mathbf{x}_\Sigma$ at the interface Σ which divides O into open sets O_1 and O_2. Let the interface $\Sigma \cap O$ be C^1 smooth, $\mathbf{n}$ be a normal vector to the interface at $\mathbf{x}_\Sigma$. Let the function ϕ, defined at least in O, belong to $C(O)$, $C^1(\overline{O}_1)$, $C^1(\overline{O}_2)$. Then, for any tangential vector $\mathbf{t}$ which is perpendicular to $\mathbf{n}$, the derivative of ϕ in the direction of $\mathbf{t}$ is continuous through the interface (In general $\nabla\phi$ can be discontinuous through Σ):*

$$\lim_{\substack{\mathbf{x} \to \mathbf{x}_\Sigma \\ \mathbf{x} \in O_1}} \frac{\partial \phi}{\partial \mathbf{t}} = \lim_{\substack{\mathbf{x} \to \mathbf{x}_\Sigma \\ \mathbf{x} \in O_2}} \frac{\partial \phi}{\partial \mathbf{t}}, \qquad \frac{\partial \phi}{\partial \mathbf{t}} = \mathbf{t} \cdot \nabla\phi.$$

We also use the continuity of tangential derivatives in the section 3.1.3 to derive a numerical scheme.

Now we can return to the interface conditions in a laboratory system (2.45). Due to incompressibility condition and continuity of the derivatives in the direction parallel to the interface, we have:

$$\left.\frac{\partial v}{\partial y}\right|_{\Sigma_f} = -\left.\frac{\partial u}{\partial x}\right|_{\Sigma_f}, \qquad \left.\frac{\partial v}{\partial y}\right|_{\Sigma_p} = -\left.\frac{\partial u}{\partial x}\right|_{\Sigma_p}, \qquad \left.\frac{\partial u}{\partial x}\right|_{\Sigma_f} = \left.\frac{\partial u}{\partial x}\right|_{\Sigma_p}.$$

If $\mu_{eff} = \mu$, then the second condition from (2.45), can be rewritten as

$$-[p]_\Sigma = M_{21}u + M_{22}v$$

In 3D laboratory system we have a similar interface conditions as (2.45) ($\mathbf{n} = (0, 0, 1)^T$):

$$\begin{array}{rcl} \mu\frac{\partial u}{\partial z}|_{\Sigma_f} - \mu_{eff}\frac{\partial u}{\partial z}|_{\Sigma_p} & = & M_{11}u + M_{12}v + M_{13}w \\ \mu\frac{\partial v}{\partial z}|_{\Sigma_f} - \mu_{eff}\frac{\partial v}{\partial z}|_{\Sigma_p} & = & M_{21}u + M_{22}v + M_{23}w \\ \mu\frac{\partial w}{\partial z}|_{\Sigma_f} - \mu_{eff}\frac{\partial w}{\partial z}|_{\Sigma_p} - p|_{\Sigma_f} + p|_{\Sigma_p} & = & M_{31}u + M_{32}v + M_{33}w \end{array} \qquad (2.49)$$

Like in 2D case, $\mu_{eff} = \mu$ implies

$$\left[\frac{\partial w}{\partial z}\right]_\Sigma = -\left[\frac{\partial u}{\partial x} + \frac{\partial v}{\partial y}\right]_\Sigma = 0$$

and the last condition is

$$-[p]_\Sigma = M_{31}u + M_{32}v + M_{33}w$$

Remark 11 *As it was already mentioned in Section 1.3.2, in general, $\mathbf{T} \neq \bar{\mathbf{T}}$, and if we use (1.35) instead of (1.34), then the stress jump interface conditions would have a form:*

$$(2D): \quad \begin{array}{rcl} \mu\frac{\partial u}{\partial y}|_{\Sigma_f} - \mu_{eff}\frac{\partial u}{\partial y}|_{\Sigma_p} + \mu\frac{\partial v}{\partial x}|_{\Sigma_f} - \mu_{eff}\frac{\partial v}{\partial x}|_{\Sigma_p} & = & M_{11}u + M_{12}v \\ 2\mu\frac{\partial v}{\partial y}|_{\Sigma_f} - 2\mu_{eff}\frac{\partial v}{\partial y}|_{\Sigma_p} - p|_{\Sigma_f} + p|_{\Sigma_p} & = & M_{21}u + M_{22}v \end{array}$$

$$(3D): \quad \begin{array}{rcl} \mu\frac{\partial u}{\partial z}|_{\Sigma_f} - \mu_{eff}\frac{\partial u}{\partial z}|_{\Sigma_p} + \mu\frac{\partial w}{\partial x}|_{\Sigma_f} - \mu_{eff}\frac{\partial w}{\partial x}|_{\Sigma_p} & = & M_{11}u + M_{12}v + M_{13}w \\ \mu\frac{\partial v}{\partial z}|_{\Sigma_f} - \mu_{eff}\frac{\partial v}{\partial z}|_{\Sigma_p} + \mu\frac{\partial w}{\partial y}|_{\Sigma_f} - \mu_{eff}\frac{\partial w}{\partial y}|_{\Sigma_p} & = & M_{21}u + M_{22}v + M_{23}w \\ 2\mu\frac{\partial w}{\partial z}|_{\Sigma_f} - 2\mu_{eff}\frac{\partial w}{\partial z}|_{\Sigma_p} - p|_{\Sigma_f} + p|_{\Sigma_p} & = & M_{31}u + M_{32}v + M_{33}w \end{array}$$

However, if $\mu_{eff} = \mu$, $\mathbf{u}$ satisfies (1.29) and the incompressibility condition $\nabla \cdot \mathbf{u} = 0$ then the conditions in (2D), and (3D) in the "laboratory system"

$$(2D): \quad \begin{array}{rcl} \mu[\frac{\partial u}{\partial y}]_\Sigma & = & M_{11}u + M_{12}v \\ -[p]_\Sigma & = & M_{21}u + M_{22}v \end{array}, \quad (3D): \quad \begin{array}{rcl} \mu[\frac{\partial u}{\partial z}]_\Sigma & = & M_{11}u + M_{12}v + M_{13}w \\ \mu[\frac{\partial v}{\partial z}]_\Sigma & = & M_{21}u + M_{22}v + M_{23}w \\ -[p]_\Sigma & = & M_{31}u + M_{32}v + M_{33}w \end{array}$$

are the same for both (1.34), (1.35). If $[\mathbf{T}]_\Sigma\mathbf{n} = [\bar{\mathbf{T}}]_\Sigma\mathbf{n}$ in some coordinate system then we can multiply the equality by $\mathbf{C}$ from the left side to conclude that in the other orthogonal coordinates $[\mathbf{T}']_{\Sigma'}\mathbf{n}' = [\bar{\mathbf{T}}']_{\Sigma'}\mathbf{n}'$ is also satisfied.

2.3   Generalized solution

When a mathematical model is chosen, one of the most important questions is its solvability. Investigating this question is the main purpose of the current section.

2.3.1   The variational formulation

Let

$$\mathcal{I}_p : L^2(\Omega) \to L^2(\Omega_p), \qquad \mathcal{I}_f : L^2(\Omega) \to L^2(\Omega_f)$$

be natural embeddings. Assume, that there is a solution $(\mathbf{u}, p)$ which satisfies in a classical sense (1.2) in Ω_f, (1.37) in Ω_p, interface conditions (1.29) and (1.34) on Σ, and some Dirichlet boundary conditions on $\partial\Omega$, Suppose, the following smoothness assumptions hold for the solution:

$$\mathcal{I}_p\mathbf{u} \in C^2(\overline{\Omega_p}), \quad \mathcal{I}_f\mathbf{u} \in C^2(\overline{\Omega_f}), \qquad \mathcal{I}_p p \in C^1(\overline{\Omega_p}), \quad \mathcal{I}_f p \in C^1(\overline{\Omega_f}). \qquad (2.50)$$

For the coefficients, right hand side, and the known velocity on $\partial\Omega$ suppose:

$$\mu_{eff} \in C^1(\overline{\Omega_p}), \mathbf{K}^{-1} \in [C(\overline{\Omega_p})]^{d\times d}, \mathbf{M} \in [C(\Sigma)]^{d\times d}, \mathbf{f} \in [C(\overline{\Omega})]^d, \mathbf{u}_{\partial\Omega} \in [C(\partial\Omega)]^d. \qquad (2.51)$$

The equations (1.2), (1.37) are of Stokes type ((1.2) is exactly Stokes). To derive the variational formulation for the coupled problem, we can follow, for example, [30],[53],[17]. We consider

systems in Ω_p and Ω_f separately: we multiply the k-th momentum equation by the k-th component of an arbitrary test vector-function $\mathbf{v} \in [C_0^\infty(\Omega)]^d$, integrate either over Ω_p or over Ω_f, and, at the end, take a sum over k from 1 to d.

For the further transformations (namely, integration by parts) we will need some auxiliary equalities based on the Green's formula [57, p.23] (or [41, p.121]). If $\mathcal{E}$ is either Ω_p or Ω_f, with the boundary at least from $\mathcal{C}^{0,1}$ (Lipschitz-continuous) then due to the Green's formula, we have

$$\int_{\mathcal{E}} v^k \frac{\partial}{\partial x^i}\left(\tilde{\mu}\frac{\partial u^k}{\partial x^i}\right) d\mathbf{x} = \int_{\partial\mathcal{E}} v^k \left(\tilde{\mu}\frac{\partial u^k}{\partial x^i}\right) n^i \, d\sigma - \int_{\mathcal{E}} \tilde{\mu}\frac{\partial u^k}{\partial x^i}\frac{\partial v^k}{\partial x^i} \, d\mathbf{x},$$

where $\mathbf{n}$ is the outer normal to $\partial\mathcal{E}$. If we take a sum over $i = 1, \ldots, d$, we obtain:

$$\int_{\mathcal{E}} v^k \nabla \cdot (\tilde{\mu}\nabla u^k) \, d\mathbf{x} = \int_{\partial\mathcal{E}} v^k(\tilde{\mu}\nabla u^k \cdot \mathbf{n}) \, d\sigma - \int_{\mathcal{E}} \tilde{\mu}\nabla v^k \cdot \nabla u^k \, d\mathbf{x},$$

and over $k = 1, \ldots, d$:

$$\sum_k \int_{\mathcal{E}} v^k \nabla \cdot (\tilde{\mu}\nabla u^k) \, d\mathbf{x} = \int_{\partial\mathcal{E}} \mathbf{v}^T (\tilde{\mu}\nabla \mathbf{u}) \, \mathbf{n} \, d\sigma - \int_{\mathcal{E}} \tilde{\mu}\nabla \mathbf{v} : \nabla \mathbf{u} \, d\mathbf{x}.$$

In a similar way, using the Green's formula, we obtain ($\mathbf{I}$ is a unit matrix)

$$\sum_k \int_{\mathcal{E}} v^k \frac{\partial p}{\partial x^k} \, d\mathbf{x} = \sum_k \left[\int_{\partial\mathcal{E}} v^k p n^k \, d\sigma - \int_{\mathcal{E}} p \frac{\partial v^k}{\partial x^k} \, d\mathbf{x}\right] = \int_{\partial\mathcal{E}} \mathbf{v}^T p \mathbf{I} \mathbf{n} \, d\sigma - \int_{\mathcal{E}} p(\nabla \cdot \mathbf{v}) \, d\mathbf{x}.$$

Using the expressions above with either Ω_p or Ω_f instead of $\mathcal{E}$, the results of the "integration by parts" are the following:

• in Ω_p: ($\mathbf{n}_p$ is an outer normal for Ω_p)

$$\int_{\Omega_p} \left(\mu_{eff}\nabla \mathbf{v} : \nabla \mathbf{u} - p(\nabla \cdot \mathbf{v}) + \mu \mathbf{v}^T \mathbf{K}^{-1}\mathbf{u}\right) d\mathbf{x} - \int_{\partial\Omega_p} \mathbf{v}^T \left(\mu_{eff}\nabla \mathbf{u} - p\mathbf{I}\right) \mathbf{n}_p \, d\sigma = \int_{\Omega_p} \mathbf{f} \cdot \mathbf{v} \, d\mathbf{x}$$
$$(2.52)$$

• and in Ω_f: ($\mathbf{n}_f$ is an outer normal for Ω_f)

$$\int_{\Omega_f} (\mu\nabla \mathbf{v} : \nabla \mathbf{u} - p(\nabla \cdot \mathbf{v})) \, d\mathbf{x} - \int_{\partial\Omega_f} \mathbf{v}^T (\mu\nabla \mathbf{u} - p\mathbf{I}) \mathbf{n}_f \, d\sigma = \int_{\Omega_f} \mathbf{f} \cdot \mathbf{v} \, d\mathbf{x}. \qquad (2.53)$$

If we take a sum of (2.52) and (2.53) and use that $\mathbf{v} = \mathbf{0}$ on $\partial\Omega$, $\mathbf{n}_f = -\mathbf{n}_p$ on Σ, the jump condition (1.33) on the interface Σ implies

$$\int_\Sigma \mathbf{v}^T \left[(\mu\nabla \mathbf{u} - p\mathbf{I})|_{\Sigma_f} - (\mu_{eff}\nabla \mathbf{u} - p\mathbf{I})|_{\Sigma_p}\right] \mathbf{n}_p \, d\sigma = \int_\Sigma \mathbf{v}^T[\tilde{\mu}\nabla \mathbf{u} - p\mathbf{I}]_\Sigma \mathbf{n}_p \, d\sigma = \int_\Sigma \mathbf{v}^T \mathbf{M}\mathbf{u} \, d\sigma.$$

Then we obtain:

$$\int_\Omega \tilde{\mu}\nabla \mathbf{v} : \nabla \mathbf{u} \, d\mathbf{x} - \int_\Omega p(\nabla \cdot \mathbf{v}) \, d\mathbf{x} + \int_{\Omega_p} \mu \mathbf{v}^T \mathbf{K}^{-1}\mathbf{u} \, d\mathbf{x} + \int_\Sigma \mathbf{v}^T \mathbf{M}\mathbf{u} \, d\sigma = \int_\Omega \mathbf{f} \cdot \mathbf{v} \, d\mathbf{x} \qquad (2.54)$$

for all $\mathbf{v} \in [C_0^\infty(\Omega)]^d$. After restriction to solenoidal test functions only

$$\mathbf{v} \in \widetilde{V}_0 = \{\mathbf{v} \in [C_0^\infty(\Omega)]^d \mid \nabla \cdot \mathbf{v} = 0\},$$

the pressure term disappears from (2.54):

$$\underbrace{\int_\Omega \tilde{\mu}\nabla\mathbf{v} : \nabla\mathbf{u}\,dx + \int_{\Omega_p} \mu\mathbf{v}^T\mathbf{K}^{-1}\mathbf{u}\,dx + \int_\Sigma \mathbf{v}^T\mathbf{M}\mathbf{u}\,d\sigma}_{a(\mathbf{u},\mathbf{v})} = \int_\Omega \mathbf{f}\cdot\mathbf{v}\,dx \qquad (2.55)$$

The next important question is the choice of appropriate spaces for generalized solutions, which contains our classical solutions. From the interface conditions (1.29) and (1.34) we cannot conclude that the pressure should be continuous through the interface Σ, so we can consider it as a member of $L^2(\Omega)$ (it is also a standard choice of a functional space for the pressure when dealing with the Stokes system).

From (2.50) we can conclude that $\mathcal{I}_p\mathbf{u} \in [H^1(\Omega_p)]^d$, $\mathcal{I}_f\mathbf{u} \in [H^1(\Omega_f)]^d$. The trace operators

$$T_{\partial\Omega_p} : H^1(\Omega_p) \to L^2(\partial\Omega_p), \qquad T_{\partial\Omega_f} : H^1(\Omega_f) \to L^2(\partial\Omega_f)$$

generalizing a concept of boundary values for H^1 functions, are well defined and bounded, provided that $\partial\Omega_p$, $\partial\Omega_f$ are at least $\mathcal{C}^{0,1}$ regular (see e.g. [57, p.22],[41, Sec.2.4],[56]). The trace operators

$$\begin{array}{llll}
(T_{\partial\Omega_p} & \Rightarrow &) & T_{\Sigma_p} : H^1(\Omega_p) \to L^2(\Sigma); \quad T_{\partial\Omega\cap\partial\Omega_p} : H^1(\Omega_p) \to L^2(\partial\Omega \cap \partial\Omega_p); \\
(T_{\partial\Omega_f} & \Rightarrow &) & T_{\Sigma_f} : H^1(\Omega_f) \to L^2(\Sigma); \quad T_{\partial\Omega\cap\partial\Omega_f} : H^1(\Omega_f) \to L^2(\partial\Omega \cap \partial\Omega_f);
\end{array}$$

are the restrictions of $T_{\partial\Omega_p}$, $T_{\partial\Omega_f}$ to Σ, $\partial\Omega \cap \partial\Omega_p$, and $\partial\Omega \cap \partial\Omega_f$, respectively. For our $\mathbf{u}$ which is smooth in $\overline{\Omega_p}$, $\overline{\Omega_f}$, the traces are just usual restrictions to the boundaries. Then, the solution satisfies the condition for traces:

$$T_{\Sigma_p}(\mathcal{I}_p\mathbf{u}) = T_{\Sigma_f}(\mathcal{I}_f\mathbf{u}) \qquad (2.56)$$

due to (1.29), and

$$T_{\partial\Omega\cap\partial\Omega_p}(\mathcal{I}_p\mathbf{u}) = \mathbf{u}_{\partial\Omega\cap\partial\Omega_p} \qquad T_{\partial\Omega\cap\partial\Omega_f}(\mathcal{I}_f\mathbf{u}) = \mathbf{u}_{\partial\Omega\cap\partial\Omega_f}.$$

which follows from the Dirichlet boundary conditions ($\mathbf{u}_{\partial\Omega\cap\partial\Omega_p}$, $\mathbf{u}_{\partial\Omega\cap\partial\Omega_f}$ are restrictions of $\mathbf{u}_{\partial\Omega}$ to $\partial\Omega \cap \partial\Omega_p$ and $\partial\Omega \cap \partial\Omega_f$ respectively).

Let us check that we can consider $\mathbf{u}$ as a member of $[H^1(\Omega)]^d$. First, $\mathbf{u} \in [L^2(\Omega)]^d$. Second, the $L^2(\Omega)$ functions, constructed from classical derivatives in Ω_p and Ω_f:

$$g_i^k = \left\{ \begin{array}{ll} \frac{\partial u^k}{\partial x^i} & \text{in } \Omega_p \\ \frac{\partial u^k}{\partial x^i} & \text{in } \Omega_f \end{array} \right.$$

are candidates for the distributional derivatives $\frac{\partial u^k}{\partial x^i}$ in the whole Ω. In fact, for arbitrary $\phi \in C_0^\infty(\Omega)$, the distributional (generalized, weak) derivative is

$$\left\langle \frac{\partial u^k}{\partial x^i}, \phi \right\rangle = -\int_\Omega u^k \frac{\partial\phi}{\partial x^i}\,d\mathbf{x} = -\sum_{j\in\{f,p\}} \int_{\Omega_j} u^k \frac{\partial\phi}{\partial x^i}\,d\mathbf{x}.$$

Using the Green's formula [57, p. 23], (2.56), and $\mathbf{n}_p = -\mathbf{n}_f$, we obtain

$$\left\langle \frac{\partial u^k}{\partial x^i}, \phi \right\rangle = \sum_{j\in\{f,p\}} \left[\int_{\Omega_j} \frac{\partial u^k}{\partial x^i}\phi\,dx - \int_{\Sigma_j} T_{\Sigma_j}(\mathcal{I}_j u^k)\phi n_j^i\,d\sigma \right] = \sum_{j\in\{f,p\}} \int_{\Omega_j} \frac{\partial u^k}{\partial x^i}\phi\,dx = \int_\Omega g_i^k\phi\,d\mathbf{x},$$

since the boundary integrals cancel each other. So, g_i^k are the distributional derivatives for $\mathbf{u}$, and $\mathbf{u} \in [H^1(\Omega)]^d$. Consequently,

$$\mathbf{u} \in \widehat{V} = \{\mathbf{u} \in [H^1(\Omega)]^d \mid \nabla \cdot \mathbf{u} = 0\}.$$

$a(\mathbf{u}, \mathbf{v})$ from (2.55) can be considered as a bilinear form on $[H^1(\Omega)]^d \times [H_0^1(\Omega)]^d$, where $\nabla \mathbf{u}$, $\nabla \mathbf{v}$ are distributional gradients, the interface term $\mathbf{v}^T \mathbf{M} \mathbf{u}$ is generalized to $(T_\Sigma \mathbf{v})^T \mathbf{M}(T_\Sigma \mathbf{u})$ (due to continuity of the trace for $H^1(\Omega)$ on Σ, we denote $T_\Sigma = T_{\Sigma_p} = T_{\Sigma_f}$). The bilinear form is continuous on $[H^1(\Omega)]^d \times [H_0^1(\Omega)]^d$: for all $\mathbf{u} \in [H^1(\Omega)]^d$, $\mathbf{v} \in [H_0^1(\Omega)]^d$

$$|a(\mathbf{u}, \mathbf{v})| \leq C(\Omega, \Sigma, \tilde{\mu}, \mathbf{K}, \mathbf{M}) \|\mathbf{u}\|_{[H^1(\Omega)]^d} \|\mathbf{v}\|_{[H^1(\Omega)]^d}.$$

The right hand side term from (2.54), (2.55) can be considered as a continuous linear functional on $[H_0^1(\Omega)]^d$:

$$|\int_\Omega \mathbf{f} \cdot \mathbf{v} \, d\mathbf{x}| \leq \|\mathbf{f}\|_{[L^2(\Omega)]^d} \|\mathbf{v}\|_{[H^1(\Omega)]^d}.$$

Therefore, the equality (2.55), being true for the classical solution $\mathbf{u}$, all $\mathbf{v} \in \widetilde{V}_0$, is also true for all $\mathbf{v} \in V_0$, where V_0 is the closure of $\widetilde{V}_0$ in the norm of $[H^1(\Omega)]^d$. In a similar way,

$$|\int_\Omega p(\nabla \cdot \mathbf{v}) \, d\mathbf{x}| \leq d\|p\|_{L^2(\Omega)} \|\mathbf{v}\|_{[H^1(\Omega)]^d}$$

implies that (2.54) is true when $(\mathbf{u}, p)$ is a classical solution not only for all smooth test functions $\mathbf{v} \in [C_0^\infty(\Omega)]^d$, but also for all $\mathbf{v} \in [H_0^1(\Omega)]^d$. From the other side, (2.54) can be used to define a generalized solution.

Definition 1 *Any pair* $(\mathbf{u}, p) \in \widehat{V} \times L^2(\Omega)$ *is called a generalized (weak) solution for our problem, if (2.54) is true for all* $\mathbf{v} \in [H_0^1(\Omega)]^d$, *and* $\mathbf{u}$ *satisfies the Dirichlet boundary conditions:*

$$T_{\partial\Omega \cap \partial\Omega_p}(\mathbf{u}) = \mathbf{u}_{\partial\Omega \cap \partial\Omega_p}, \qquad T_{\partial\Omega \cap \partial\Omega_f}(\mathbf{u}) = \mathbf{u}_{\partial\Omega \cap \partial\Omega_f}. \tag{2.57}$$

At least this gives a more general concept of the solution to our problem. Conditions on the input quantities can be significantly weaker than what is necessary for the classical case (2.51):

$$\tilde{\mu} \in L^\infty(\Omega), \mathbf{K}^{-1} \in [L^\infty(\Omega_p)]^{d \times d}, \mathbf{M} \in [L^\infty(\Sigma)]^{d \times d}, \mathbf{f} \in [H^{-1}(\Omega)]^d, \mathbf{u}_{\partial\Omega} \in [H^{1/2}(\partial\Omega)]^d.$$

Let us try to simplify the previous definition. First, the pressure can be taken out from the consideration: a vector function $\mathbf{u} \in \widehat{V}$, which satisfies the boundary conditions (2.57), and

$$a(\mathbf{u}, \mathbf{v}) = \langle \mathbf{f}, \mathbf{v} \rangle \qquad \forall \mathbf{v} \in V_0,$$

is a velocity from the generalized solution $(\mathbf{u}, p)$. The pressure field $p \in L^2(\Omega)$ exists due to the result related to the De Rahm's theorem (see [53, p.15,p.19],[17, p.186]): the functional $\mathbf{g}_p \in [H^{-1}(\Omega)]^d$

$$\langle \mathbf{g}_p, \mathbf{v} \rangle = \langle \mathbf{f}, \mathbf{v} \rangle - a(\mathbf{u}, \mathbf{v}), \qquad \forall \mathbf{v} \in [H_0^1(\Omega)]^d,$$

such that $\langle \mathbf{g}_p, \mathbf{v} \rangle = 0$ for all $\mathbf{v} \in V_0$, can be represented through the function $p \in L^2(\Omega)$ (unique up to a constant), as

$$\langle \mathbf{g}_p, \mathbf{v} \rangle = \langle \nabla p, \mathbf{v} \rangle = -\int_\Omega p(\nabla \cdot \mathbf{v}) \, d\mathbf{x},$$

and (2.54) is true for all $\mathbf{v} \in [H_0^1(\Omega)]^d$.

Second, we can substitute the problem for homogeneous Dirichlet boundary conditions for the non-homogeneous one. Vector fields $\mathbf{u} \in \widehat{V}$ satisfy

$$0 = \int_\Omega \nabla \cdot \mathbf{u}\, d\mathbf{x} = \int_{\partial\Omega} T_{\partial\Omega} \mathbf{u} \cdot \mathbf{n}\, d\sigma,$$

where $\mathbf{n}$ is the outer normal to $\partial\Omega$. On the other hand, if the given data $\mathbf{u}_{\partial\Omega} \in [H^{1/2}(\partial\Omega)]^d$ from the Dirichlet boundary condition satisfy the compatibility condition:

$$\int_{\partial\Omega} \mathbf{u}_{\partial\Omega} \cdot \mathbf{n}\, d\sigma = 0, \tag{2.58}$$

then (see [17, p.131],[53, p.31-32]) there exist a vector $\mathbf{u}_D \in \widehat{V}$, such that $T_{\partial\Omega} \mathbf{u}_D = \mathbf{u}_{\partial\Omega}$. We can seek the generalized solution $\mathbf{u}$ in a form $\mathbf{u} = \mathbf{u}_0 + \mathbf{u}_D$, where $\mathbf{u}_0 \in \widehat{V}_0$ is a new unknown,

$$\widehat{V}_0 = \{\mathbf{u} \in [H_0^1(\Omega)]^d \mid \nabla \cdot \mathbf{u} = 0\}.$$

For the Lipschitz domains, we have $V_0 = \widehat{V}_0$ (see [53, p.18, T. 1.6] or discussion in [17, III.4]).

$$a(\mathbf{u}_0, \mathbf{v}) = \langle \mathbf{f}, \mathbf{v}\rangle - a(\mathbf{u}_D, \mathbf{v}), \qquad \forall \mathbf{v} \in V_0, \tag{2.59}$$

where $\langle \mathbf{f}, \mathbf{v}\rangle - a(\mathbf{u}_D, \mathbf{v})$ is a new linear functional on $\mathbf{v} \in V_0$. If we can find $\mathbf{u}_0 \in V_0$ satisfying (2.59), then the generalized solution $(\mathbf{u}, p)$ can be constructed. Is it unique? The vector function $\mathbf{u}_D$ is, for example, not unique. Assume, there are two generalized solutions $\mathbf{u}_1$ and $\mathbf{u}_2$ from $\widehat{V}$, which satisfy the boundary conditions (2.57), and

$$a(\mathbf{u}_1, \mathbf{v}) = \langle \mathbf{f}, \mathbf{v}\rangle, \qquad a(\mathbf{u}_2, \mathbf{v}) = \langle \mathbf{f}, \mathbf{v}\rangle, \qquad \forall \mathbf{v} \in V_0.$$

Then the difference $\mathbf{w} = \mathbf{u}_1 - \mathbf{u}_2 \in V_0$ satisfies

$$a(\mathbf{w}, \mathbf{v}) = 0, \qquad \forall \mathbf{v} \in V_0.$$

Instead of investigating the problem from Def.1, it is sufficient to investigate existence and uniqueness of the problem:

$$\text{Find } \mathbf{u} \in V_0, \text{ such that} \qquad a(\mathbf{u}, \mathbf{v}) = \langle \mathbf{f}, \mathbf{v}\rangle \qquad \forall \mathbf{v} \in V_0, \tag{2.60}$$

where $\mathbf{f} \in [H^{-1}(\Omega)]^d$.

2.3.2   Coercivity of $a(\mathbf{u}, \mathbf{v})$

$$a(\mathbf{u}, \mathbf{v}) = a_c(\mathbf{u}, \mathbf{v}) + \int_\Sigma (T_\Sigma \mathbf{v})^T \mathbf{M}(T_\Sigma \mathbf{u})\, d\sigma, \qquad a_c(\mathbf{u}, \mathbf{v}) = \int_\Omega \tilde{\mu} \nabla \mathbf{v} : \nabla \mathbf{u}\, d\mathbf{x} + \int_{\Omega_p} \mu \mathbf{v}^T \mathbf{K}^{-1} \mathbf{u}\, d\mathbf{x}$$

where $a_c(\mathbf{u}, \mathbf{v})$ is a bilinear form that corresponds to the Stokes-Brinkman system with continuous stress condition $\mathbf{M} \equiv \mathbf{0}$ (see [3]). As it is shown in [3], $a_c(\mathbf{u}, \mathbf{v})$ is V_0–elliptic:

$$a_c(\mathbf{u}, \mathbf{u}) \geq C_1 \|\mathbf{u}\|_{V_0}^2, \qquad \forall \mathbf{v} \in V_0$$

If the function $\mathbf{M}$ is accidently semi-positive definite on the whole interface Σ then $a(\mathbf{u}, \mathbf{v})$ is also elliptic. Hence (2.60) has unique solution for any $\mathbf{f} \in [H^{-1}(\Omega)]^d$. But unfortunately this assumption (which has a physical background for some particular cases) doesn't seem to be realistic for our problem. Similar is the situation with the symmetry of $\mathbf{M}$, and therefore

$a(\mathbf{u}, \mathbf{u})$ is not necessarily symmetric. In general, $a(\mathbf{u}, \mathbf{v})$ is not V_0–elliptic, since we can find $\mathbf{u}_* \in V_0$ such that $T_\Sigma \mathbf{u}_* \neq \mathbf{0}$. Defining

$$m = -a_c(\mathbf{u}_*, \mathbf{u}_*) \Big/ \iint_\Sigma (T_\Sigma \mathbf{u}_*)^2 \, d\sigma \ ,$$

and setting $\mathbf{M} := m\mathbf{I}$, we come to $a(\mathbf{u}_*, \mathbf{u}_*) = 0$. That is, $a(\mathbf{u}, \mathbf{v})$ is not V_0–elliptic.

Now we can check V_0–coercivity of $a(\mathbf{u}, \mathbf{v})$. To do this, we should first define an appropriate Hilbert space H for the Gelfand triple

$$V_0 \hookrightarrow H = H' \hookrightarrow V_0' \tag{2.61}$$

(see for example [20, p.133]) where the injection of V_0 into H is continuous and dense.

To construct H, let us consider the linear space $\widetilde{V}_0$, equipped with the scalar product

$$(\mathbf{u}, \mathbf{v})_H = \int_\Omega \mathbf{u} \cdot \mathbf{v} \, d\mathbf{x} + \int_\Sigma \mathbf{u} \cdot \mathbf{v} \, d\sigma.$$

The scalar product is well defined for smooth vector functions from $\widetilde{V}_0$. Let H be a closure of $\widetilde{V}_0$ with respect to the norm associated with the scalar product: $\|\mathbf{u}\|_H^2 = \|\mathbf{u}\|_{[L^2(\Omega)]^d}^2 + \|\mathbf{u}\|_{[L^2(\Sigma)]^d}^2$.

The norm in V_0 is stronger than the norm in H: for $\mathbf{u} \in \widetilde{V}_0$

$$\|\mathbf{u}\|_H^2 = \|\mathbf{u}\|_{[L^2(\Omega)]^d}^2 + \|T_\Sigma \mathbf{u}\|_{[L^2(\Sigma)]^d}^2 \leq \|\mathbf{u}\|_{[L^2(\Omega)]^d}^2 + C_{T_\Sigma}^2 \|\mathbf{u}\|_{[H_0^1(\Omega)]^d}^2 = (1 + C_{T_\Sigma}^2)\|\mathbf{u}\|_{V_0}^2$$

since the trace operator is continuous on V_0. For each element $\mathbf{u} \in V_0$, there exists a sequence $\mathbf{u}_n$ in $\widetilde{V}_0$ that converges to $\mathbf{u}$ in V_0 norm. And the same sequence is convergent in H to some limit $\mathbf{u}_H \in H$ which can be identified with $\mathbf{u}$ through the embedding operator. V_0 is dense in H since $\widetilde{V}_0$ is dense in both spaces. To ensure that different elements in V_0 correspond to different elements in H, it is enough to show that if $\mathbf{u}_n$ is a Cauchy sequence in $\widetilde{V}_0 \cap V_0$ and $\|\mathbf{u}_n\|_H \to 0$, then $\|\mathbf{u}_n\|_{V_0} \to 0$. First, $\mathbf{u}_n \to \mathbf{u}$ in $[H_0^1(\Omega)]^d$ since V_0 is a subspace of $[H_0^1(\Omega)]^d$. Second, from $\|\mathbf{u}_n\|_H \to 0$ one can conclude that $\|\mathbf{u}_n\|_{[L^2(\Omega)]^d} \to 0$. This means that $\mathbf{u} = \mathbf{0}$ in $[H_0^1(\Omega)]^d$ and $\|\mathbf{u}_n\|_{V_0} = \|\mathbf{u}_n\|_{[H_0^1(\Omega)]^d} \to 0$.

Definition 2 *(see [20, p.141]). Let (2.61) be a Gelfand triple. A bilinear form $a(\cdot, \cdot)$ is said to be V_0-coercive if it is continuous and if there exists $C_1 > 0$ and $C_2 \in \mathbb{R}$ such that*

$$a(\mathbf{u}, \mathbf{u}) + C_2 \|\mathbf{u}\|_H^2 \geq C_1 \|\mathbf{u}\|_{V_0}^2 \qquad \text{for all } \mathbf{u} \in V_0.$$

Let us estimate the integral over Σ in $a(\mathbf{u}, \mathbf{u})$ from above. For a matrix $\mathbf{M}$ and a vector $\mathbf{t}$ we have:

$$|\mathbf{t}^T \mathbf{M} \mathbf{t}| \leq \sum_i \sum_j |M_{ij} t^i t^j| \leq \max_{i,j} |M_{ij}| \sum_i \sum_j \frac{(t^i)^2 + (t^j)^2}{2} \leq d|\mathbf{t}|^2 \max_{i,j} |M_{ij}|.$$

The bilinear form $a(\mathbf{u}, \mathbf{u})$ is V_0–coercive, since there exists a constant $C_2 \geq d \max\limits_{i,j} \|M_{ij}\|_{L^\infty(\Sigma)}$, such that for all $\mathbf{u} \in V_0$

$$a(\mathbf{u}, \mathbf{u}) + C_2 \|\mathbf{u}\|_H^2 = a_c(\mathbf{u}, \mathbf{u}) + \int_\Sigma (T_\Sigma \mathbf{u})^T \mathbf{M}(T_\Sigma \mathbf{u}) \, d\sigma + C_2 \|\mathbf{u}\|_H^2 \geq a_c(\mathbf{u}, \mathbf{u}) \geq C_1 \|\mathbf{u}\|_{V_0}^2.$$

Remark 12 *In [3, p. 1404] the following inequality was used:*

$$\|T_\Sigma \phi\|_{L^2(\Sigma)} \leq C_\Sigma(\Omega)\|\phi\|_{H^1(\Omega)}^{1/2}\|\phi\|_{L^2(\Omega)}^{1/2}, \qquad \forall \phi \in H^1(\Omega).$$

Using this inequality for each component of $\mathbf{u}$*, we estimate the integral over* Σ

$$\left| \int_\Sigma (T_\Sigma \mathbf{u})^T \mathbf{M}(T_\Sigma \mathbf{u})\, d\sigma \right| \leq C_2 \sum_i \|T_\Sigma u^i\|_{L^2(\Sigma)}^2 \leq C_2 C_\Sigma^2 \sum_i \|u^i\|_{H^1(\Omega)}\|u^i\|_{L^2(\Omega)} \leq$$

$$\leq C_2 C_\Sigma^2 \sqrt{\sum_i \|u^i\|_{H^1(\Omega)}^2}\sqrt{\sum_i \|u^i\|_{L^2(\Omega)}^2} = C_2 C_\Sigma^2 \|\mathbf{u}\|_{[H^1(\Omega)]^d}\|\mathbf{u}\|_{[L^2(\Omega)]^d}.$$

From the Cauchy's inequality $ab \leq \frac{\delta}{2}a^2 + \frac{1}{2\delta}b^2$ *(* $\delta > 0$ *), where* $a = \|\mathbf{u}\|_{[H^1(\Omega)]^d}$*,* $b = C_2 C_\Sigma^2 \|\mathbf{u}\|_{[L^2(\Omega)]^d}$*,* $\delta = C_1$*, we obtain*

$$\left| \int_\Sigma (T_\Sigma \mathbf{u})^T \mathbf{M}(T_\Sigma \mathbf{u})\, d\sigma \right| \leq \frac{C_1}{2}\|\mathbf{u}\|_{[H^1(\Omega)]^d}^2 + \frac{C_2^2 C_\Sigma^4(\Omega)}{2C_1}\|\mathbf{u}\|_{[L^2(\Omega)]^d}^2.$$

The coercivity of $a(\mathbf{u}, \mathbf{v})$ *can also be obtained, using the standard space* H*,*
$H = \{$*the closure of* $\tilde{V}_0$ *in* $[L^2(\Omega)]^d\}$ *(see [53, p.248])*

$$a(\mathbf{u}, \mathbf{u}) + \frac{C_2^2 C_\Sigma^4(\Omega)}{2C_1}\|\mathbf{u}\|_{[L^2(\Omega)]^d}^2 \geq \frac{C_1}{2}\|\mathbf{u}\|_{[H^1(\Omega)]^d}^2.$$

For smooth domains Ω_p and Ω_f the trace operator T_Σ is not only continuous, but also compact. But in some important practical situations, the smoothness assumption for both Ω_p and Ω_f is too strong: for example the case when Σ has a non-empty intersection with $\partial\Omega$ (see [3]). Also our numerical method (see Chapter 3) is based on rectangular control volumes, so that Ω^h, Ω_p^h, Ω_f^h has only piecewise smooth boundary. The compactness result for Lipschitz boundaries can be found in [33, p.344] or in [41, p.107].

It means that if we have a bounded sequence $\{\mathbf{u}_n\}$ in V_0 then there exists a subsequence $\{\mathbf{u}_n'\}$ such that $\mathbf{u}_n'$ is a Cauchy sequence in $[L^2(\Omega)]^d$ due to compact embedding of $H^1(\Omega) \hookrightarrow L^2(\Omega)$, and $T_\Sigma \mathbf{u}_n'$ is a Cauchy sequence in $[L^2(\Sigma)]^d$ due to compactness of T_Σ. Hence $\mathbf{u}_n'$ is a Cauchy sequence in H, and the embedding of V_0 to H in (2.61) is compact.

Having a compact embedding in the Gelfand triple (2.61), one can apply results of the Riesz-Schauder theory (see for example [20, p.142] or [56, p.169,266]) for the spectrum of the linear operator $\mathcal{A} : V_0 \to V_0'$ defined as $\langle \mathcal{A}\mathbf{u}, \mathbf{v}\rangle_{V_0' \times V_0} = a(\mathbf{u}, \mathbf{v})$. $\mathcal{I}$ here is the compact embedding operator from V_0 through H to V_0'.

Proposition 4 *The spectrum of* $\mathcal{A}$*:* $Sp(\mathcal{A})$ *consists of at most countably many eigenvalues which cannot accumulate in* $\mathbb{C}$*.*
• *If* $\lambda \in \mathbb{C}$ *is not an eigenvalue then the variational problem:*

$$\text{find } \mathbf{u} \in V_0 \text{ such that} \quad a(\mathbf{u}, \mathbf{v}) - \lambda(\mathbf{u}, \mathbf{v})_H = \langle \mathbf{f}, \mathbf{v}\rangle_{V_0' \times V_0}, \qquad \forall\, \mathbf{v} \in V_0 \qquad (2.62)$$

has unique solution for all $\mathbf{f} \in V_0'$*. (this corresponds to the operator equation* $(\mathcal{A} - \lambda\mathcal{I})\mathbf{u} = \mathbf{f}$*)*
• *If* $\lambda \in \mathbb{C}$ *is an eigenvalue then there exists finite-dimensional eigenspace* $E(\lambda) \neq \{\mathbf{0}\}$ *that for* $\mathbf{u}^* \in E(\lambda)$

$$a(\mathbf{u}^*, \mathbf{v}) = \lambda(\mathbf{u}^*, \mathbf{v})_H, \qquad \forall\, \mathbf{v} \in V_0.$$

In this case the solution of (2.62) exists not for all $\mathbf{f} \in V_0'$*, and when* $\mathbf{u}$ *exists, for some* $\mathbf{f}$*, then it is not unique (* $\mathbf{u} + \mathbf{u}^*$ *is also a solution).*

In connection with (2.60) we are interested only in the question if $0 \in Sp(\mathcal{A})$. In general it is difficult to solve the eigenvalue problem for some given Ω, Ω_p, Ω_f, $\mathbf{K}$, $\mathbf{M}$, $\tilde{\mu}$. The practical meaning of Prop. 4 is given by the following Remark from [20, p.143]: "*The spectrum $Sp(\mathcal{A})$ has measure zero so that the solvability of (2.62) is guaranteed for almost all λ. The problem (2.60) is uniquely solvable if not 'accidentally' $0 \in Sp(\mathcal{A})$*".

There is a quite large class of $\mathbf{M} \in [L^\infty(\Sigma)]^{d \times d}$ (which includes semi-positive definite matrix functions on Σ) that guarantees $0 \notin Sp(\mathcal{A})$. The following question can arise: would it be possible (by using some advanced technique) to show that the case $0 \in Sp(\mathcal{A})$ never occurs for general $\mathbf{M}$? A hint that the answer could be negative comes from the 1D solution of a fully developed flow in the channel presented above for $M_{11} = M_{11}^\emptyset$ (2.27). We cannot use that example since the channel problem is not a common Dirichlet problem that we consider here and the weak formulation is valid for $d > 1$. But we can try to construct a 2D Dirichlet problem which leads to ODE in polar coordinates and for some $\mathbf{M}$ has some problems with the solution. From the Prop.4 we need to investigate the uniqueness of the homogeneous solution to conclude if $0 \in Sp(\mathcal{A})$, or not. This is done in the next subsection.

2.3.3 Example of non-unique solution for some M

Let us consider the Stokes–Brinkman system (1.37) in Ω_f and Ω_p, which in the particular case has the form of a ring drawn in Fig.2.5. Consider interface conditions (1.29), (1.34) on the fluid–porous interface Σ, no-slip conditions on the solid core, and some Dirichlet boundary conditions on the outer boundary $\partial\Omega$ (they will be specified later). We consider only the case when μ_{eff} is a constant in Ω_p. Hence, the Stokes–Brinkman system can be written as

$$-\tilde{\mu} \triangle \mathbf{u} + \tilde{B}\mathbf{u} + \nabla p = \mathbf{f}, \qquad \nabla \cdot \mathbf{u} = 0, \qquad \text{in } \Omega_p \cup \Omega_f \qquad (2.63)$$

$$\text{where} \qquad \tilde{\mu} = \begin{cases} \mu & \text{in } \Omega_f \\ \mu_{eff} & \text{in } \Omega_p \end{cases}, \qquad \tilde{B} = \begin{cases} 0 & \text{in } \Omega_f \\ \frac{\mu}{K} & \text{in } \Omega_p \end{cases}.$$

The relation between Cartesian (x, y) and polar (r, θ) coordinates is the following: $x = r \cos\theta$,
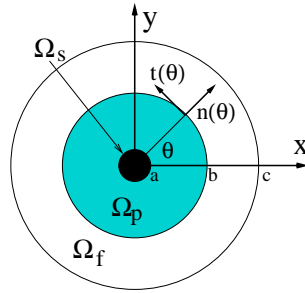

Figure 2.5: Ω_f, Ω_p, Ω_s for the example in polar coordinates

$y = r \sin\theta$; $r = \sqrt{x^2 + y^2}$, $\theta = arctg\frac{y}{x}$. We will often use the vector functions $\mathbf{n}(\theta)$, $\mathbf{t}(\theta)$, $\mathbf{t} \perp \mathbf{n}$ (see Fig. 2.5):

$$\mathbf{n} = \frac{(x, y)^T}{\sqrt{x^2 + y^2}} = \begin{bmatrix} \cos\theta \\ \sin\theta \end{bmatrix}, \qquad \mathbf{t} = \frac{(-y, x)^T}{\sqrt{x^2 + y^2}} = \begin{bmatrix} -\sin\theta \\ \cos\theta \end{bmatrix}, \qquad \frac{\partial\mathbf{n}}{\partial\theta} = \mathbf{t}, \quad \frac{\partial\mathbf{t}}{\partial\theta} = -\mathbf{n}.$$

Let us look for the solution in a form (we are interested in "1D" solution that comes from ODE since in this case it can be easily investigated): $\mathbf{u}(r, \theta) = \mathbf{t}(\theta)\xi(r)$, $p(r, \theta) = p(r)$. This form

guarantees that $\nabla \cdot \mathbf{u} = 0$:

$$\nabla \cdot \mathbf{u} = \mathbf{n}^T \frac{\partial \mathbf{u}}{\partial r} + \frac{1}{r} \mathbf{t}^T \frac{\partial \mathbf{u}}{\partial \theta} = \mathbf{n}^T \mathbf{t} \xi'(r) + \frac{1}{r} \mathbf{t}^T \xi(r)(-\mathbf{n}) = 0$$

For any scalar function $v(r, \theta)$ we have

$$\triangle v(r, \theta) = \frac{1}{r} \frac{\partial}{\partial r} \left(r \frac{\partial v}{\partial r} \right) + \frac{1}{r^2} \frac{\partial^2 v}{\partial \theta^2}, \qquad \nabla v(r, \theta) = \mathbf{n} \frac{\partial v}{\partial r} + \frac{1}{r} \mathbf{t} \frac{\partial v}{\partial \theta}$$

The momentum equation then can be written in polar coordinates as follows:

$$-\tilde{\mu} \left[\mathbf{t}(\theta) \frac{1}{r} \frac{\partial}{\partial r} \left(r \frac{\partial \xi(r)}{\partial r} \right) - \frac{\xi(r)}{r^2} \mathbf{t}(\theta) \right] + \tilde{B} \mathbf{t}(\theta) \xi(r) + \mathbf{n}(\theta) \frac{\partial p(r)}{\partial r} = f(r) \mathbf{t}(\theta) + g(r) \mathbf{n}(\theta) \quad (2.64)$$

We have restricted ourselves to $\mathbf{f}(r, \theta) = f(r) \mathbf{t}(\theta) + g(r) \mathbf{n}(\theta)$. It is a vector equation and we can group terms in it according to vectors $\mathbf{t}$ and $\mathbf{n}$:

$$\mathbf{t}(\theta) \left[-\tilde{\mu} \xi'' - \frac{\tilde{\mu}}{r} \xi' + \left(\frac{\tilde{\mu}}{r^2} + \tilde{B} \right) \xi \right] + \mathbf{n}(\theta) \frac{\partial p(r)}{\partial r} = f(r) \mathbf{t}(\theta) + g(r) \mathbf{n}(\theta)$$

Since $\mathbf{t}(\theta) \perp \mathbf{n}(\theta)$ then we can split (2.64) into

$$\begin{cases} -\tilde{\mu} \left(\xi'' + \frac{\xi'}{r} \right) + \frac{1}{r^2} (\tilde{\mu} + \tilde{B} r^2) \xi = f(r) \\ p'(r) = g(r) \end{cases}$$

From the second equation, the pressure can be calculated by $p(r) = p(b) + \int_b^r g(x)\,dx$. $p(b)$ will have a condition on the interface, and can be specified either in Ω_p, or in Ω_f by an arbitrary constant. For simplicity, let us set $g \equiv 0$. Then $p(r) = p(b) = const$. Further, consider the first equation.

$$r^2 \xi'' + r \xi' - (1 + r^2 \tilde{B} / \tilde{\mu}) \xi = -\frac{f(r) r^2}{\tilde{\mu}}$$

In order to have a solution in a closed analytical form, we choose $K(r) = K_0 r^2$ in Ω_p, so that

$$\text{in } \Omega_p: \quad 1 + \frac{r^2 \tilde{B}}{\tilde{\mu}} = 1 + \frac{r^2 \mu}{\mu_{eff} K(r)} = 1 + \frac{\mu}{\mu_{eff} K_0} = \tilde{\lambda}^2 = const; \qquad \text{in } \Omega_f: \quad 1 + \frac{r^2 \tilde{B}}{\tilde{\mu}} = 1.$$

Then, the second order ODE has the form:

$$r^2 \xi'' + r \xi' - \tilde{\lambda}^2 \xi = \frac{f(r) r^2}{\mu_{eff}}, \quad \text{in } (a, b); \qquad \text{and} \qquad r^2 \xi'' + r \xi' - \xi = \frac{f(r) r^2}{\mu}, \quad \text{in } (b, c). \quad (2.65)$$

The homogeneous equations for (2.65) have two linear independent solutions: $\xi_1^p(r) = r^{\tilde{\lambda}}$, $\xi_2^p(r) = r^{-\tilde{\lambda}}$, in Ω_p; $\xi_1^f(r) = r$, $\xi_2^f(r) = 1/r$ in Ω_f. For our purposes the homogeneous problems are enough, since non-zero solution to homogeneous problem means non-uniqueness. The solution is then the linear combination of ξ_1^p, ξ_2^p in (a, b), and ξ_1^f, ξ_2^f in (b, c). In order to obtain 4 constants needed to determine the solution of the boundary value problem in Ω, one should use interface and boundary conditions.

Interface conditions. First, we need to calculate $\mathbf{T} = \tilde{\mu}\nabla\mathbf{u} - p\mathbf{I}$ in polar coordinates.

$$\nabla\mathbf{u}(r, \theta) = \frac{\partial\mathbf{u}}{\partial r}\mathbf{n}^T + \frac{1}{r}\frac{\partial\mathbf{u}}{\partial\theta}\mathbf{t}^T = \mathbf{t}\xi'\mathbf{n}^T + \frac{\xi}{r}(-\mathbf{n})\mathbf{t}^T$$

Thus, using that $\mathbf{n}^T\mathbf{n} = 1$ and $\mathbf{t}^T\mathbf{n} = 0$, in the left hand side of the stress jump condition (1.34) we have

$$\mathbf{Tn} = \tilde{\mu}\xi'\mathbf{tn}^T\mathbf{n} - \tilde{\mu}\frac{\xi}{r}\mathbf{nt}^T\mathbf{n} - p(r)\mathbf{In} = \tilde{\mu}\xi'(r)\mathbf{t}(\theta) - p(r)\mathbf{n}(\theta). \tag{2.66}$$

Now we consider the right hand side of (1.34). Assume that M is known in a laboratory system (at the point $(x, y) = (0, b)$, where $\mathbf{n} = (0, 1)^T$):

$$\mathbf{M}' = \left[\begin{array}{cc} M'_{11} & M'_{12} \\ M'_{21} & M'_{22} \end{array}\right]$$

Other points on the interface we assume to be similar to the point $(x, y) = (0, b)$ (see Section 2.2). This means that $\mathbf{M}$ is not a constant matrix on the interface, but a function of θ (since the normal vector is not constant). In order to calculate it, we need (see (2.43)) a matrix $\mathbf{C}$ ($\mathbf{C}$ gives a rotation from the current system into the laboratory system. $\mathbf{n}' = \mathbf{Cn}$). $\mathbf{C}$ is the matrix of the counterclockwise rotation on the angle $\frac{\pi}{2} - \theta$. It is given by (to make the notations shorter we will use $c = \cos\theta$, $s = \sin\theta$)

$$\mathbf{C} = \left[\begin{array}{cc} \cos(\frac{\pi}{2} - \theta) & -\sin(\frac{\pi}{2} - \theta) \\ \sin(\frac{\pi}{2} - \theta) & \cos(\frac{\pi}{2} - \theta) \end{array}\right] = \left[\begin{array}{cc} s & -c \\ c & s \end{array}\right], \qquad \mathbf{C}^T = \left[\begin{array}{cc} s & c \\ -c & s \end{array}\right].$$

Now we can calculate $\mathbf{M}(\theta)$, and group terms corresponding to each of M'_{ij}:

$$\mathbf{M}(\theta) = \mathbf{C}^T\mathbf{M}'\mathbf{C} = M'_{11}\left[\begin{array}{cc} s^2 & -sc \\ -sc & c^2 \end{array}\right] + M'_{21}\left[\begin{array}{cc} sc & -c^2 \\ s^2 & -sc \end{array}\right] + M'_{12}\left[\begin{array}{cc} sc & s^2 \\ -c^2 & -sc \end{array}\right] + M'_{22}\left[\begin{array}{cc} c^2 & sc \\ sc & s^2 \end{array}\right].$$

In the stress jump condition (1.34) the right hand side is $\mathbf{Mu}$:

$$\mathbf{M}(\theta)\mathbf{u} = \xi(r)\mathbf{M}(\theta)\left[\begin{array}{c} -s \\ c \end{array}\right] = \xi(r)\left(M_{11}\left[\begin{array}{c} -s^3 - sc^2 \\ s^2c + c^3 \end{array}\right] + M_{21}\left[\begin{array}{c} -s^2c - c^3 \\ -s^3 - sc^2 \end{array}\right]\right).$$

The vectors corresponding to M'_{12}, M'_{22} are identically zero. The identity $s^2 + c^2 = 1$ is used in order to obtain

$$\mathbf{M}(\theta)\mathbf{u} = \xi(r)\left(M'_{11}\left[\begin{array}{c} -s \\ c \end{array}\right] + M'_{21}\left[\begin{array}{c} -c \\ -s \end{array}\right]\right) = \xi(r)\left[M'_{11}\mathbf{t}(\theta) - M'_{21}\mathbf{n}(\theta)\right]. \tag{2.67}$$

Now we can put together (2.66), (2.67) into the interface stress jump conditions (1.34):

$$\left[\tilde{\mu}\xi'(r)\mathbf{t}(\theta) - p(r)\mathbf{n}(\theta)\right]_\Sigma = \xi(b)\left[M'_{11}\mathbf{t}(\theta) - M'_{21}\mathbf{n}(\theta)\right]$$

or, since $\mathbf{n}$, $\mathbf{t}$ don't have jumps on the interface

$$\mathbf{t}(\theta)[\tilde{\mu}\xi'(r)]_\Sigma - \mathbf{n}(\theta)[p(r)]_\Sigma = \mathbf{t}(\theta)M'_{11}\xi(b) - \mathbf{n}(\theta)M'_{21}\xi(b).$$

This vector condition can be splitted with respect to the basis vectors into two conditions from (1.34). The third interface condition comes from (1.29): $[\xi(r)]_\Sigma = 0$ (it is a continuity of the tangential component. The normal component is zero and therefore is also continuous). On the interface we have

$$\quad 1. \quad [\tilde{\mu}\xi'(r)]_\Sigma = M'_{11}\xi(b); \qquad 2. \quad [p(r)]_\Sigma = M'_{21}\xi(b); \qquad 3. \quad [\xi(r)]_\Sigma = 0. \tag{2.68}$$

Now all preliminary work is done and we are ready to formulate the current problem in Ω as ODE: $\xi = \xi(r)$, $p = p(r)$, $r \in [a, c]$ (c is no more notation for $\cos\theta$)

$$r^2\xi''(r) + r\xi'(r) - \tilde{\lambda}^2\xi(r) = 0, \quad r \in (a, b); \qquad r^2\xi''(r) + r\xi'(r) - \xi(r) = 0, \quad r \in (b, c).$$

The general solution in (a, b) (porous part):

$$\xi(r) = \tilde{C}_1 r^{\tilde{\lambda}} + \tilde{C}_2 \frac{1}{r^{\tilde{\lambda}}}, \qquad p(r) = const = \tilde{p};$$

in (b, c) (fluid part):

$$\xi(r) = C_1 r + C_2 \frac{1}{r}, \qquad p(r) = const = p;$$

with the homogeneous boundary conditions:

$$\xi(a) = \tilde{C}_1 a^{\tilde{\lambda}} + \tilde{C}_2 \frac{1}{a^{\tilde{\lambda}}} = 0, \qquad \xi(b) = C_1 c + C_2 \frac{1}{c} = 0;$$

and the interface conditions from (2.68):

$$\mu\xi'(b+0) - \mu_{eff}\xi'(b-0) = M_{11}'\xi(b), \qquad p - \tilde{p} = M_{21}'\xi(b), \qquad \xi(b+0) = \xi(b-0).$$

If we know $\xi(r)$, then the situation with the pressure is clear: we can choose an arbitrary constant $\tilde{p}$ in (porous part) and then the constant pressure in the fluid part is $p = \tilde{p} + M_{21}'\xi(b)$. The boundary and interface conditions determine a system of linear equations with unknowns $\tilde{C}_1$, $\tilde{C}_2$, C_1, C_2:

$$\begin{cases} \mu(C_1 - C_2/b^2) - \mu_{eff}\tilde{\lambda}(\tilde{C}_1 b^{\tilde{\lambda}-1} - \tilde{C}_2/b^{\tilde{\lambda}+1}) = M_{11}'(C_1 b + C_2/b) \\ \tilde{C}_1 b^{\tilde{\lambda}} + \tilde{C}_2/b^{\tilde{\lambda}} = C_1 b + C_2/b \\ \tilde{C}_1 a^{\tilde{\lambda}} + \tilde{C}_2/a^{\tilde{\lambda}} = 0 \\ C_1 c + C_2/c = 0 \end{cases} \qquad (2.69)$$

Of course our ODE has a zero solution $\xi(r) \equiv 0$ when $\tilde{C}_1 = \tilde{C}_2 = C_1 = C_2 = 0$. This corresponds to the 2D problem (2.63) where $\mathbf{f} \equiv \mathbf{0}$, no-slip conditions $\mathbf{u} = \mathbf{0}$ on $\partial\Omega$, $\partial\Omega_s$ and the solution $\mathbf{u} \equiv \mathbf{0}$. Our purpose here is to check if there exists such β that when $\mathbf{M}_{11}' = \beta$ then the system (2.69) has a non-zero solution $\tilde{C}_1$, $\tilde{C}_2$, C_1, C_2 leading to a non-zero solution $\xi(r)$, and to another, non-zero solution $\mathbf{u}$ of (2.63). The linear system (2.69) has a non-zero solution if and only if the determinant of the matrix corresponding to the system (2.69) is zero. In other words we are looking for such β that

$$0 = \begin{vmatrix} -\tilde{\lambda}\mu_{eff}b^{\tilde{\lambda}-1} & \frac{\tilde{\lambda}\mu_{eff}}{b^{\tilde{\lambda}+1}} & \mu - \beta b & -\frac{\mu}{b^2} - \frac{\beta}{b} \\ b^{\tilde{\lambda}} & b^{-\tilde{\lambda}} & -b & -b^{-1} \\ a^{\tilde{\lambda}} & a^{-\tilde{\lambda}} & 0 & 0 \\ 0 & 0 & c & c^{-1} \end{vmatrix} = -c \begin{vmatrix} -\tilde{\lambda}\mu_{eff}b^{\tilde{\lambda}-1} & \frac{\tilde{\lambda}\mu_{eff}}{b^{\tilde{\lambda}+1}} & -\frac{\mu}{b^2} - \frac{\beta}{b} \\ b^{\tilde{\lambda}} & b^{-\tilde{\lambda}} & -b^{-1} \\ a^{\tilde{\lambda}} & a^{-\tilde{\lambda}} & 0 \end{vmatrix} +$$

$$+ \frac{1}{c} \begin{vmatrix} -\tilde{\lambda}\mu_{eff}b^{\tilde{\lambda}-1} & \frac{\tilde{\lambda}\mu_{eff}}{b^{\tilde{\lambda}+1}} & \mu - \beta b \\ b^{\tilde{\lambda}} & b^{-\tilde{\lambda}} & -b \\ a^{\tilde{\lambda}} & a^{-\tilde{\lambda}} & 0 \end{vmatrix} = -c \left[\left(\frac{\mu}{b^2} + \frac{\beta}{b} \right) \left(\frac{a^{\tilde{\lambda}}}{b^{\tilde{\lambda}}} - \frac{b^{\tilde{\lambda}}}{a^{\tilde{\lambda}}} \right) - \frac{\tilde{\lambda}\mu_{eff}}{b^2} \left(\frac{a^{\tilde{\lambda}}}{b^{\tilde{\lambda}}} + \frac{b^{\tilde{\lambda}}}{a^{\tilde{\lambda}}} \right) \right] +$$

$$+ \frac{1}{c} \left[(\mu - \beta b) \left(\frac{b^{\tilde{\lambda}}}{a^{\tilde{\lambda}}} - \frac{a^{\tilde{\lambda}}}{b^{\tilde{\lambda}}} \right) - \tilde{\lambda}\mu_{eff} \left(\frac{b^{\tilde{\lambda}}}{a^{\tilde{\lambda}}} + \frac{a^{\tilde{\lambda}}}{b^{\tilde{\lambda}}} \right) \right].$$

If we put all terms with β to the left hand side and other terms to the right hand side we will get:

$$\beta \frac{b^{2\tilde{\lambda}} - a^{2\tilde{\lambda}}}{a^{\tilde{\lambda}} b^{\tilde{\lambda}}} \left[\frac{c}{b} - \frac{b}{c} \right] = \frac{\mu_{eff} \tilde{\lambda}(b^2 - c^2)(a^{2\tilde{\lambda}} + b^{2\tilde{\lambda}}) + \mu(b^2 + c^2)(a^{2\tilde{\lambda}} - b^{2\tilde{\lambda}})}{a^{\tilde{\lambda}} b^{\tilde{\lambda}+2} c}$$

Due to our geometry $0 < a < b < c$, and this guarantees that $(b^{2\tilde{\lambda}} - a^{2\tilde{\lambda}})/(ab)^{\tilde{\lambda}} > 0$, $c/b - b/c > 0$, and hence β exists:

$$\beta = -\frac{\mu_{eff} \tilde{\lambda}}{b} \frac{b^{2\tilde{\lambda}} + a^{2\tilde{\lambda}}}{b^{2\tilde{\lambda}} - a^{2\tilde{\lambda}}} - \frac{\mu}{b} \frac{c^2 + b^2}{c^2 - b^2} < 0.$$

For M'_{11} equal to β, there is a non-zero ODE solution $\xi(r)$, and consequently one can construct a pair $(\mathbf{u}, p) \in H_0^1(\Omega) \times L^2(\Omega)$: $\mathbf{u}(r, \theta) = \xi(r)\mathbf{t}(\theta) \in H_0^1(\Omega)$, $p(r, \theta) = \tilde{p}$ in Ω_p and $p(r, \theta) = \tilde{p} + M'_{21}\xi(b)$ in Ω_f. The solution is smooth and satisfies in classical sense the homogeneous equation (2.63) in each domain Ω_f, Ω_p, no-slip boundary conditions on $\partial\Omega$ and continuous velocity, stress jump condition on the porous–fluid interface. Therefore it is also a solution in a weak sense and satisfies $a(\mathbf{u}, \mathbf{v}) = 0$. Since $\mathbf{u} \neq \mathbf{0}$ then $\mathbf{u}$ should be an eigenvector corresponding to the eigenvalue $0 \in Sp(\mathcal{A})$.

Chapter 3

Numerical algorithm

In this chapter we describe a numerical algorithm for the model, considered in previous chapters. These are Navier–Stokes and Brinkman equations (1.36), (1.37), together with interface conditions (1.29), (1.33) on the porous-fluid interface, no-slip conditions on the solid walls, and Dirichlet, "Outlet", or "Symmetry" boundary conditions on remaining parts of $\partial \Omega$. The algorithm is based on a finite volume discretization on a non-uniform staggered Cartesian grid. SIMPLE-type method is used for solving the resulting coupled system of algebraic equations. At the end of this chapter we present some tests that were done in order to validate the algorithm and its implementation.

3.1 Finite volume discretization

Consider a bounded domain Ω. We can include it into some parallelepiped, Π, $\Pi = [\pi^1_-, \pi^1_+] \times [\pi^2_-, \pi^2_+] \times [\pi^3_-, \pi^3_+]$ (in 3D). We use a non-uniform Cartesian grid to subdivide Π into rectangular control volumes $P_{i,j,k}$. Denote the centre of $P_{i,j,k}$ by $\mathbf{x}_{i,j,k} = (x_i, y_j, z_k)$, and the lengths by $\mathbf{h}_{i,j,k} = (h_i, l_j, d_k)$:

$$P_{i,j,k} = \left\{ (x, y, z) \in \Pi \mid x \in (x_{i-\frac{1}{2}}, x_{i+\frac{1}{2}}), y \in (y_{j-\frac{1}{2}}, y_{j+\frac{1}{2}}), z \in (z_{k-\frac{1}{2}}, z_{k+\frac{1}{2}}) \right\}$$

where $x_{i\pm\frac{1}{2}} = x_i \pm \frac{h_i}{2}$, $y_{j\pm\frac{1}{2}} = y_j \pm \frac{l_j}{2}$, $z_{k\pm\frac{1}{2}} = z_k \pm \frac{d_k}{2}$.

If $\overline{\Omega_f}$, $\overline{\Omega_p}$, $\overline{\Omega_s}$ cannot be represented by some union of the control volumes $\overline{P_{i,j,k}}$. Then we approximate them by $\overline{\Omega_f^h}$, $\overline{\Omega_p^h}$, $\overline{\Omega_s^h}$ by expanding properties of the central point $\mathbf{x}_{i,j,k}$ to the whole control volume $P_{i,j,k}$. For example, if the centre $\mathbf{x}_{i,j,k}$ is in Ω_f then the whole $P_{i,j,k}$ belongs to Ω_f^h (see Fig.3.1). If a centre of some control volume is outside Ω then we can exclude such control volume from consideration or, alternatively, we can consider it within the framework of the Fictitious Region approach. The control volumes are supposed to contain only one phase: either solid, or fluid, or porous. That is, interfaces between different media appear only between control volumes $P_{i,j,k}$.

Remark 13 *Approximation of the domain with bricks gives $O(h)$ error estimates for Dirichlet and Neumann problems. However, it is not clear if the problem with shifted interfaces approximates the problem with original interface. In the Section 3.3 and Chapter 4 we use only those $\overline{\Omega}$, $\overline{\Omega_p}$, $\overline{\Omega_{pf}}$, $\overline{\Omega_{ps}}$, $\overline{\Omega_f}$, $\overline{\Omega_s}$ for which the interface is resolved by the grid.*

We use the Finite Volume method on staggered grid (see for example [54],[16],[14]). Continuous variables $\mathbf{u} = (u^1, u^2, u^3)$, p which are defined in Ω are substituted by discrete variables
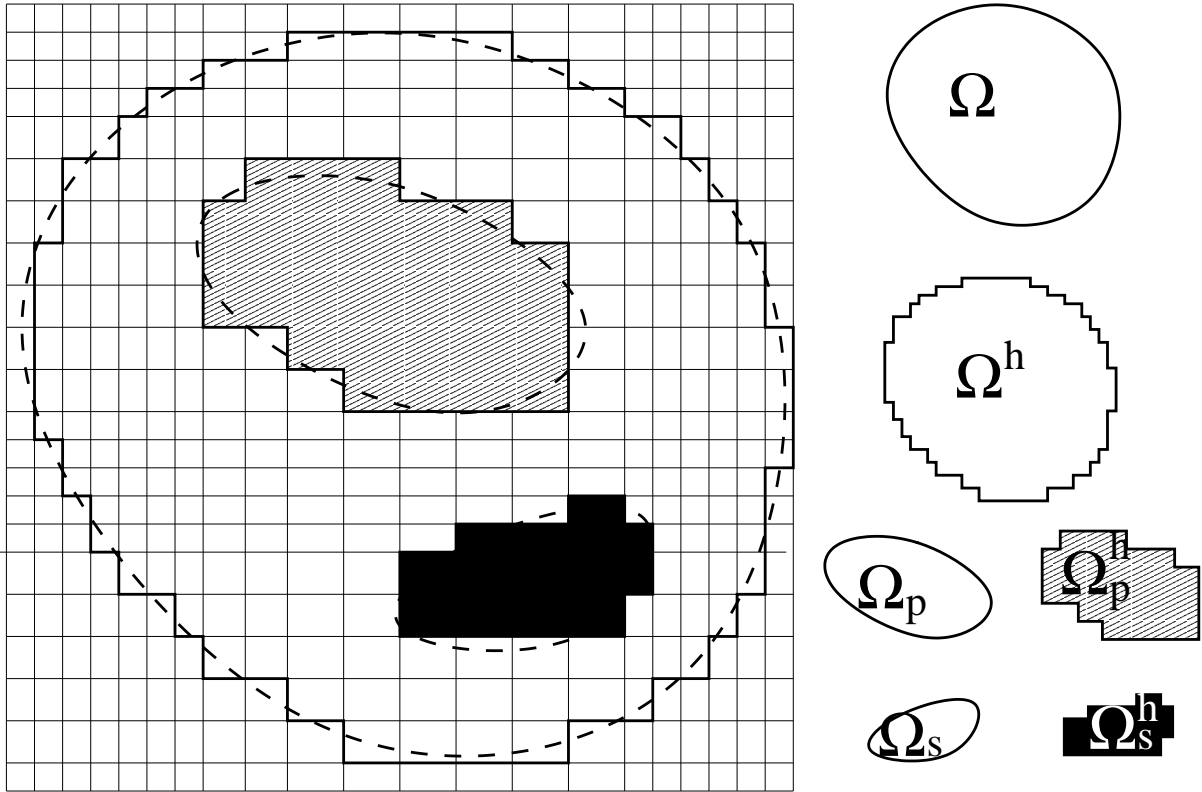
Figure 3.1: Computational domain Π with a non-uniform grid in 2D. Approximation of Ω by Ω^h, Ω_p by Ω_p^h, Ω_s by Ω_s^h.
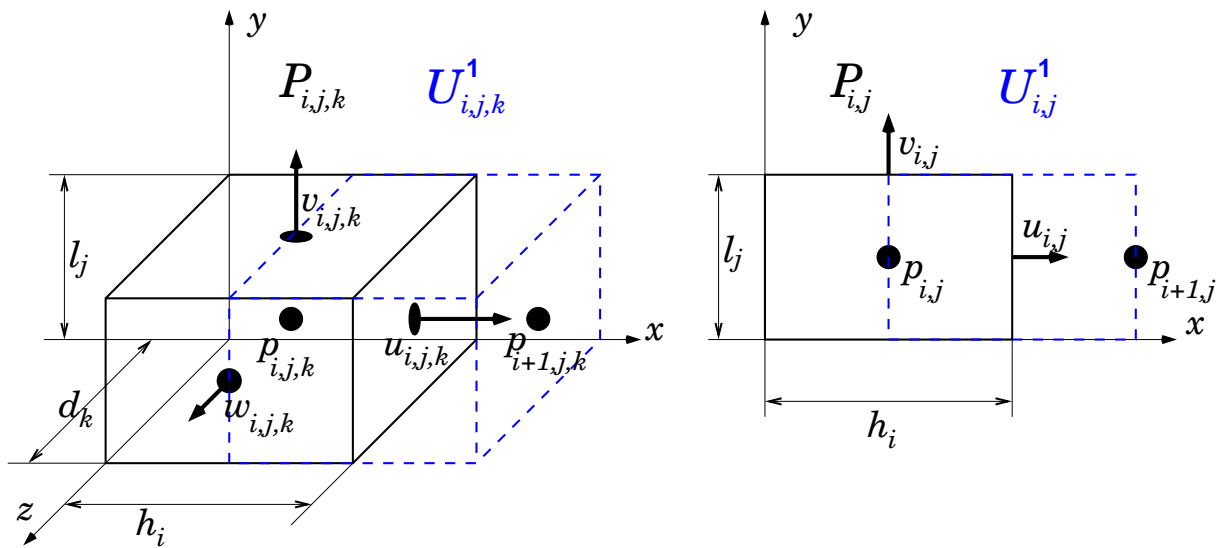

Figure 3.2: Control volumes for pressure ($P_{i,j,k}$, $P_{i,j}$, black, solid line) and for the first velocity component u ($U_{i,j,k}^1$, $U_{i,j}^1$, blue, dashed line) in 3D (left) and 2D (right)

$(u_{i,j,k}^1, u_{i,j,k}^2, u_{i,j,k}^2)$, $p_{i,j,k}$. These are defined at grid points in $\overline{\Omega^h}$. The discrete pressure $p_{i,j,k}$ is defined at $\mathbf{x}_{i,j,k}$. The capital letter P is used to denote a control volume related to the pressure – $P_{i,j,k}$. Discrete velocity components $(u_{i,j,k}^1, u_{i,j,k}^2, u_{i,j,k}^3) = (u_{i,j,k}, v_{i,j,k}, w_{i,j,k})$ are defined at different points. Namely, $u_{i,j,k}^m$ is defined at the point $\mathbf{x}_{i,j,k} + \mathbf{e}_m h_{i,j,k}^m/2$, which is the middle of $P_{i,j,k}$'s face, perpendicular to the m-th unit vector $\mathbf{e}_m$ (see Fig.3.2). $u_{i,j,k}^m$ has its own control volume $U_{i,j,k}^m = U_{\mathbf{i}}^m$, here $\mathbf{i}$ is a multi-index, ($\mathbf{i} = (i, j, k)$),

$$U_{\mathbf{i}}^m = \left\{ \mathbf{x} = (x^1, \dots, x^d) \in \Omega^h \mid x^m \in (x_{\mathbf{i}}^m, x_{\mathbf{i}+\mathbf{e}_m}^m); \quad \text{for } s \neq m : x^s \in (x_{\mathbf{i}}^s - \frac{h_{\mathbf{i}}^s}{2}, x_{\mathbf{i}}^s + \frac{h_{\mathbf{i}}^s}{2}). \right\}.$$

The control volumes $P_{\mathbf{i}}$ will be used for discretization of the continuity equation in the system (1.36). The velocity control volume $U_{\mathbf{i}}^m$ is used for discretization of the m-th momentum equation in (1.36). The divergence form of (1.36) reads:

$$-\nabla \cdot \underbrace{(\tilde{\mu} \nabla \mathbf{u} - \rho \mathbf{u}\,\mathbf{u}^T - p\mathbf{I})}_{\mathbf{W}} + \mu \mathbf{K}^{-1} \mathbf{u} = \mathbf{f} \qquad (3.1)$$

$$\nabla \cdot \mathbf{u} = 0 \qquad (3.2)$$

The system (1.37) can be discretized in the same way just ignoring the convective term. The macroscopic characteristics of the porous medium μ_{eff}, $\mathbf{K}$ can be functions in Ω_p, but we had only the porous–fluid interface. Here we can consider a more general situation where Ω_p may consist of different porous media Ω_p^k ($\overline{\Omega_p} = \bigcup_k \overline{\Omega_p^k}$). In each Ω_p^k we assume $\mu_{eff} = \mu_{eff}^k$, $\mathbf{K} = \mathbf{K}^k$ are constant (smooth) functions. Additional to the porous-fluid interface we may have porous-porous interfaces between Ω_p^k and Ω_p^m, $k \neq m$. We impose on the porous-porous interfaces the same conditions as on the porous–fluid interface (1.29), (1.34). Such generalization doesn't change the derivation of the numerical scheme, although it is not clear if the conditions are physical. We assume that the solution of (3.1), (3.2) is smooth enough in Ω_f and in each Ω_p^k. The velocity $\mathbf{u}$ is continuous in $\overline{\Omega_p \cup \Omega_f}$ due to the interface condition (1.29). The interface between porous and fluid (or different porous media), under our assumptions on the discretization is always perpendicular to a certain $\mathbf{e}_n$. Using $\mathbf{W} = \mathbf{T} - \rho \mathbf{u}\,\mathbf{u}^T$ one can rewrite the interface conditions (1.34) as

$$(\mathbf{W}^+ - \mathbf{W}^-)\,\mathbf{e}_n = \mathbf{M}\,\mathbf{u} \qquad (3.3)$$

where $\mathbf{W}^+ = \mathbf{W}(\mathbf{x} + 0\,\mathbf{e}_n)$, $\mathbf{W}^- = \mathbf{W}(\mathbf{x} - 0\,\mathbf{e}_n)$ and $\mathbf{x}$ is a point on the interface.
First, $[\mathbf{W}]|_\Sigma = [\mathbf{T}]|_\Sigma$ since $[\rho \mathbf{u}\,\mathbf{u}^T]|_\Sigma = 0$ due to the interface condition (1.29). Second:
• if $\mathbf{e}_n = \mathbf{n}_p$ then $\mathbf{W}^+ = \mathbf{W}|_{\Sigma_f}$ and $\mathbf{W}^- = \mathbf{W}|_{\Sigma_p}$;
• if $\mathbf{e}_n = -\mathbf{n}_p$ then $\mathbf{W}^+ = \mathbf{W}|_{\Sigma_p}$ and $\mathbf{W}^- = \mathbf{W}|_{\Sigma_f}$.

For brevity, let us derive the discretization in the 2D case (See Fig.3.3). We consider the coefficients $\tilde{\mu}$, $\mathbf{K}^{-1}$ to be constants (or smooth) inside each control volume $P_{i,j}$ (inside each of red, green, yellow and blue boxes in Fig.3.3), but they may have jumps on the $P_{i,j}$ boundaries. We assume that the solution of (3.1), (3.2) is smooth enough in $P_{i,j}$. The velocity $\mathbf{u}$ is continuous in $\overline{\Omega_p \cup \Omega_f}$ due to (1.29) condition on the interface. The pressure and $\nabla \mathbf{u}$ can be discontinuous through the interface. Any face between two control volumes $P_{\mathbf{i}}$, $P_{\mathbf{i}+\mathbf{e}_n}$ is a possible part of the porous-fluid (porous-porous) interface. If it is really the case then $\mathbf{W}$ may have a jump there according to the condition (3.3), where $\mathbf{M}$ is given. Otherwise, $\mathbf{W}$ is smooth, without jump through the interface, but we still can consider the condition (3.3) with $\mathbf{M} = \mathbf{0}$. So the matrix function $\mathbf{M}$ can be defined on any face of $P_{\mathbf{i}}$.

To discretize the continuity equation, (3.2) let us integrate it over $P_{i,j}$ (it is denoted by $ABFE$ in Fig.3.3, its volume is $|P_{i,j}| = h_i l_j$) and use the Gauss theorem:

$$0 = \int_{ABFE} \nabla \cdot \mathbf{u}\,d\mathbf{x} = \int_{\partial ABFE} \mathbf{u} \cdot \mathbf{n}\,d\sigma \approx \left(\frac{u_{i,j} - u_{i-1,j}}{h_i} + \frac{v_{i,j} - v_{i,j-1}}{l_j} \right) |P_{i,j}| \qquad (3.4)$$
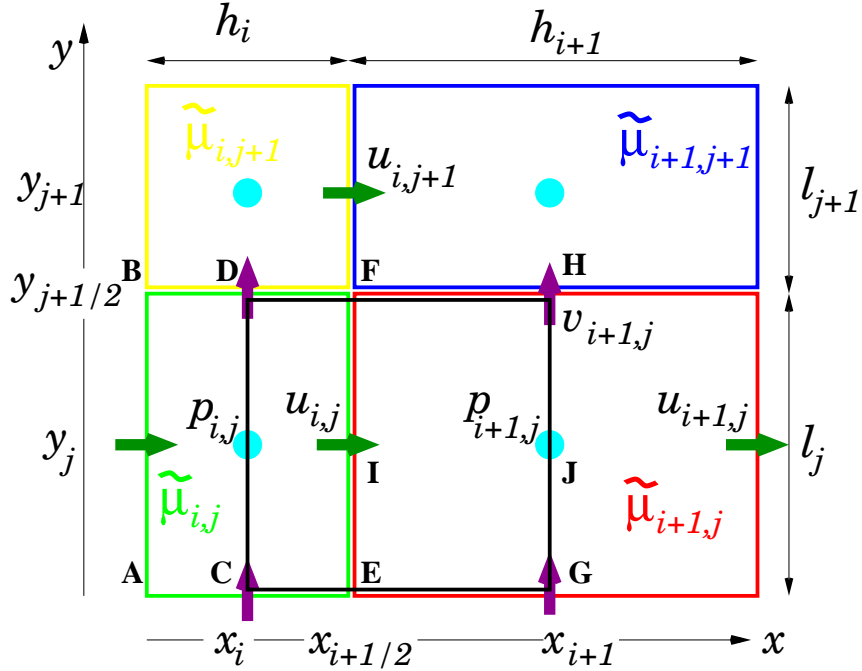
Figure 3.3: A small part of Ω^h with $P_{i,j}$ ($ABFE$) and $U^1_{i,j}$ (CDHG).

The first momentum equation from (3.1) is

$$-\nabla \cdot \underbrace{(\tilde{\mu}\nabla u - \rho u\, \mathbf{u} - p\mathbf{e}_1)}_{\mathbf{w}_1} + \mu\mathbf{k}_1 \cdot \mathbf{u} = f^1 \tag{3.5}$$

where $\mathbf{K}^{-1} = (\mathbf{k}_1, \dots, \mathbf{k}_d)^T$, $\mathbf{W} = (\mathbf{w}_1, \dots, \mathbf{w}_d)^T$. To obtain a discretized form we integrate (3.5) over $U^1_{i,j}$ (it is denoted by $CDHG$ in Fig.3.3). Let us first express the integral from $\nabla \cdot \mathbf{w}_1$. In order to use the Gauss theorem we should divide $CDHG$ into two parts $CDFE$ and $EFHG$ since EF is a possible interface with jump in stress and viscosity:

$$\int_{CDHG} \nabla \cdot \mathbf{w}_1\, d\mathbf{x} = \int_{CDFE} \nabla \cdot \mathbf{w}_1\, d\mathbf{x} + \int_{EFHG} \nabla \cdot \mathbf{w}_1\, d\mathbf{x}.$$

In $CDFE$ and $EFHG$ the Gauss theorem can be applied:

$$\int_{CDHG} \nabla \cdot \mathbf{w}_1\, d\mathbf{x} = \int_{\partial CDFE} \mathbf{w}_1(\sigma - 0\,\tilde{\mathbf{n}}) \cdot \tilde{\mathbf{n}}\, d\sigma + \int_{\partial EFHG} \mathbf{w}_1(\sigma - 0\,\hat{\mathbf{n}}) \cdot \hat{\mathbf{n}}\, d\sigma,$$

where $\tilde{\mathbf{n}}$ and $\hat{\mathbf{n}}$ are outer normals to $CDFE$ and $EFHG$ respectively, $\mathbf{w}_1(\sigma - 0\,\tilde{\mathbf{n}})$, $\mathbf{w}_1(\sigma - 0\,\hat{\mathbf{n}})$ means that we take a limit from internal part of $CDFE$ and $EFHG$ since $\mathbf{w}_1$ may be discontinuous on the interface. On EF $\tilde{\mathbf{n}} = -\hat{\mathbf{n}} = \mathbf{e}_1$ then

$$\int_{CDHG} \nabla \cdot \mathbf{w}_1\, d\mathbf{x} = \int_{\partial CDHG} \mathbf{w}_1(\sigma - 0\,\mathbf{n}) \cdot \mathbf{n}\, d\sigma - \int_{EF} (\mathbf{w}_1^+ - \mathbf{w}_1^-) \cdot \mathbf{e}_1\, d\sigma$$

where $\mathbf{n}$ is an outer normal to $CDHG$. From the stress jump condition (3.3) we know that $(\mathbf{w}_1^+ - \mathbf{w}_1^-) \cdot \mathbf{e}_1 = \mathbf{m}_1 \cdot \mathbf{u}$, for given $\mathbf{M} = (\mathbf{m}_1, \dots, \mathbf{m}_d)^T$:

$$\int_{CDHG} \nabla \cdot \mathbf{w}_1\, d\mathbf{x} = \int_{\partial CDHG} \mathbf{w}_1(\sigma - 0\,\mathbf{n}) \cdot \mathbf{n}\, d\sigma - \int_{EF} \mathbf{m}_1 \cdot \mathbf{u}\, d\sigma.$$

Hence (3.5) integrated over $CDHG$ leads to the equation

$$-\int_{\partial CDHG} \mathbf{w}_1 \cdot \mathbf{n}\, d\sigma + \int_{EF} \mathbf{m}_1 \cdot \mathbf{u}\, d\sigma + \int_{CDHG} (\mu \mathbf{k}_1 \cdot \mathbf{u} - f^1)\, d\mathbf{x} = 0. \qquad (3.6)$$

Below we will approximate consecutively each of the integrals in (3.6). The discretized momentum equation for u will be a result of substitution of all approximations to (3.6). To approximate the integrals we will often use the following standard technique. Assume $f(x)$ is a continuous function and $g(x)$ is possibly a discontinuous one. Let x^* be some intermediate point within a volume V. Then

$$\int_V f(x)g(x)\, dx \approx f(x^*) \int_V g(x)\, dx$$

The diameter of V should be small. In our case it is bounded by the largest discretization step.

$$\int_{\partial CDHG} \mathbf{w}_1 \cdot \mathbf{n}\, d\sigma = \int_{CD} \mathbf{w}_1 \cdot \mathbf{n}\, d\sigma + \int_{DH} \mathbf{w}_1 \cdot \mathbf{n}\, d\sigma + \int_{HG} \mathbf{w}_1 \cdot \mathbf{n}\, d\sigma + \int_{CG} \mathbf{w}_1 \cdot \mathbf{n}\, d\sigma$$

It is enough to consider integrals over HG and DH. The integral over CD is approximated similar to HG, CG similar to DH.

3.1.1 Approximation of the integrals over $CDHG$ and EF

First, we approximate the volume integral in (3.6):

$$\int_{CDHG} (\mu \mathbf{k}_1 \cdot \mathbf{u} - f^1)\, d\mathbf{x} \approx \mu \mathbf{u}(x_{i+\frac{1}{2}}, y_j) \cdot \int_{CDHG} \mathbf{k}_1\, d\mathbf{x} - \int_{CDHG} f^1\, d\mathbf{x} \qquad (3.7)$$

– the continuity of $\mathbf{u}$ was used. Similar we approximate the integral over EF:

$$\int_{EF} \mathbf{m}_1 \cdot \mathbf{u}\, d\sigma \approx \mathbf{u}(x_{i+\frac{1}{2}}, y_j) \cdot \int_{EF} \mathbf{m}_1\, d\sigma = \mathbf{u}(x_{i+\frac{1}{2}}, y_j) \cdot \mathbf{m}_{i,j}^1, \qquad \mathbf{m}_{i,j}^1 = \int_{EF} \mathbf{m}_1\, d\sigma \qquad (3.8)$$

The first component of $\mathbf{u}(x_{i+\frac{1}{2}}, y_j)$ is just a discrete variable $u_{i,j}$. The second component $v(x_{i+\frac{1}{2}}, y_j)$ (and the third, appearing in 3D case) can be obtained by interpolation from discrete variables in the neighbourhood due to continuity of $\mathbf{u}$, for example:

$$v(x_{i+\frac{1}{2}}, y_j) \approx \frac{(v_{i,j} + v_{i,j-1})h_{i+1} + (v_{i+1,j} + v_{i+1,j-1})h_i}{2(h_i + h_{i+1})}. \qquad (3.9)$$

These are possible approximations for the integrals over $CDHG$ and EF. But we need here some additional care. $\mathbf{k}_1$ can have very large values (of order $\bar{\varepsilon}^{-2}$) in one of $CDFE$, $EFHG$ and zeros in another (one belongs to porous phase, another to fluid). Also the discrete variables for velocities tangential to the interface (in our case v and in 3D w) can have very small values in the porous part and significantly larger values in the fluid part (like the flow behaviour in the Beavers–Joseph experiment). Then the values of v on EF obtained by linear interpolation from $v_{i,j}$, $v_{i+1,j}$, $v_{i,j-1}$, $v_{i+1,j}$ is not the best choice to approximate the integral on EF (we note also that $\mathbf{m}_1$ can have large values (of order $\bar{\varepsilon}^{-1}$)). As a consequence, a good approximation for the integrals $\int_{CDHG} \mu \mathbf{k}_1 \cdot \mathbf{u}\, d\mathbf{x}$, $\int_{EF} \mathbf{m}_1 \cdot \mathbf{u}\, d\sigma$ by the formulae proposed above may need a very small discretization step. One other way to interpolate v on EF (which we believe leads to a weaker restriction on the discretization step) is to use the analytical solution in the channel

(see Section 2.1.3). For example, if $P_{i,j}$ is porous and $P_{i+1,j}$ is fluid then we can take
- $l = h_i/2$, $h = h_{i+1}/2$ in order to determine the geometry of Ω_{far};

$$\bullet \qquad 2\frac{p_{i,j+1} - p_{i,j-1}}{2l_j + l_{j+1} + l_{j-1}} \qquad \text{or similar expressions}$$

to determine P – the pressure gradient in the direction tangential to the interface;
- $(v_{i,j} + v_{i,j-1})/2$ to determine u_{-l} for the Dirichlet boundary condition $u(-l) = u_{-l}$ on the lower boundary of the channel; and
- $(v_{i+1,j} + v_{i+1,j-1})/2$ to determine u_h for the Dirichlet boundary condition $u(h) = u_h$ on the upper boundary of the channel. The notation: $u(y)$, h, l, P, Ω_{far} was used in the section 2.1. The analytical solution for non-homogeneous Dirichlet boundary condition is given in the section 2.1.3. The velocity on the interface (C_2 in 2.38) linearly depends on P, u_h, u_{-l} (2.41) and hence on discrete variables $v.$, $p.$. This expression can be used for the value of $v(x_{i+\frac{1}{2}}, y_j)$

$$v(x_{i+\frac{1}{2}}, y_j) \approx a\frac{2(p_{i,j+1} - p_{i,j-1})}{2l_j + l_{j+1} + l_{j-1}} + b\frac{v_{i+1,j} + v_{i+1,j-1}}{2} + c\frac{v_{i,j} + v_{i,j-1}}{2} \qquad (3.10)$$

instead of linear interpolation (3.9) which uses only $v..$. (3.10) can be used in the approximation of the integral over EF (3.8). It can also be useful for approximation of $\int_{CDHG} \mu\mathbf{k}_1 \cdot \mathbf{u}\, d\mathbf{x}$ different from those given in (3.7). We can divide the integral into two, and approximate each of them, separately (2D):

$$\int_{CDHG} \mu\mathbf{k}_1 \cdot \mathbf{u}\, d\mathbf{x} \approx \mu u_{i,j} \int_{CDHG} \kappa_{11}\, d\mathbf{x} + \frac{\mu}{2}\left(\frac{v_{i,j} + v_{i,j-1}}{2} + v(x_{i+\frac{1}{2}}, y_j)\right) \int_{CDFE} \kappa_{12}\, d\mathbf{x} +$$

$$+ \frac{\mu}{2}\left(\frac{v_{i+1,j} + v_{i+1,j-1}}{2} + v(x_{i+\frac{1}{2}}, y_j)\right) \int_{EFHG} \kappa_{12}\, d\mathbf{x}.$$

3.1.2 Approximation of the integral over HG.

Let us return to the approximation of (3.6). We consider now the integral over HG. The integrand is

$$(\mathbf{w}_1 \cdot \mathbf{n})|_{HG} = (\mathbf{w}_1 \cdot \mathbf{e}_1)|_{HG} = \tilde{\mu}\frac{\partial u}{\partial x} - \rho[u]^2 - p$$
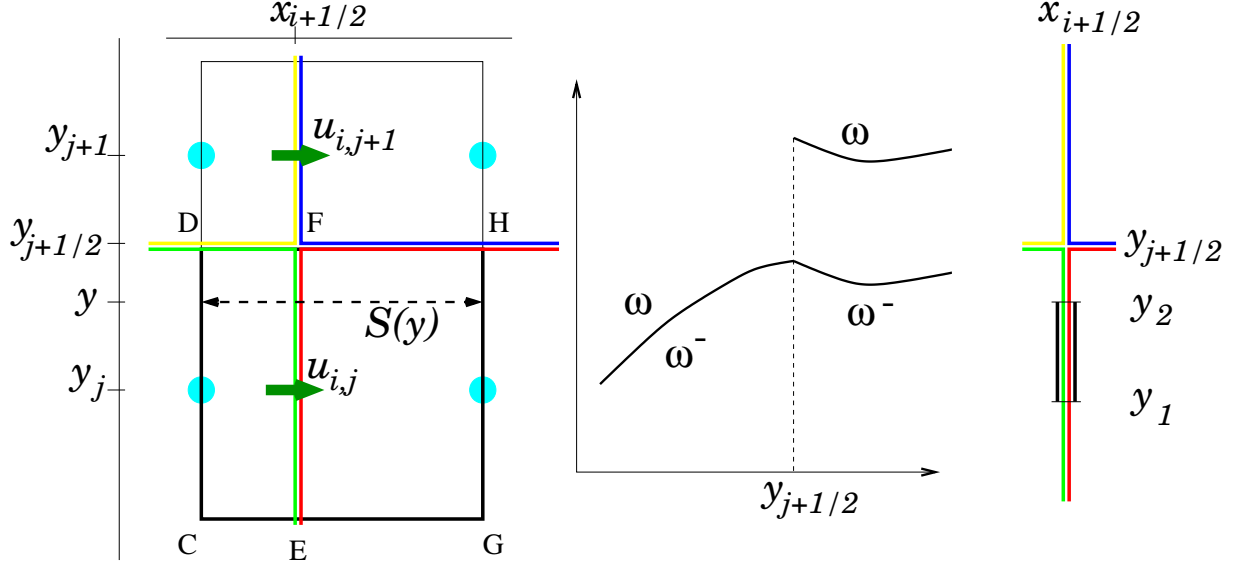
HG is inside $P_{i+1,j}$ where the solution is assumed to be smooth, $\mathbf{w}_1 \cdot \mathbf{e}_1$ is continuous on HG and we can use central point approximation for the integral:

$$\int_{HG} \mathbf{w}_1 \cdot \mathbf{n} \approx (\mathbf{w}_1 \cdot \mathbf{n})|_{(x_{i+1}, y_j)} \cdot |HG| \approx \left(\tilde{\mu}_{i+1,j}\frac{u_{i+1,j} - u_{i,j}}{h_{i+1}} - \rho[u(x_{i+1}, y_j)]^2 - p_{i+1,j}\right)|HG|$$
$$(3.11)$$

Similar

$$\int_{CD} \mathbf{w}_1\, \mathbf{n} \approx -\left(\tilde{\mu}_{i,j}\frac{u_{i,j} - u_{i-1,j}}{h_i} - \rho[u(x_i, y_j)]^2 - p_{i,j}\right)|CD|$$

The terms $[u(x_{i+1}, y_j)]^2$, $[u(x_i, y_j)]^2$ needs a special care due to non-linearity. Their interpolation will be discussed in Section 3.1.4.

Figure 3.4: Approximation of the surface integral over DH

3.1.3 Approximation of the integral over DH.

Approximation of the surface integral over DH is somewhat more interesting since four different media may contact at the point F. (see Fig.3.4, left). The integrand is

$$(\mathbf{w}_1 \cdot \mathbf{n})|_{DH} = (\mathbf{w}_1 \cdot \mathbf{e}_2)|_{DH} = \tilde{\mu}\frac{\partial u}{\partial y} - \rho uv.$$

Let us define an auxiliary function $\omega(y)$, $y \in [y_j, y_{j+1}] \setminus \{y_{j+1/2}\}$

$$\omega(y) = \int_{S(y)} \left(\tilde{\mu}\frac{\partial u}{\partial y} - \rho uv \right) dx, \qquad \text{where } S(y) = \{(x, y) : x \in [x_i, x_{i+1}]\}. \tag{3.12}$$

If DH is a part of the porous-fluid interface interface where $\mathbf{m}_1 \neq \mathbf{0}$ then $\omega(y)$ may be discontinuous at $y = y_{j+1/2}$. The jump is anyway known from (3.3):

$$\omega(y_{j+1/2} + 0) - \omega(y_{j+1/2} - 0) = \int_{DH} \mathbf{m}_1 \cdot \mathbf{u} \, d\sigma \tag{3.13}$$

Let $\omega^-(y)$ be a continuous part of $\omega(y)$:

$$\omega^-(y) = \begin{cases} \omega(y) & y \in [y_j, y_{j+1/2}) \\ \omega(y) - \int_{DH} \mathbf{m}_1 \cdot \mathbf{u} \, d\sigma & y \in (y_{j+1/2}, y_{j+1}] \end{cases} \tag{3.14}$$

$\omega^-(y)$ is continuous on $[y_j, y_{j+1}]$. (see Fig.3.4, middle) Our purpose is to approximate

$$\omega(y_{j+1/2} - 0) = \omega^-(y_{j+1/2})$$

since it is exactly the interface integral we are looking for. If $y \neq y_{j+1/2}$ then $u'_y(x, y)$ is continuous on $S(y)$: in $P_{i,j}$, $P_{i+1,j}$ we assume u to be enough smooth; there is also no discontinuity through the possible interface EF since u'_y is a derivative along the direction tangential to the interface (see Prop.3). We approximate (3.12) by taking the continuous function through the integral:

$$\omega(y) \approx u'_y(x_{i+\frac{1}{2}}, y) \int_{S(y)} \tilde{\mu} \, dx - \rho \int_{S(y)} uv \, dx, \qquad y \neq y_{j+1/2}. \tag{3.15}$$

Let us introduce $\Lambda(y) = \int_{S(y)} \tilde{\mu}\, dx > 0$, $UV(y) = \rho \int_{S(y)} uv\, dx$. From (3.15) we can express

$$u'_y(x_{i+\frac{1}{2}}, y) \approx \Big(\omega(y) + UV(y)\Big)/\Lambda(y) \qquad \text{for } y \neq y_{j+1/2}.$$

Even if $u'_y(x_{i+\frac{1}{2}}, y)$ is not defined at $y = y_{j+1/2}$, the following integral relation holds:

$$u_{i,j+1} - u_{i,j} = \int_{y_j}^{y_{j+1}} u'_y(x_{i+\frac{1}{2}}, y)\, dy \approx \int_{y_j}^{y_{j+1}} \Big(\omega(y) + UV(y)\Big)/\Lambda(y)\, dy =$$

$$= \int_{y_j}^{y_{j+\frac{1}{2}}} \Big(\omega^-(y) + UV(y)\Big)/\Lambda(y)\, dy + \int_{y_{j+\frac{1}{2}}}^{y_{j+1}} \Big(\omega(y) + UV(y)\Big)/\Lambda(y)\, dy =$$

$$= \int_{y_j}^{y_{j+1}} \frac{\omega^-(y) + UV(y)}{\Lambda(y)}\, dy + \left(\int_{DH} \mathbf{m}_1 \cdot \mathbf{u}\, dx\right) \int_{y_{j+\frac{1}{2}}}^{y_{j+1}} \frac{dy}{\Lambda(y)}$$

we have expressed $\omega(y)$ in $[y_{j+\frac{1}{2}}, y_{j+1}]$ using the continuous function $\omega^-(y)$ defined in (3.14). The continuous functions $\omega^-(y) + UV(y)$, $\mathbf{u}$ we can take out from the integrals at the points $y_{j+\frac{1}{2}}$, $(x_{i+\frac{1}{2}}, y_{j+\frac{1}{2}})$ respectively to obtain the approximation for $u_{i,j+1} - u_{i,j}$:

$$u_{i,j+1} - u_{i,j} \approx \Big(\omega^-(y_{j+\frac{1}{2}}) + UV(y_{j+\frac{1}{2}})\Big) \int_{y_j}^{y_{j+1}} \frac{dy}{\Lambda(y)} + \left(\mathbf{u}(x_{i+\frac{1}{2}}, y_{j+\frac{1}{2}}) \cdot \int_{DH} \mathbf{m}_1\, dx\right) \int_{y_{j+\frac{1}{2}}}^{y_{j+1}} \frac{dy}{\Lambda(y)}$$
$$\tag{3.16}$$

Using the following notation for the coefficients

$$\Lambda_{i,j+\frac{1}{2}} = \left[\int_{y_j}^{y_{j+1}} \frac{dy}{\Lambda(y)}\right]^{-1}, \qquad \Lambda^+_{i,j+\frac{1}{2}} = \left[\int_{y_{j+1/2}}^{y_{j+1}} \frac{dy}{\Lambda(y)}\right]^{-1}, \qquad \Lambda^-_{i,j+\frac{1}{2}} = \left[\int_{y_j}^{y_{j+1/2}} \frac{dy}{\Lambda(y)}\right]^{-1},$$

$$\mathbf{m}^+_{i,j+\frac{1}{2}} = \frac{\Lambda_{i,j+\frac{1}{2}}}{\Lambda^+_{i,j+\frac{1}{2}}} \int_{DH} \mathbf{m}_1\, dx, \qquad \mathbf{m}^-_{i,j+\frac{1}{2}} = \frac{\Lambda_{i,j+\frac{1}{2}}}{\Lambda^-_{i,j+\frac{1}{2}}} \int_{DH} \mathbf{m}_1\, dx.$$

we can resolve (3.16) for $\omega^-(y_{j+\frac{1}{2}})$:

$$\omega^-(y_{j+\frac{1}{2}}) \approx \Lambda_{i,j+\frac{1}{2}}(u_{i,j+1} - u_{i,j}) - \rho(uv)(x_{i+\frac{1}{2}}, y_{j+\frac{1}{2}})|DH| - \mathbf{u}(x_{i+\frac{1}{2}}, y_{j+\frac{1}{2}}) \cdot \mathbf{m}^+_{i,j+\frac{1}{2}}. \tag{3.17}$$

To approximate the surface integral over CG we need an expression for $-\omega^+(y_{j-\frac{1}{2}})$. From (3.13) we approximate $\omega^+(y_{j+\frac{1}{2}}) = \omega(y_{j+\frac{1}{2}} + 0)$ by

$$\omega^+(y_{j+\frac{1}{2}}) \approx \Lambda_{i,j+\frac{1}{2}}(u_{i,j+1} - u_{i,j}) - \rho(uv)(x_{i+\frac{1}{2}}, y_{j+\frac{1}{2}})|DH| + \mathbf{u}(x_{i+\frac{1}{2}}, y_{j+\frac{1}{2}}) \cdot \mathbf{m}^-_{i,j+\frac{1}{2}}$$

and use it in approximation of momentum equation for the control volume $P_{i,j+1}$. The expression for $\omega^+(y_{j-\frac{1}{2}})$ can be obtained if we substitute j by $j-1$:

$$\omega^+(y_{j-\frac{1}{2}}) \approx \Lambda_{i,j-\frac{1}{2}}(u_{i,j} - u_{i,j-1}) - \rho(uv)(x_{i+\frac{1}{2}}, y_{j-\frac{1}{2}})|DH| + \mathbf{u}(x_{i+\frac{1}{2}}, y_{j-\frac{1}{2}}) \cdot \mathbf{m}^-_{i,j-\frac{1}{2}}.$$

If in each control volume $P_{i,j}$, the effective viscosities $\tilde{\mu}$ are constants equal to $\tilde{\mu}_{i,j}$ then it is easy to calculate the integrals in the expressions for the coefficients:

$$\Lambda(y) = \begin{cases} \frac{1}{2}(\tilde{\mu}_{i,j} h_i + \tilde{\mu}_{i+1,j} h_{i+1}) & y \in [y_j, y_{j+\frac{1}{2}}] \\ \frac{1}{2}(\tilde{\mu}_{i,j+1} h_i + \tilde{\mu}_{i+1,j+1} h_{i+1}) & y \in [y_{j+\frac{1}{2}}, y_{j+1}] \end{cases}$$

$$\Lambda_{i,j+\frac{1}{2}} = \left(\frac{l_j}{\tilde{\mu}_{i,j}h_i + \tilde{\mu}_{i+1,j}h_{i+1}} + \frac{l_{j+1}}{\tilde{\mu}_{i,j+1}h_i + \tilde{\mu}_{i+1,j+1}h_{i+1}} \right)^{-1} \tag{3.18}$$

$$\Lambda^+_{i,j+\frac{1}{2}} = \left(\frac{l_{j+1}}{\tilde{\mu}_{i,j+1}h_i + \tilde{\mu}_{i+1,j+1}h_{i+1}} \right)^{-1} \qquad \Lambda^-_{i,j+\frac{1}{2}} = \left(\frac{l_j}{\tilde{\mu}_{i,j}h_i + \tilde{\mu}_{i+1,j}h_{i+1}} \right)^{-1}$$

To complete the approximation of (3.17) we need to express the velocity vector at $(x_{i+\frac{1}{2}}, y_{j+\frac{1}{2}})$. Due to continuity of **u** we can use the linear interpolation:

$$u(x_{i+\frac{1}{2}}, y_{j+\frac{1}{2}}) \approx u_{i,j+\frac{1}{2}} := \frac{u_{i,j}l_{j+1} + u_{i,j+1}l_j}{l_j + l_{j+1}}, \qquad v(x_{i+\frac{1}{2}}, y_{j+\frac{1}{2}}) \approx v_{i+\frac{1}{2},j} := \frac{v_{i,j}h_{i+1} + v_{i+1,j}h_i}{h_i + h_{i+1}} \tag{3.19}$$

$u(x_{i+\frac{1}{2}}, y_{j+\frac{1}{2}})$ is a velocity tangential to the interface. If, for example, both $P_{i,j}$, $P_{i+1,j}$ contain one phase (e.g. porous), and $P_{i,j+1}$, $P_{i+1,j+1}$ contain another phase (e.g. fluid) then like in the section 3.1.1 we may use the analytical solution in the channel to interpolate $u(x_{i+\frac{1}{2}}, y_{j+\frac{1}{2}})$. In our case it is possible to choose the input parameters: $l = l_j/2$, $h = l_{j+1/2}$,

$$P = 2\frac{(p_{i+1,j} - p_{i,j})l_{j+1} + (p_{i+1,j+1} - p_{i,j+1})l_j}{(h_{i+1} + h_i)(l_{j+1} + l_j)}$$

$u_{-l} = u_{i,j}$, $u_h = u_{i,j+1}$. Then the interpolation has a form:

$$u(x_{i+\frac{1}{2}}, y_{j+\frac{1}{2}}) \approx a \left(2\frac{(p_{i+1,j} - p_{i,j})l_{j+1} + (p_{i+1,j+1} - p_{i,j+1})l_j}{(h_{i+1} + h_i)(l_{j+1} + l_j)} \right) + bu_{i,j+1} + cu_{i,j} \tag{3.20}$$

The interpolation (3.20) might be better than $u_{i,j+\frac{1}{2}}$ from (3.19) (we note also that $\mathbf{m}^+_{i,j+\frac{1}{2}}$ can be large $(\bar{\varepsilon}^{-1})$). But in the term from (3.17) containing $(uv)(x_{i+\frac{1}{2}}, y_{j+\frac{1}{2}})$ it is preferable to use (3.19) since the behaviour of (3.20) together with non-linearity is not clear.

3.1.4 Approximation of the non-linear convective terms

We still have to approximate the non-linear terms $[u(x_{i+1}, y_j)]^2$ from (3.11), and $(uv)(x_{i+\frac{1}{2}}, y_{j+\frac{1}{2}})$ from (3.17). They don't appear if we deal with the Stokes–Brinkman model (1.37).

The so-called central differencing approximation is:

$$u_{i+\frac{1}{2},j} := \frac{u_{i,j} + u_{i+1,j}}{2}, \quad [u(x_{i+1}, y_j)]^2 \approx u_{i+\frac{1}{2},j}u_{i+\frac{1}{2},j}, \quad (uv)(x_{i+\frac{1}{2}}, y_{j+\frac{1}{2}}) \approx u_{i,j+\frac{1}{2}}v_{i+\frac{1}{2},j}. \tag{3.21}$$

where the expressions from (3.19) were used. Unfortunately the scheme doesn't work well when the Reynolds number is high. To weaken this restriction one can use the so-called upwind differencing scheme:

$$[u(x_{i+1}, y_j)]^2 \approx \begin{cases} \tilde{u}_{i+\frac{1}{2},j}u_{i,j} & \text{if } \tilde{u}_{i+\frac{1}{2},j} \geq 0 \\ \tilde{u}_{i+\frac{1}{2},j}u_{i+1,j} & \text{if } \tilde{u}_{i+\frac{1}{2},j} < 0 \end{cases}, \ (uv)(x_{i+\frac{1}{2}}, y_{j+\frac{1}{2}}) \approx \begin{cases} \tilde{v}_{i+\frac{1}{2},j}u_{i,j} & \text{if } \tilde{v}_{i+\frac{1}{2},j} \geq 0 \\ \tilde{v}_{i+\frac{1}{2},j}u_{i,j+1} & \text{if } \tilde{v}_{i+\frac{1}{2},j} < 0 \end{cases} \ . \tag{3.22}$$

where $\tilde{u}_{i+\frac{1}{2},j}$, $\tilde{v}_{i+\frac{1}{2},j}$ are a priory known predictions for the values of $u_{i+\frac{1}{2},j}$, $v_{i+\frac{1}{2},j}$. This already couples the creation of the system of non-linear algebraic equations (where the discrete variables play a role of unknowns) with solving it by an iterative process. The expressions with *tilde* are calculated using the known discrete variables from the previous iteration. Assuming a convergence of the iterative process the discrete variables on previous iteration (marked with

tilde) approximate the current discrete variables. The approximations from (3.21) can be also made linear:

$$[u(x_{i+1}, y_j)]^2 \approx u_{i+\frac{1}{2},j} \tilde{u}_{i+\frac{1}{2},j} \qquad (uv)(x_{i+\frac{1}{2}}, y_{j+\frac{1}{2}}) \approx u_{i,j+\frac{1}{2}} \tilde{v}_{i+\frac{1}{2},j}.$$

The upwind scheme (3.22) can be applied for problems with much higher Reynolds numbers than the central differencing approximation (3.21), but it is less precise. A compromise solution is the so-called deferred correction with upwind as a low order scheme and central differences as a high order scheme (see [15, p.76]):

$$[u(x_{i+1}, y_j)]^2 \approx \begin{cases} \tilde{u}_{i+\frac{1}{2},j}(u_{i,j} - \tilde{u}_{i,j}) + (\tilde{u}_{i+\frac{1}{2},j})^2 & \text{if } \tilde{u}_{i+\frac{1}{2},j} \geq 0 \\ \tilde{u}_{i+\frac{1}{2},j}(u_{i+1,j} - \tilde{u}_{i+1,j}) + (\tilde{u}_{i+\frac{1}{2},j})^2 & \text{if } \tilde{u}_{i+\frac{1}{2},j} < 0 \end{cases}$$

$$(uv)(x_{i+\frac{1}{2}}, y_{j+\frac{1}{2}}) \approx \begin{cases} \tilde{v}_{i+\frac{1}{2},j}(u_{i,j} - \tilde{u}_{i,j}) + \tilde{u}_{i,j+\frac{1}{2}} \tilde{v}_{i+\frac{1}{2},j} & \text{if } \tilde{v}_{i+\frac{1}{2},j} \geq 0 \\ \tilde{v}_{i+\frac{1}{2},j}(u_{i,j+1} - \tilde{u}_{i,j+1}) + \tilde{u}_{i,j+\frac{1}{2}} \tilde{v}_{i+\frac{1}{2},j} & \text{if } \tilde{v}_{i+\frac{1}{2},j} < 0 \end{cases}$$

3.1.5   Vector-index form and 3D case

In a similar way one can discretize another momentum equations and consider the third velocity component for the 3D case. Although there are no principal difficulties in writing down or implementing in a computer program other momentum equations, a heightened attention is required, since a large number of similar cases should be taken into account.

   An alternative approach is to discretize the momentum equation only once, using Fig. 3.3 as it was done above, but to abstract from particular directions. The first momentum equation (3.5) we can substitute by the m-th momentum equation

$$-\nabla \cdot \underbrace{(\tilde{\mu}\nabla u^m - \rho u^m \mathbf{u} - p\mathbf{e}_m)}_{\mathbf{w}_m} + \mu \mathbf{k}_m \cdot \mathbf{u} = f^m, \tag{3.23}$$

where m is a parameter that can take values from $1, \dots, d$. Further, when we integrate (3.23) over $U_{\mathbf{i}}^m$, we obtain

$$-\int_{\partial U_{\mathbf{i}}^m} \mathbf{w}_m \cdot \mathbf{n}\, d\sigma + \int_{\partial P_{\mathbf{i}} \cap \partial P_{\mathbf{i}+\mathbf{e}_m}} \mathbf{m}_m \cdot \mathbf{u}\, d\sigma + \int_{U_{\mathbf{i}}^m} (\mu \mathbf{k}_m \cdot \mathbf{u} - f^m)\, d\mathbf{x} = 0 \tag{3.24}$$

instead of (3.6). $\partial U_{\mathbf{i}}^m = \bigcup_k F_k$, where F_k is a union of two faces of $U_{\mathbf{i}}^m$ perpendicular to $\mathbf{e}_k$: $F_k = [\partial U_{\mathbf{i}}^m \cap \partial U_{\mathbf{i}+\mathbf{e}_k}^m] \cup [\partial U_{\mathbf{i}}^m \cap \partial U_{\mathbf{i}-\mathbf{e}_k}^m]$. ($\mathbf{n}$ is either $\mathbf{e}_k$ or $-\mathbf{e}_k$ on F_k). Then the first integral can be represented as a sum

$$\int_{\partial U_{\mathbf{i}}^m} \mathbf{w}_m \cdot \mathbf{n}\, d\sigma = \sum_k \int_{F_k} \mathbf{w}_m \cdot \mathbf{n}\, d\sigma = \int_{F_m} \mathbf{w}_m \cdot \mathbf{n}\, d\sigma + \sum_{s \neq m} \int_{F_s} \mathbf{w}_m \cdot \mathbf{n}\, d\sigma.$$

In 2D there is only one F_s, $s \neq m$: $s = 3 - m$. In 3D we have two F_s, and integrals over them are approximated in a similar way, like it was done in the section 3.1.3. s is the second parameter after m. The integral over F_m is different (see the section 3.1.2). So, it is enough to write the discretizations for the momentum equations in a vector form, depending on the parameters m, s. The third parameter t appears only in 3D. It is uniquely determined by $t = 6 - m - s$. We will not write the approximation of (3.24) up to the end in the vector-index form, but we used

this way in order to implement the algorithm. The discretization of the continuity equation (see (3.4) in 2D) is

$$\sum_{m=1}^{d} \frac{u_{\mathbf{i}}^m - u_{\mathbf{i}-\mathbf{e}_m}^m}{h_{\mathbf{i}}^m} |P_{\mathbf{i}}| = 0, \tag{3.25}$$

where $|P_{\mathbf{i}}|$ is either the volume (in 3D) or the area (in 2D) of the pressure control volume $P_{\mathbf{i}}$.

From here we will use mostly the vector-index notation.

3.1.6 Discrete unknowns and corresponding algebraic equations

At the end of the discretization process one should obtain a system of algebraic equations. Those discrete variables, which are unknowns in that system, let us call as discrete unknowns. It is important to have the number of equations in the system equal to the number of discrete unknowns. To satisfy this criteria we may think that each discrete unknown should have its own equation and the only one. Let $\mathbf{i}(\Omega^h)$ be a set of all indexes $\mathbf{i} \in \mathbb{Z}^d$ such that $P_{\mathbf{i}} \subset \Omega^h$. The number of such indexes (and the number of $P_{\mathbf{i}}$) we denote by N_{CV}. Let us define the set of all discrete unknowns as those $u_{\mathbf{i}}^1, \ldots, u_{\mathbf{i}}^d, p_{\mathbf{i}}$ that $\mathbf{i} \in \mathbf{i}(\Omega^h)$. We note that the discrete variable $u_{\mathbf{i}}^m$, defined on the boundary $\partial\Omega^h$, belongs to the set of discrete unknowns only if the outer normal to $\partial\Omega^h$ coincides with $\mathbf{e}_m$ at the point where $u_{\mathbf{i}}^m$ is defined. It means, that one should treat the parts of the boundary with and without discrete unknowns in a different way.

If the discrete unknown $u_{\mathbf{i}}^m$ is not on the boundary then $\mathbf{i} + \mathbf{e}_m \in \mathbf{i}(\Omega^h)$, and $U_{\mathbf{i}}^m$ can be defined as usual, containing a half of $P_{\mathbf{i}}$ and a half of $P_{\mathbf{i}+\mathbf{e}_m}$. (3.24) makes sense, and the algebraic equation for this $u_{\mathbf{i}}^m$ is an approximation of (3.24). Above, we have discussed the approximation for the case when $U_{\mathbf{i}}^m$ is away from the boundary (all discrete variables used in the approximation were discrete unknowns). When $U_{\mathbf{i}}^m$ is close to the boundary it is also possible to write the approximation of (3.24), using the approach proposed above since the grid can be also defined outside Ω^h (see Fig.3.1), but some discrete variables needed for the approximation are not discrete unknowns and we should also somehow extrapolate the properties of the medium (like $\tilde{\mu}$) from Ω^h to some region outside Ω^h (since the expressions like (3.18) in the approximation may depend on the properties outside Ω^h). All discrete variables which are not discrete unknowns cannot be used in the resulting system of algebraic equations. They should be excluded with the help of boundary conditions. This will be discussed in the next subsection as well as the case when the discrete unknown $u_{\mathbf{i}}^m$ is on the boundary. In the latter case the algebraic equation corresponding to $u_{\mathbf{i}}^m$ is an approximation of the boundary condition.

To the discrete pressure unknown $p_{\mathbf{i}}$ we correspond the discretization of the continuity equation (3.25) even if there is no pressure variable itself (it is one of the difficult points of incompressible Navier-Stokes system of equations). If $P_{\mathbf{i}}$ does not touch the boundary, then (3.25) is well defined in terms of discrete unknowns. Otherwise the boundary conditions should be used to express the missing velocities in (3.25). It is also the task of the next subsection.

At the end we should have a system of $(d+1)N_{CV}$ algebraic equations for $(d+1)N_{CV}$ discrete unknowns.

3.1.7 Boundary conditions

We will consider here and use for solving numerical problems in the Section 3.3 and the Chapters 4, 5 only three types of boundary conditions:

- *Dirichlet boundary condition.* Let S_{in} be a part of the boundary $\partial\Omega^h$, where the Dirichlet condition is imposed. At any point $\mathbf{x} \in S_{in}$ we have d conditions: $\mathbf{u}(\mathbf{x}) = \mathbf{u}_{\partial\Omega}$. If it is the

only boundary condition in use, then the input data $\mathbf{u}_{\partial\Omega}$ should satisfy the compatibility condition (2.58). A particular case is the no-slip condition imposed on the solid-fluid, solid-porous boundaries: $\mathbf{u}(\mathbf{x}) = \mathbf{0}$. The Dirichlet condition will be used in all our numerical tests, usually together with the "Outlet" condition.

- *"Outlet" boundary condition.* Let S_{out} be a part of the boundary $\partial\Omega^h$, where the "Outlet" condition is imposed, and $\mathbf{n}$ be an outer normal to $\partial\Omega^h$. The "Outlet" conditions at the point $\mathbf{x} \in S_{out}$ results in d conditions $\frac{\partial\mathbf{u}}{\partial\mathbf{n}} = \mathbf{0}$ (Neumann conditions for each velocity component).

  The solution $\mathbf{u}$ of the differential system satisfies the incompressibility condition leading to $\int_{\partial\Omega^h} \mathbf{u} \cdot \mathbf{n}\, d\sigma = 0$. If the mass flux through $\partial\Omega^h \setminus S_{out}$: $\int_{\partial\Omega^h \setminus S_{out}} \mathbf{u} \cdot \mathbf{n}\, d\sigma$ can be calculated, then we have a necessary integral condition for S_{out}:

  $$F_{out} = \int_{S_{out}} \mathbf{u} \cdot \mathbf{n}\, d\sigma = - \int_{\partial\Omega^h \setminus S_{out}} \mathbf{u} \cdot \mathbf{n}\, d\sigma, \qquad (3.26)$$

  that can be used in the numerical algorithm for solving the resulting system of algebraic equations.

  The "Outlet" condition is usually used far from the region of interest, where the flow is assumed to be fully developed. We will use this condition on the boundaries perpendicular to some pipe where the outlet of the flow is expected.

- *"Symmetry" boundary condition.* Let S_{sym} be a part of the boundary $\partial\Omega^h$, where the "Outlet" condition is imposed. This condition one can impose on a symmetry plane for the case when the solution is expected to be symmetric with respect to this plane. The boundary (plane) is perpendicular to some $\mathbf{e}_m$ ($\mathbf{n} \parallel \mathbf{e}_m$). Other unit vectors $\mathbf{e}_s$ (and $\mathbf{e}_t$ in 3D) are tangential to the boundary. Then for $\mathbf{x} \in S_{sym}$ we have d conditions: $u^m = 0$, $\frac{\partial}{\partial\mathbf{n}}u^s = 0$ (and $\frac{\partial}{\partial\mathbf{n}}u^t = 0$ in 3D).

  There is no mass flux through such boundary: $\int_{S_{sym}} \mathbf{u} \cdot \mathbf{n}\, d\sigma = 0$.

  We will use the symmetry condition only in one problem (see the problem's geometries in Fig.4.10,4.11) together with Dirichlet and "Outlet" boundary conditions.

If we deal only with these three boundary conditions, then (3.26) can be rewritten as

$$F_{out} = \int_{S_{out}} \mathbf{u} \cdot \mathbf{n}\, d\sigma = - \int_{S_{in}} \mathbf{u} \cdot \mathbf{n}\, d\sigma, \qquad (3.27)$$

Let us assume that the boundary lies between $P_\mathbf{i}$ and $P_{\mathbf{i}+\mathbf{e}_m}$ ($S = \overline{P_\mathbf{i}} \cap \overline{P_{\mathbf{i}+\mathbf{e}_m}}$). Then either $\mathbf{i}$ or $\mathbf{i} + \mathbf{e}_m$ is not in $\mathrm{i}(\Omega^h)$. (in the Fig.3.3 we can choose for example $S = EF$, $P_\mathbf{i} = P_{i,j}$, $P_{\mathbf{i}+\mathbf{e}_m} = P_{i+1,j}$, $u_\mathbf{i}^m = u_{i,j}$, $u_\mathbf{i}^s = v_{i,j}$, $u_{\mathbf{i}+\mathbf{e}_m}^s = v_{i+1,j}$).

If $\mathbf{i} \in \mathrm{i}(\Omega^h)$ then $u_\mathbf{i}^m$ is a discrete unknown. The corresponding algebraic equation is a discretization of the boundary condition (the momentum equation is not used for this case). We have the following possibilities:

- if $S \subset S_{in}$ then $u_\mathbf{i}^m = u_S^m$, where u_S^m is the given value ($u_S^m = \frac{1}{|S|}\int_S \mathbf{u}_{\partial\Omega} \cdot \mathbf{n}\, d\sigma$).
- if $S \subset S_{out}$ then we equate $u_\mathbf{i}^m$ with the discrete unknown $u_{\mathbf{i}-\mathbf{e}_m}^m$. The unknown $u_{\mathbf{i}-\mathbf{e}_m}^m$ is placed one step in the direction opposite to $\mathbf{n}$ from the boundary (the case $\mathbf{i} - \mathbf{e}_m \notin \mathrm{i}(\Omega^h)$ is not in agreement with imposing "Outlet" condition on S). The equation for $u_\mathbf{i}^m$ is $u_\mathbf{i}^m = u_{\mathbf{i}-\mathbf{e}_m}^m$.
- if $S \subset S_{sym}$ then the equation for $u_\mathbf{i}^m$ is $u_\mathbf{i}^m = 0$ (no-penetration).

If $\mathbf{i} + \mathbf{e}_m \in \mathrm{i}(\Omega^h)$ then $u_\mathbf{i}^m$ is not a discrete unknown and hence doesn't need an equation. But it can be used in the equations for other discrete unknowns. We have similar cases:

- if $S \subset S_{in}$ then $u_\mathbf{i}^m = u_S^m$: we substitute the value u_S^m for each entry of $u_\mathbf{i}^m$.
- if $S \subset S_{out}$ then we identify $u_\mathbf{i}^m$ and the discrete unknown $u_{\mathbf{i}+\mathbf{e}_m}^m$: we substitute the discrete unknown $u_{\mathbf{i}+\mathbf{e}_m}^m$ for each entry of $u_\mathbf{i}^m$.
- if $S \subset S_{sym}$ we substitute 0 for each entry of $u_\mathbf{i}^m$.

Now we consider velocity components tangential to the boundary. If only one from $\mathbf{i}$, $\mathbf{i}+\mathbf{e}_m$ is in $\mathbf{i}(\Omega^h)$, then only one from the discrete variables $u_\mathbf{i}^s$, $u_{\mathbf{i}+\mathbf{e}_m}^s$ is the discrete unknown ($s \neq m$). The discrete variable being outside Ω^h still can be used in expressions approximating some momentum equation. In order to exclude it we can do the following:

- if $S \subset S_{in}$. Let $\mathbf{x} \in S$ be the intersection point of the segment connecting points where $u_\mathbf{i}^s$ and $u_{\mathbf{i}+\mathbf{e}_m}^s$ are defined with the boundary (according to our example, $\mathbf{x}$ coincides with the point F in Fig.3.3). Due to the Dirichlet condition the velocity is known at that point. The s-th component is $\mathbf{u}^s(\mathbf{x}) = \mathbf{u}_S^s$. Using the linear interpolation

$$u_S^s \approx \frac{u_\mathbf{i}^s h_{\mathbf{i}+\mathbf{e}_m}^m + u_{\mathbf{i}+\mathbf{e}_m}^s h_\mathbf{i}^m}{h_\mathbf{i}^m + h_{\mathbf{i}+\mathbf{e}_m}^m} \qquad \left(\text{in Fig.3.3} \quad v(F) \approx \frac{v_{i,j} h_{i+1} + v_{i+1,j} h_i}{h_i + h_{i+1}} \right).$$

and the known value u_S^s, we can express either $u_\mathbf{i}^s$ or $u_{\mathbf{i}+\mathbf{e}_m}^s$. One of them, which is not a discrete unknown, can be replaced in this way from all equations.

- if $S \subset S_{out}$ then $u_\mathbf{i}^s = u_{\mathbf{i}+\mathbf{e}_m}^s$. We substitute the discrete unknown for another one in all equations.
- if $S \subset S_{sym}$: the same as in the case $S \subset S_{out}$.

These are the main ideas how to exclude the discrete variables being not in the set of discrete unknowns from approximations of momentum and continuity equations.

3.1.8 Numerical solution

As we have mentioned in the subsection 3.1.6, the main purpose of the discretization procedure is to determine the system of $(d+1)N_{CV}$ algebraic equations with $(d+1)N_{CV}$ discrete unknowns. Any set of values for the discrete unknowns that satisfies the system of (non-linear) algebraic equations we can call a numerical solution for our problem (discrete unknowns marked with *tilde* (in the subsection 3.1.4) has the same meaning here as the discrete unknowns without *tilde*). We discuss here neither existence nor uniqueness of the numerical solution. Using the values of the discrete unknowns it is possible to determine also the values of the discrete variables near the boundary which were excluded with the help of the boundary conditions (see Section 3.1.7). In particular, we can determine the discrete velocity field consisting of all discrete variables which are defined in $\overline{\Omega^h}$.

One possibility to solve the system of equations, based on the SIMPLE method, we consider in the next section.

3.2 On solving the coupled system of algebraic equations

Iteration methods are often used when one have to solve systems of non-linear algebraic equations as well as systems of linear algebraic equations (especially in the case of large number of unknowns). In the subsection 3.1.4 some discrete unknowns were marked with the *tilde* sign, meaning that on the current iteration this variable is not an unknown, but has a known value from previous iteration. If the iterative process converges, then, after enough large number of iterations, the values of the discrete unknowns on the current and on the previous iteration are close to each other and satisfy approximately the initial system of algebraic equations. This means the convergence to the numerical solution. Additional to discrete unknowns marked

with the *tilde* sign in the subsection 3.1.4 to make the equations linear, we can mark some other discrete unknowns with the *tilde* sign in order to simplify the current iteration. For example, in the algebraic equation that corresponds to some discrete unknown $u_{\mathbf{i}}^m$ we can mark with the *tilde* sign all discrete unknown u^s ($s \neq m$). If we use the expressions (3.10), (3.20) then the pressure variables there we also mark with the *tilde* sign. Due to our discretization the algebraic equation for $u_{\mathbf{i}}^m$ contains no more than $2d + 1$ discrete velocity unknowns without *tilde* sign, namely the main (diagonal) unknown $u_{\mathbf{i}}^m$ and $2d$ neighbours $u_{\mathbf{j}}^m$, where $\mathbf{j} = \mathbf{i} \pm \mathbf{e}_k$, $k = 1, \dots d$, $\mathbf{j} \in \mathbf{i}(\Omega^h)$ and two discrete pressure unknowns $p_{\mathbf{i}}$, $p_{\mathbf{i}+\mathbf{e}_m}$. The pressure unknowns appear only in the discretized momentum equations (not in the discretized continuity equations), therefore we have to consider them as unknowns on the current iteration.

If we numerate somehow the elements of the finite set $\mathbf{i}(\Omega^h)$ then we can define the vectors $\mathbf{U}^k \in \mathbb{R}^{N_{CV}}$, $k = 1, \dots, d$, containing all discrete unknowns $u_{\mathbf{i}}^k$, $\mathbf{i} \in \mathbf{i}(\Omega^h)$; $\mathbf{P} \in \mathbb{R}^{N_{CV}}$ containing all $p_{\mathbf{i}}$, $\mathbf{i} \in \mathbf{i}(\Omega^h)$; $\mathbf{U} = (\mathbf{U}^1, \dots, \mathbf{U}^d) \in \mathbb{R}^{dN_{CV}}$ containing all discrete velocity unknowns (we note that this notation is different from $U_{\mathbf{i}}^k$, $P_{\mathbf{i}}$ denoting the velocity and pressure control volumes).

The iterative process is the sequence

$$(\mathbf{U}, \mathbf{P})^{(1)}, (\mathbf{U}, \mathbf{P})^{(2)}, \dots, (\mathbf{U}, \mathbf{P})^{(n)}, (\mathbf{U}, \mathbf{P})^{(n+1)}, \dots$$

Each element $(\mathbf{U}, \mathbf{P})^{(n)}$ contains values of all discrete variables after $n \in \mathbb{N}$ iterations. The values of all discrete velocity variables which are defined in $\overline{\Omega^h}$, but are not discrete unknown can be calculated from $\mathbf{U}^{(n)}$ by the same expressions used to exclude them (for example from discrete continuity equation). These values make up the discrete velocity field, corresponding to $\mathbf{U}^{(n)}$.

In order to describe the iterative process, it is enough to describe one step, namely how to obtain $(\mathbf{U}, \mathbf{P})^{(n+1)}$ from $(\mathbf{U}, \mathbf{P})^{(n)}$. With the *tilde* sign ($\tilde{\cdot}$) we mark the discrete unknowns on the previous iteration (n): $(\widetilde{\mathbf{U}}, \widetilde{\mathbf{P}}) := (\mathbf{U}, \mathbf{P})^{(n)}$. With the *hat* sign ($\hat{\cdot}$) we mark the intermediate velocity $\widehat{\mathbf{U}}$. With the *overline* sign ($\overline{\cdot}$) we mark the numerical solution – the main goal of the algorithm: $\overline{\mathbf{U}}, \overline{\mathbf{P}}$. $\mathbf{U}, \mathbf{P}, u, p$ without *tilde*, *hat* or *overline* we use to denote the values on the new iteration: $(\mathbf{U}, \mathbf{P}) := (\mathbf{U}, \mathbf{P})^{(n+1)}$.

Let us consider the linear algebraic equation for the discrete unknown $u_{\mathbf{i}}^m$. It has a form:

$$a_{\mathbf{i},\mathbf{i}}^m[\widetilde{\mathbf{U}}]u_{\mathbf{i}}^m - \sum_{s=1}^{d} \sum_{\gamma=\pm 1} a_{\mathbf{i},\mathbf{i}+\gamma\mathbf{e}_s}^m[\widetilde{\mathbf{U}}]\, u_{\mathbf{i}+\gamma\mathbf{e}_s}^m + b_{\mathbf{i}}^m(p_{\mathbf{i}+\mathbf{e}_m} - p_{\mathbf{i}}) = c_{\mathbf{i}}^m[\widetilde{\mathbf{U}}] \qquad (3.28)$$

where the coefficients $a_{\mathbf{i},\mathbf{j}}^m$, $c_{\mathbf{i}}^m$ depend only on the known values of $\widetilde{\mathbf{U}}$ ($a_{\mathbf{i},\mathbf{j}}^m$ depends on $\widetilde{\mathbf{U}}$ due to convective terms, $c_{\mathbf{i}}^m$ may depend also on $\widetilde{\mathbf{P}}$ when (3.10),(3.20) are used), $b_{\mathbf{i}}^m$ is a constant. In (3.28) $a_{\mathbf{i},\mathbf{i}}^m > 0$, other coefficients may be equal to zero. When $u_{\mathbf{i}}^m$ is on the boundary then we still have (3.28) with $b_{\mathbf{i}}^m = 0$.

Using again that if the iterative process converges, then $u_{\mathbf{i}}^m \approx \tilde{u}_{\mathbf{i}}^m$, we can add the term $(\frac{1}{\alpha_u} - 1)a_{\mathbf{i},\mathbf{i}}^m[\widetilde{\mathbf{U}}]u_{\mathbf{i}}^m$ ($0 < \alpha_u \leq 1$) to both sides of (3.28) and then substitute in the right hand side the known value $\tilde{u}_{\mathbf{i}}^m$ for $u_{\mathbf{i}}^m$. We will obtain the under-relaxed form of (3.28):

$$\frac{a_{\mathbf{i},\mathbf{i}}^m[\widetilde{\mathbf{U}}]}{\alpha_u}u_{\mathbf{i}}^m - \sum_{s=1}^{d} \sum_{\gamma=\pm 1} a_{\mathbf{i},\mathbf{i}+\gamma\mathbf{e}_s}^m[\widetilde{\mathbf{U}}]\, u_{\mathbf{i}+\gamma\mathbf{e}_s}^m + b_{\mathbf{i}}^m(p_{\mathbf{i}+\mathbf{e}_m} - p_{\mathbf{i}}) = c_{\mathbf{i}}^m[\widetilde{\mathbf{U}}] + \frac{1-\alpha_u}{\alpha_u}a_{\mathbf{i},\mathbf{i}}^m[\widetilde{\mathbf{U}}]\tilde{u}_{\mathbf{i}}^m. \quad (3.29)$$

If we choose $\alpha_u = 1$ then (3.29) coincides with (3.28). Hence, we don't need to consider (3.28) any more. The relaxation parameter $\alpha_u < 1$ improves the main (diagonal) term in (3.29) comparing to (3.28). This simplifies each iteration step, and sometimes it is even necessary to use the under-relaxation in order to obtain a convergent iterative process.

But, for $u_{\mathbf{i}}^m$, defined on the boundary with Dirichlet or "Symmetry" conditions, there are several reasons to use the left equation (without under-relaxation) than the right one:

$$u_{\mathbf{i}}^m = \text{given value}, \qquad \frac{u_{\mathbf{i}}^m}{\alpha_u} = \text{given value} + \frac{1 - \alpha_u}{\alpha_u} \tilde{u}_{\mathbf{i}}^m. \tag{3.30}$$

First, the left equation has the diagonal dominance. Second, in the right equation we artificially introduce an error which disappear only on convergent solution, when $\tilde{u}_{\mathbf{i}}^m = u_{\mathbf{i}}^m$; but the left equation is exactly the discretized form of the boundary condition. Third, if on $\partial\Omega$ we have only Dirichlet and "Symmetry" boundary conditions ($S_{out} = \emptyset$), satisfying the compatibility condition (2.58) then the discrete velocity field, obtained after solving the momentum equations (3.29), (3.30,left) satisfies the discretized compatibility condition. Using (3.30,right) we don't have this property, which will be important for the pressure–correction equation (see the Subsection 3.2.3). In the case $S_{out} \neq \emptyset$, we will combine solving the momentum equations with "Outlet" condition and the momentum equations where the "Outlet" conditions are substituted by some Dirichlet conditions.

The equations (3.29) for all discrete velocity unknowns $u_{\mathbf{i}}^m$, $m = 1, \ldots, d$, $\mathbf{i} \in \mathbf{i}(\Omega^h)$ and discrete continuity equations (3.25) make up a system of linear algebraic equations. The linear system has the following block–structure (3D):

$$\begin{bmatrix} \mathbf{A}_{11} & \mathbf{0} & \mathbf{0} & \mathbf{G}_1 \\ \mathbf{0} & \mathbf{A}_{22} & \mathbf{0} & \mathbf{G}_2 \\ \mathbf{0} & \mathbf{0} & \mathbf{A}_{33} & \mathbf{G}_3 \\ \mathbf{D}_1 & \mathbf{D}_2 & \mathbf{D}_3 & \mathbf{0} \end{bmatrix} \begin{bmatrix} \mathbf{U}^1 \\ \mathbf{U}^2 \\ \mathbf{U}^3 \\ \mathbf{P} \end{bmatrix} = \begin{bmatrix} \mathbf{c}^1 \\ \mathbf{c}^2 \\ \mathbf{c}^3 \\ \mathbf{d}_{in} \end{bmatrix} \tag{3.31}$$

where $\mathbf{A}_{kk}$, $\mathbf{G}_k$, $\mathbf{D}_k$ ($k = 1, \ldots, d$) are $\mathbb{R}^{N_{CV} \times N_{CV}}$ matrixes, having non-zero elements (we note that marking with the *tilde* sign has linearized the initial system of equations, and has simplified the resulting matrix: $\mathbf{A}_{ij} = \mathbf{0}$, $i \neq j$). Solving the system and considering the solution $(\mathbf{U}, \mathbf{P})$ as the values on the new iteration would define a possible iterative process (we note that due to our boundary conditions, the pressure is defined up to a constant). But we use another way to construct $(\mathbf{U}, \mathbf{P})$ from $(\widetilde{\mathbf{U}}, \widetilde{\mathbf{P}})$ based on the SIMPLE method proposed by Patankar (see e.g. [14],[54],[16]). The values of $(\mathbf{U}, \mathbf{P})$ (obtained by the SIMPLE method) in general doesn't satisfy (3.31). In order to describe the algorithm, we need to define some discrete operators.

3.2.1 The operators $\mathcal{U}$, ∇_h.

The operators $\mathcal{U}$, $\mathcal{U}_O/\mathcal{U}_D$. Let us consider the algebraic equations (3.29), (3.30,left) where $\widetilde{\mathbf{U}}$ is known from the previous iteration and assume that $\mathbf{P}$ is given. Then we have a system of dN_{CV} linear equations with dN_{CV} unknowns $\mathbf{U}$. We have simplified the equations in such a way that $\mathbf{U}^m$ can be found independently from other velocity components, by solving a system of linear equations with the matrix $\mathbf{A}_{mm}$ (see (3.31)). Then we can define a solution operator $\mathcal{U}$ for this linear system:

$$\mathcal{U} : \mathbb{R}^{N_{CV}} \times \mathbb{R}^{dN_{CV}} \to \mathbb{R}^{dN_{CV}}, \qquad \mathbf{U} = \mathcal{U}[\mathbf{P}, \widetilde{\mathbf{U}}] = (\mathcal{U}^1[\mathbf{P}, \widetilde{\mathbf{U}}], \ldots, \mathcal{U}^d[\mathbf{P}, \widetilde{\mathbf{U}}]).$$

The matrixes $\mathbf{A}_{mm}$ can be made diagonal–dominant by a proper choice of the relaxation parameter α_u. Therefore $\mathcal{U}$ exists and can be efficiently implemented in a computer program. We note that the matrixes $\mathbf{A}_{mm}$ are not necessarily symmetric (for example due to upwind scheme). In the implementation of $\mathcal{U}^m$ we have used the *BiCGSTAB* solver for sparse matrixes with the *ILU* preconditioner.

If $S_{out} \neq \emptyset$ then we will use two versions of $\mathcal{U}$: $\mathcal{U}_O[\mathbf{P}, \mathbf{U}]$, $\mathcal{U}_D[\mathbf{P}, \mathbf{U}]$. The former solves the momentum equations with "Outlet" conditions, and the latter solves momentum equations where Dirichlet conditions substitute for "Outlet" conditions (in the section 3.2.4 we discuss how to obtain values for the Dirichlet conditions, needed in $\mathcal{U}_D$).

The operators $\nabla_h \cdot$, $\overline{\nabla}_h \cdot$. Let us define now the discrete divergence operator $\nabla_h \cdot$ for the case when on the the boundary we have either Dirichlet or "Symmetry" boundary conditions:

$$\nabla_h \cdot : \mathbb{R}^{dN_{CV}} \to \mathbb{R}^{N_{CV}}, \qquad (\nabla_h \cdot \mathbf{U})(\mathbf{i}) = \sum_{m=1}^{d} \frac{u_{\mathbf{i}}^m - u_{\mathbf{i}-\mathbf{e}_m}^m}{h_{\mathbf{i}}^m} |P_{\mathbf{i}}|, \qquad \mathbf{i} \in \mathbf{i}(\Omega^h), \qquad (3.32)$$

where the discrete variables $u_{\mathbf{i}-\mathbf{e}_m}^m$ defined on the boundary are substituted due to the boundary condition as it was proposed in the Subsection 3.1.7 ($u_{\mathbf{i}}^m$ is a discrete unknown). According to (3.31) the operator $\nabla_h \cdot$ has a matrix form:

$$\nabla_h \cdot \mathbf{U} = \mathbf{D}_1 \mathbf{U}^1 + \ldots + \mathbf{D}_d \mathbf{U}^d - \mathbf{d}_{in},$$

where the non-zero elements of $\mathbf{d}_{in}$ come from the non-zero Dirichlet conditions on the boundary with the normal $\mathbf{n}$ directed opposite to some $\mathbf{e}_k$. Therefore $\nabla_h \cdot$ is not a linear operator. $\nabla_h \cdot \mathbf{U}$ depends only on the discrete vector field related to $\mathbf{U}$. We will apply $\nabla_h \cdot$ to those $\mathbf{U}$, which satisfies (3.30,left).

The operator $\nabla_h \cdot$ can be modified to obtain a linear operator $\overline{\nabla}_h \cdot$: $\mathbb{R}^{dN_{CV}} \to \mathbb{R}^{N_{CV}}$. To define $(\overline{\nabla}_h \cdot \mathbf{U})(\mathbf{i})$ we use the expression from (3.32) where we substitute the zero for $u_{\mathbf{i}}^m$ or $u_{\mathbf{i}-\mathbf{e}_m}^m$ whenever these discrete variables are defined on the boundary. Therefore, the operator $\overline{\nabla}_h \cdot$ depends only on the discrete unknowns $u_{\mathbf{i}}^m$ from $\mathbf{U}$ which are defined between two control volumes for pressure, $P_{\mathbf{i}}$ and $P_{\mathbf{i}+\mathbf{e}_m}$ from Ω^h ($\mathbf{i}, \mathbf{i} + \mathbf{e}_m \in \mathbf{i}(\Omega^h)$). Hence the algebraic equation (3.29) for such $u_{\mathbf{i}}^m$ contains the discrete pressure unknowns.

If $\mathbf{U}$ and $\mathbf{V}$ satisfy the boundary conditions (3.30,left), $\partial\Omega^h = S_{in} \cup S_{sym}$, then

$$\nabla_h \cdot \mathbf{U} - \nabla_h \cdot \mathbf{V} = \overline{\nabla}_h \cdot (\mathbf{U} - \mathbf{V}), \qquad (3.33)$$

since the discrete unknowns $u_{\mathbf{i}}^m$, $v_{\mathbf{i}}^m$ on the boundary has the same values due to the boundary conditions, and the constant values from $\mathbf{d}_{in}$ cancel each other.

Another important property is the following: if $\mathbf{U}$ satisfies the boundary conditions (3.30,left), $\partial\Omega^h = S_{in} \cup S_{sym}$ and $\mathbf{V}$ is arbitrary then

$$\sum_{\mathbf{i} \in \mathbf{i}(\Omega^h)} (\nabla_h \cdot \mathbf{U})(\mathbf{i}) = 0, \qquad \sum_{\mathbf{i} \in \mathbf{i}(\Omega^h)} (\overline{\nabla}_h \cdot \mathbf{V})(\mathbf{i}) = 0 \qquad (3.34)$$

In (3.32) $u_{\mathbf{i}}^m$, $u_{\mathbf{i}-\mathbf{e}_m}^m$ are defined on the faces with the area $|P_{\mathbf{i}}|/h_{\mathbf{i}}^m$. The sum (3.34) contains terms $u_{\mathbf{i}}^m |P_{\mathbf{i}}|/h_{\mathbf{i}}^m$ and $-u_{\mathbf{i}}^m |P_{\mathbf{i}+\mathbf{e}_m}|/h_{\mathbf{i}+\mathbf{e}_m}^m$ cancelling each other for all $u_{\mathbf{i}}^m$ defined between two pressure control volumes $P_{\mathbf{i}}$ and $P_{\mathbf{i}+\mathbf{e}_m}$ from Ω^h. Therefore the second sum is zero. The rest in the first sum contains only mass fluxes through the boundary determined by the boundary conditions. The first sum is exactly the total mass flux from Ω^h and it should be zero due to the compatibility condition (2.58) for the Dirichlet data.

3.2.2 SIMPLE and SIMPLEC algorithms

Using the discrete operators defined above, the numerical problem can be written as:

$$\text{Find} \quad (\overline{\mathbf{U}}, \overline{\mathbf{P}}) \quad \text{such that:} \quad \overline{\mathbf{U}} = \mathcal{U}[\overline{\mathbf{P}}, \overline{\mathbf{U}}], \quad \nabla_h \cdot \overline{\mathbf{U}} = \mathbf{0}. \qquad (3.35)$$

Using the values on the previous iteration $(\widetilde{\mathbf{U}}, \widetilde{\mathbf{P}})$ we can get a preliminary vector $\widehat{\mathbf{U}}$ on the new iteration:

$$\widehat{\mathbf{U}} = \mathcal{U}[\widetilde{\mathbf{P}}, \widetilde{\mathbf{U}}].$$

$\widehat{\mathbf{U}}$ satisfies the boundary conditions $(\partial\Omega^h = S_{in} \cup S_{sym})$, but, in general, $\nabla_h \cdot \widehat{\mathbf{U}} \neq \mathbf{0}$. Using (3.33), (3.35), we have

$$\nabla_h \cdot \overline{\mathbf{U}} - \nabla_h \cdot \widehat{\mathbf{U}} = \overline{\nabla}_h \cdot \left(\overline{\mathbf{U}} - \widehat{\mathbf{U}}\right) = -\nabla_h \cdot \widehat{\mathbf{U}}. \tag{3.36}$$

The main goal is to find $\mathbf{U}$, possibly close to $\overline{\mathbf{U}}$, satisfying the discrete incompressibility condition $\nabla_h \cdot \mathbf{U} = \mathbf{0}$. Then we want to approximate the difference

$$\overline{\mathbf{U}} - \widehat{\mathbf{U}} = \mathcal{U}[\overline{\mathbf{P}}, \overline{\mathbf{U}}] - \mathcal{U}[\widetilde{\mathbf{P}}, \widetilde{\mathbf{U}}]. \tag{3.37}$$

First of all, on the boundary $\overline{\mathbf{U}} - \widehat{\mathbf{U}}$ is zero. Hence we have to approximate $\bar{u}_{\mathbf{i}}^m - \widehat{u}_{\mathbf{i}}^m$ defined between two pressure control volumes. The algebraic equations for $\bar{u}_{\mathbf{i}}^m$ and $\widehat{u}_{\mathbf{i}}^m$ are

$$\frac{a_{\mathbf{i},\mathbf{i}}^m[\overline{\mathbf{U}}]}{\alpha_u}\bar{u}_{\mathbf{i}}^m = \sum_{s,\gamma} a_{\mathbf{i},\mathbf{i}+\gamma\mathbf{e}_s}^m[\overline{\mathbf{U}}]\bar{u}_{\mathbf{i}+\gamma\mathbf{e}_s}^m - b_{\mathbf{i}}^m(\bar{p}_{\mathbf{i}+\mathbf{e}_m} - \bar{p}_{\mathbf{i}}) + c_{\mathbf{i}}^m[\overline{\mathbf{U}}] + \frac{1-\alpha_u}{\alpha_u}a_{\mathbf{i},\mathbf{i}}^m[\overline{\mathbf{U}}]\bar{u}_{\mathbf{i}}^m,$$

$$\frac{a_{\mathbf{i},\mathbf{i}}^m[\widetilde{\mathbf{U}}]}{\alpha_u}\widehat{u}_{\mathbf{i}}^m = \sum_{s,\gamma} a_{\mathbf{i},\mathbf{i}+\gamma\mathbf{e}_s}^m[\widetilde{\mathbf{U}}]\widehat{u}_{\mathbf{i}+\gamma\mathbf{e}_s}^m - b_{\mathbf{i}}^m(\widetilde{p}_{\mathbf{i}+\mathbf{e}_m} - \widetilde{p}_{\mathbf{i}}) + c_{\mathbf{i}}^m[\widetilde{\mathbf{U}}] + \frac{1-\alpha_u}{\alpha_u}a_{\mathbf{i},\mathbf{i}}^m[\widetilde{\mathbf{U}}]\widetilde{u}_{\mathbf{i}}^m$$

respectively. Let us subtract the second equation from the first, denoting $v_{\mathbf{i}}^m = \bar{u}_{\mathbf{i}}^m - \widehat{u}_{\mathbf{i}}^m$, $q_{\mathbf{i}} = \bar{p}_{\mathbf{i}} - \widetilde{p}_{\mathbf{i}}$, $\mathbf{V} = \overline{\mathbf{U}} - \widehat{\mathbf{U}}$, $\mathbf{Q} = \overline{\mathbf{P}} - \widetilde{\mathbf{P}}$:

$$\frac{a_{\mathbf{i},\mathbf{i}}^m[\widetilde{\mathbf{U}}]}{\alpha_u}v_{\mathbf{i}}^m = \sum_{s,\gamma} a_{\mathbf{i},\mathbf{i}+\gamma\mathbf{e}_s}^m[\widetilde{\mathbf{U}}]v_{\mathbf{i}+\gamma\mathbf{e}_s}^m - b_{\mathbf{i}}^m(q_{\mathbf{i}+\mathbf{e}_m} - q_{\mathbf{i}}) + \frac{1-\alpha_u}{\alpha_u}a_{\mathbf{i},\mathbf{i}}^m[\widetilde{\mathbf{U}}](\bar{u}_{\mathbf{i}}^m - \widetilde{u}_{\mathbf{i}}^m) + Rest \tag{3.38}$$

where the *Rest* is:

$$\sum_{s,\gamma}\left(a_{\mathbf{i},\mathbf{i}+\gamma\mathbf{e}_s}^m[\overline{\mathbf{U}}] - a_{\mathbf{i},\mathbf{i}+\gamma\mathbf{e}_s}^m[\widetilde{\mathbf{U}}]\right)\bar{u}_{\mathbf{i}+\gamma\mathbf{e}_s}^m + \left[\frac{1-\alpha_u}{\alpha_u} - \frac{1}{\alpha_u}\right](a_{\mathbf{i},\mathbf{i}}^m[\overline{\mathbf{U}}] - a_{\mathbf{i},\mathbf{i}}^m[\widetilde{\mathbf{U}}])\bar{u}_{\mathbf{i}}^m + c_{\mathbf{i}}^m[\overline{\mathbf{U}}] - c_{\mathbf{i}}^m[\widetilde{\mathbf{U}}] =$$

$$= \sum_{s,\gamma}\left(a_{\mathbf{i},\mathbf{i}+\gamma\mathbf{e}_s}^m[\overline{\mathbf{U}}] - a_{\mathbf{i},\mathbf{i}+\gamma\mathbf{e}_s}^m[\widetilde{\mathbf{U}}]\right)\bar{u}_{\mathbf{i}+\gamma\mathbf{e}_s}^m - (a_{\mathbf{i},\mathbf{i}}^m[\overline{\mathbf{U}}] - a_{\mathbf{i},\mathbf{i}}^m[\widetilde{\mathbf{U}}])u_{\mathbf{i}}^m + c_{\mathbf{i}}^m[\overline{\mathbf{U}}] - c_{\mathbf{i}}^m[\widetilde{\mathbf{U}}].$$

Formally, assuming that $\overline{\mathbf{U}}$, $\widetilde{\mathbf{U}}$ are known, we can consider equations (3.38) together with $v_{\mathbf{i}}^m = 0$ on the boundary as a linear system for $\mathbf{V}$, and define its solution operator $\overline{\mathcal{V}}[\mathbf{Q}; \overline{\mathbf{U}}, \widetilde{\mathbf{U}}]$. From (3.38), (3.36) we obtain a system for $\mathbf{V}$, $\mathbf{Q}$:

$$\mathbf{V} = \overline{\mathcal{V}}[\mathbf{Q}; \overline{\mathbf{U}}, \widetilde{\mathbf{U}}], \qquad \overline{\nabla}_h \cdot \mathbf{V} = -\nabla_h \cdot \widehat{\mathbf{U}}, \tag{3.39}$$

leading to one equation for $\mathbf{Q}$:

$$\overline{\nabla}_h \cdot \overline{\mathcal{V}}[\mathbf{Q}; \overline{\mathbf{U}}, \widetilde{\mathbf{U}}] = -\nabla_h \cdot \widehat{\mathbf{U}}. \tag{3.40}$$

This form is of no use, except that we can demonstrate the idea of the SIMPLE method on it: instead of $\overline{\mathcal{V}}$ in (3.39), (3.40) we will use its coarse simplification which depends explicitly and linearly on the unknown $\mathbf{Q}$, and may depend on the known parameters like $\widetilde{\mathbf{U}}$, $\widehat{\mathbf{U}}$. Although it

is not possible to get $(\overline{\mathbf{U}}, \overline{\mathbf{P}})$ from $(\widehat{\mathbf{U}}, \widetilde{\mathbf{P}})$, using such $\mathbf{V}$ and $\mathbf{Q}$, we still can obtain good values for the new iteration $(\mathbf{U}, \mathbf{P})$, where $\mathbf{U} = \widehat{\mathbf{U}} + \mathbf{V}$ is divergence free: $\nabla_h \cdot \mathbf{U} = \mathbf{0}$.

In order to obtain the simplification of $\overline{\mathcal{V}}$, let us try to express $v_{\mathbf{i}}^m$ from (3.38) explicitly. First, we neglect in (3.38) the *Rest* term. Second, we can either neglect $(\theta_1 = 0)$ or use $(\theta_1 = 1)$ the term

$$\frac{1 - \alpha_u}{\alpha_u} a_{\mathbf{i},\mathbf{i}}^m[\widetilde{\mathbf{U}}](\bar{u}_{\mathbf{i}}^m - \widetilde{u}_{\mathbf{i}}^m) = \frac{1 - \alpha_u}{\alpha_u} a_{\mathbf{i},\mathbf{i}}^m[\widetilde{\mathbf{U}}](v_{\mathbf{i}}^m + \widehat{u}_{\mathbf{i}}^m - \widetilde{u}_{\mathbf{i}}^m).$$

Third, we have the non-diagonal terms $a_{\mathbf{i},\mathbf{i}+\gamma\mathbf{e}_s}^m[\widetilde{\mathbf{U}}]v_{\mathbf{i}+\gamma\mathbf{e}_s}^m$ that still prevent us to express $v_{\mathbf{i}}^m$. In the SIMPLE method we simply neglect them $(\theta_2 = 0)$ and in the SIMPLEC method they are approximated by $a_{\mathbf{i},\mathbf{i}+\gamma\mathbf{e}_s}^m[\widetilde{\mathbf{U}}]v_{\mathbf{i}}^m$ $(\theta_2 = 1)$. Then, instead of (3.38) we have

$$\frac{a_{\mathbf{i},\mathbf{i}}^m[\widetilde{\mathbf{U}}]}{\alpha_u}v_{\mathbf{i}}^m = \theta_2 \sum_{s,\gamma} a_{\mathbf{i},\mathbf{i}+\gamma\mathbf{e}_s}^m[\widetilde{\mathbf{U}}]v_{\mathbf{i}}^m - b_{\mathbf{i}}^m(q_{\mathbf{i}+\mathbf{e}_m} - q_{\mathbf{i}}) + \theta_1\frac{1 - \alpha_u}{\alpha_u} a_{\mathbf{i},\mathbf{i}}^m[\widetilde{\mathbf{U}}](v_{\mathbf{i}}^m + \widehat{u}_{\mathbf{i}}^m - \widetilde{u}_{\mathbf{i}}^m),$$

or, collecting the terms with $v_{\mathbf{i}}^m$ in the left hand side:

$$D_{\mathbf{i}}^m v_{\mathbf{i}}^m = -b_{\mathbf{i}}^m(q_{\mathbf{i}+\mathbf{e}_m} - q_{\mathbf{i}}) + \theta_1\frac{1 - \alpha_u}{\alpha_u} a_{\mathbf{i},\mathbf{i}}^m[\widetilde{\mathbf{U}}](\widehat{u}_{\mathbf{i}}^m - \widetilde{u}_{\mathbf{i}}^m),$$

$$\text{where} \qquad D_{\mathbf{i}}^m = \frac{1 - \theta_1(1 - \alpha_u)}{\alpha_u} a_{\mathbf{i},\mathbf{i}}^m[\widetilde{\mathbf{U}}] - \theta_2 \sum_{s,\gamma} a_{\mathbf{i},\mathbf{i}+\gamma\mathbf{e}_s}^m[\widetilde{\mathbf{U}}].$$

We note that the choice $\theta_1 = 1$, $\theta_2 = 1$ leads to $D_{\mathbf{i}}^m = a_{\mathbf{i},\mathbf{i}}^m[\widetilde{\mathbf{U}}] - \sum_{s,\gamma} a_{\mathbf{i},\mathbf{i}+\gamma\mathbf{e}_s}^m[\widetilde{\mathbf{U}}]$. It is better not to use this case, since we will expect in (3.43) that all $D_{\mathbf{i}}^m$ are positive.

We can define two operators, in order to have a simple expression for $\mathbf{V}$:

$$\mathbf{V} = \mathcal{V}[\widetilde{\mathbf{U}}]\mathbf{Q} + \mathcal{R}[\widetilde{\mathbf{U}}, \widehat{\mathbf{U}}],$$

where the operators $\mathcal{V}$ and $\mathcal{R}$ are defined by

$$\left(\mathcal{V}[\widetilde{\mathbf{U}}]\mathbf{Q}\right)^m(\mathbf{i}) := -\frac{b_{\mathbf{i}}^m}{D_{\mathbf{i}}^m}(q_{\mathbf{i}+\mathbf{e}_m} - q_{\mathbf{i}}), \qquad \mathcal{R}[\widetilde{\mathbf{U}}, \widehat{\mathbf{U}}]^m(\mathbf{i}) := \theta_1\frac{1 - \alpha_u}{\alpha_u}\frac{a_{\mathbf{i},\mathbf{i}}^m[\widetilde{\mathbf{U}}]}{D_{\mathbf{i}}^m}(\widehat{u}_{\mathbf{i}}^m - \widetilde{u}_{\mathbf{i}}^m)$$

when $u_{\mathbf{i}}^m$ is between two pressure control volumes, and are defined by zero otherwise. Returning back to (3.40) we have the so-called pressure-correction equation:

$$\overline{\nabla}_h \cdot \left(\mathcal{V}[\widetilde{\mathbf{U}}]\mathbf{Q}\right) = -\overline{\nabla}_h \cdot \mathcal{R}[\widetilde{\mathbf{U}}, \widehat{\mathbf{U}}] - \nabla_h \cdot \widehat{\mathbf{U}}. \tag{3.41}$$

If we can solve it, then the velocity and pressure on the new iteration are:

$$\mathbf{U} = \widehat{\mathbf{U}} + \mathcal{V}[\widetilde{\mathbf{U}}]\mathbf{Q} + \mathcal{R}[\widetilde{\mathbf{U}}, \widehat{\mathbf{U}}], \qquad \mathbf{P} = \widetilde{\mathbf{P}} + \alpha_p\mathbf{Q}. \tag{3.42}$$

As well as $\mathbf{V} \neq \overline{\mathbf{U}} - \widetilde{\mathbf{U}}$ (after our simplifications), the solution of the pressure correction equation $\mathbf{Q}$ is also different from $\overline{\mathbf{P}} - \widetilde{\mathbf{P}}$. Therefore it is reasonable to make a smaller step from $\widetilde{\mathbf{P}}$ in the direction $\mathbf{Q}$: $0 < \alpha_p \leq 1$. The new velocity $\mathbf{U}$ is divergence–free:

$$\nabla_h \cdot \mathbf{U} = \nabla_h \cdot \widehat{\mathbf{U}} + \overline{\nabla}_h \cdot \left(\mathcal{V}[\widetilde{\mathbf{U}}]\mathbf{Q}\right) + \overline{\nabla}_h \cdot \mathcal{R}[\widetilde{\mathbf{U}}, \widehat{\mathbf{U}}] = \mathbf{0}.$$

3.2.3 Pressure-correction equation

The vector form of the pressure correction equation (3.41) is a system of N_{CV} linear algebraic equations with N_{CV} unknowns that can be written explicitly. Let us take a look at the matrix $\mathbf{G}$ for the linear system. In each row we have a linear equation corresponding to some pressure control volume $P_{\mathbf{i}}$, $\mathbf{i} \in \mathbf{i}(\Omega^h)$. All non-zero elements in this row correspond either to $\mathbf{i}$ or to those $\mathbf{j} \in \mathbf{i}(\Omega^h)$ that $\overline{P_{\mathbf{j}}}$ and $\overline{P_{\mathbf{i}}}$ have a common face. We deal with the connected domain $\Omega = \Omega^h$, therefore each $P_{\mathbf{i}}$ has at least one neighbour. The non-zero coefficients in the row are $(m = 1, \ldots, d)$:

$$g_{\mathbf{i},\mathbf{i}+\mathbf{e}_m} = -\frac{b_{\mathbf{i}}^m}{D_{\mathbf{i}}^m} \frac{|P_{\mathbf{i}}|}{h_{\mathbf{i}}^m} < 0, \quad \text{if } \mathbf{i} + \mathbf{e}_m \in \mathbf{i}(\Omega^h);$$

$$g_{\mathbf{i},\mathbf{i}-\mathbf{e}_m} = -\frac{b_{\mathbf{i}-\mathbf{e}_m}^h}{D_{\mathbf{i}-\mathbf{e}_m}^m} \frac{|P_{\mathbf{i}}|}{h_{\mathbf{i}}^m} < 0, \quad \text{if } \mathbf{i} - \mathbf{e}_m \in \mathbf{i}(\Omega^h); \qquad g_{\mathbf{i},\mathbf{i}} = -\sum_{\mathbf{j} \in \mathbf{i}(\Omega^h) \setminus \{\mathbf{i}\}} g_{\mathbf{i},\mathbf{j}} > 0. \qquad (3.43)$$

Proposition 5 *The matrix $\mathbf{G}$ is symmetric, degenerate, with one dimensional subspace $\ker \mathbf{G} = \{\mathbf{Q} \in \mathbb{R}^{N_{CV}} : \mathbf{G}\mathbf{Q} = \mathbf{0}\}$. The pressure correction equation (3.41) has a solution, unique up to a constant.*

- Symmetry of $\mathbf{G}$.

if we take some $g_{\mathbf{i},\mathbf{j}} \neq 0$, then $\mathbf{i}$ has a neighbour $\mathbf{j}$ as well as $\mathbf{j}$ has a neighbour $\mathbf{i}$. It is enough to consider the case $\mathbf{j} = \mathbf{i} + \mathbf{e}_m$. Then from (3.43) we have

$$g_{\mathbf{i},\mathbf{j}} = g_{\mathbf{i},\mathbf{i}+\mathbf{e}_m} = -\frac{b_{\mathbf{i}}^m}{D_{\mathbf{i}}^m} \frac{|P_{\mathbf{i}}|}{h_{\mathbf{i}}^m}, \qquad g_{\mathbf{j},\mathbf{i}} = g_{\mathbf{j},\mathbf{j}-\mathbf{e}_m} = -\frac{b_{\mathbf{j}-\mathbf{e}_m}^m}{D_{\mathbf{j}-\mathbf{e}_m}^m} \frac{|P_{\mathbf{j}}|}{h_{\mathbf{j}}^m} = -\frac{b_{\mathbf{i}}^m}{D_{\mathbf{i}}^m} \frac{|P_{\mathbf{j}}|}{h_{\mathbf{j}}^m}.$$

$g_{\mathbf{i},\mathbf{j}} = g_{\mathbf{j},\mathbf{i}}$ since $|P_{\mathbf{j}}|/h_{\mathbf{j}}^m = |P_{\mathbf{i}}|/h_{\mathbf{i}}^m$ is the area of the common face.
- $\mathbf{G}$ is degenerate.

Let us take a vector $\mathbf{Q}_0$ with all elements equal to 1. $\mathbf{G}\mathbf{Q}_0 = \mathbf{0}$ since in any row

$$\sum_{\mathbf{j} \in \mathbf{i}(\Omega^h)} g_{\mathbf{i},\mathbf{j}} \times 1 = g_{\mathbf{i},\mathbf{j}} + \sum_{\mathbf{j} \in \mathbf{i}(\Omega^h) \setminus \{\mathbf{i}\}} g_{\mathbf{i},\mathbf{j}} = 0.$$

- rank $\mathbf{G} = N_{CV} - 1$.

rank $\mathbf{G} \leq N_{CV} - 1$ since $\mathbf{Q}_0 \in \ker \mathbf{G}$. Let us construct a minor $\mathbf{G}'$ of order $N_{CV} - 1$, by excluding a row and a column, corresponding to some index $\overline{\mathbf{i}} \in \mathbf{i}(\Omega^h)$. In each row, corresponding to a neighbour of $\overline{\mathbf{i}}$ we will have

$$|g_{\mathbf{i},\mathbf{i}}| > \sum_{\mathbf{j} \in \mathbf{i}(\Omega^h) \setminus \{\mathbf{i},\overline{\mathbf{i}}\}} |g_{\mathbf{i},\mathbf{j}}|,$$

and in other rows of $\mathbf{G}'$:

$$|g_{\mathbf{i},\mathbf{i}}| = \sum_{\mathbf{j} \in \mathbf{i}(\Omega^h) \setminus \{\mathbf{i}\}} |g_{\mathbf{i},\mathbf{j}}|,$$

Therefore, $\mathbf{G}'$ has a weak diagonal dominance. After the control volume $P_{\overline{\mathbf{i}}}$ is deleted from Ω^h, the rest can become disconnected, but any connected part will contain a neighbour of $P_{\overline{\mathbf{i}}}$. This means that if $\mathbf{G}'$ is not irreducible (see [55, p.267]) then every independent subsystem will have a weak diagonal dominance. Consequently, $\det \mathbf{G}' \neq 0$ and rank $\mathbf{G} = N_{CV} - 1$.
- Solvability of the pressure-correction equation (3.41).

The pressure-correction equation is solvable only if the right hand side belongs to $\operatorname{im} \mathbf{G}$. From $\mathbb{R}^{N_{CV}} = \operatorname{im} \mathbf{G} \oplus \ker \mathbf{G}^T$, $\mathbf{G} = \mathbf{G}^T$ we conclude that the vector belongs to $\operatorname{im} \mathbf{G}$ only if it is orthogonal to $\mathbf{Q}_0$, meaning that the sum of all its elements is 0. According to (3.34) we have this property for the right hand side of (3.41).

- To any solution one can add a vector from $\ker \mathbf{G}$: $C\mathbf{Q}_0$ (where C is a constant) to obtain another solution. A difference of two solutions should belong to $\ker \mathbf{G}$. Therefore the solution is unique up to a constant.

Remark 14 *Let $\mathbf{Q}$ and $\mathbf{Q}' = \mathbf{Q} + C\mathbf{Q}_0$ are two solutions of the pressure correction equation. The velocity $\mathbf{U}$ on the new iteration (3.42) is the same since $\mathcal{V}[\widetilde{\mathbf{U}}]\mathbf{Q} = \mathcal{V}[\widetilde{\mathbf{U}}]\mathbf{Q}'$. The new pressure vector is different (3.42): $\mathbf{P} = \widetilde{\mathbf{P}} + \alpha_p \mathbf{Q}$ in the first case and $\mathbf{P} = \widetilde{\mathbf{P}} + \alpha_p \mathbf{Q} + \alpha_p C\mathbf{Q}_0$ in the second. Nevertheless, it is not a problem since the pressure is defined up to a constant.*

Remark 15 *One can fix a value of the solution at some control volume $P_{\bar{1}}$, for example: $q_{\bar{1}} = 0$. Then the modified matrix $\widetilde{\mathbf{G}}$ has only one non-zero element in the $\bar{1}$-th row and column, namely it is 1 on the diagonal. Other part of $\mathbf{G}$ is unchanged. Its determinant is $\det \widetilde{\mathbf{G}} = 1 \times \det \mathbf{G}' \neq 0$.*

Remark 16 *The pressure correction equation is another system of linear algebraic equations that should be solved in the program (after the systems needed for the operators $\mathcal{U}^m$). We use the CG method with ILU preconditioner to solve it.*

3.2.4 Some final remarks about the algorithm.

Up to now we were dealing with the case $\Omega^h = S_{in} \cup S_{sym}$, $S_{out} = \emptyset$: no "Outlet" conditions on $\partial\Omega$. Now we consider the case: $S_{out} \neq \emptyset$. Let us assume that the exact solution for the problem with the "Outlet" conditions $(\mathbf{u}, p)$ exists. It is possible to construct a corresponding problem with Dirichlet conditions on S_{out}, setting the values of $\mathbf{u}$ on S_{out} as a known data. Then $(\mathbf{u}, p)$ can be recovered as a solution of the modified problem, without "Outlet" condition.

This suggests a strategy of interchanging problems with "Outlet" and Dirichlet conditions in approaching the numerical solution by iterative process. Like before, let $\widetilde{\mathbf{U}}$, $\widetilde{\mathbf{P}}$ be the values on the previous iteration. We can solve the system of algebraic equations (with discretized "Outlet" conditions on S_{out}) to obtain

$$\widehat{\mathbf{U}}_O = \mathcal{U}_O(\widetilde{\mathbf{P}}, \widetilde{\mathbf{U}}) \qquad (\text{"O" stands for "Outlet"}).$$

The velocity field related to $\widehat{\mathbf{U}}_O$ (the discrete unknowns together with the discrete variables excluded due to boundary conditions) satisfies neither the discrete continuity equations nor the discrete compatibility condition in general. The latter prevents us to construct the pressure-correction equation (namely, the operator $\nabla_h \cdot$ was defined only for Dirichlet and "Symmetry" boundary conditions). Therefore we add an additional step: we substitute the "Outlet" conditions by Dirichlet conditions that satisfies the discrete compatibility condition, and solve the system of algebraic equations again (but with Dirichlet conditions on S_{out}):

$$\widehat{\mathbf{U}} = \mathcal{U}_D(\widetilde{\mathbf{P}}, \widetilde{\mathbf{U}}) \qquad (\text{"D" stands for Dirichlet}). \tag{3.44}$$

$\widehat{\mathbf{U}}$ satisfies the boundary conditions (Dirichlet, "Symmetry"). We can proceed further with solving the pressure-correction equation (3.41) and constructing the approximation on the new iteration $(\mathbf{U}, \mathbf{P})$ using (3.42).

In general, the Dirichlet conditions on S_{out} and consequently the operator $\mathcal{U}_D$ are not the same on different iterations. In order to obtain values for the Dirichlet condition on S_{out} we do the following. First, we calculate the values of $\widehat{\mathbf{U}}_O$ on S_{out} (the discrete unknowns for velocity components, directed tangential to the boundary can be extrapolated to S_{out} using the Neumann condition). Second, we use the velocity to calculate the total flux $\widehat{F}_{out}$ through S_{out}. The correct value F_{out} (which is in accordance with the compatibility condition) is given by (3.27). In fact,

we need to modify the Dirichlet conditions only for the discrete velocity variables which are defined on the boundary (they determine the fluxes through the boundary). If $\widehat{F}_{out} \neq 0$, then

$$F_{out} = \frac{F_{out}}{\widehat{F}_{out}} \int_{S_{out}} \mathbf{u} \cdot \mathbf{n} \, d\sigma = \int_{S_{out}} \left(\frac{F_{out}}{\widehat{F}_{out}} \mathbf{u} \right) \cdot \mathbf{n} \, d\sigma.$$

Therefore we can use in $\mathcal{U}_D$ the Dirichlet condition $u_{\mathbf{i}}^m = \widehat{u}_{\mathbf{i},O}^m F_{out}/\widehat{F}_{out}$ for any discrete variable $u_{\mathbf{i}}^m$ defined on the boundary S_{out}, where $\widehat{u}_{\mathbf{i},O}^m$ is the value on S_{out}, obtained from $\widehat{\mathbf{U}}_O$. Another case, $\widehat{F}_{out} = 0$ usually happens on the first iteration, if we start from $\widetilde{\mathbf{U}} = \mathbf{0}$. Using, that

$$F_{out} = \int_{S_{out}} \frac{F_{out}}{|S_{out}|} \, d\sigma$$

we can use in $\mathcal{U}_D$ a uniform velocity profile $u_{\mathbf{i}}^m = F_{out}/|S_{out}|$ for any discrete variable $u_{\mathbf{i}}^m$, defined on the boundary S_{out}.

If the iterative process converges (meaning also that $\widehat{\mathbf{U}}_O - \widetilde{\mathbf{U}}$ tends to zero) then the limit solution satisfies the continuity condition ($\widetilde{\mathbf{U}}$) and the discrete momentum equation with "Outlet" boundary conditions on S_{out} ($\widehat{\mathbf{U}}_O$).

$S_{out} = \emptyset$ means that we don't need the operator $\mathcal{U}_O$, we just start from (3.44) where $\mathcal{U}_D$ is the same as the operator $\mathcal{U}$ defined in the Section 3.2.1. If the iterative process converges (meaning also that $\widehat{\mathbf{U}} - \widetilde{\mathbf{U}}$ tends to zero) then the limit solution satisfies the continuity condition ($\widetilde{\mathbf{U}}$) and the discrete momentum equation ($\widehat{\mathbf{U}}$).

We have often used the assumption that the iterative process converges, to be sure that what we obtain at the end is the numerical solution $\overline{\mathbf{U}}, \overline{\mathbf{P}}$ that we are looking for. In general, we cannot guarantee the convergence. This may depend for example on the parameters of the continuous problem, like Reynolds number and the choice of the boundary conditions; or on the chosen discretization formulae; or on the internal parameters of the iterative method, like α_u, α_p, θ_1, θ_2. The algorithm implemented in a computer program needs much more additional parameters, absent in the idealized case that we discussed above. For example, the operators $\mathcal{U}^m$ and $(\nabla_h \cdot \mathcal{V})^{-1}$ give in fact only an approximate solution of the underlying systems of linear algebraic equations. The additional parameters in this case control the precision of the linear solver. It is often the case that solving the linear systems on each iteration with high precision needs much more time resources than just a coarse approximation, and in addition has no advantage in number of iterations needed to approach the final solution.

Remark 17 *We thankfully acknowledge the use in our program of the SparceLib++, IML++, MV++ libraries for solving systems of linear algebraic equations, created by R. Pozo, K. Remington, and A. Lumsdaine. http://math.nist.gov/sparselib/*

3.3 Numerical validation of the algorithm

The algorithm that we used is a modification of the SIMPLE algorithm for Navier-Stokes equations and in particular (for example when $\Omega_p = \emptyset$) it should be able to solve Navier–Stokes system of equations. This suggests that the first tests can be just some standard test for Navier-Stokes solvers.

The 2D lid-driven cavity test Let us consider a 2D cavity $[0,1] \times [0,1]$ with Dirichlet boundary conditions $\mathbf{u} = (1,0)$ on the top $y = 1$ and the no-slip condition $\mathbf{u} = \mathbf{0}$ on the other boundaries.

The Reynolds number is calculated with $L = 1$, $U = 1$, $\rho = 1$: $Re = 1/\mu$. The geometry and computed velocity fields are presented in Fig.3.5 for Reynolds numbers equal to 1000 (left) and 3200 (right).
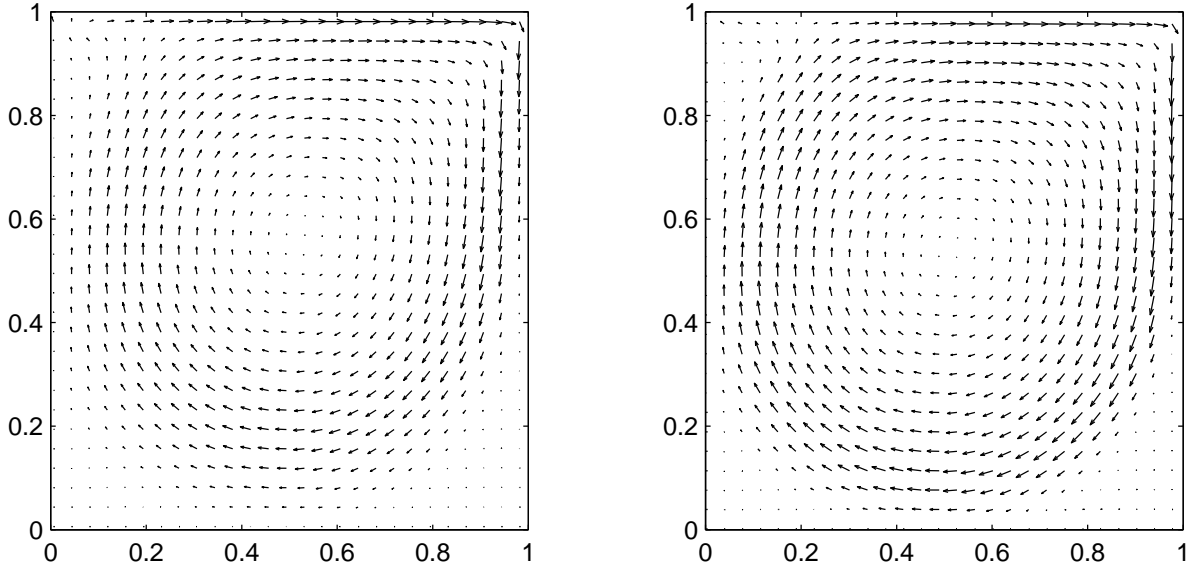
Figure 3.5: Velocity fields for the lid-driven cavity test problem. Re=1000 (left) and Re=3200 (right)

We have compared our velocity solution with the results presented in [18] see Fig.3.6 (Re=1000) and Fig.3.7 (Re=3200). The comparison was done on two lines $x = 0.5$ and $y = 0.5$ for velocity components ($\mathbf{u} = (u, v)$) which are perpendicular to the corresponding lines: $u(0.5, y)$, $y \in [0, 1]$ (blue color) and $v(x, 0.5)$, $x \in [0, 1]$ (red color). The circles are values presented in [18] and the continuous lines show our solution calculated on different uniform grids. The line numbers are related to the grid size in the following way: 1:20x20; 2:40x40; 3:80x80; 4: 160x160; 5:320x320. Similar comparisons were obtained also for smaller Reynolds numbers: 100, 400.

A flow in a channel with porous media   In the Section 2.1 we considered a fully developed flow in a channel and an exact solution was obtained in Ω_{far} provided $\frac{\partial u}{\partial y} = 0$ there.

Here we consider a 2D problem in a channel (see Fig.3.8) $\Omega = (0, 6) \times (0, 1)$ where porous media domain is $\Omega_p = (1, 6) \times (0, 0.5)$. The boundary conditions are: no-slip conditions on the solid boundaries of the channel $y = 0$ and $y = 1$, given inlet velocity $\mathbf{u} = (1, 0)$ on the left side $x = 0$ and "Outlet" condition on the right side $x = 6$ (this condition seems to be consistent with our assumptions for the fully-developed flow).

Our purpose is to use the model (1.2) in Ω_f, (1.37) in Ω_p with the interface conditions (1.29), (1.34) for numerical solution in 2D and to compare the solution in Ω_{far} with the (ODE) analytical solution from the Section 2.1.

For the calculations we need to specify $\mathbf{f}$, μ, $\tilde{\mu}$, $\mathbf{M}$, $\mathbf{K}$. The right hand side was not taken into account in the Section 2.1 therefore $\mathbf{f} \equiv \mathbf{0}$ for the numerical calculations. To make our tests more rich in content, we can require effective viscosity in Ω_p to be different from the fluid viscosity: $\mu = 1$, $\mu_{eff} = 5$.

We present here results of two tests, different in the parameters $\mathbf{M}$ and $\mathbf{K}$. The parameter
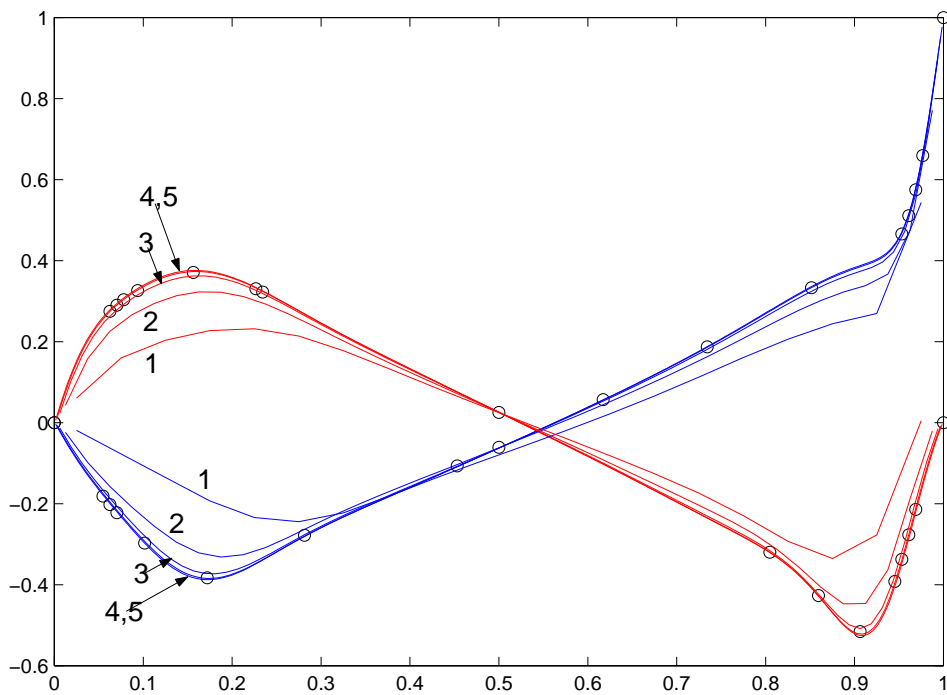
Figure 3.6: Velocity profiles $u(0.5, \cdot)$ (blue), $v(x, 0.5)$ (red). Circles – benchmark solution. $Re = 1000$
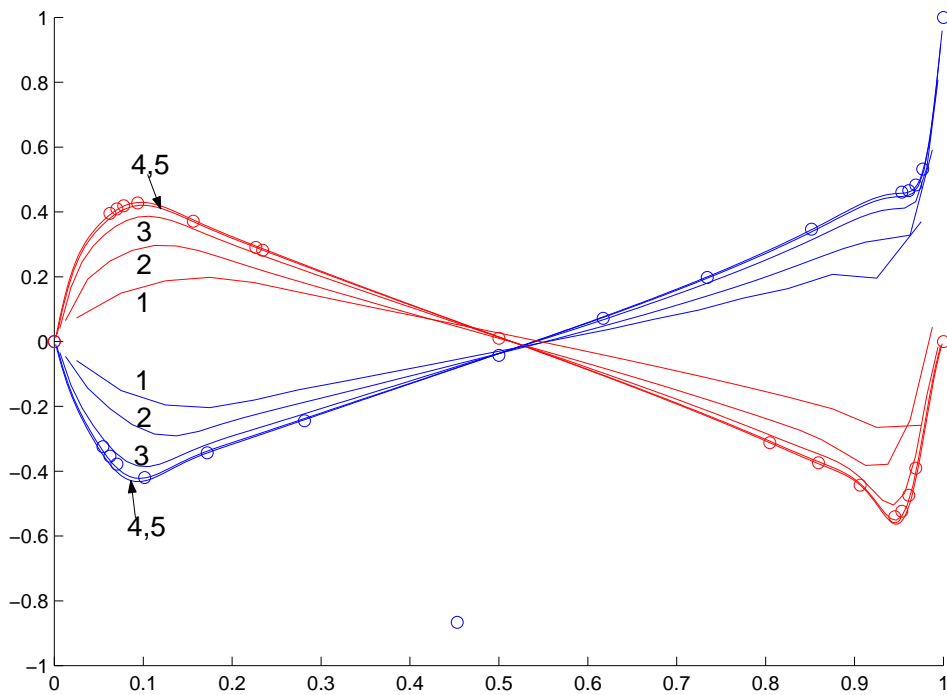
Figure 3.7: Velocity profiles $u(0.5, \cdot)$ (blue), $v(x, 0.5)$ (red). Circles – benchmark solution. $Re = 3200$

$\mathbf{M}'$ in the "laboratory system" and the permeability $\mathbf{K}$ in Ω_p are

$$\text{test 1:} \qquad \mathbf{M}' = \begin{bmatrix} 40 & 0 \\ 30 & 0 \end{bmatrix}, \qquad \mathbf{K} = 0.08^2 \mathcal{K}_{II}$$

$$\text{test 2:} \qquad \mathbf{M}' = \begin{bmatrix} 800 & 0 \\ 600 & 0 \end{bmatrix}, \qquad \mathbf{K} = 0.008^2 \mathcal{K}_{II},$$

where the non-scalar permeability $\mathcal{K}_{II}$ is from (1.16). $\mathbf{K}$ and $\mathbf{M}$ were chosen to have a magnitude of order $\bar{\varepsilon}^2$, $\bar{\varepsilon}^{-1}$ respectively. The porous medium for the second test has smaller pores than the porous medium for the test 1.

$\mathbf{M}'$ we will use to define $\mathbf{M}$ on the interface:

on (x, y): $x \in [1, 6], y = 0.5$ we can set $\mathbf{M} = \mathbf{M}'$ since $\mathbf{n} = (0, 1)^T$;

in order to obtain $\mathbf{M}$ on (x, y): $x = 1$, $y \in [0, 0.5]$ we should choose coordinate transformation $\mathbf{C}$ which transforms the normal $\mathbf{n} = (-1, 0)$ into $(0, 1)$ and to use (2.43). In 2D there are two possibilities:

$$\mathbf{C} = \begin{bmatrix} 0 & 1 \\ -1 & 0 \end{bmatrix} \qquad \text{or} \qquad \mathbf{C} = \begin{bmatrix} 0 & -1 \\ -1 & 0 \end{bmatrix}$$

depending on whether the tangential vector $(0, 1)$ transforms into $(1, 0)$ or $(-1, 0)$. We have chosen the first variant. Then $\mathbf{M}$ on $x = 1$ is given by

$$\mathbf{M} = \begin{bmatrix} 0 & -1 \\ 1 & 0 \end{bmatrix} \begin{bmatrix} M'_{11} & M'_{12} \\ M'_{21} & M'_{22} \end{bmatrix} \begin{bmatrix} 0 & 1 \\ -1 & 0 \end{bmatrix} = \begin{bmatrix} M'_{22} & -M'_{21} \\ -M'_{12} & M'_{11} \end{bmatrix} \tag{3.45}$$

The 2D solution $(\mathbf{u}_N, p_N)$ (N is for "numerical") was calculated using two grids for the first test: 120x100, 240x200 and tree grids for the second test: 120x100, 240x200, 480x400. The geometry and velocity fields calculated on the finest grids are presented in Fig.3.8 (test 1), Fig.3.12 (test 2); the pressure fields are plotted in Fig.3.9 (test 1) and Fig.3.13 (test 2).

We suppose that the channel is long enough and the region $(4.5, 5.5) \times (0, 1)$ can be taken as Ω_{far} since the velocity profiles $u_N(4.5, \cdot)$ and $u_N(5.5, \cdot)$ almost coincide for all calculations see for example Fig.3.10 (test 1, grid 120x100), Fig.3.14 (test 2, grid 480x400) where blue points and red circles correspond to the 2D numerical velocity component u_N plotted on blue and red lines in Fig.3.8,3.12. The pressures along blue and red lines in Ω_f are almost constants also for all calculations: $p_N(4.5, \cdot) \approx P_1$ and $p_N(5.5, \cdot) \approx P_2$ (the values P_1, P_2 are of course test and grid dependent:

	120×100	240×200	120×100	240×200	480×400
P_1 :	-350.7871	-350.3349	-362.2892	-362.3589	-361.977
P_2 :	-443.47185	-443.1095	-457.76195	-458.0489	-457.7385

the left table contains values for the first test, right for the second. The pressure was fixed by setting $p_N(0.5, 0.5) = 0$

These values can be used to calculate "input" parameters for the ODE problem $P = (P_1 - P_2)/(x_{max} - x_{min})$ and $p^0 = P_1$. Then 1D solution $(\mathbf{u}_A, p_A)$ (A is for "analytical") can be explicitly written in Ω_{far} using (2.15), (2.16), (2.13), (2.14), (2.24)-(2.26) and (2.33). We note that the analytical solution $(\mathbf{u}_A, p_A)$ depends on the calculated numerical solution $(\mathbf{u}_N, p_N)$. On other grids the values P_1 and P_2 are different and consequently the analytical solutions are also different.

The comparison of u_N with u_A and p_N with p_A are presented in Fig.3.10, 3.11 (test 1) and Fig.3.14, 3.15 (test 2).

The Fig.3.10 shows the comparison of the horizontal velocity components $u_N(4.5, \cdot)$ (blue points), $u_N(5.5, \cdot)$ (red circles) calculated on the grid 120x100 for the test 1 and the corresponding $u_A(5, \cdot)$ (black dashed line) (they are given at different x since we additionally need to check the assumption for Ω_{far} that $\frac{\partial u}{\partial x} \approx 0$). Two small subfigures on the right show magnifications of two critical places: around the interface point $y = 0.5$ (down) and near the maximal velocity where the maximal numerical error is expected.

Similar, the Fig.3.14 shows the velocity comparison for the second test. Different from the previous case the grid for numerical solution is 480x400 and due to the large number (400), the blue points and the red circles were substituted by blue and red continuous lines to indicate $u_N(4.5, \cdot)$ and $u_N(5.5, \cdot)$ respectively in the large subfigure. We note that it is not easy to distinguish these three lines there.

The pressure p_N and p_A from the first test are compared in Fig.3.11. Two left subfigures show $p_N(5, \cdot)$ (green continuous line) calculated on the grids 120x100 (left subfigure), 240x200 (middle subfigure) and corresponding $p_A(5, \cdot)$ (black dashed line). In both cases p_N and p_A are quite close to each other. The difference can be seen in the right subfigure where both left and middle subfigures are combined and magnified around $x = 0.3$. Blue lines are for the grid 240x200: continuous (num. 1) $- p_N(5, \cdot)$, dashed (num. 2) $- p_A(5, \cdot)$. Red lines are for the grid 120x100: continuous (num. 3) $- p_N(5, \cdot)$, dashed (num. 4) $- p_A(5, \cdot)$.

Fig.3.15 presents a similar comparison for the second test. There is no magnification since the difference is visible, all three subfigures corresponds to different grids: 120x100 (left), 240x200 (middle), 480x400 (right). According to the pressure comparison for tests 1 and 2 the numerical solution corresponding to porous media with smaller pores is less accurate than those with large pores. The accuracy obtained on the grid 120x100 for the first test was not achieved even on the grid 480x400 for the second test.

The relative difference between p_N and p_A is much smaller if we take into account the total pressure variation for the problem (see for example Fig.3.9) is around 450 instead of the pressure variation over the line $x = 5$ which is around 20 (see Fig.3.11). But we should also note that in the numerical scheme the interface velocity was calculated using the 1D solution (see expressions (3.10) (3.20)). It means that the scheme was optimized for the parallel flow problems. We can compare with the standard case where the linear interpolations (from (3.9), (3.19)) were used to predict the tangential velocity on the interface without employing the 1D solution. In the Fig.3.16 the pressure $p_N(5, \cdot)$ calculated by this way is compared with corresponding $p_A(5, \cdot)$. The left subfigure is for the grid 120x100, test 1; other two are for the test 2 calculated for the grid 240x200 (middle) and 480x400 (right).
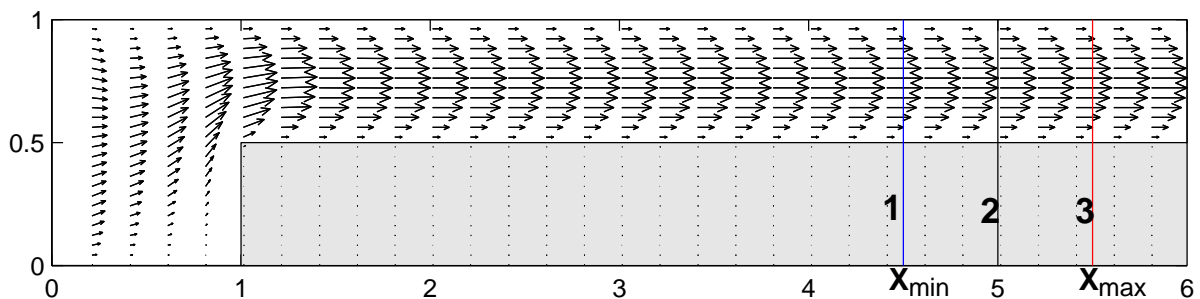
Figure 3.8: Geometry and velocity field in the channel, test 1
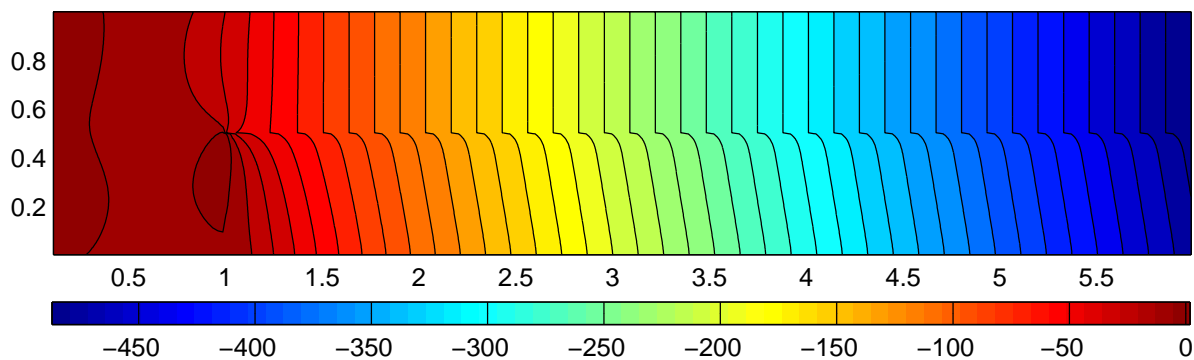
Figure 3.9: Pressure field in the channel, test 1
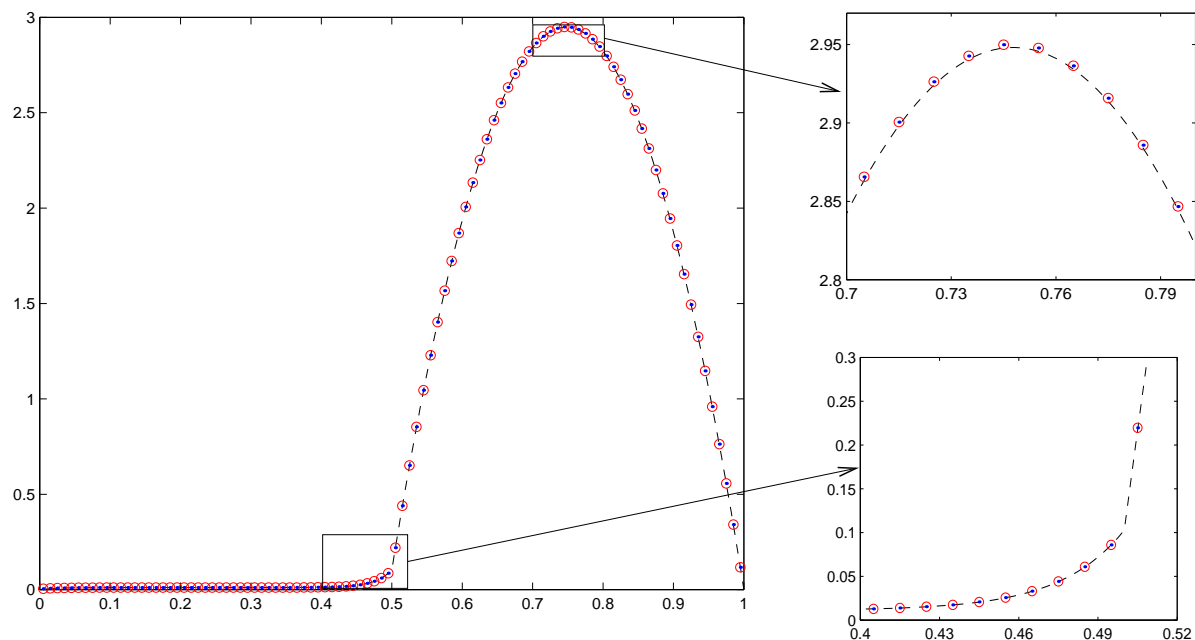
Figure 3.10: Velocity comparison: $u_N(x_{min}, \cdot)$ (blue points), $u_N(x_{max}, \cdot)$ (red circles) and corresponding $u_A(5, \cdot)$ (dashed black line), test 1
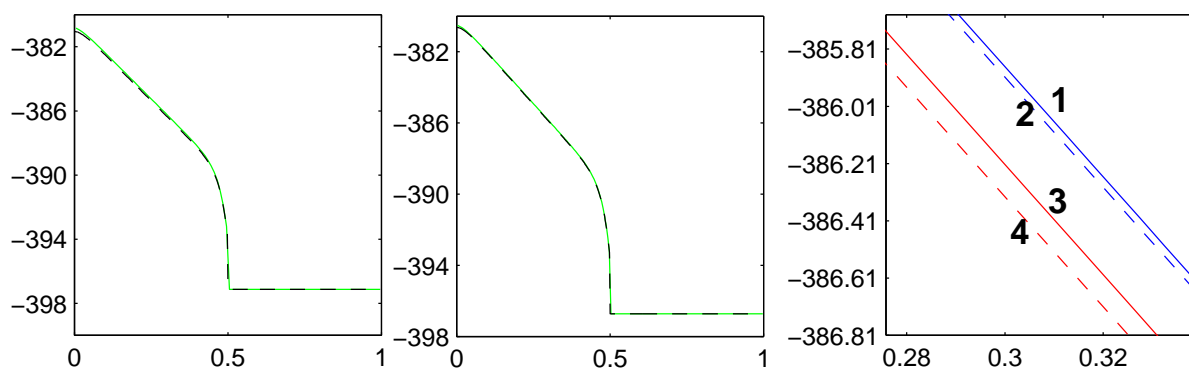
Figure 3.11: Pressure comparison: $p_N(5, \cdot)$ (continuous line) and corresponding $p_A(5, \cdot)$ (dashed line). Grids for $p_N(5, \cdot)$: 120x100(left), 240x200(middle), magnification of both (right), test 1
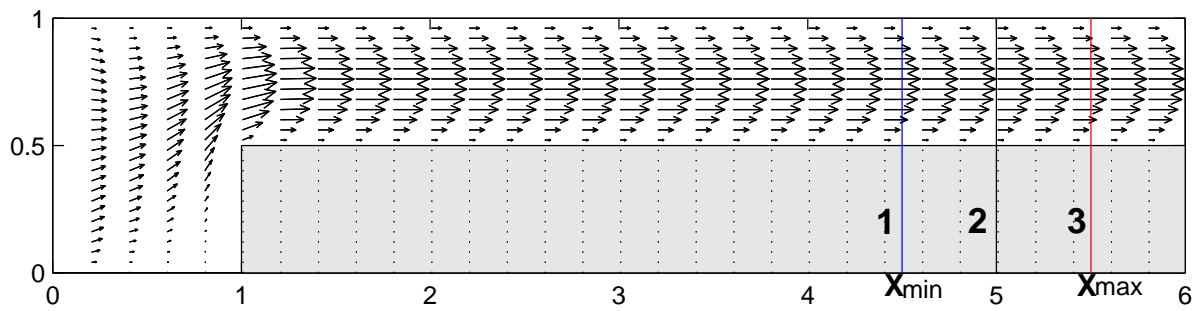
Figure 3.12: Geometry and velocity field in the channel, test 2
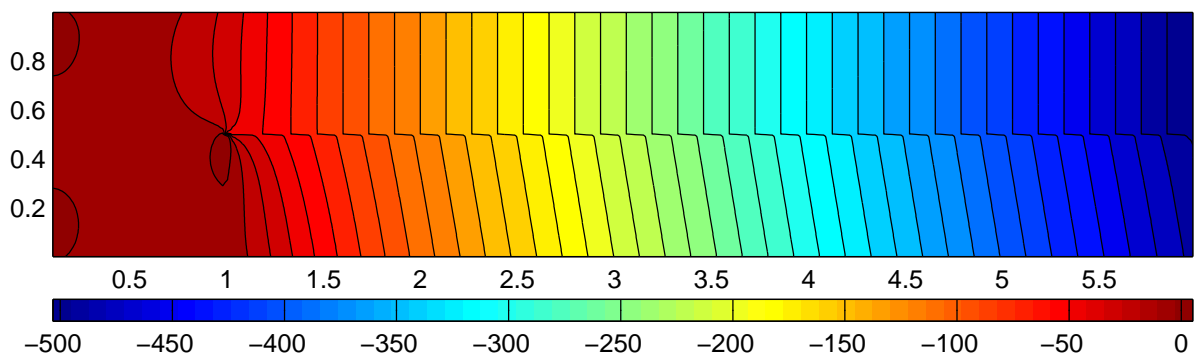
Figure 3.13: Pressure field in the channel, test 2
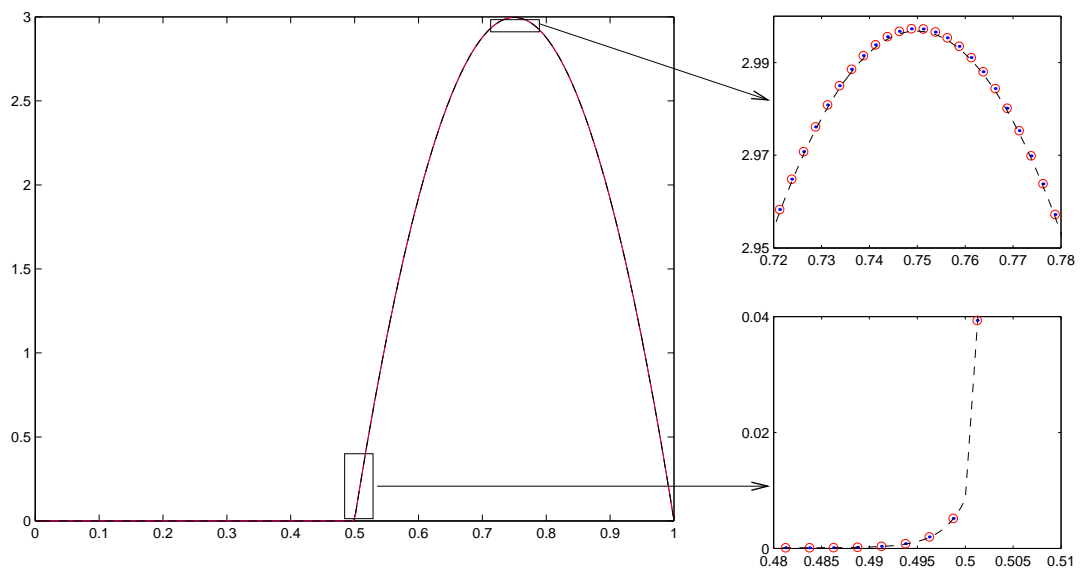
Figure 3.14: Velocity comparison: $u_N(x_{min}, \cdot)$ (blue), $u_N(x_{max}, \cdot)$ (red) and corresponding $u_A(5, \cdot)$ (dashed black line), test 2
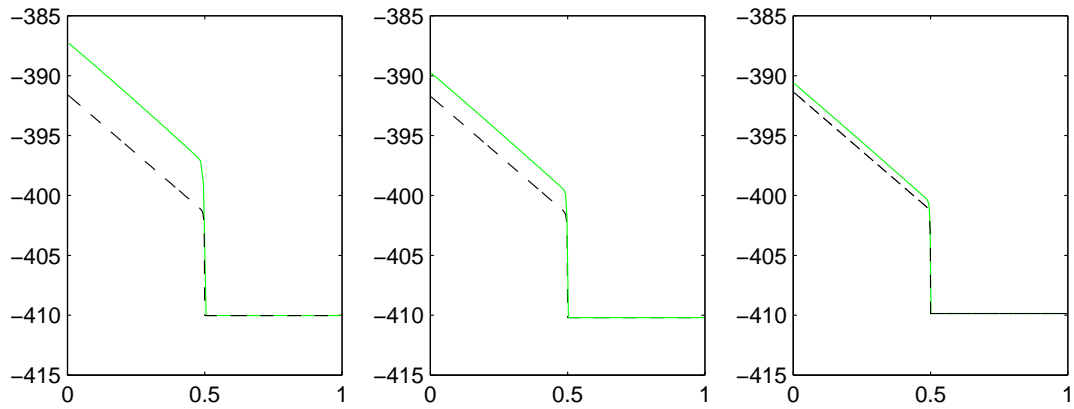
Figure 3.15: Pressure comparison: $p_N(5, \cdot)$ (continuous line) and corresponding $p_A(5, \cdot)$ (dashed line). Grids for $p_N(5, \cdot)$: 120x100(left), 240x200(middle), 480x400 (right), test 2
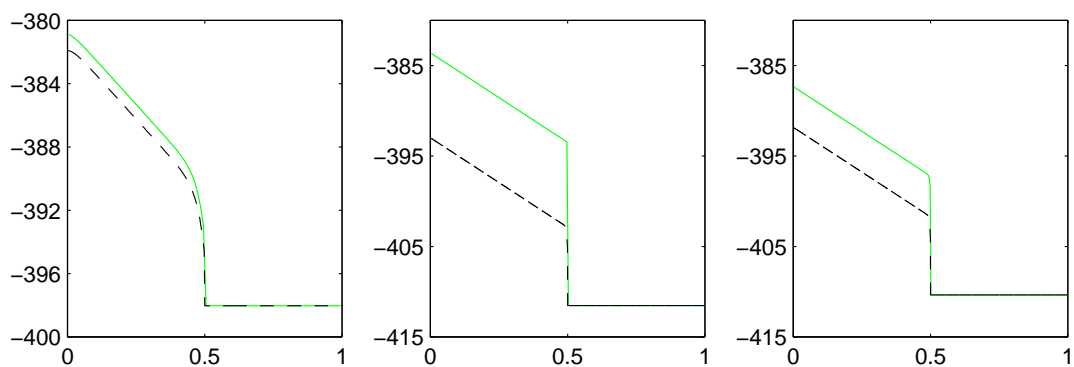
Figure 3.16: p_N without 1D interpolation: $p_N(5, \cdot)$ (continuous line) and corresponding $p_A(5, \cdot)$ (dashed line). Grids: test 1, 120x100(left); test 2, 240x200(middle), 480x400 (right)

Chapter 4

Validation of the models

In the preceding Chapters we described the (Navier-)Stokes-Brinkman model (equipped with the Ochoa-Tapia&Whitaker interface conditions), as well as the numerical algorithm for solving the arisen system of PDEs. This Chapter deals with the validation of the model via comparisons with direct numerical simulation of flows at micro-level. The idea is to compare the solution at a micro level, when the Stokes (or Navier–Stokes) equations are governing the flow in the complex (micro) geometry, with the solution at a macro level, when the (Navier–)Stokes-Brinkman model is used in homogeneous domain. That is, direct numerical simulations are used for validation of the model. Nowadays this can not be done for arbitrary porous media due to limitations on the computer resources. Therefore, we consider relatively simple samples of porous media, which are chosen in accordance with the following requirements.

(i). First of all, we restrict ourselves to 2D case (the real porous media are tree-dimensional). This restriction allows us to have around 1000 discretization points in each direction on the finest grid.

(ii). Second, the ratio of typical pore size to the characteristic size of the problem (usually assumed to be a small parameter for porous materials) for our calculations is bounded from below, due to the need to resolve pores by a grid. Moreover, we want to be able to evaluate the numerical error on a consequence of refined grids. As a result, the ratio that we are able to deal with is much larger than what can be found in many practical problems.

(iii). Third, we do not use micro-geometries, obtained (e.g. via micro tomography) from some real porous material. Instead, we design ourselves (artificial) micro-geometry, which satisfies the following requirements:

- the solid structure should be aligned with the used grid elements (in our case it means that a rectangular should be the basic element for assembling the solid matrix);

- the solid matrix is periodic.

The last requirement, the periodicity of the porous media, is suitable for a straightforward calculation of the permeability (see also (1.11)). We use two different unit cells (see Fig.1.2), from which we assemble periodic porous media. We use I or II signs to emphasize that the porous medium is assembled from the periodic repetition of the unit cell CG I or CG II respectively. The permeability, used in the macro problem is determined from (1.14), where $\varepsilon = \bar{\varepsilon}$, $\mathcal{K}$ is either $\mathcal{K}_I$ or $\mathcal{K}_{II}$ (1.16), depending on what cell geometry (i.e., CG I or CG II) was used to construct the solid matrix.

To solve the macroscopic problem, one needs also to define the porous domain Ω_p. This is equivalent to defining the exact location of the porous–fluid interface $\Sigma = \partial\Omega_p \cap \partial\Omega_f$. Our porous medium is built from unit cells. Therefore it is reasonable to define Ω_p as an union

of the unit cells. That is, the interface coincides with the outer cell boundaries (not with the boundary of the solid matrix).

All flow problems, considered here, are solved in open regions. If nothing else is specified, a velocity profile is prescribed at the inlet, while soft "Outlet" boundary conditions are prescribed at the outlet.

Several test problems for coupled flows in plain and porous media are solved and analyzed in the next sections. They cover separately the cases when the main flow is perpendicular to the porous medium, when it is parallel to the porous medium, and when it is inclined. In some of the test cases the inlet and the outlet are completely separated by the porous medium, in other cases there exist pure liquid subregion, connecting the inlet and the outlet. In our understanding, these test cases represent qualitatively the most of the plain and porous media combinations, observed in the real life problems. In the most of our test problems we consider the (Navier-)Stokes-Brinkman system, equipped with continuous stress tensor, or with jump stress tensor interface conditions as a macroscopic model. The first section, however, deals with the usage of another model: the Navier-Stokes equations in the free fluid subregion, and the Darcy law in the porous subregion.

4.1   Can there be a pressure jump on the interface when coupling Navier–Stokes and Darcy equations?

The aim of the results, presented in this section, is to contribute to the discussions on the coupling conditions between Navier-Stokes and Darcy equations. Although this thesis is devoted to the Navier–Stokes–Brinkman model, analysis of the above mentioned coupling is also of interest for us (in the Section 2.1 we investigated how the Beavers–Joseph and the pressure jump conditions can be approximated with the proper choice of $\mathbf{M}$). The used here direct numerical simulation at a micro level allows us to discuss validity of the different coupling conditions and of different models for the porous media.

One of the intuitive interface conditions for coupling Navier–Stokes in Ω_f with Darcy law in Ω_p is the continuity of the pressure (see the literature review in Chapter 1). Such a condition was proposed in [12] for the case of the Stokes equations and Darcy law on the base of asymptotical considerations. The authors concluded, that in the considered case the pressure variation across the interface is of the same order, as the pressure variation along a cell face, aligned with the interface. Using the fact, that the length of the unit cell is small, compared to the size of the domain, they suggested to use the pressure continuity condition on the interface, as a low order asymptotic approximation. In [50], the pressure interface condition was investigated numerically. A channel with periodic porous media, constructed either from in-line, or from staggered arrangement cylinders, was considered there. Solving the Navier-Stokes equations, the authors calculated the pressure difference across the interface. This difference is calculated from two limit values for the pressure on the interface: one is computed by averaging the pressure from the fluid side, and another by averaging the pressure from the porous medium side. The conclusion, made in [50] was that for small Reynolds number, the pressure difference across the interface is negligible even in comparison with the pressure variation along the cell side, aligned with the interface. That is, for the flow without convective terms and geometries considered in from [50], the pressure jump effect is even smaller than it was expected in [12]. Thus, the pressure continuity condition is a correct assumption in this case. It was further reported in [50], that the pressure difference across the interface becomes more significant for higher Reynolds numbers. These results are presented in [50, Fig. 6(c)] for the in-line arrangement of the cylinders. It has to be noted that the 2-D geometry, chosen in [50] for the direct numerical

simulation, is symmetric with respect to the vertical line passing through centers of all solid circles in a certain column; and the in-line arrangement is square-periodic, and as such it belongs to the case considered in [25]. Therefore, the constant C_ω^{bl} from (1.28) should be zero for the in-line arrangement due to Remark 3.9 in [25], meaning that no pressure jump is expected for that geometry. In this way, the theoretical analysis from [25] explains the observed in [50] zero pressure jump by the symmetry of the particular microgeometry. For more general (periodic) geometries, the pressure jump condition (1.26) was suggested in [25] on the base of asymptotic analysis. The article [25] contains also a numerical method for solving the boundary layer problem (1.27) and for calculating the coefficients C_1^{bl}, C_ω^{bl} from (1.28) for two types of cell geometries. The cell with inclined ellipse as an obstacle leads to a non-zero coefficient C_ω^{bl} (namely $C_1^{bl} = -0.52$, $C_\omega^{bl} = -0.45$). Therefore, the theory from [25] predicts a pressure jump on the interface of the porous media constructed from this periodicity cell. Up to our knowledge, the direct numerical simulations were not performed earlier to demonstrate the pressure jump effect. Therefore, we present such simulations in this section.

We have chosen the periodic geometries drawn in Fig.1.2: symmetric (CG I) and non-symmetric (CG II) with respect to the vertical line $y^1 = 1/2$. For the case CG I the constant $C_{\omega,I}^{bl}$ should be zero. Although the constant $C_{\omega,II}^{bl}$ related to the case CG II is not known, the solid obstacle there is somehow similar to the inclined ellipse from [25] reflected with respect to the line $y^1 = 1/2$. The constants $\tilde{C}_1^{bl}$, $\tilde{C}_\omega^{bl}$ related to the cell with the reflected ellipse can be calculated using C_1^{bl}, C_ω^{bl}:

$$\tilde{C}_1^{bl} = C_1^{bl} = -0.52, \qquad \tilde{C}_\omega^{bl} = -C_\omega^{bl} = 0.45 \qquad (4.1)$$

The reason is that the solutions of these two boundary layer problems (see (1.27)) for the inclined ellipse from [25] and for the reflected ellipse are related as follows:

$$\tilde{\beta}_{bl}^1(y^1, y^2) = \beta_{bl}^1(1 - y^1, y^2), \quad \tilde{\beta}_{bl}^2(y^1, y^2) = -\beta_{bl}^2(1 - y^1, y^2), \quad \tilde{\omega}_{bl}(y^1, y^2) = -\omega_{bl}(1 - y^1, y^2).$$

since, for example, the first momentum equation in (1.27) is:

$$-\triangle_{\mathbf{y}} \tilde{\beta}_{bl}^1(y^1, y^2) + \frac{\partial \tilde{\omega}_{bl}}{\partial y^1}(y^1, y^2) = -\frac{\partial^2 \beta_{bl}^1}{\partial (y^1)^2}(1 - y^1, y^2)(-1)^2 - \frac{\partial^2 \beta_{bl}^1}{\partial (y^2)^2}(1 - y^1, y^2)$$

$$-\frac{\partial \omega_{bl}}{\partial y^1}(1 - y^1, y^2)(-1) = -\triangle_{\mathbf{y}} \beta_{bl}^1(1 - y^1, y^2) + \frac{\partial}{\partial y^1} \omega_{bl}(1 - y^1, y^2) = 0.$$

This idea was used in the Remark 3.9 from [25] to show that the symmetry implies $C_\omega^{bl} = 0$.

Although the geometry for the case CG II is only a rude approximation to the reflected ellipse, we expect that $C_{\omega,II}^{bl}$ is non-zero, and the pressure jump effect can be observed. Let us describe the setup for our direct numerical simulation. The geometry for both test problems (test I and test II), as well as the calculated pressure fields, are presented in Fig.4.1 and Fig.4.6. The channels $\Omega = (0, 4) \times (0, 0.8)$ have solid top and bottom walls. Uniform velocity is given on the left side, while "Outlet" condition is prescribed on the right side. The artificial porous media $\Omega_p = (0.51, 2.99) \times (0, 0.48)$ for the test II is obtained as a periodic ensemble from the cell geometry CG II. For the test I, $\Omega_p = (0.5, 3.02) \times (0, 0.48)$, and it is based on the cell geometry CG I. We have $\varepsilon_{II} = 0.08$ and $\varepsilon_I = 0.06$, respectively. We could not set the porous media up to the end of the channel, otherwise the "Outlet" conditions would violate the flow. The flow is governed by the Stokes equations. The calculations were done on three nested grids: 1600x320 (solid line), 800x160 (dashed line), 400x80 (dotted line) to check the convergence of the numerical solution.

Magnifications of the pressure field near the interface are given in Fig.4.2 and 4.7. Although the pressure field is not periodic, one can see that there are two patterns for isobars: one of them is periodically repeated in both directions inside Ω_p and another is periodically repeated in the horizontal direction near the interface.

The plots of the (microscopical) pressure along the various vertical lines (namely, $x = 1.5$, $x = 1.55$, $x = 2.0$, $x = 2.05$) are presented in the four figures. First two figures, Fig.4.3 and Fig.4.4, concern the cell geometry CG II. Next two figures, Fig.4.8, and Fig.4.9, concern the cell geometry CG I. The pressure plot is not a continuous line: the gaps appear when the vertical lines intersect the solid obstacles. The pressure variation near the interface is definitely higher, compared to the pressure variation inside Ω_p. This is true for both microgeometries, CG II and CG I, as it can be seen in Fig.4.2, Fig.4.7, as well as in Fig.4.3, Fig.4.4, Fig.4.8, and Fig.4.9. The symmetry of the geometry CG I is the reason why the pressure values below the narrow interfacial region are practically the same, as the pressure values above the interface. (see Fig.4.7). However, this is not the case for the geometry CG II. As it can be seen in Fig.4.2, Fig.4.3, and Fig.4.4, the pressure values above and below the interface are different for the cell geometry CG II. More informative are the plots of the pressure averaged over the ε_{II}-squares. They are presented in Fig.4.5: the averaged pressures in the porous part are inclined black lines which rapidly decrease near the interface to match the constant values in the free fluid part. This rapid change in the interfacial region can be understood as a jump in the effective pressure (given, e.g., by the green dashed lines).

The pressure gradient in Ω_p (see Fig.4.5 (left)) is approximately given by:

$$P = \frac{\partial p}{\partial x} \simeq \frac{1211.3 - 1199.6}{0.05} = 234,$$

where $1211.3 - 1199.6$ is approximately the gap between two pressure profiles at $x = 1.5$ and $x = 1.55$ in Fig.4.5 (left). Then, the pressure difference across the cell in the longitudinal direction, $\varepsilon_{II}P$, $\varepsilon_{II}P \simeq 0.08 \times 234 \simeq 18.7$, is comparable with the value of the jump which is $\simeq 9$ (see the green dashed line in Fig.4.5,left). Does this mean that the jump effect is small and can be neglected (in our problem the total pressure difference is around 700 (see Fig.4.1))? Let us make a rough estimation for the jump, using the approach from [25]. The profile for the horizontal velocity component $u(y)$ is given by $u(y) = u_{eff}(y - 0.48)$ where u_{eff} is from (2.17) since the interface is not at $y = 0$, but at $y = 0.48$. The pressure jump condition (1.26) is written as

$$p(x, 0.48 - 0) - p(x, 0.48 + 0) = \mu C_{\omega,II}^{bl}\frac{\partial u}{\partial y}(0.48) = \mu C_{\omega,II}^{bl}\frac{\partial u_{eff}}{\partial y}(0) = C_{\omega,II}^{bl}\frac{Ph^2}{2(h + \alpha)} \quad (4.2)$$

where $\alpha = -\varepsilon_{II}C_{1,II}^{bl}$, $\mu = 1$. Taking into account the approximate nature of our calculations, let us substitute the unknown coefficients $C_{1,II}^{bl}$, $C_{\omega,II}^{bl}$, by the known $\tilde{C}_1^{bl}$, $\tilde{C}_\omega^{bl}$ from (4.1). h is the width of the pure fluid part in the channel: $h = 0.8 - 0.48 = 0.32$. Thus, the pressure jump can be estimated by

$$p(x, 0.48 - 0) - p(x, 0.48 + 0) \simeq P\frac{\tilde{C}_\omega^{bl}h^2}{2(h - \varepsilon_{II}\tilde{C}_1^{bl})} = P\frac{0.45 \times 0.32^2}{2(0.32 + 0.08 \times 0.52)} = 0.064P = 15.0$$

This estimation for the pressure jump, $0.064P = 15$, is comparable with our numerical jump, which is 9. Further on, for this problem it is comparable also with the pressure difference across the cell in the longitudinal direction, $\varepsilon_{II}P \simeq 18.7$.

If one considers a sequence of problems with $\varepsilon_{II} \to 0$, then according to [24],[25] the pressure jump (4.2) should tend to $PC_{\omega,II}^{bl}h/2$. This constant doesn't depend on ε_{II} and hence cannot

be neglected (although in particular cases it can be small in comparison with the total pressure variation). On the other hand, the pressure difference across the cell in the longitudinal direction tends to zero, when ε_{II} does. In our test, ε_{II} is not enough small in comparison with h (in our calculations $h/\varepsilon_{II} = 4$). Therefore we cannot completely confirm the pressure jump condition, but we observe at least such a tendency.
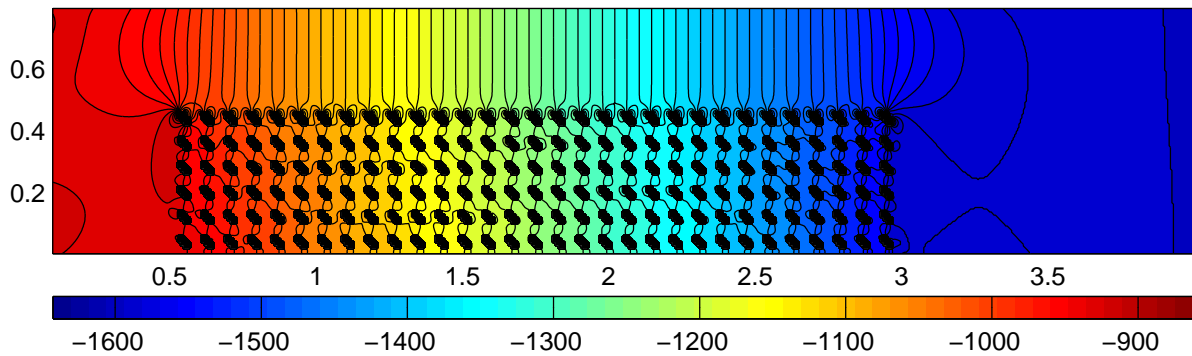

Figure 4.1: Geometry CG II and the pressure field. Sec.4.1,4.3
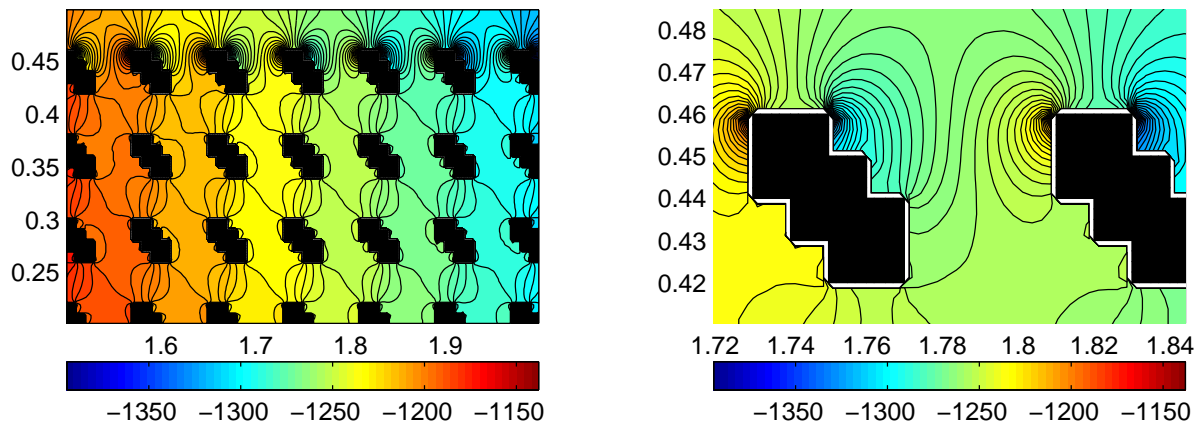
Figure 4.2: Pressure field near the porous-fluid interface. CG II

4.2 Flow, perpendicular to the porous medium

After the above short discussion on coupling conditions between (Navier-)Stokes and Darcy models, we return to the main topic of our investigations, namely, to the (Navier–)Stokes–Brinkman model. Analysis of the interface conditions for this system is the topic for the next three sections. We will use the dimensionless form of the equations (see section 1.4.1). μ_{eff} different from μ will not be used. The Darcy number is needed only for macro calculations and can be easily obtained from geometry of the corresponding micro-problem: it is just the squared size of one periodicity cell, measured in unit lengths of the computational domain. This unit length corresponds to L in the dimensional problem. The characteristic velocity U is the normal component of the uniform Inlet velocity (so, the dimensionless velocity is a unit vector there).

The first test is a simple filtration problem, which is often considered in conjunction with
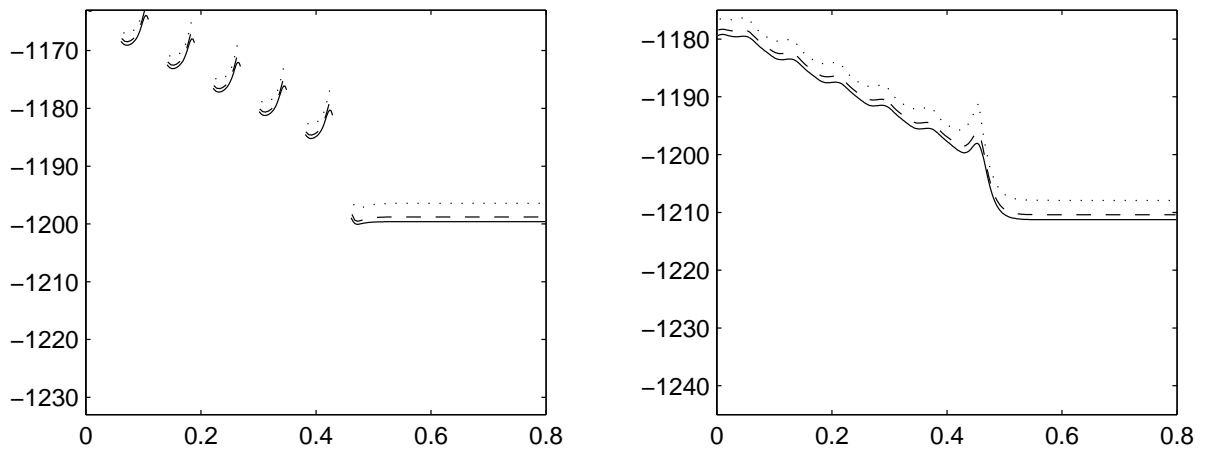
Figure 4.3: Pressure along the lines $x = 1.5$ (left) and $x = 1.55$ (right). CG II
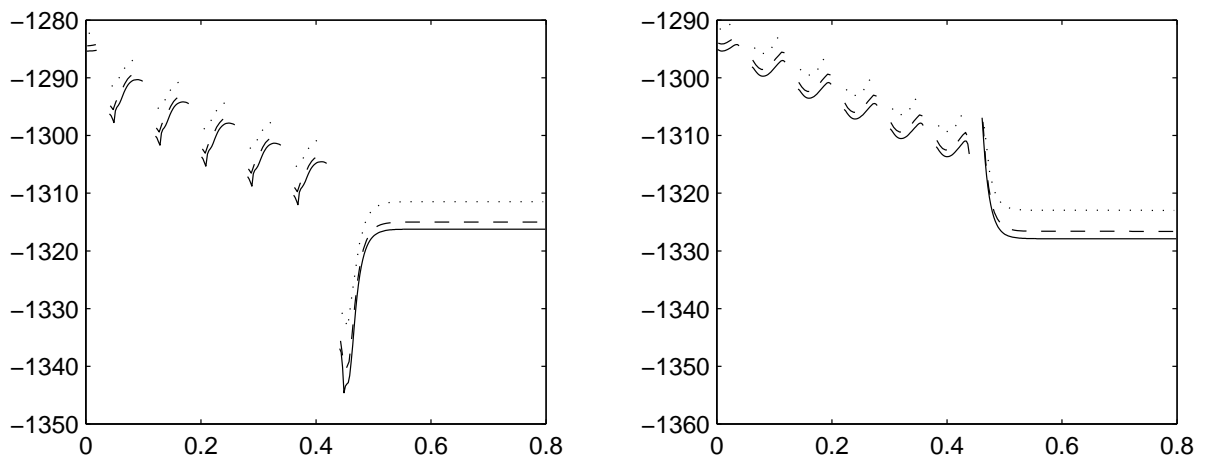
Figure 4.4: Pressure along the lines $x = 2.0$ (left) and $x = 2.05$ (right). CG II
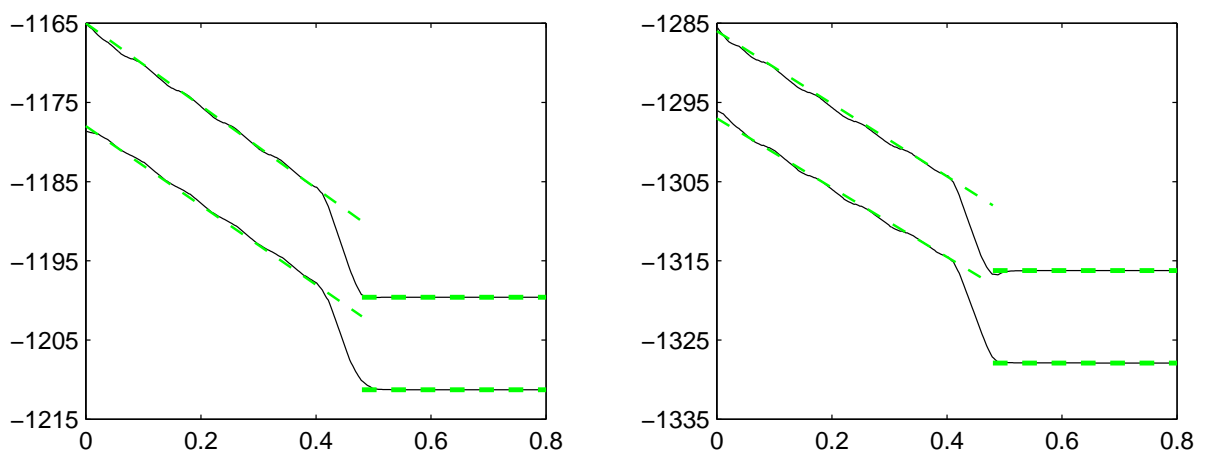
Figure 4.5: cell-averaged pressure along the lines $x = 1.5$, $x = 1.55$ (left) and $x = 2.0$, $x = 2.05$ (right). CG II
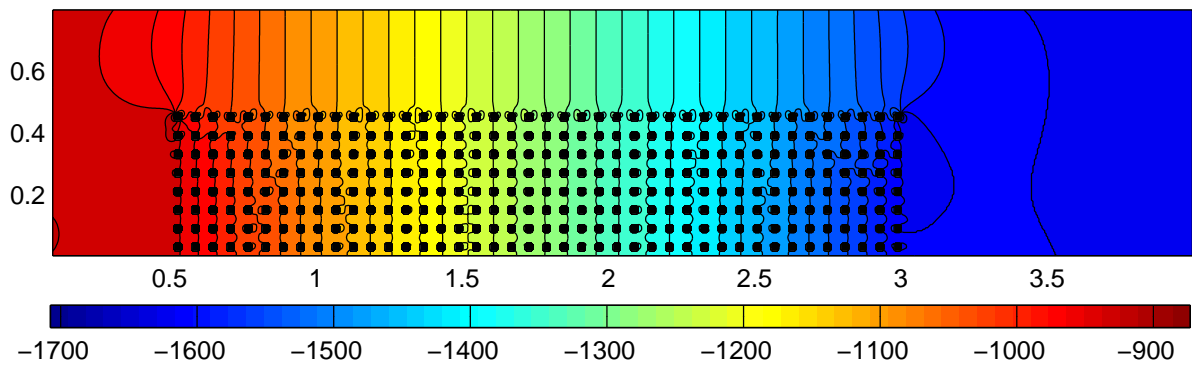
Figure 4.6: Geometry CG I and the pressure field. Sec.4.1
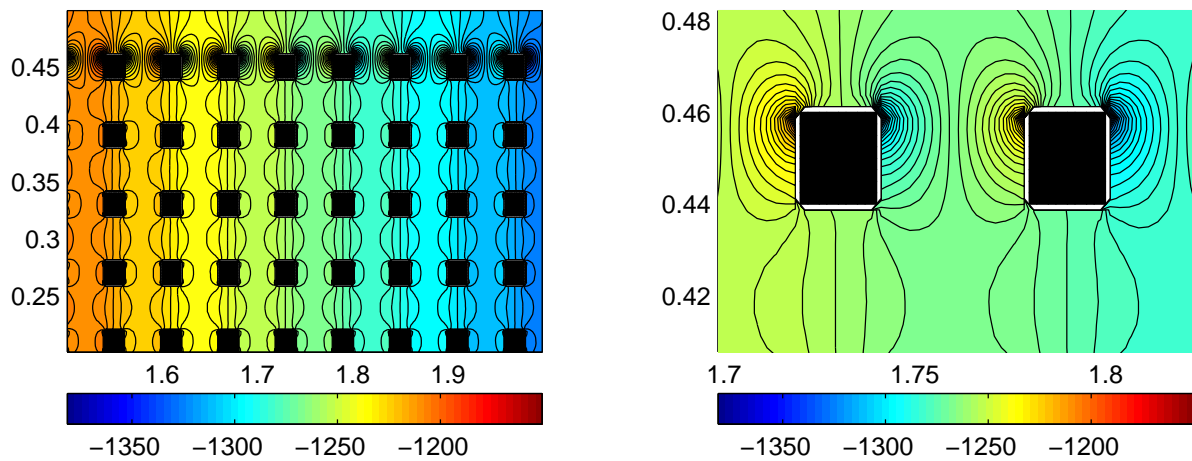
Figure 4.7: Pressure field near the porous-fluid interface. CG I
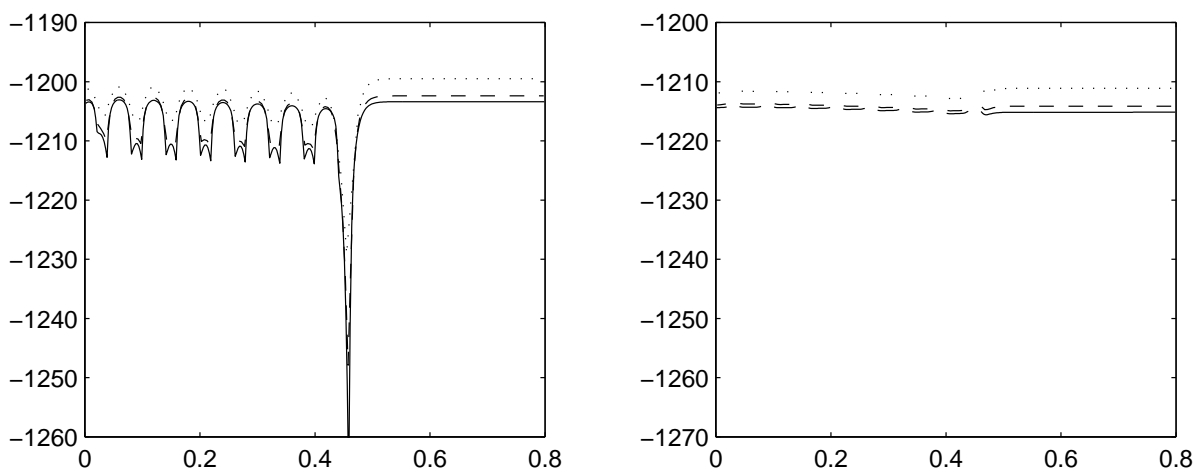
Figure 4.8: Pressure along the line $x = 1.5$ (left) and $x = 1.55$ (right). CG I
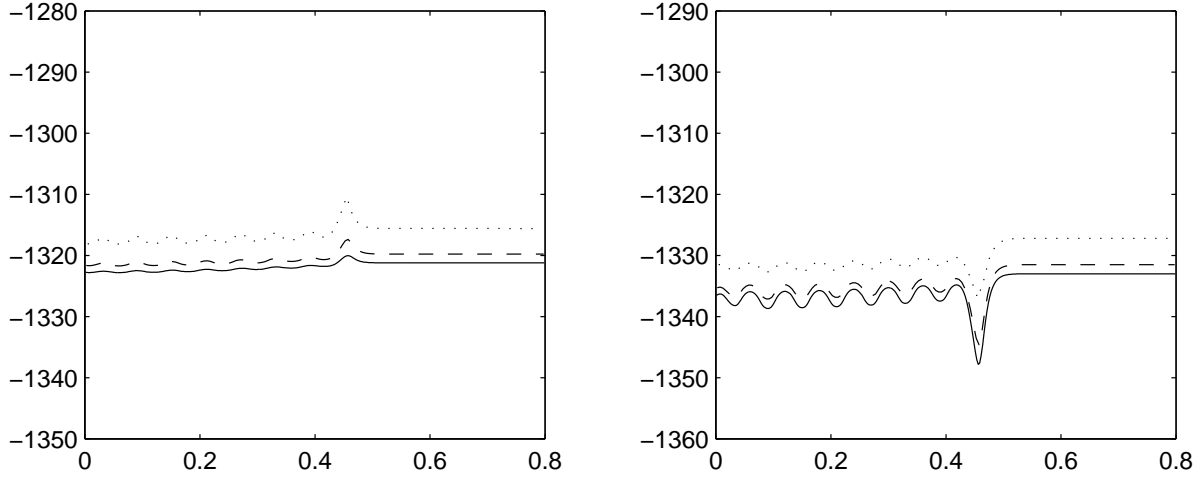
Figure 4.9: Pressure along the line $x = 2.0$ (left) and $x = 2.05$ (right). CG I

the Darcy law, as a way to measure the scalar permeability of porous media. We investigate it in conjunction with the Stokes–Brinkman model.

Consider a semi-infinite domain, $(0, 1.5) \times (-\infty, +\infty)$. The porous medium, which is a periodic arrangement of square obstacles, occupies the subdomain $(0.3, 1.2) \times (-\infty, +\infty)$. Accounting for the periodicity of the porous medium, we restrict our considerations to the subdomain $(0, 1.5) \times (0, 0.12)$. Geometry for the corresponding microscopical problem, and the computed there velocity field, are shown in Fig.4.10. The flow at the microscale (e.g. in the free fluid region around the solid obstacles) is governed by the 2D Stokes equations (1.44).

The left boundary ($x = 0$) is the Inlet boundary ($\mathbf{u} = (1, 0)$ there). At the outflow, $x = 1.5$, we set the "Outlet" boundary conditions. "Symmetry" boundary conditions are prescribed at $y = 0$ and at $y = 0.12$ as if there would be many similar rows below $y = 0$ and above $y = 0.12$. (consult the section 3.1.7 for the "Symmetry" and "Outlet" boundary conditions).

The consideration of only a small part of the periodic porous medium (in vertical direction) allows us to use fine grids in simulations. This micro problem is solved on a sequence of refined grids, containing 75x6, 150x12, 300x24, 600x48, 1200x96, and 2400x192 control volumes, respectively.

The geometry for the corresponding macro problem is given in Fig.4.11. The Stokes-Brinkman equations (1.43) are governing the (macro) flow there. The Darcy number is 0.06^2 (see Fig.4.10), and the permeability $\mathcal{K} = \mathcal{K}_I$ from (1.16). Boundary conditions in this case are the same as for the micro problem. The interface conditions on $x = 0.3$ and $x = 1.2$ are the continuous velocity, (1.42), and the continuous stress tensor condition, (1.46). We note that the first square in Fig.4.10 has the minimal x coordinate equal to $0.3 + \sqrt{Da}/3$, since we decided to locate the interface in accordance with the cell's boundary.

Two grids were used to calculate the macro solution: 75x6 and 150x12. It is easy to check, that the macroscopic problem has an exact solution. It is given by $\mathbf{u} \equiv (1, 0)^T$ for $(x, y) \in \Omega$, together with $p(x, \cdot) = p_1$ when $x < 0.3$; $p(x, \cdot) = p_2$, when $x > 1.2$, and $p(x)$ satisfies the 1D Darcy law

$$u = -Da\mathcal{K}\frac{\partial p}{\partial x} \qquad x \in (0.3, 1.2) \tag{4.3}$$

where $u = 1$, either p_1 or p_2 can be chosen arbitrarily.

The comparison of pressure profiles along the line $y = 0.04$, calculated using the microscopical as well as the macroscopic problems on nested grids, is given in Fig.4.12. One can observe a

very good agreement between the solutions of the micro and the macro models for this problem.
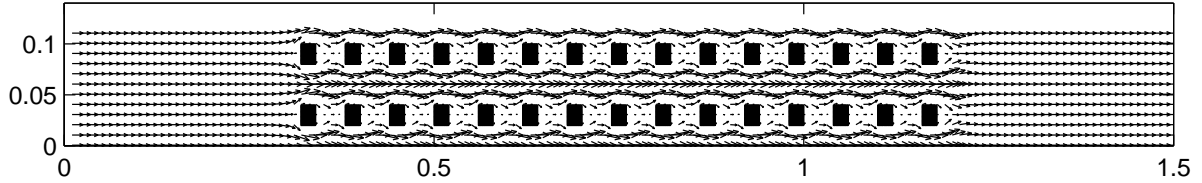
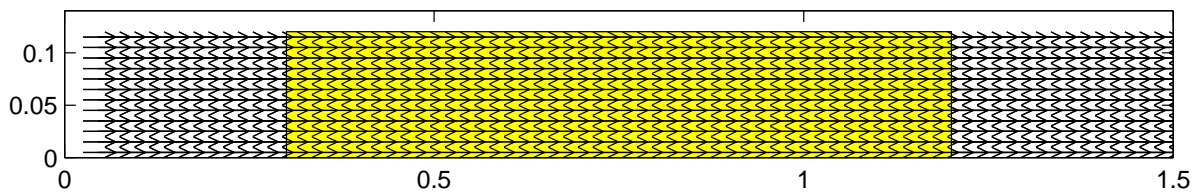Figure 4.10: Microgeometry (CG I) and the velocity field. Sec.4.2

Figure 4.11: Macrogeometry (CG I) and the velocity field. Sec.4.2

4.3 Flow in a channel with a long porous obstacle

We continue to compare the microscopical calculations with macroscopic ones, considering now more interesting types of flows. In contrast to the preceding section, now the flow is not perpendicular to the porous medium, it is mainly parallel to it. For the first test (test I), the porous medium is built from squares with the cell geometry CG I (see Fig.4.13). The second test (test II) is the same test from the section 4.1 used to demonstrate the pressure jump (see Fig. 4.1). The Stokes model (1.44) is used for the flow at a microlevel, while at a macrolevel the Stokes model is used in Ω_f, and the Stokes–Brinkman model (1.43) is used in Ω_p for both tests. The domains Ω represent channels with solid top and bottom walls. The left and right boundaries of the channels are Inlet and Outlet boundaries with Dirichlet and "Outlet" conditions, respectively. For both test I and test II we consider two variants for the interface conditions at a macrolevel. In the first variant, the continuous stress condition (1.46) is used. In the second variant, the stress jump condition (1.45) is used. In both variants, the second interface condition, as usual, is the continuity of the velocity across the interface (1.42).

Dealing with (1.45) we should specify the tensorial coefficient $\mathcal{M}$ on the interface Σ. The interface can be divided into three parts Σ_1, Σ_2, Σ_3 having the normals $(0, 1)^T$, $(-1, 0)^T$, $(1, 0)^T$, respectively. On each part Σ_i we are going to use the same matrix $\mathcal{M}$. The coefficient $\mathcal{M}$ on Σ_2, Σ_3 we will calculate by (2.43) from the values of $\mathcal{M}$ on Σ_1, playing a role of $\mathbf{M}'$ in the "laboratory system" ((2.43) can be applied to $\mathcal{M}$ instead of $\mathbf{M}$). The values of $\mathcal{M}$ on Σ_1 we treat as parameters to be fitted. Below we describe both tests and the numerical results separately.

Test I (see Fig. 4.13) The computational domain and the porous media are $\Omega = (0, 6) \times (0, 1.44)$, $\Omega_p = (1.44, 3.84) \times (0, 0.84)$. The Darcy number is $Da = 0.12^2$ (since the cell size is 0.12 in Fig.4.13) and the dimensionless permeability is $\mathcal{K} = \mathcal{K}_I$ (from 1.16).
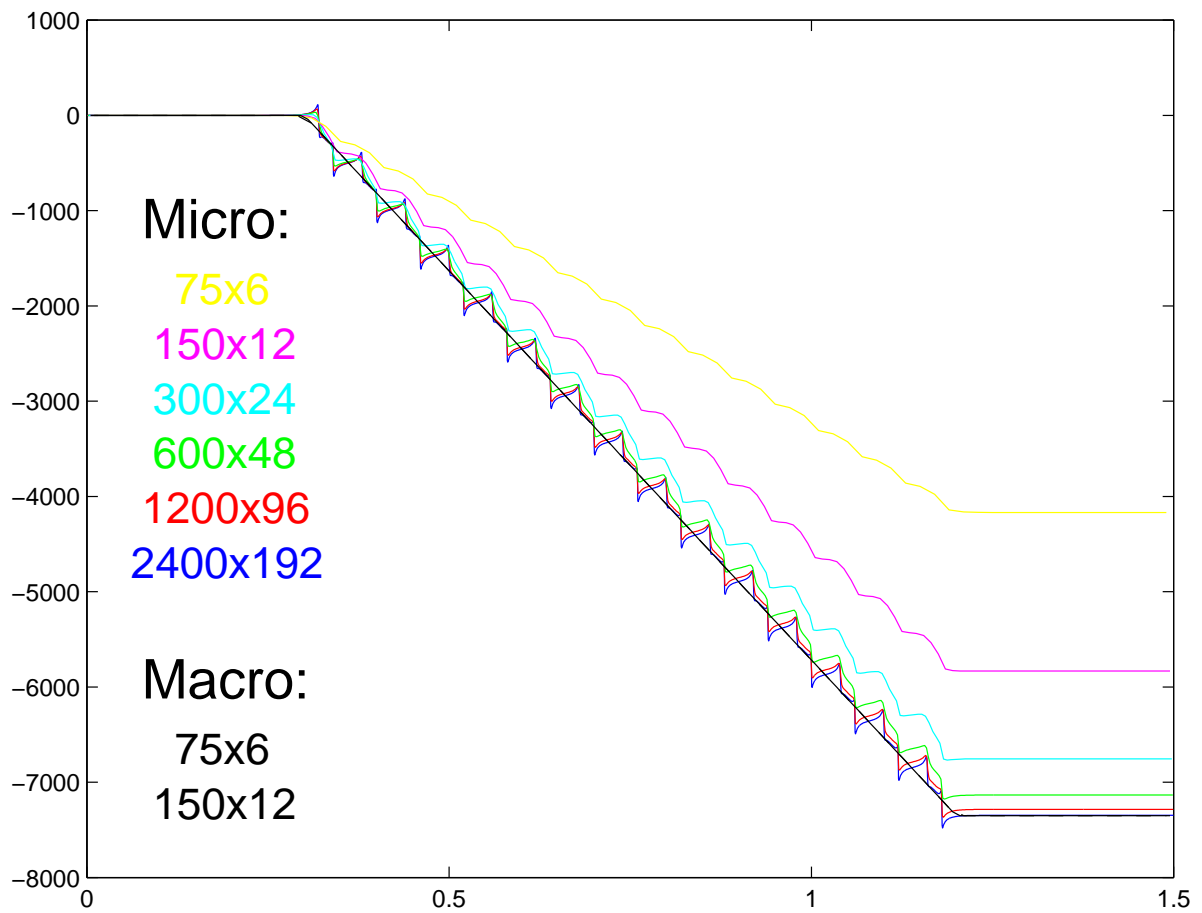
Figure 4.12: Comparison micro pressure on 6 nested grids with macro pressure on 2 nested grids

Let us assume first that $\mathcal{M}_1$ on $\Sigma_1 = [1.44, 3.84] \times \{0.84\}$ is known and equal to $\mathcal{M}'$ (in the "laboratory" system). Using $\mathcal{M}'$ we can calculate $\mathcal{M}_2$, $\mathcal{M}_3$. To obtain $\mathcal{M}_2$ on $\Sigma_2 = \{1.44\} \times [0, 0.84]$ we use (3.45). For $\Sigma_3 = \{3.84\} \times [0, 0.84]$ ($\mathbf{n} = (1, 0)^T$), we can calculate $\mathcal{M}_3$ from

$$\mathbf{C} = \left[\begin{array}{cc} \cos\frac{\pi}{2} & -\sin\frac{\pi}{2} \\ \sin\frac{\pi}{2} & \cos\frac{\pi}{2} \end{array} \right], \qquad \mathcal{M} = \mathbf{C}^T \left[\begin{array}{cc} \mathcal{M}'_{11} & \mathcal{M}'_{12} \\ \mathcal{M}'_{21} & \mathcal{M}'_{22} \end{array} \right] \mathbf{C} = \left[\begin{array}{cc} \mathcal{M}'_{22} & -\mathcal{M}'_{21} \\ -\mathcal{M}'_{12} & \mathcal{M}'_{11} \end{array} \right].$$

Now the only undetermined parameters are the values in $\mathcal{M}'$. We did not find in the literature how they can be determined. Therefore, we tried to fit them in a heuristic way. Starting from $\mathcal{M}' = \mathbf{0}$ which corresponds to the continuous stress condition (1.46), we looked for such $\mathcal{M}'$, which leads to a better agreement (if possible) of the macro-solutions with the micro-solutions for this particular problem. In general, $\mathcal{M}'$ has four entries (2D). The cell geometry CG I leads to the scalar permeability and is symmetric with respect to the vertical line going through the center. This implies that $\varkappa_{21} = 0$ and $C_\omega^{bl} = 0$. Then the expression (2.36) suggests to choose $\mathcal{M}'_{21} = 0$. Furthermore, the analytical solution for the parallel flow from the Section 2.1 was independent from the values M_{12} and M_{22}. Then let us restrict ourselves, by setting $\mathcal{M}'_{12} = \mathcal{M}'_{22} = 0$. The only remaining entry, which we had to fit, is $\mathcal{M}'_{11}$. After several attempts, we found that the best agreement between the micro- and the macro- solutions is obtained for the following $\mathcal{M}'$:

$$\frac{\mathcal{M}'}{\sqrt{Da}} = \left[\begin{array}{cc} -20 & 0 \\ 0 & 0 \end{array} \right] \tag{4.4}$$

The resulting coefficients on Σ_1, Σ_2, Σ_3 are

$$\frac{\mathcal{M}_1}{\sqrt{Da}} = \left[\begin{array}{cc} -20 & 0 \\ 0 & 0 \end{array} \right], \qquad \frac{\mathcal{M}_2}{\sqrt{Da}} = \frac{\mathcal{M}_3}{\sqrt{Da}} = \left[\begin{array}{cc} 0 & 0 \\ 0 & -20 \end{array} \right]. \tag{4.5}$$

The micro-calculations were done on two grids, containing 1200×288 and 600×144 control volumes, respectively. The macro-problems were solved on grids with 600×144 and 300×72 control volumes (for both variants of the interface conditions).

The numerical solutions of the microproblem are compared with the numerical solutions of the macroproblems along the colored lines, shown on Fig.4.13. More precisely, we compare pressures (calculated from micro- and from macro models) along the magenta (4) and and along the cyan (5) colored lines. Horizontal velocities are compared along the blue (1), the red (2), and the green (3) colored lines. The results are presented in Fig.4.14, 4.15 for the case of the continuous stress tensor condition, and in Fig.4.16, 4.17 for the case of the stress jump condition (using the already fitted values for $\mathcal{M}'$).

The macroscopic solution, computed with the continuous stress interface condition, has an irreducible error, when compared to the microsolution. The term "irreducible" is used here in the sense, that further refining of the grid does not ensure proximity of the macro- and micro- solutions in this case. It can be seen, that the macroscopic model with the stress jump interface condition approximates the microsolutions with better accuracy on all lines where the comparison was made. Recall, that this was achieved by changing only one entry, namely, $\mathcal{M}'_{11}$.

Remark 18 *In the previous section 4.2 we obtained a good approximation of the microscopical solution by the macroscopic solution when the continuous stress condition was used. The microgeometry in the interfacial regions near $x = 0.3$, $x = 1.2$ (see Fig.4.10) for that problem is similar to the microgeometry near $x = 1.44$, $x = 3.84$ (see Fig.4.13). Therefore, instead of the continuous stress interface conditions $\widetilde{\mathcal{M}}_2 = \mathbf{0}$ (on $x = 0.3$), $\widetilde{\mathcal{M}}_3 = \mathbf{0}$ (on $x = 1.2$) we can try*

to use $\widetilde{\mathcal{M}}_2 = \mathcal{M}_2$, $\widetilde{\mathcal{M}}_3 = \mathcal{M}_3$, where $\mathcal{M}_2$, $\mathcal{M}_3$ can be expressed from (4.5) ($\sqrt{Da}$ was equal to 0.12 there). In the problem from Section.4.2, $\sqrt{Da} = 0.06$. Therefore

$$\frac{\widetilde{\mathcal{M}}_2}{\sqrt{Da}} = \frac{0.12}{0.06} \begin{bmatrix} 0 & 0 \\ 0 & -20 \end{bmatrix}, \qquad \frac{\widetilde{\mathcal{M}}_3}{\sqrt{Da}} = \frac{0.12}{0.06} \begin{bmatrix} 0 & 0 \\ 0 & -20 \end{bmatrix}$$

The macrosolution given explicitly for the continuous stress interface condition in the Section 4.2 ($\mathbf{u} \equiv (1,0)^T$) also satisfies the stress jump condition with $\widetilde{\mathcal{M}}_2$, $\widetilde{\mathcal{M}}_3$ since the right hand side of (1.45) is zero in both cases:

$$\frac{\widetilde{\mathcal{M}}_2}{\sqrt{Da}}\mathbf{u} = \frac{\widetilde{\mathcal{M}}_3}{\sqrt{Da}}\mathbf{u} = \begin{bmatrix} 0 & 0 \\ 0 & -40 \end{bmatrix} \begin{bmatrix} 1 \\ 0 \end{bmatrix} = \mathbf{0} \quad = \begin{bmatrix} 0 & 0 \\ 0 & 0 \end{bmatrix} \mathbf{u}.$$

Test II (see Fig.4.1) The computational domain and the porous media are $\Omega = (0,4) \times (0,0.8)$, $\Omega_p = (0.51, 2.99) \times (0,0.48)$. The Darcy number is $Da = 0.08^2$ (since the cell size is 0.08) and the dimensionless permeability is $\mathcal{K} = \mathcal{K}_{II}$ (from 1.16). We still have to specify $\mathcal{M}$ on $\Sigma_1 = [0.51, 2.99] \times \{0.48\}$, $\Sigma_2 = \{0.51\} \times [0, 0.48]$, $\Sigma_3 = \{2.99\} \times [0, 0.48]$.

On $\Sigma_1 = [0.51, 2.99] \times \{0.48\}$ the coefficient was fitted:

$$\frac{\mathcal{M}_1}{\sqrt{Da}} = \frac{\mathcal{M}''}{\sqrt{Da}} := \begin{bmatrix} -49 & 0 \\ -10 & 0 \end{bmatrix}. \tag{4.6}$$

For the cell geometry CG II we fitted two parameters $\mathcal{M}''_{11}$ and $\mathcal{M}''_{21}$ (similar to the test I, we restrict ourselves to the case $\mathcal{M}''_{12} = \mathcal{M}''_{22} = 0$).

Remark 19 *We note that using (2.37) with $\tilde{C}^{bl}_1$ $\tilde{C}^{bl}_\omega$ from the Section 4.1 we would obtain*

$$\frac{\mathcal{M}_1}{\sqrt{Da}} = \frac{1}{0.08} \begin{bmatrix} -\frac{1}{-0.52} - \sqrt{\frac{1}{53.8}}53.8 & \cdot \\ -\frac{0.45}{-0.52} - \sqrt{\frac{1}{53.8}}11.1 & \cdot \end{bmatrix} = \begin{bmatrix} -67.7 & \cdot \\ -8.1 & \cdot \end{bmatrix}$$

From one side the values of $\tilde{C}^{bl}_1$, $\tilde{C}^{bl}_\omega$ are only some approximations to the constants $C^{bl}_{1,II}$, $C^{bl}_{\omega,II}$ for the cell geometry CG II, from another side the form (2.37) for $\mathcal{M}$ is derived for periodic microstructure under the assumption that the Darcy number is small enough (in other words $\varepsilon \ll L$) and may lead to rough results in the case of moderate Darcy numbers that we are dealing with. Hence, we will use the fitted $\mathcal{M}''$ from (4.6).

The value of $\mathcal{M}$ on $\Sigma_2 = \{0.51\} \times [0, 0.48]$ ($\mathcal{M}_2$) we calculate from (4.6), since the microgeometries are similar. But rotations are not enough to transform a neighbourhood of Σ_2 to some neighbourhood of Σ_1. We also need a reflection. The matrix $\mathbf{C}$ transforms $\mathbf{n} = (-1,0)$ to $\mathbf{n}' = (0,1)$ and $\mathbf{t} = (0,-1)$ to $\mathbf{t}' = (1,0)$. Therefore

$$\mathbf{C} = \begin{bmatrix} 0 & -1 \\ -1 & 0 \end{bmatrix}, \qquad \mathcal{M}_2 = \mathbf{C}^T \mathcal{M}'' \mathbf{C} = \begin{bmatrix} \mathcal{M}''_{22} & \mathcal{M}''_{21} \\ \mathcal{M}''_{12} & \mathcal{M}''_{11} \end{bmatrix}.$$

Similar situation we have on $\Sigma_3 = 2.99 \times [0, 0.48]$: $\mathbf{C}$ transforms $\mathbf{n} = (1,0)$ to $\mathbf{n}' = (0,1)$ and $\mathbf{t} = (0,1)$ to $\mathbf{t}' = (1,0)$. Hence,

$$\mathbf{C} = \begin{bmatrix} 0 & 1 \\ 1 & 0 \end{bmatrix}, \qquad \mathcal{M}_3 = \mathbf{C}^T \mathcal{M}'' \mathbf{C} = \begin{bmatrix} \mathcal{M}''_{22} & \mathcal{M}''_{21} \\ \mathcal{M}''_{12} & \mathcal{M}''_{11} \end{bmatrix}.$$

The resulting coefficients are

$$\frac{\mathcal{M}_1}{\sqrt{Da}} = \left[\begin{array}{cc} -49 & 0 \\ -10 & 0 \end{array} \right], \qquad \frac{\mathcal{M}_2}{\sqrt{Da}} = \frac{\mathcal{M}_3}{\sqrt{Da}} = \left[\begin{array}{cc} 0 & -10 \\ 0 & -49 \end{array} \right].$$

The following grids were chosen for the numerical calculations: 400×80, 800×160 control volumes for the macroscopic solutions and 400×80, 800×160, 1600×320 control volumes for the microscopical solutions. The microsolution is compared with the macrosolution in Fig.4.18,4.19. In Fig.4.18 the pressure is plotted on two horizontal lines with $y = 0.22$ (black), $y = 0.5$ (red). In the left subfigure the microscopical solution (black and red solid lines) is compared with the macroscopic solution for the model with the stress jump interface condition (black and red dashed lines). In the right subfigure we have a similar comparison, only the continuous stress condition was used to obtain the macroscopic solution. The horizontal velocities plotted on three vertical lines $x = 0.25$ (blue), $x = 1.5$ (red), $x = 3$ (green) are presented in Fig.4.19. The micro velocities (solid lines) are compared with the macro velocities (dashed lines), obtained for the stress jump interface condition (left subfigure), and for the continuous stress condition (right subfigure). We note that the line $x = 3$ (green) lies partially on the porous-fluid interface.

Like for the test I, the macro solution with the stress jump condition approximates well the microsolution, while the macro solution with the continuous stress condition has significant quantitative discrepancies. We note that according to some authors, the continuous stress condition can provide approximation to the microsolution, if μ_{eff} is set different from μ. We do not consider this case here.
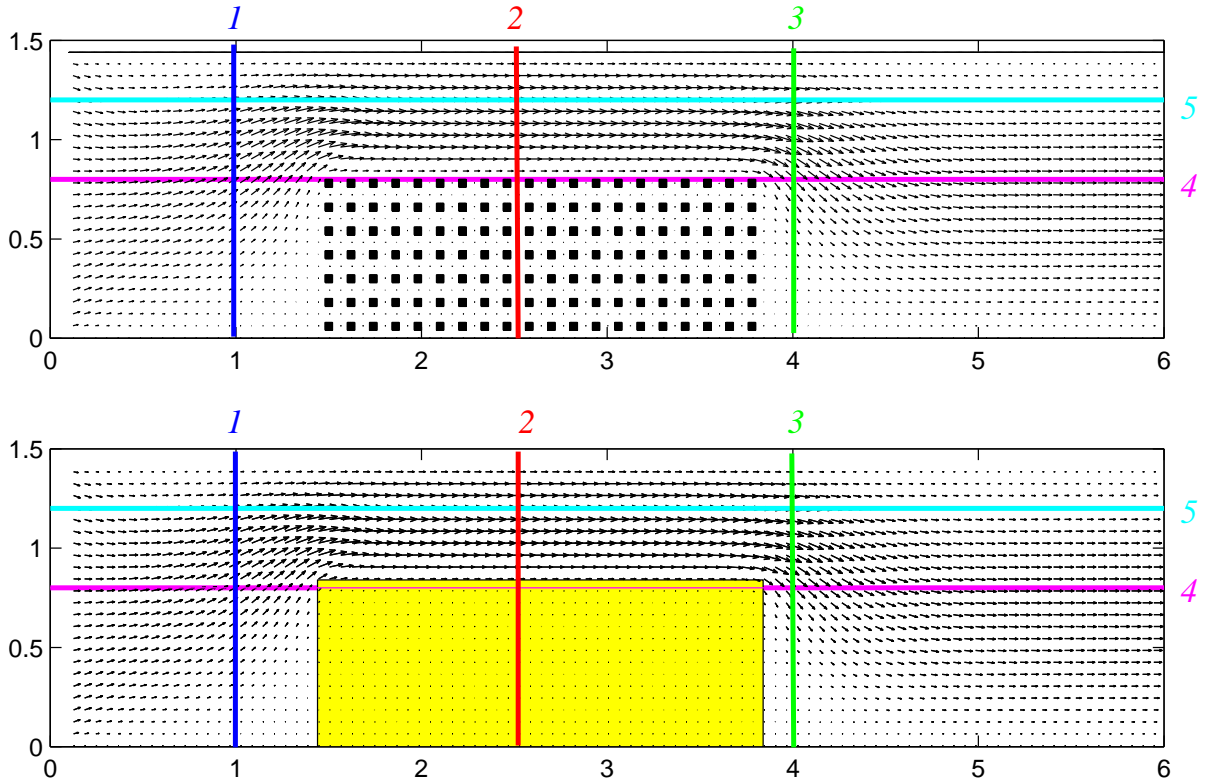
Figure 4.13: Geometries for micro and macro problems. Colored lines and their reference numbers $1, 2, 3, 4, 5$. test I. Sec.4.3
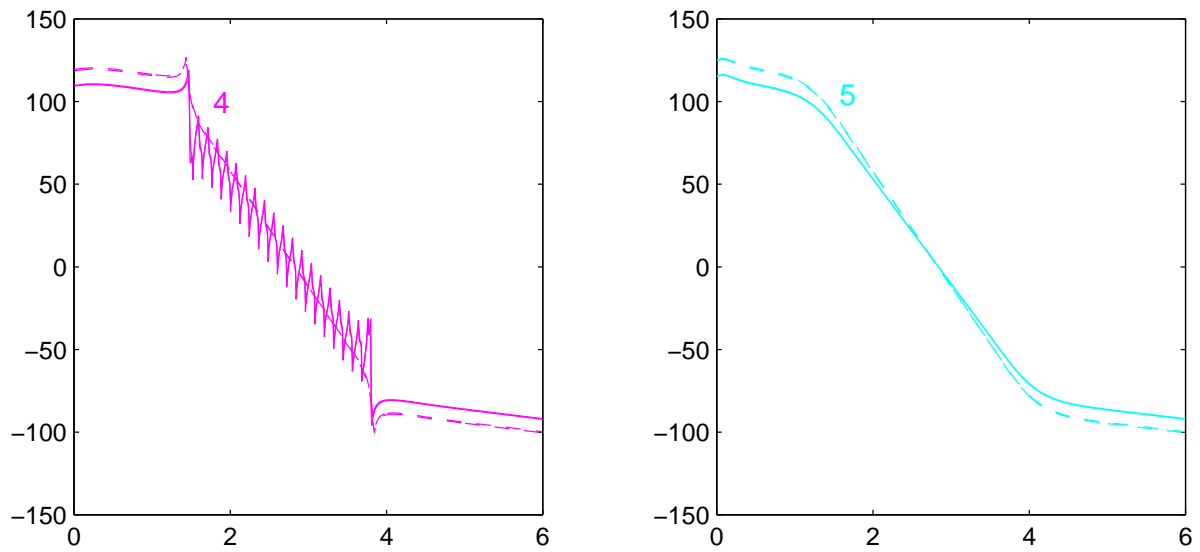
Figure 4.14: p along color lines $4, 5$ (Fig.4.13). Solid lines – microsolutions 1200×288, 600×144, dashed lines – macrosolutions 600×144, 300×72 (Continuous stress). test I
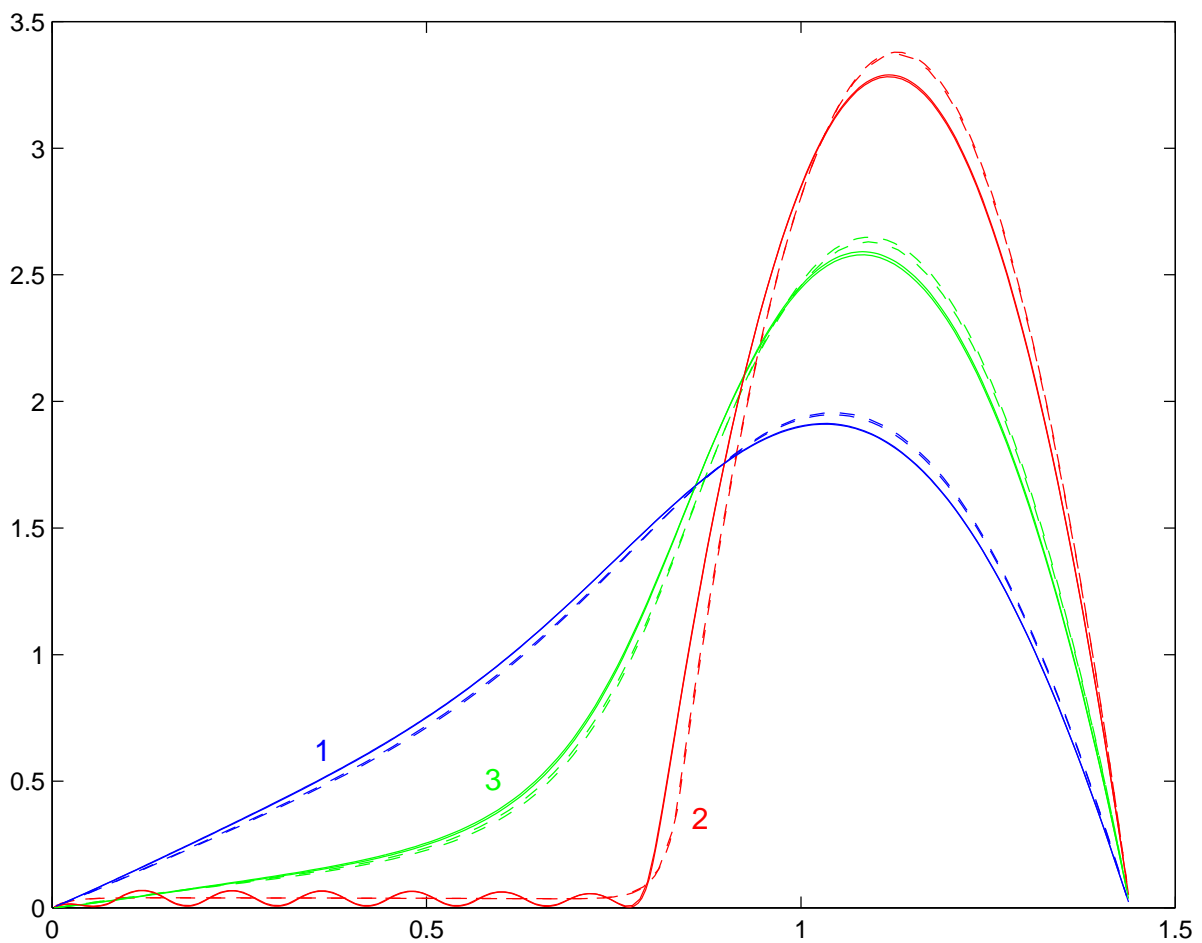
Figure 4.15: u along color lines $1, 2, 3$ (Fig.4.13). Solid lines – microsolutions 1200×288, 600×144, dashed lines – macrosolutions 600×144, 300×72 (Continuous stress). test I
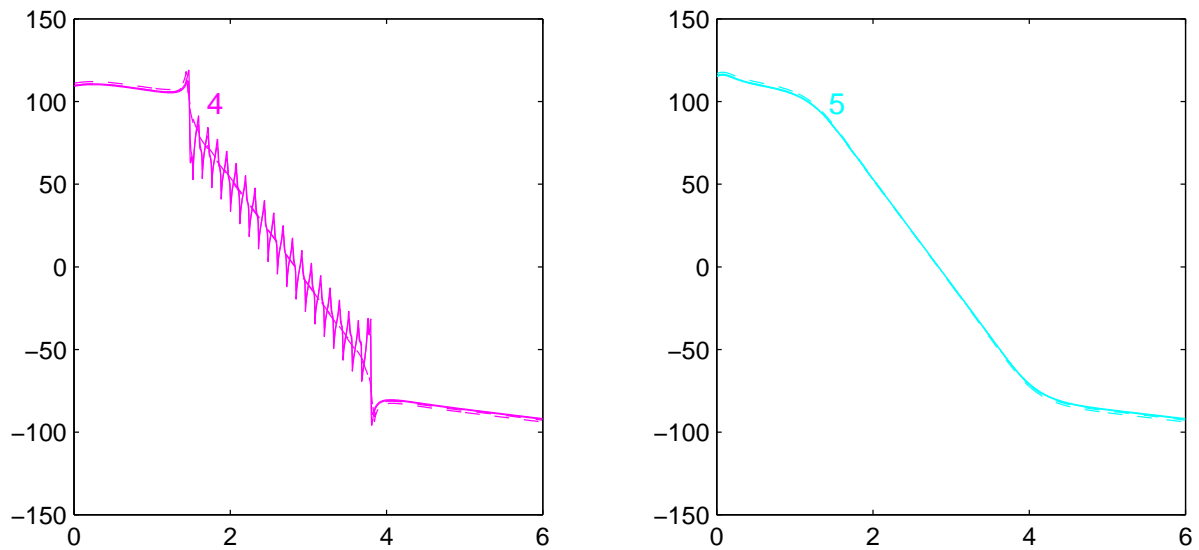
Figure 4.16: p along color lines $4, 5$ (Fig.4.13). Solid lines – microsolutions 1200×288, 600×144, dashed lines – macrosolutions 600×144, 300×72 (Stress jump). test I
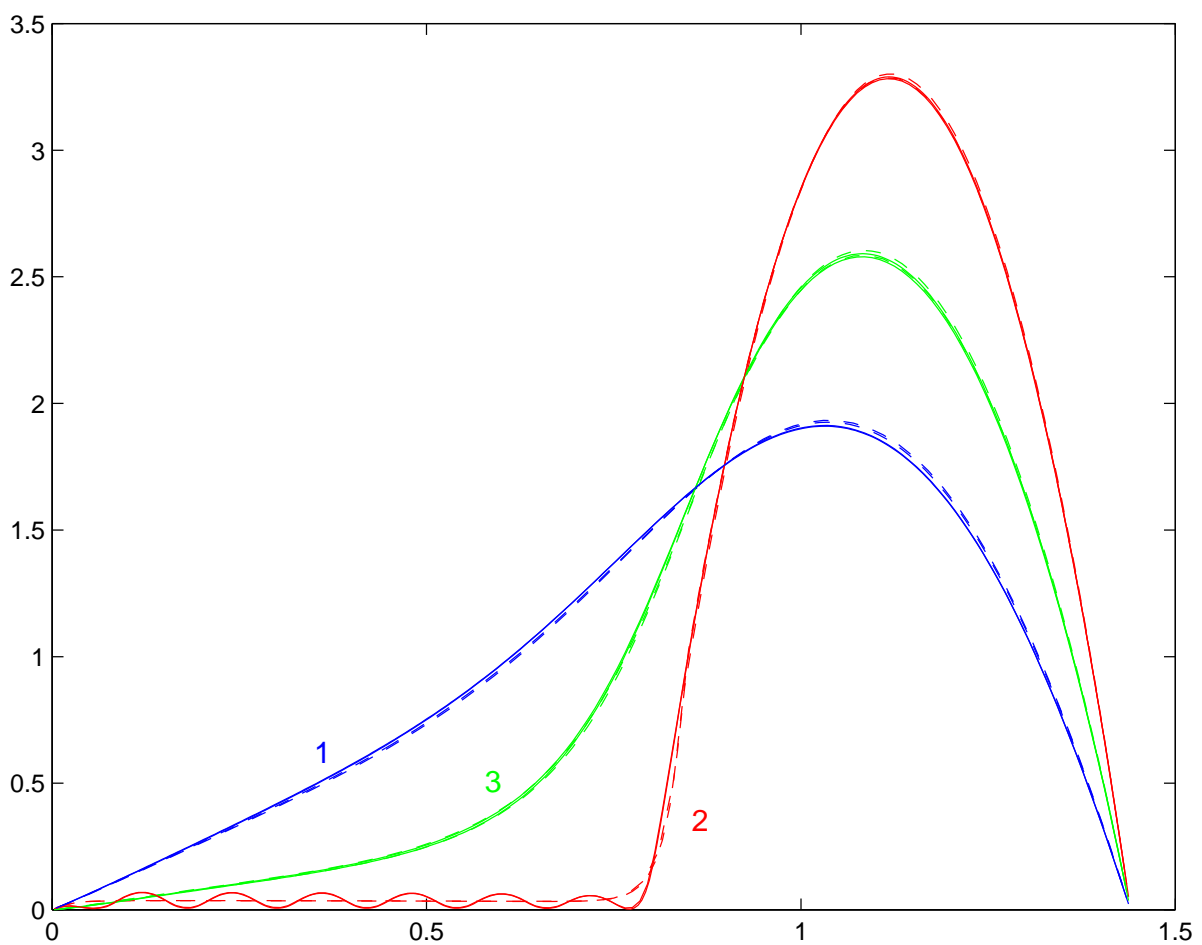
Figure 4.17: u along color lines $1, 2, 3$ (Fig.4.13). Solid lines – microsolutions 1200×288, 600×144, dashed lines – macrosolutions 600×144, 300×72 (Stress jump). test I
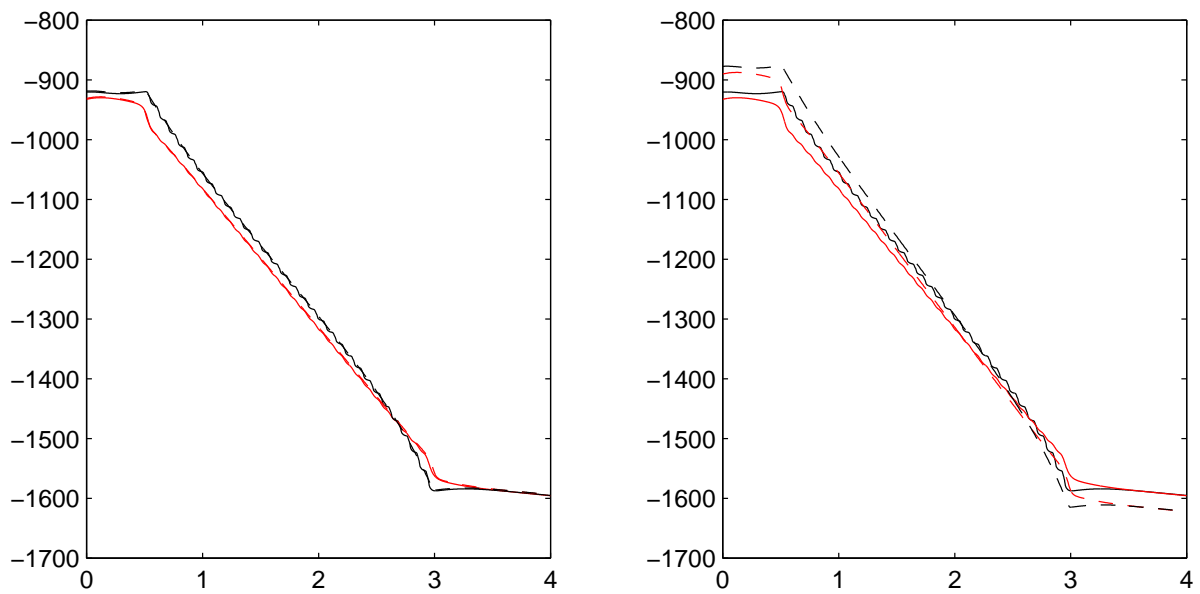
Figure 4.18: p along colored lines $y = 0.22$ (black), $y = 0.5$ (red). Solid lines – microsolutions 1600×320, dashed lines – macrosolutions 800×160. Stress jump condition - left; continuous stress condition - right. test II
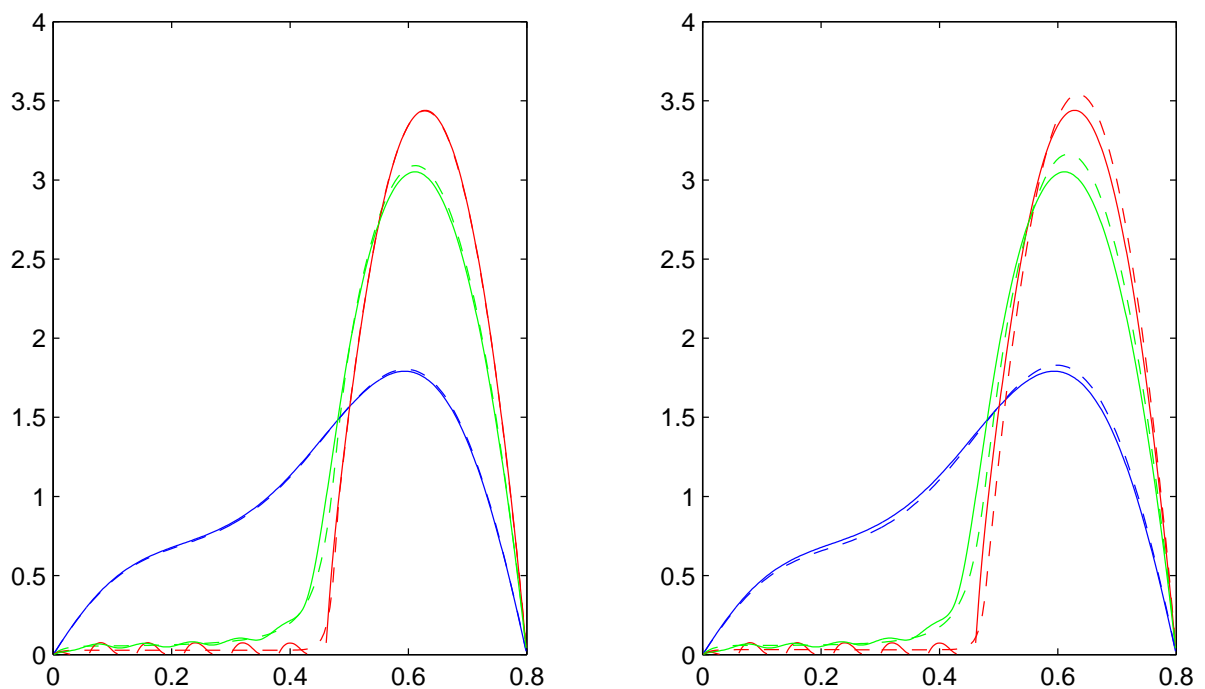
Figure 4.19: u along colored lines $x = 0.25$ (blue), $x = 1.5$ (red), $x = 3$ (green) Solid lines – microsolutions 1600×320, dashed lines – macrosolutions 800×160, Stress jump condition - left; continuous stress condition - right. test II

4.4   A model industrial filtration problem

In the last series of micro/macro comparisons we consider a 2D model geometry, which is a cross section of a simplified oil filter presented in Fig.4.20. The microscopical geometry is shown in the left subfigure, while the macroscopic one is shown in the right subfigure. The computational (macro) domain, Ω, $\Omega = (0, 2.5) \times (0, 2)$, consists of solid, porous, and fluid parts. The solid part (colored in black in the figures), Ω_s, is defined as $\overline{\Omega_s} = [0, 0.2] \times [0.3, 1.2] \cup [0, 2.1] \times [1.2, 2]$. The porous part (colored in yellow) is defined as $\overline{\Omega_p} = [0.2, 2.5] \times [0.32, 0.92]$. Finally, the fluid part (colored in white), is given by $\Omega_f = \Omega \setminus (\overline{\Omega_s} \cup \overline{\Omega_p})$ (see Fig.4.20, right).

   The boundary conditions for the problem are prescribed as follows. No-slip condition is prescribed on solid walls. At the Inlet $\{0\} \times [0, 0.3]$ uniform Dirichlet boundary conditions are given. The inlet velocity is used again as a characteristic velocity, U (thus the dimensionless inlet velocity is equal to 1). At the outlet $[2.1, 2.5] \times \{2\}$ the soft "Outlet" boundary conditions are prescribed . These boundary conditions are appropriate for all models we consider.

   The above problem is a typical filtration problem: the Inlet and the Outlet are separated by the porous medium. The microgeometry of the porous media is formed by a periodic repetition of the cell CG I from Fig. 1.2 (see Fig.4.20, left), The period is $\bar{\varepsilon} = 0.12L$. The Darcy number is $Da = 0.12^2$.

   We compare numerical solutions of microscopical with those of the macroscopic models. The flow at a microscopic level is governed by Stokes, or by Navier–Stokes equations . The following grids are used for the computations at a microlevel: 125×100, 250×200, 500×400, 1000×800. The flow at a macroscopic level is governed by the Stokes–Brinkman system, or by the Navier–Stokes–Brinkman system. Again, two variants of the interface conditions are considered: one including the continuous stress condition, the other including the stress jump condition. In both variants, the continuity of the velocity is the second interface condition. Three grids are used for macroscopic simulations: 125×100, 250×200, 500×400. The comparison between the microscopic and the macroscopic solution is done at five locations: on two horizontal lines, and on three vertical lines (see Fig.4.20). The vertical lines are marked by 1, 2, and 5, and they are colored in blue (1), in red (2), and in magenta (5), respectively. The horizontal lines are marked by 3 and 4, and they are colored in green (3) and in black (4), respectively. The solutions of microscopical problems are plotted with solid lines and the solutions of macroscopic problems – with dashed lines. As it was mentioned above, we used consecutively refined grids, in order to observe convergence of the numerical solution with respect to the grid size. Here we plot only numerical solutions calculated on two finest grids. We note that on certain intervals two of the dashed lines can overlap, and to look like one solid line.

Direct Simulation (Stokes) vs Stokes–Brinkman with Continuous Stress   In the first test for the geometry from Fig.4.20, the microscopical model is the Stokes system (1.44) in $\Omega_f \cup \Omega_{pf}$. The macroscopic model is based on Stokes, (1.44) in Ω_f, and on Brinkman, (1.43) in Ω_p, equations. As in all tests in this Chapter, $\mu_{eff}/\mu = 1$. The interface conditions for this case are continuous velocity (1.42) and continuous stress tensor (1.46).

   The pressure, computed on a microlevel, is compared with the pressure computed on a macrolevel, at four different locations (see Fig.4.21). We note that the black (4) and the green (3) lines on Fig.4.20 are horizontal ones, while and the blue (1), the red (2) lines are vertical. The results for all four notations are plotted in one figure, and in their interpretation one has to remember, that the abscissa in Fig.4.21 has different meaning: it corresponds to OX for the black (4) and for the green (3) lines, while it corresponds to OY for the blue (1) and for the red (2) lines. The horizontal velocity component u and the vertical velocity component v
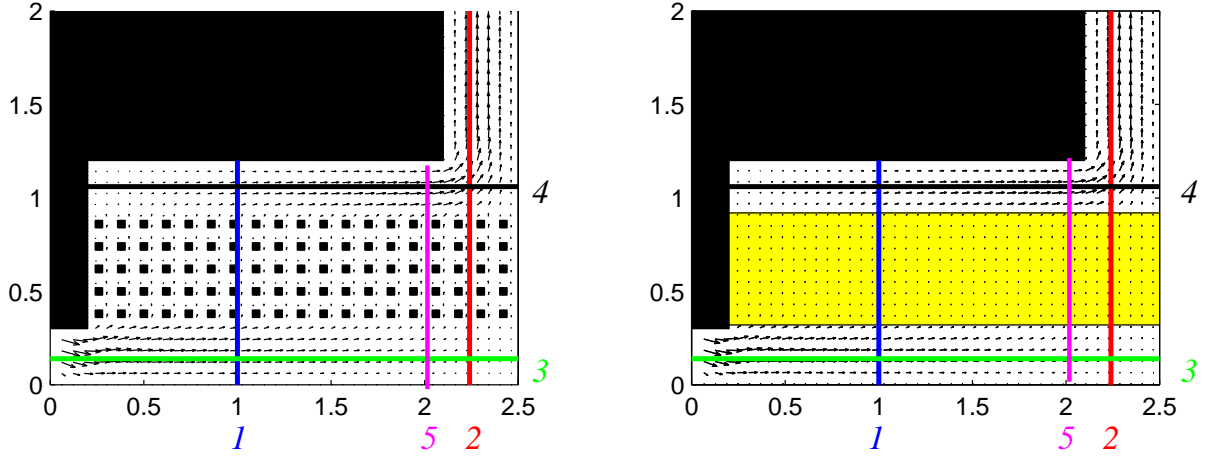
Figure 4.20: Geometries for micro and macro problems. Colored lines and their reference numbers $1, 2, 3, 4, 5$. Sec.4.4

($\mathbf{u} = (u, v)$) are compared in Fig.4.22 and 4.23, respectively. The microscopic solutions (solid lines) were calculated on grids 1000×800, 500×400 and the macroscopic solutions (dashed lines) were calculated on grids with 500×400, 250×200 control volumes. As it can be seen, the continuous stress tensor interface condition can not ensure satisfactory results in this case. Significant differences are observed between the macro- and the micro- solutions, and these differences do not decrease when the grid is refined. These differences are for the pressure and for horizontal component of the velocity. On the other hand, the macroscopic computations ensure a reasonable approximation for the vertical component of the velocity (compared to the one, obtained in the microscopic simulations). Thus, in this case we observe the typical behaviour of the solutions from the preceding sections: the continuous stress tensor is a reasonable interface conditions for flow perpendicular to the porous medium, while it is not relevant for flows, parallel to the porous medium.

Direct Simulation (Stokes) vs Brinkman with Stress Jump   In the second test for the geometry from Fig.4.20 we use the same equations in the fluid and in the porous subdomains, and the same grids as above. However, the stress jump interface condition, (1.45), is used instead of the continuous stress interface condition, (1.46). The tensor coefficient $\mathcal{M}$ has to be prescribed on the interface in the stress jump condition.

There are two disconnected interfaces between the porous and the plain media (see Fig.4.20), $\Sigma_1 = [0.2, 2.5] \times \{0.92\}$ and $\Sigma_2 = [0.2, 2.5] \times \{0.32\}$ having the same interfacial microstructures. As usual, we assume that $\mathcal{M}$ should be a constant along each of the interfaces, and that $\mathcal{M}_1$ on the upper interface Σ_1 is related to $\mathcal{M}_2$ on the lower interface Σ_2 by (2.43):

$$\mathbf{C} = \begin{bmatrix} \cos \pi & -\sin \pi \\ \sin \pi & \cos \pi \end{bmatrix} \qquad \mathcal{M}_2 = \begin{bmatrix} -1 & 0 \\ 0 & -1 \end{bmatrix} \mathcal{M}_1 \begin{bmatrix} -1 & 0 \\ 0 & -1 \end{bmatrix} = (-\mathbf{I})\mathcal{M}_1(-\mathbf{I}) = \mathcal{M}_1. \quad (4.7)$$

In the Section 4.3 we have obtained the values for $\mathcal{M}'$ fitted for that problem (4.4). The interfacial microstructure there was the same as for the current problem. Therefore, it is interesting to check if $\mathcal{M}_1 = \mathcal{M}'$ (and consequently $\mathcal{M}_2 = \mathcal{M}'$ due to (4.7)) also gives a better approximation to the microscopical solution comparing with the continuous stress interface condition. Thus, we set $\mathcal{M}_1 = \mathcal{M}_2 = \mathcal{M}'$, where $\mathcal{M}'$ is from (4.4). The macrosolution corresponding to this $\mathcal{M}'$ is compared with the microsolution on Fig.4.24, 4.25, and 4.26. We should note that like in the
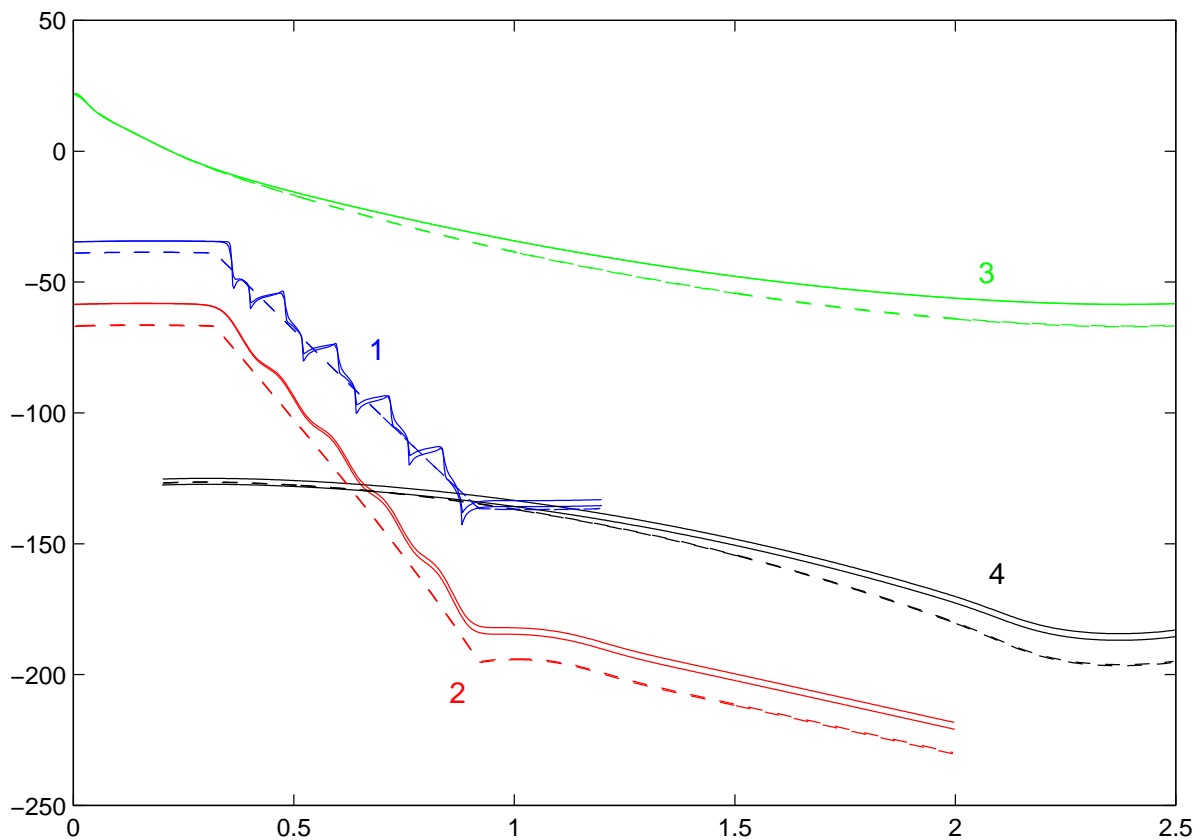
Figure 4.21: p along colored lines $1, 2, 3, 4$ (Fig.4.20). Solid lines − microsolutions 1000×800, 500×400, dashed lines − macrosolutions 500×400, 250×200 (Continuous stress)
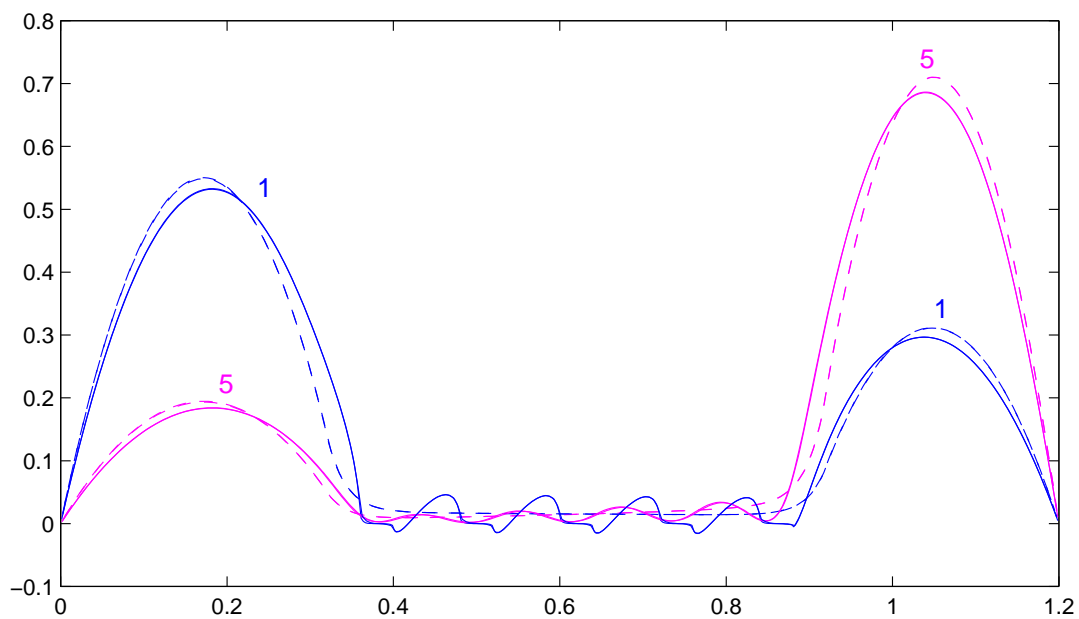
Figure 4.22: u along colored lines $1, 5$ (Fig.4.20). Solid lines − microsolutions 1000×800, 500×400, dashed lines − macrosolutions 500×400, 250×200 (Continuous stress)
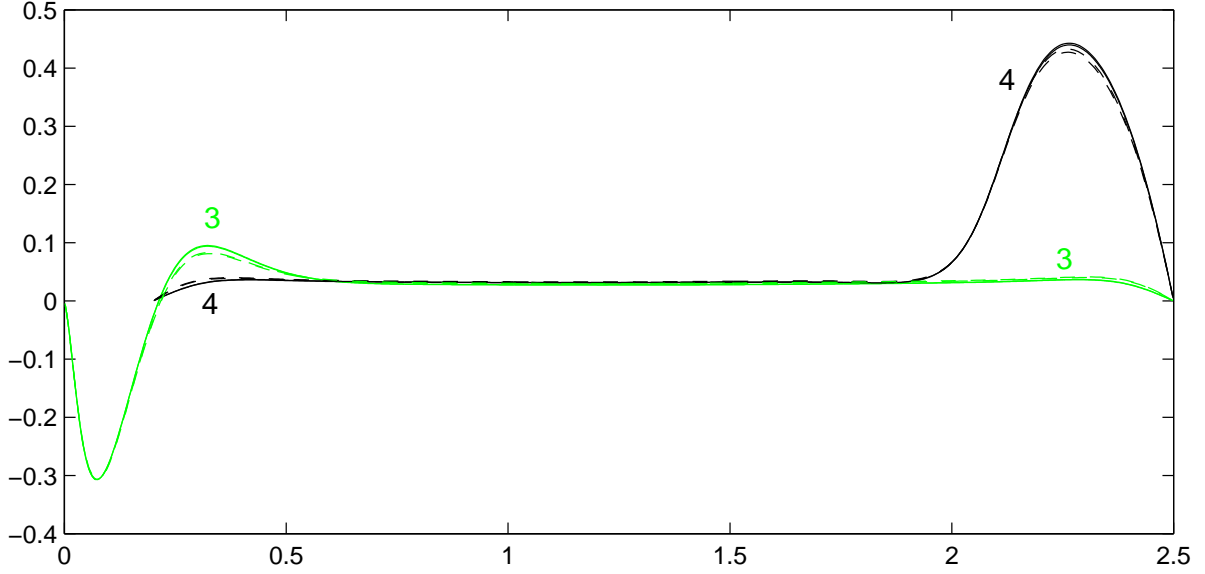
Figure 4.23: v along colored lines $3, 4$ (Fig.4.20). Solid lines – microsolutions 1000×800, 500×400, dashed lines – macrosolutions 500×400, 250×200 (Continuous stress)

Section 4.3 the improvement (compared to continuous stress interface condition) was achieved for all the variables, and on all the lines, where the comparison was made.

Direct simulation (Navier–Stokes, Re100) vs Brinkman with Continuous Stress   In the third and in the fourth tests for the geometry in Fig.4.20 we change the models by adding the convective terms: the microscopical model is the Navier–Stokes system (1.39) in $\Omega_f \cup \Omega_{pf}$. The macroscopic model is (1.38) in Ω_p with $\mu_{eff}/\mu = 1$, (1.39) in Ω_f. The right hand side **f** is identically zero for both tests. The interface conditions are: continuous velocity (1.42), and continuous stress tensor (1.41) conditions. The Reynolds number (Re) appearing here is set to 100. The same grids as before were used. The comparison of the computed solutions at micro- and at macro- level are shown on Fig.4.27, Fig.4.28, and Fig. 4.29. The meaning of the colors and of the lines is the same as above.

Direct simulation (Navier–Stokes, Re100) vs Brinkman with Stress Jump   In the last test for the geometry plotted in Fig.4.20 we use the same models as in the previous test, but the stress jump condition (1.40) is used instead of the continuous stress condition. The coefficient $\mathcal{M}'$ is taken the same, as for the second test, i.e., from (4.4). The results are presented in Fig.4.30, Fig.4.31, and Fig.4.32. Again, as in the second test, the usage of the stress jump condition allows to obtain a good agreement between the micro- and the macro- solutions.

4.5   Summary of the models validation

Our main purpose in this Chapter was to show that the macrosolutions of the (Navier–) Stokes –Brinkman system of equations together with the continuous velocity, jump in stress interface conditions are able to approximate the corresponding microsolutions (at least for the test problems we consider) for some choice of the interface coefficient **M**. In particular we conclude that
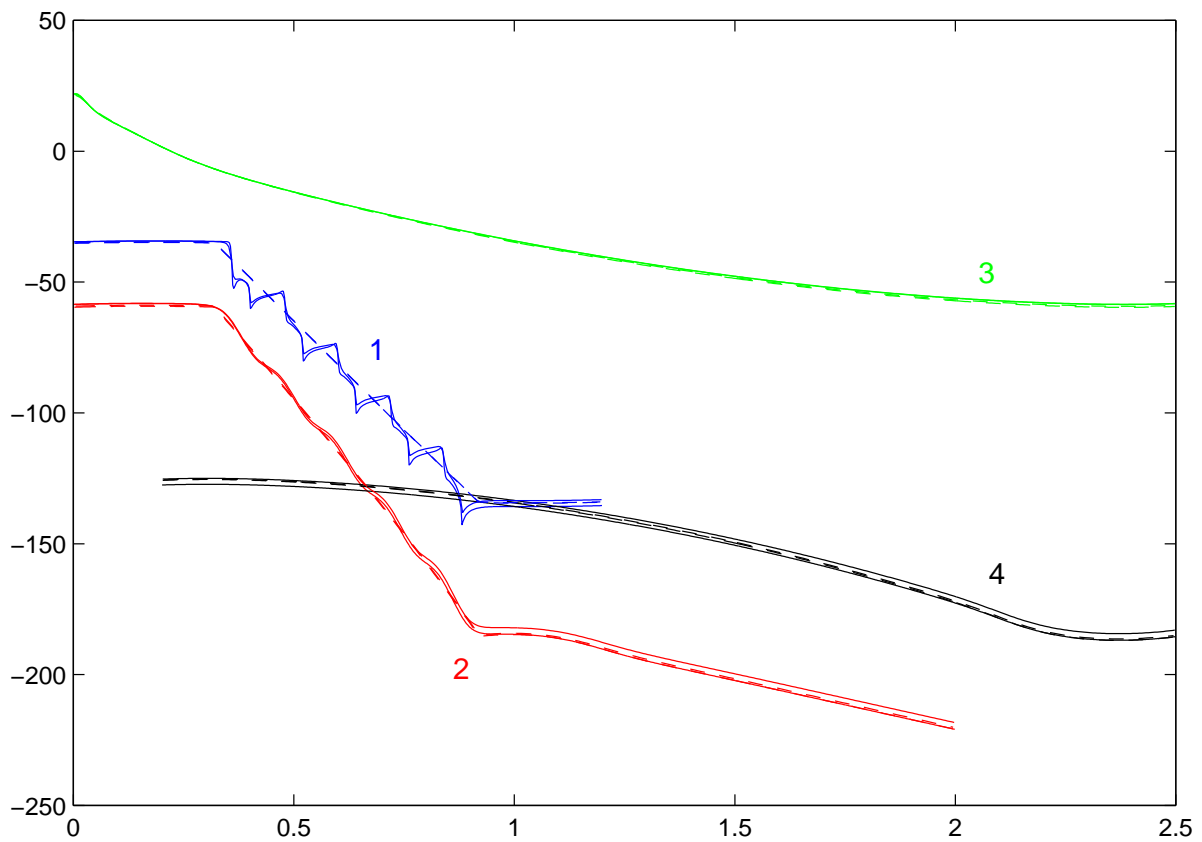
Figure 4.24: p along colored lines $1, 2, 3, 4$ (Fig.4.20). Solid lines – microsolutions 1000×800, 500×400, dashed lines – macrosolutions 500×400, 250×200 (Stress jump)
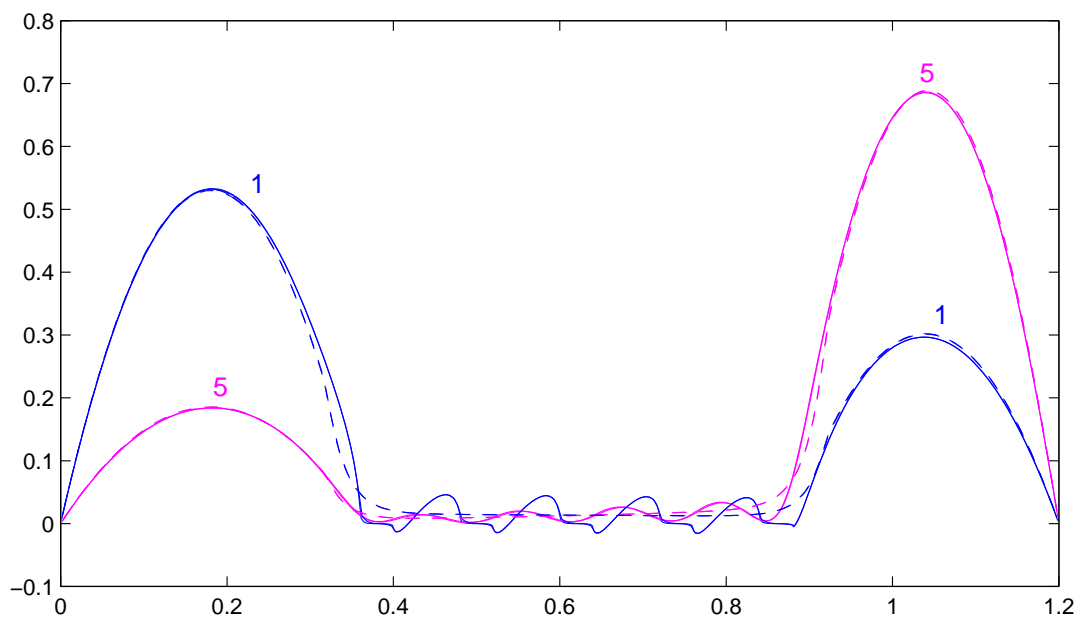
Figure 4.25: u along colored lines $1, 5$ (Fig.4.20). Solid lines – microsolutions 1000×800, 500×400, dashed lines – macrosolutions 500×400, 250×200 (Stress jump)
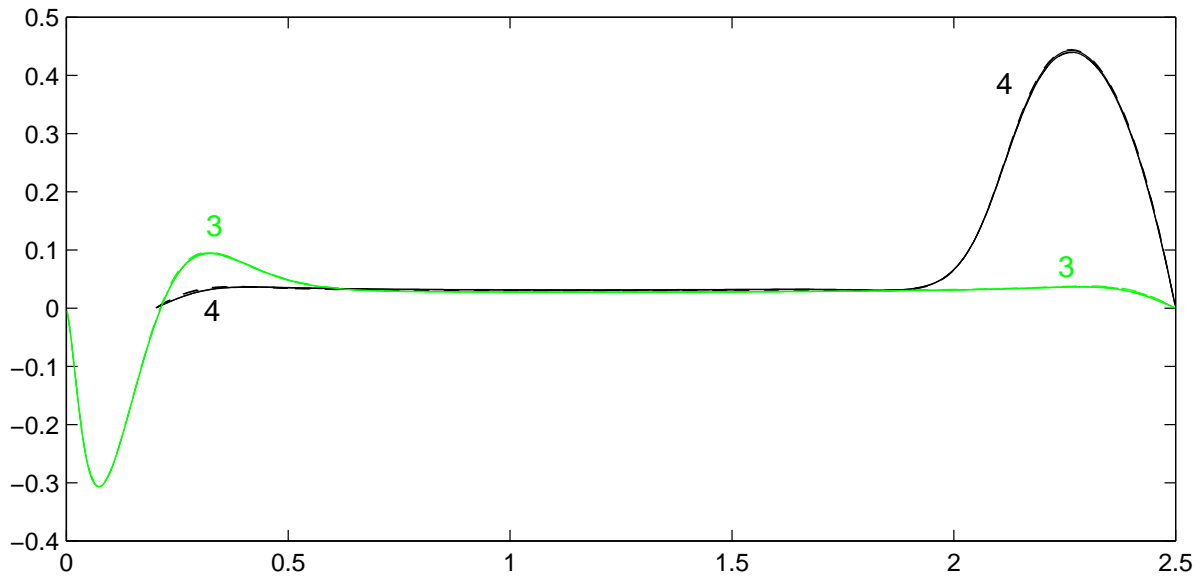
Figure 4.26: v along colored lines $3, 4$ (Fig.4.20). Solid lines – microsolutions 1000×800, 500×400, dashed lines – macrosolutions 500×400, 250×200 (Stress jump)
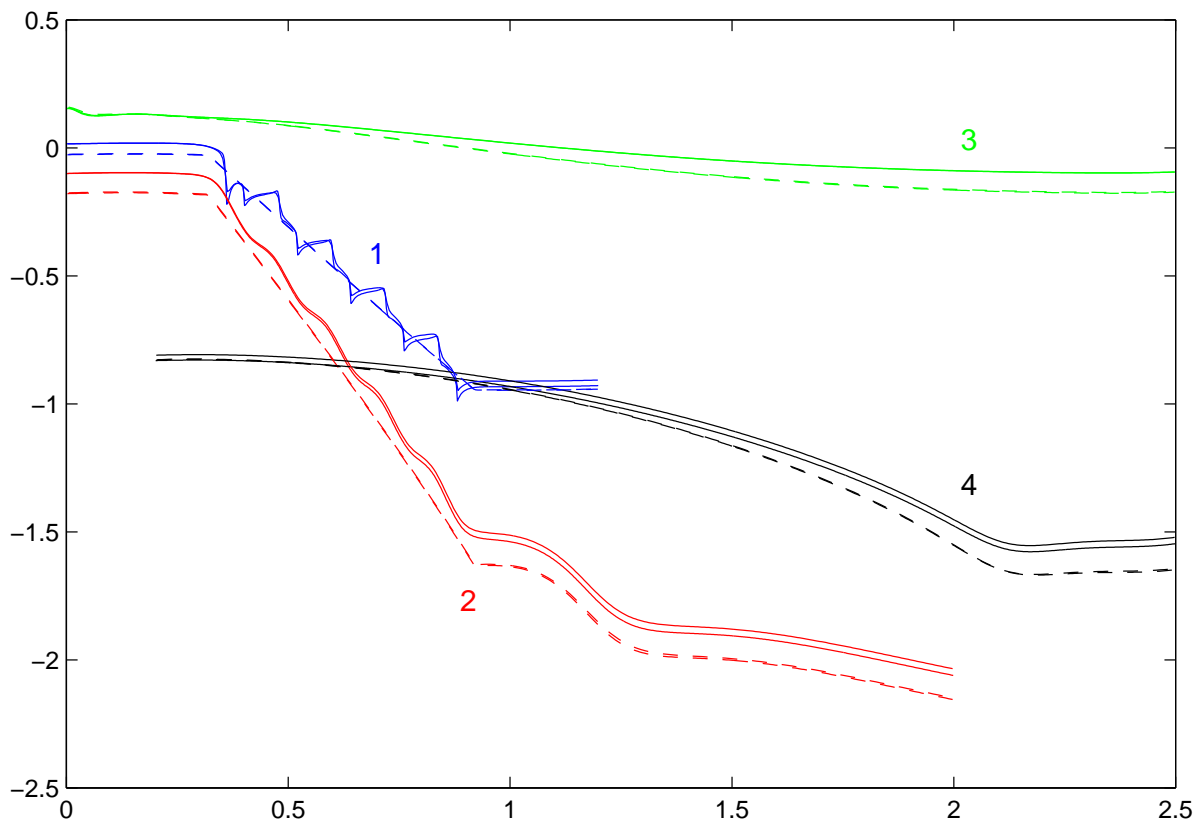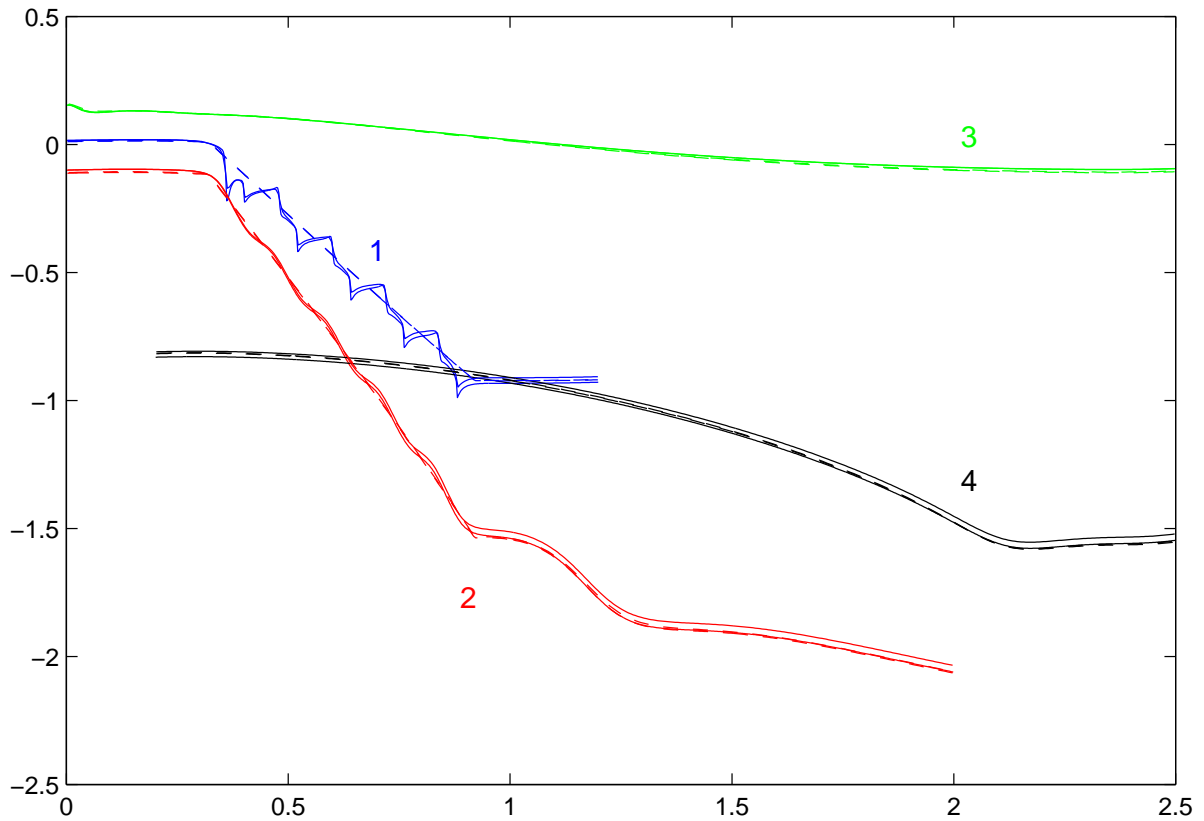

Figure 4.27: p along colored lines $1, 2, 3, 4$ (Fig.4.20). $Re = 100$. Solid lines – microsolutions 1000×800, 500×400, dashed lines – macrosolutions 500×400, 250×200 (Continuous stress)
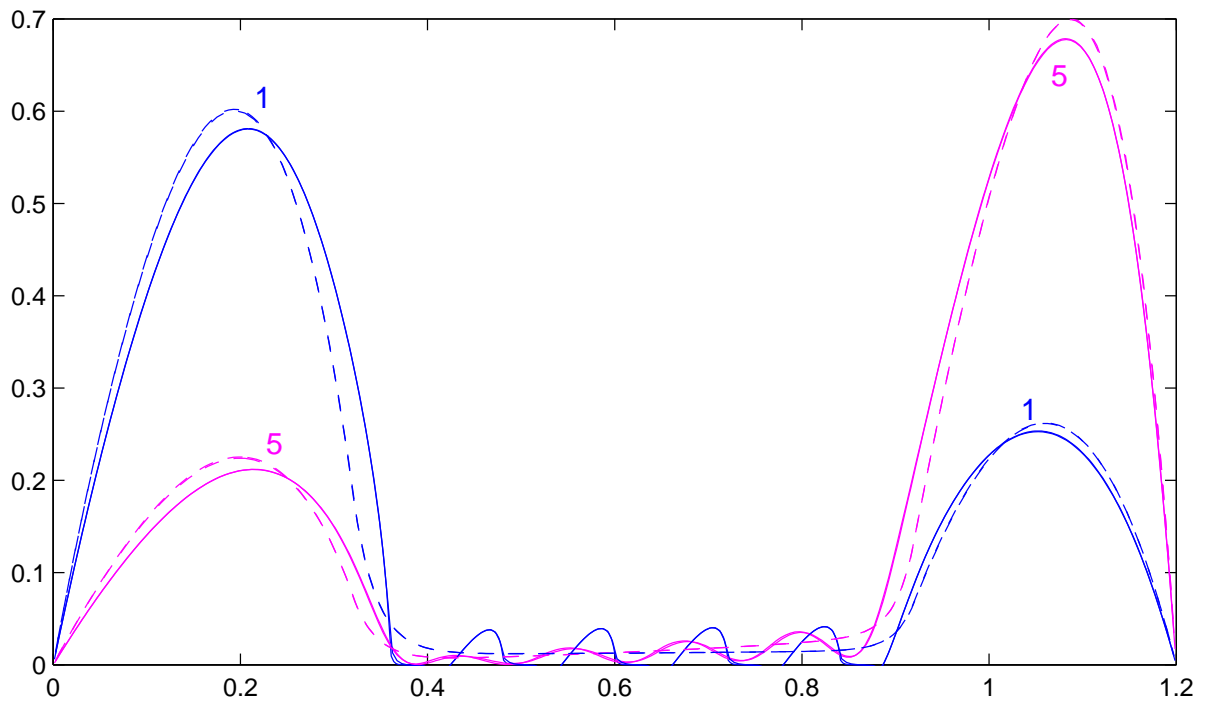
Figure 4.28: u along colored lines $1, 5$ (Fig.4.20). $Re = 100$. Solid lines – microsolutions 1000×800, 500×400, dashed lines – macrosolutions 500×400, 250×200 (Continuous stress)
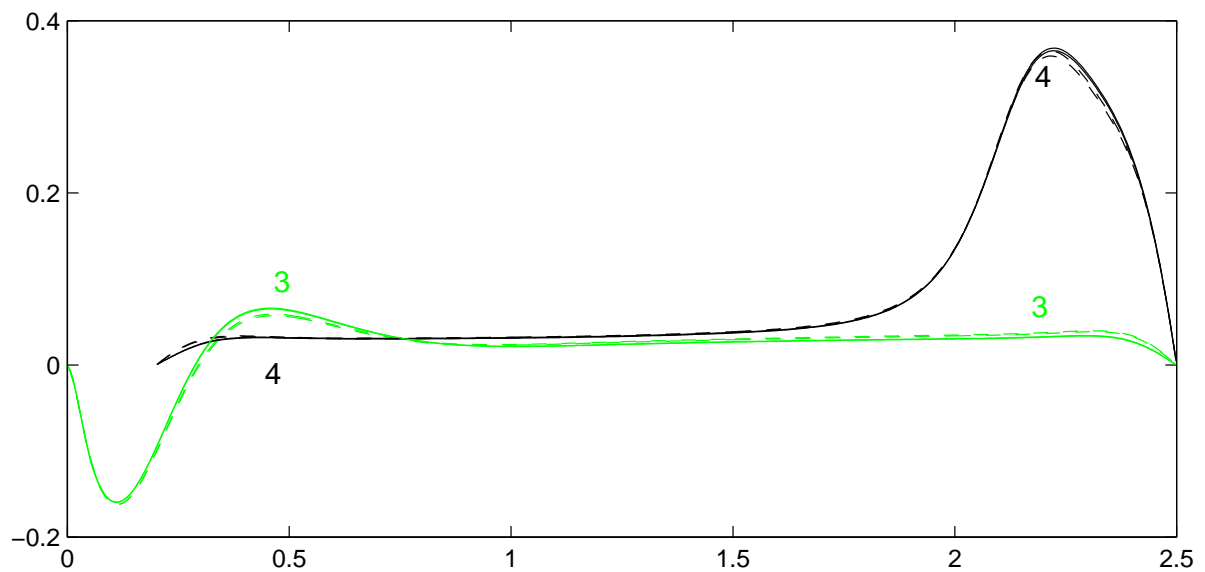
Figure 4.29: v along colored lines $3, 4$ (Fig.4.20). $Re = 100$. Solid lines – microsolutions 1000×800, 500×400, dashed lines – macrosolutions 500×400, 250×200 (Continuous stress)

Figure 4.30: p along colored lines $1, 2, 3, 4$ (Fig.4.20). $Re = 100$. Solid lines – microsolutions 1000×800, 500×400, dashed lines – macrosolutions 500×400, 250×200 (Stress jump)
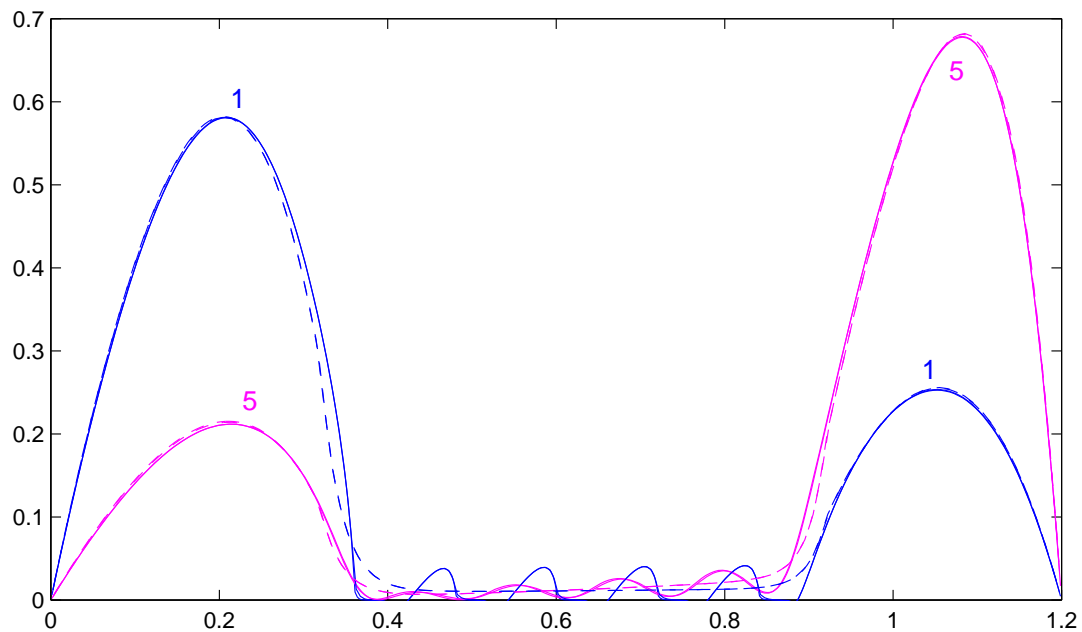
Figure 4.31: u along colored lines $1, 5$ (Fig.4.20). $Re = 100$. Solid lines – microsolutions 1000×800, 500×400, dashed lines – macrosolutions 500×400, 250×200 (Stress jump)
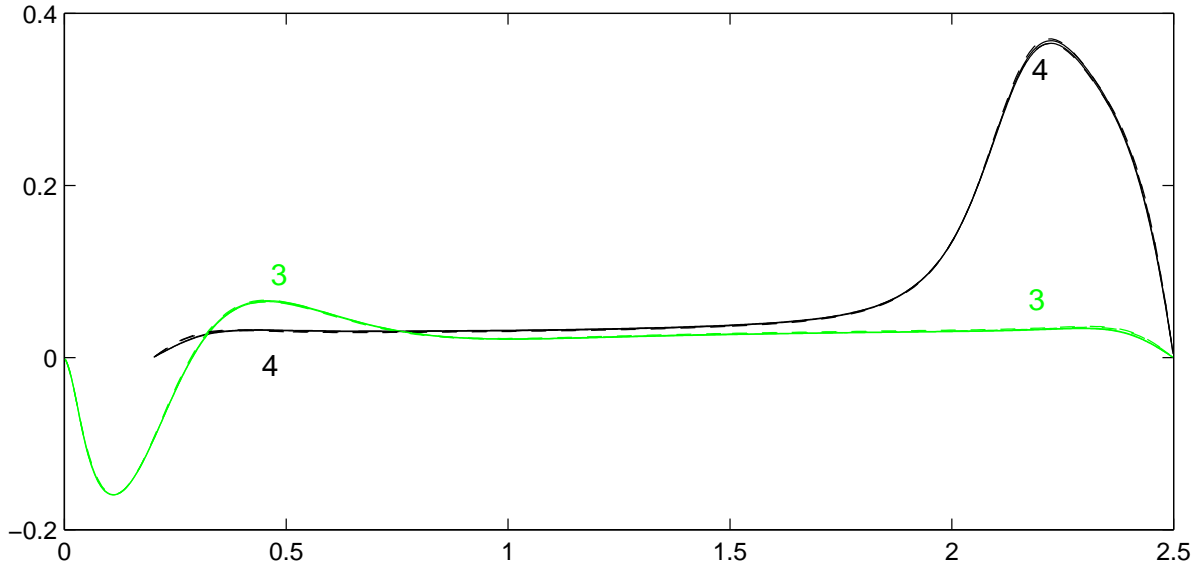
Figure 4.32: v along colored lines $3, 4$ (Fig.4.20). Solid lines – microsolutions 1000×800, 500×400, dashed lines – macrosolutions 500×400, 250×200 (Stress jump)

the (Navier–)Stokes – Brinkman system was a reasonable model to describe the flow inside the porous media (for all tests).

From a practical point of view it is desirable that $\mathbf{M}$ would be a property of the microstructure in the interfacial region. This hypothesis is very strong if we apply it without restrictions since it means that whenever $\mathbf{M}$ is somehow determined then one is able to solve different types of coupled flows. We don't know whether the hypothesis in this general form can be justified or whether it is true. More probably it has some applicability area (like almost all models), describing at what situations and for which types of flow it can be applied. For example, in the section 2.1 we investigated the model in the case of the parallel flow in a channel for small Da numbers and proposed the way to calculate $\mathbf{M}$ in accordance with experimental and theoretical results.

Nevertheless, we used the hypothesis in order to minimize the effort while fitting $\mathbf{M}$: we chose one $\mathcal{M}'$ for the plain interface corresponding to CG I microgeometry and one $\mathcal{M}''$ for the plain interface corresponding to CG II microgeometry, in the "laboratory" system and used these values to calculate $\mathbf{M}$ for the test problems at different points on the same interface; on different interfaces provided they have similar microgeometries; for different types of flow (only for CG I); and for models with and without convective terms (only for CG I). In all the cases the macroscopic solution for such $\mathbf{M}$ was rather close to the microscopical solution. Although we tried to choose the series of test problems to be representative in the area of moderately small Darcy numbers, it is not enough to confirm the hypothesis and to claim that the given $\mathcal{M}'$, $\mathcal{M}''$ should be always used in other test problems for the microgeometries CG I, CG II (there might be other coefficients $\widetilde{\mathcal{M}}'$, $\widetilde{\mathcal{M}}''$, e.g. containing non-zero $\mathcal{M}_{12}$, $\mathcal{M}_{22}$, still giving appropriate results in a larger applicability area).

From our point of view the Navier-Stokes Brinkman model with continuous velocity, stress jump condition on the porous–fluid interface is a promising model for solving the coupled flow. But it is still not clear how to determine $\mathbf{M}$ in practical situations. In such situations it is possible to choose for example $\mathbf{M} = \mathbf{0}$ and to deal with the continuous stress condition on the interface (or to choose some $\mathbf{M}$, not necessarily the best one). Our test results for this model

were qualitatively correct, even if the discrepancies with the microsolution were significant. The model with the Navier–Stokes–Brinkman system and $\mathbf{M} = \mathbf{0}$ is used in the next Chapter to simulate flows in some 2D/3D filters. For a 3D car filter we compared the computational results with experimental in a large diapason of Reynolds numbers and for a very small Darcy number (too small for microscopical simulations). A reasonable prediction was obtained if we take into account the measurement errors and the discussed weakness of the macroscopic model with the continuous stress interface condition to give precise results.

Chapter 5

Numerical simulation of a class of industrial flows

In this chapter we present results from numerical simulations of certain industrial flows. The first section deals with simulation of 3D oil flows through car filters, while the second section deals with 2D,3D flows through ceramic filters. The simulations were performed using our own software, which is an object–oriented implementation of the presented here algorithm. For the case of oil filters this software works together with a Preprocessor, developed by A. Vaikuntam and A. Wiegmann [58, p.35] in the Fraunhofer Institute for Industrial Mathematics. The Preprocessor reads the CAD data (describing the filter housing and the filtering medium) in STL format, and generates a Cartesian grid within the filter housing. This grid is further used in the computations presented below. The visualization is done with MatLab.

5.1 Simulation of 3-D oil flow through car filters

5.1.1 Introduction

The purpose of oil filters is to filter out (small) dirt particles from the oil. Top and bottom pans of a filter housing are shown in Fig.5.1, a sketch of a cross-section of a filter assembly is shown on Fig.5.2. Several challenging mathematical problems have to be solved to support the design of oil filters: detailed simulation of coupled flows through filters (i.e., through pure liquid interior of the filter housing and through the porous filtering medium); modeling and simulation of capturing of dirt particles by the filtering media, interaction of the flow and the deformable filtering medium, optimal shape design, etc. Here we discuss the first of these problems, i.e. coupled flows simulations. The main aspects in this case are:

- choice of an adequate mathematical model for the flow in each of subregions;

- usage of proper interface conditions between different media;

- development of efficient and robust numerical algorithms and software;

- usage of correct input parameters (e.g., permeability, viscosity, etc.).

The used in this Chapter mathematical model corresponds to the Navier–Stokes–Brinkman system of equations (1.38, $\mathbf{f} \equiv \mathbf{0}$) with continuous velocity (1.42) continuous stress tensor *interface conditions* on the porous–fluid interface (1.46). The interface conditions are set in accordance with the results from the preceding Chapter. As it was shown there, continuous

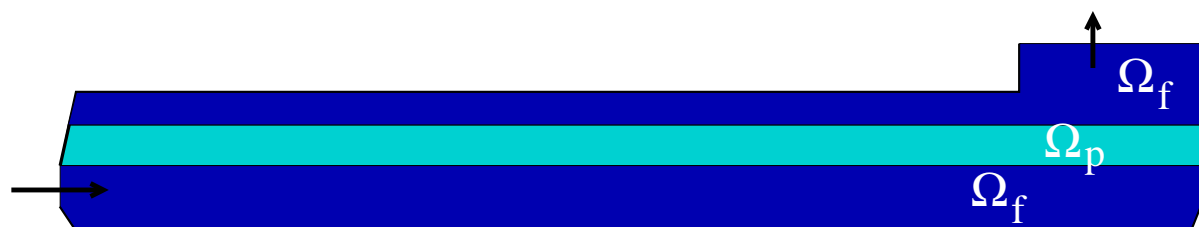Figure 5.1: Top pan (left) and bottom pan (right) of a filter housing;

Figure 5.2: A schematic drawing of a vertical cross-section of the filter

stress tensor condition is a good choice for the case when the direction of the flow is mostly perpendicular to the interface between the plain and the porous media. Because the aim of the designers is to achieve such a flow within the filter housing, we choose this interface condition in our simulations below.

Numerical algorithms for solving the coupled system can be conventionally subdivided into two groups. In the first group there are algorithms, using different systems of equations in different subdomains (e.g., Navier-Stokes in liquid zones, and Darcy or Brinkman in the porous zones), and coupling them through the interface conditions. Such algorithms are (naturally) based on domain decomposition (DD). This approach has an advantage: one can use existing algorithms and software for solving Navier-Stokes equations and for solving porous media flows. But it also has a drawback: the convergence (at least for the additive and multiplicative versions of DD) might be slow in the case when the inlet and the outlet are completely separated by the porous medium, which is the case with the oil filters. For more details on this approach see, for example, [31] and references therein.

In the second group there are algorithms, using one system of equations in the whole domain, for example, the Navier-Stokes-Brinkman system. In some of commercial CFD software (e.g. Star-CD, Fluent, etc.) the Navier-Stokes-Brinkman system is solved by algorithms developed for the Navier-Stokes system, which are modified so that the main term describing the flow through the porous media is treated explicitly (i.e., taken from the previous time step in the unsteady case, or taken from the previous iteration in the algorithms for the steady state problems). From our point of view it is preferable to treat this term implicitly, as it was already described in Chapter 3.

The usage of correct parameters might be critical for some of the applications. The manufacturers continuously offer new filtering media, and usually their permeabilities are not known. The traditional approach here is to calculate the permeability on the basis of laboratory experiments. A more recent approach supposes an usage of microstructure simulations (see for details [59],[58, p.32]). In this case, a 3D picture of a piece of the filtering medium is taken (say, by X-ray computer tomography), and after that 3-D image analysis is performed in order to obtain a computer representation of the microstructure of the porous material. Next, one solves Stokes equations in the complex microlevel-geometry, to calculate permeability on the basis of homogenization theory [13]. Among others, this approach has an advantage: it is a natural component of virtual material design [59]. Such a way for determining the permeability, although more advanced, is still not realized in our case although the first step (3D image) is done. Instead, the permeability of the filtering medium is determined from measurements.

The interface conditions and the algorithm are described in the preceding Chapters. Below we will discuss the particular way for determining the permeability from measurements, the comparison of the measurements and the simulations, and the results from the numerical simulations. We note, here we will present only a part of the obtained results, namely those for which we have a permission from industrial partners. Also, most of the particular parameters, which are used in simulations, will not be specified. Anyway, the presented results should give an impression about the abilities of the developed algorithm and software.

5.1.2 Calculation of permeability from measurements and comparison between simulations and measurements

The permeability of the filtering medium, used in most of simulations, was measured in a laboratory. For this purpose a special filter was constructed in such a way that the flow was essentially perpendicular to the filtering medium (we assume an isotropic medium). The flow rate Q of the oil was prescribed, and the pressure drop Δp was measured. Below we shortly explain how the permeability was extracted from the measurements.

To calculate the permeability, we use the Darcy law:

$$u = -\frac{K}{\mu}\nabla p$$

u stands for the Darcy velocity, K stands for the permeability, μ for the viscosity, p for the pressure. The pressure gradient can be approximated as $\nabla p = \frac{\Delta p}{\Delta l}$, where Δl is the thickness of the porous media. Rearranging the terms in the Darcy law, we obtain

$$K = -\frac{\mu\,u}{\nabla p} = -\frac{\frac{\mu}{\rho}\,\rho\,u}{\frac{\Delta p}{\Delta l}} = -\frac{\nu\,\rho\,(u\,S)\,\frac{1}{S}\,\Delta l}{\Delta p} = -\frac{\nu\,\rho\,Q\,\Delta l}{S\,\Delta p}.$$

Here S, ν, ρ stand for the surface of the porous material, for the kinematic viscosity and for the fluid density, respectively. It will be more suitable for us to change some of the measurements units.

$$K[m^2] = -\frac{\nu[m^2/s]\,\rho[kg/m^3]\,Q[m^3/s]\,\Delta l[m]}{S[m^2]\,\Delta p[kg/(m\,s^2)]} =$$

$$= -\frac{(10^{-6} * \nu[mm^2/s])\,\rho[kg/m^3]\,\left(\frac{10^{-3}}{60} * Q[l/min]\right)\,\Delta l[m]}{S[m^2]\,(10^2 * \Delta p[mbar])} =$$

Finally we have

$$K[m^2] = -\frac{1}{6} * 10^{-12}\,\frac{\nu[mm^2/s]\,\rho[kg/m^3]\,Q[l/min]\,\Delta l[m]}{S[m^2]\,(\Delta p[mbar])}. \tag{5.1}$$

A series of experiments was performed for different flow rates and temperatures. The resulting permeability values calculated by (5.1) belong to some interval (K_{min}, K_{max}) with $(K_{max} - K_{min})/K_{max} \approx 0.25$. We have noted some temperature dependence of these values. The averaged value $(K_{max} + K_{min})/2$ we refer as K_{av}.

Further, we need the permeability values for simulations of oil flows through a particular filter (i.e., particular filter housing and particular filtering medium, see for example Fig. 5.5, right). The filters we consider are designed to be used at temperature range of $60°C$ and flow rates differing more then one order of magnitude. As it is known, viscosity of the oil ($\nu = \nu(T)$) strongly depends on the temperature: at the lowest temperature it is 40 times larger than at the highest temperature. This leads to a difference of more than two orders of magnitude in the Reynolds number. We (and industrial partners), were mainly interested in flows at low Re, because these are the so called cold regimes. For cold regimes significant pressure is needed, therefore optimization of the flow for such regimes is especially important. The density may also be the temperature–dependent function: $\rho = \rho(T)$. The experimental data of the total pressure difference ΔP between Inlet and Outlet of the filter for the series of flow rates Q and temperatures T were available to compare the simulations and measurements.

According to our model, if the permeability of the porous medium is fixed, then we have only one dimensionless parameter Re (Da number is fixed). Therefore some pairs (Q, T) with different Q and T may correspond to the same dimensionless calculation. We can use Q and the area S of the Inlet region of the filter to define a characteristic velocity $U = Q/S$, and choose some characteristic length L of the filter. Then the experimental data $(Q, T, \Delta P)$ can be transformed into dimensionless numbers $(Re, \Delta P_*)$ by

$$Re = \frac{UL}{\nu(T)} \quad (\text{where } U = \frac{Q}{S}), \qquad \Delta P_* = \frac{\Delta P}{\rho(T)U^2} \tag{5.2}$$

(see subsection 1.4.1). Since Re and ΔP_* vary in orders of magnitude, it is reasonable to deal with their logarithms. We found out that the data $(logRe, log\Delta P_*)$ corresponding to the same T and different Q perfectly lie on smooth lines (see Fig. 5.5, left). The lines corresponding to high temperatures T overlap very well, but for low temperatures the lines are shifted one with respect to another. This means that using dimensionless simulations (macroscopic or microscopic) for the whole range of Reynolds numbers it is not possible to fit well all the experimental data. This discrepancy can occur due to measurement errors as well as presence of significant factors which were not taken into account in our models. As a result of macroscopic simulations we also have pairs $(Re, \Delta P_*)$. If one is mostly interested in the total pressure difference at some flow rate, temperature $(\Delta P(Q, T))$ then it is possible to obtain several pairs $(Re, \Delta P_*)$ from macroscopic simulations, and then to construct the function $\Delta P_*(Re)$ by interpolation. Again, it is better to do it on the log-log plot, where the points $(logRe, log\Delta P_*)$ are disperse and lie almost on a line. The interpolation can be done for example by the least squares approximation method. Then for a given (Q, T) we can calculate the corresponding Reynolds number Re from (5.2) and use $\Delta P_* = \Delta P_*(Re)$ to calculate the dimensional pressure ΔP from (5.2).

The relative errors (in %) between the experimentally measured pressure drop and predicted by four calculations (the black boxes in Fig.5.5, left) and interpolation (the black line in Fig.5.5, left) are presented in the following table. For all calculations the value K_{av} was used for permeability. The blank entries ” ” in the table mean that no experiments were done for this (T,Q), ”−” corresponds to the flow regime with high Reynolds number where only the experimental data were available:

$T\backslash Q$	4.0	6.0	8.0	10.0	15.0	20.0	30.0	32.5	40.0	50.0
24	-23.8			-25.7		–	–		–	–
10	-21.1			-22.8		-23.5	–		–	–
-4	-23.8			-19.4		-18.5	-20.4		-22.0	–
-18	-7.8	-0.8	0.6	-2.8	1.0	5.7	12.4	11.3		
-26	34.9	36.9	41.1	45.4						

Since the experimental results corresponding to different temperatures represented as points on the log-log plot don't lie on the same line, it was not possible to approximate all of them using the same K and different Re. Only the group of results for $T = -18°C$ is well approximated. We tried to find the specific values of K for the other group of experimental results for $T = -4°C$, $T = 10°C$, $T = 24°C$ (the corresponding points lie almost on the same line). The relative errors for two other values of K are presented in the following tables. In both cases the approximations for this particular group become better.

$T\backslash Q$	4.0	10.0	20.0	30.0
24	-11.3	-14.9	-22.3	–
10	-8.4	-10.3	-12.3	-19.2
-4	-11.4	-6.4	-5.2	-7.8

$T\backslash Q$	4.0	10.0	20.0	30.0
24	3.1	-1.5	-11.5	–
10	7.1	4.3	1.5	-7.0
-4	3.7	9.5	10.4	7.1

5.1.3 Simulation of 3-D flow though oil filters

Here we present some 3-D simulations of oil flows through filters shown in Fig.5.1 and in Fig.5.5 (right), respectively. While the first figure shows the top and bottom pan for one filter, the second figure represents the computational domain for another filter. The computational domain is formed by the interior of the filter housing, thus the second figure gives also impression about the internal shape of a filter housing.

First, we will present some illustrative results for the filter from Fig.5.1. In this case we use some model data, aiming at a qualitative study of the flow. Pressure distribution (illustrated by the colors) and velocity distribution vectors (illustrated by the arrows) in two horizontal cross-sections are presented in Fig.5.3. A very useful information is presented in Fig.5.4. The
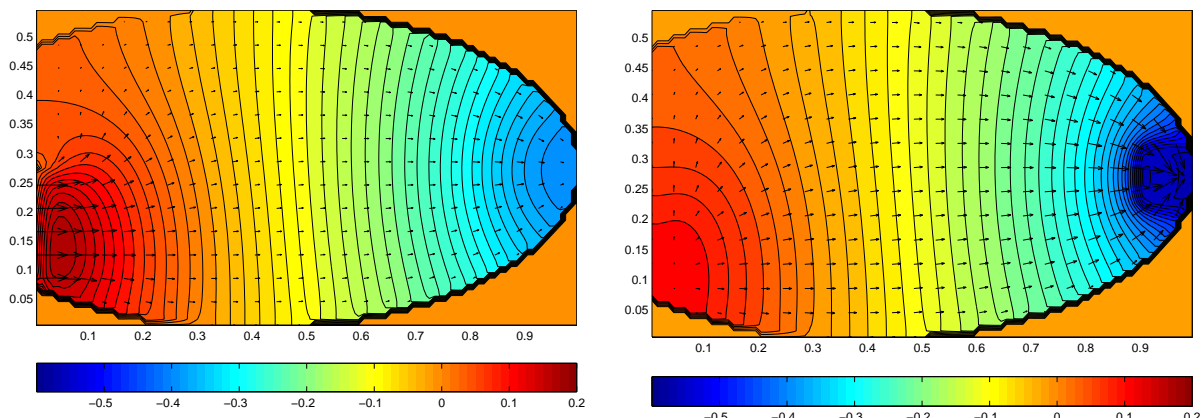

Figure 5.3: Pressure (colors) and velocity (arrows) at horizontal cross-section near the bottom (left) and near the top (right)

mass flow rate from the upper surface of the filtering media is shown there. It can be seen, that the filtering medium is non-uniformly loaded in this case. Of course, the aim of the designers is
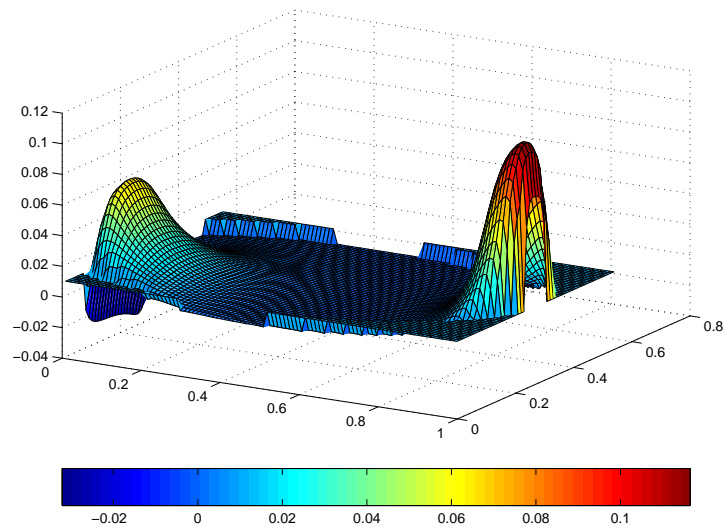
to avoid such situations.

Figure 5.4: Mass flow rate from the upper surface of filtering media

To discretize the problem from Fig.5.5 (right), we used about 200 control volumes in OX and in OZ directions (see also Fig.5.6,5.7). In OY direction, the grid was non-uniform and the pipe was prolongated upwards to have a fully developed flow near the boundary with "Outlet" boundary conditions. In the main part of the filter the discretization step in OY was smaller than 0.002. The (scalar) permeability of the filter was experimentally determined, as explained above.

In Fig. 5.6, 5.7 some typical velocity and pressure fields are presented in a vertical (OX, OY) and two horizontal (OX, OZ) cross-sections, respectively. Such information is used by designers, in particular, for locating ribs (these are elements of the top pan, which have the task to support the soft filtering medium, see Fig.5.5 (right)).

Such simulations make it possible to obtain the flow properties of the filter during the design stage without creating a prototype needed for the experiments. The important properties are the total pressure difference that a pump should provide for the given flow rate and the detailed flow field needed to design the ribs supporting the filter.
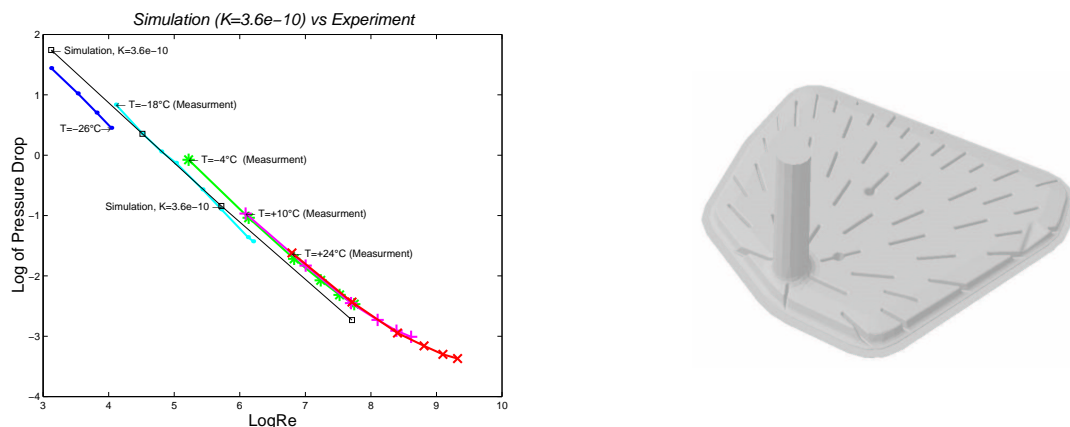

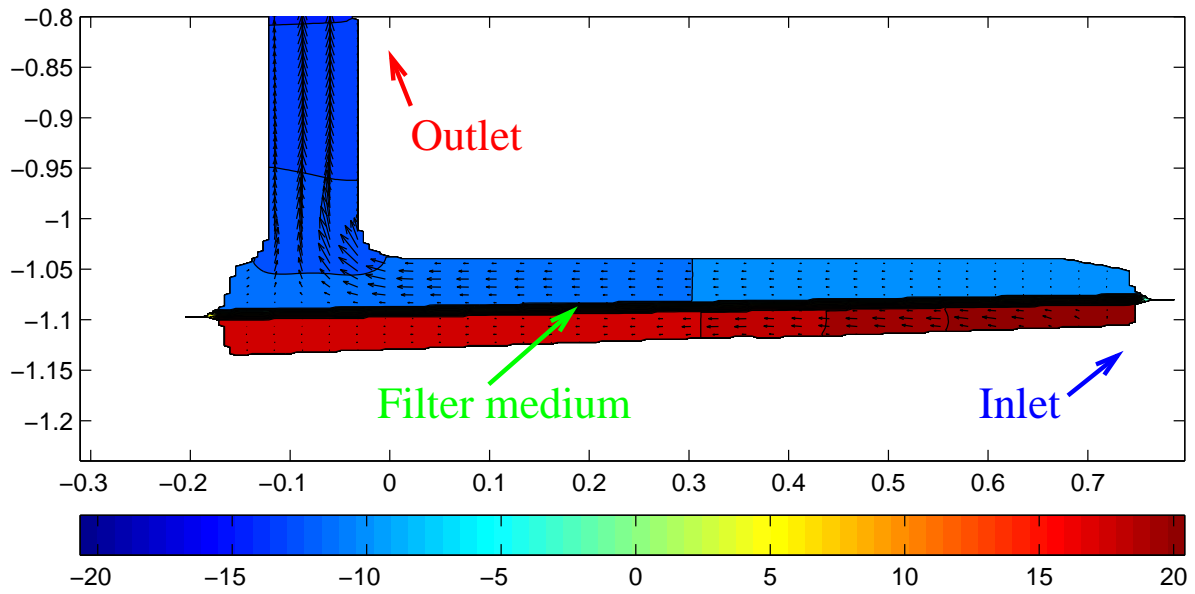Figure 5.5: Exper. and simul. results on log-log plot (left). 3D Filter box with ribs (right).

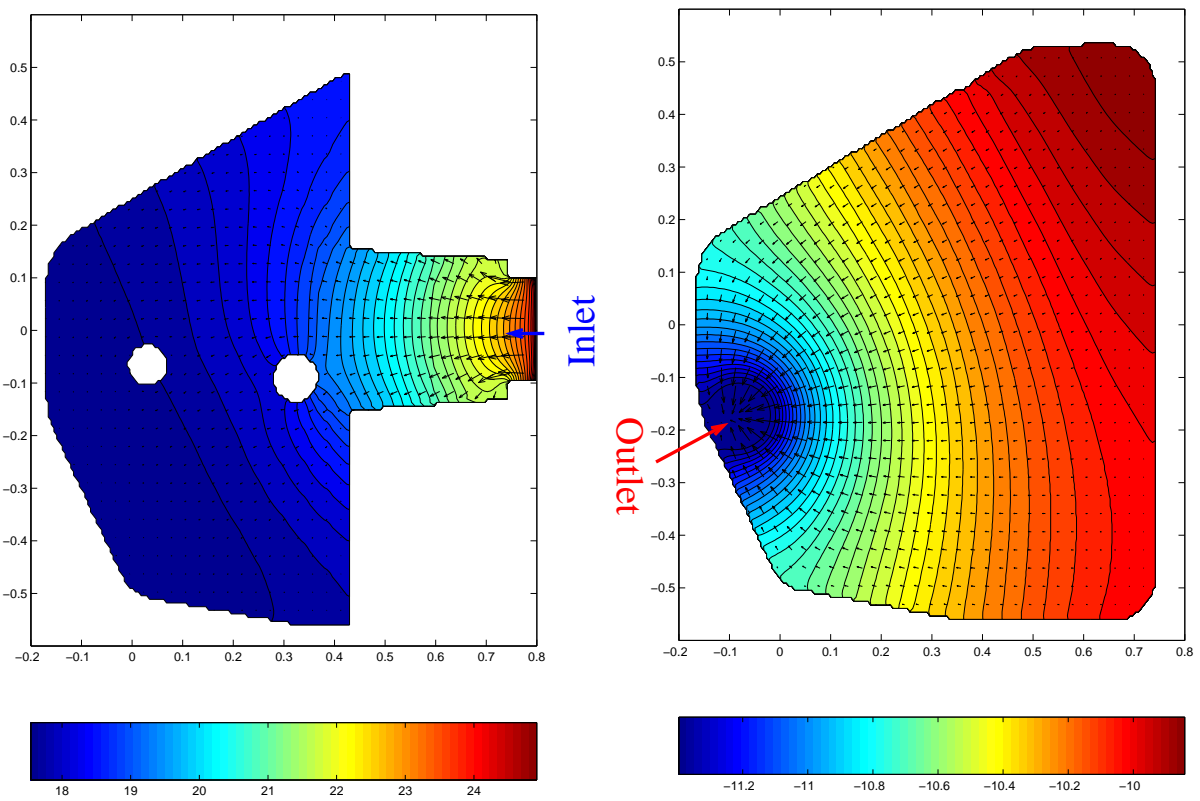Figure 5.6: 3D Filter. pressure and velocity fields vertical cross-section (OXY plane)

Figure 5.7: 3D Filter. pressure and velocity fields below (left) and above (right) the filter medium (OXZ plane)

5.2   Simulation of 2D,3D flows through ceramic filters

In this section we present some simulations for flows through ceramic filters. Such filters have been more and more often used. Our particular task was to support the understanding of the influence of the geometry and the permeability on the pressure drop. Thus, we carried out simulations for the case of a rectangular isotropic filtering media, rectangular anisotropic filtering media in 2D, and a 3D filtering media with the shape of a cylinder with drilled holes from the inflow side. The idea in the last case is to reduce the pressure drop by drilling holes, which have a smaller depth, compared to the depth of the filtering medium. The pressure drop in such a case should be lower, but the interesting question is what the velocity and pressure distributions within the filtering medium are in this case. We note that in these cases we did not use in the simulations the real data, but some model values, just to study the phenomena qualitatively.

In the 2D test the isotropic permeability tensor, $\mathbf{K_{is}}$, and the anisotropic permeability tensor, $\mathbf{K_{anis}}$, used in simulations, are given by

$$Da \times \mathcal{K}_{is} = \begin{pmatrix} 0.0174 & 0 \\ 0 & 0.0174 \end{pmatrix}, \quad Da \times \mathcal{K}_{anis} = \begin{pmatrix} 0.0174 & -0.0139 \\ -0.0139 & 0.0174 \end{pmatrix}$$

$\Omega = (0,2) \times (0,1)$, $\Omega_p = (0.5,1.5) \times (0,1)$, $Re = 100$. The channel has solid walls $y = 0$, $y = 1$. The uniform Dirichlet condition is prescribed on the left boundary and the "Outlet" condition on the right boundary. In Fig.5.8 the calculated pressure is represented by colors, while the velocity is illustrated by arrows.
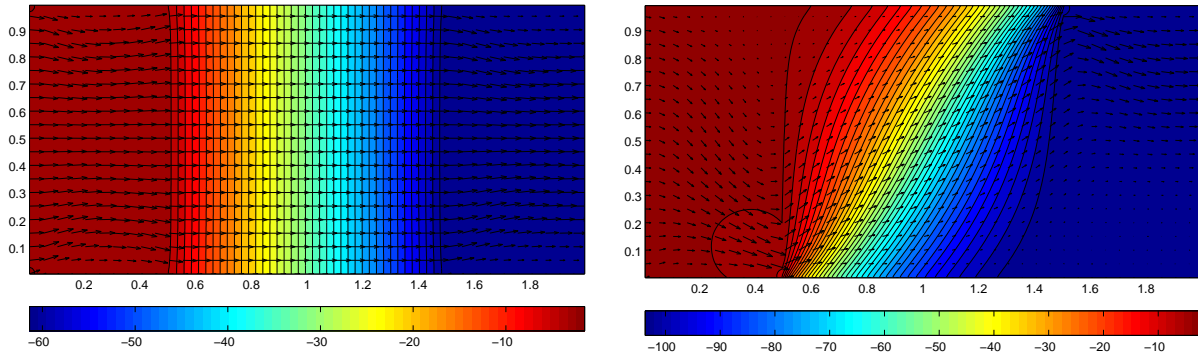

Figure 5.8: Pressure (colors) and velocity vectors (arrows) for coupled flow through isotropic (left) and through anisotropic (right) porous media.

In the 3D test we consider a cylindrical channel, directed according to OZ with length 15.0 and radius 5.4. A 3D ceramic filter placed between $z = 4$ and $z = 9$ separates Inlet with uniform Dirichlet boundary conditions from the right boundary with "Outlet" boundary conditions. Other boundaries are solid walls. The filter medium was a cylinder before holes with different diameter and length were drilled (see Fig.5.9). The parameters used for the simulation are $Re = 3000$, $Da \times \mathcal{K} = 3 \times 10^{-5}\mathbf{I}$. For this problem with high Reynolds number the 1st order Upwind differencing scheme was used. (see Subsection 3.1.4). The Grid was $100 \times 100 \times 100$. We have checked that similar results can be obtained if one consider only a quarter of the domain: $x > 5.4$, $y > 5.4$ with "Symmetry" boundary condition on the planes $x = 5.4$, $y = 5.4$. In the Fig.5.10,5.11,5.12 the pressure and velocity fields are plotted in some crossections of the quarter of the initial computational domain (other parts can be reconstructed by symmetry).
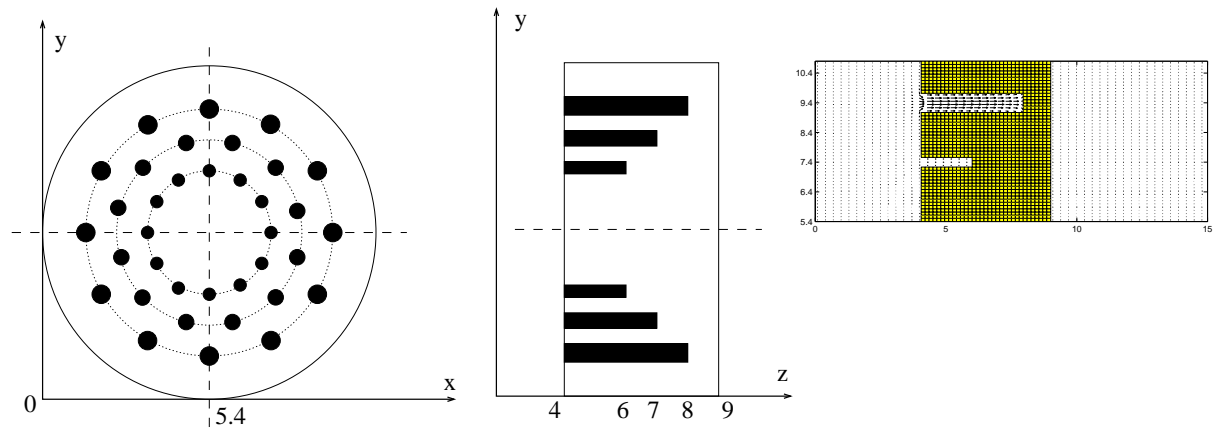
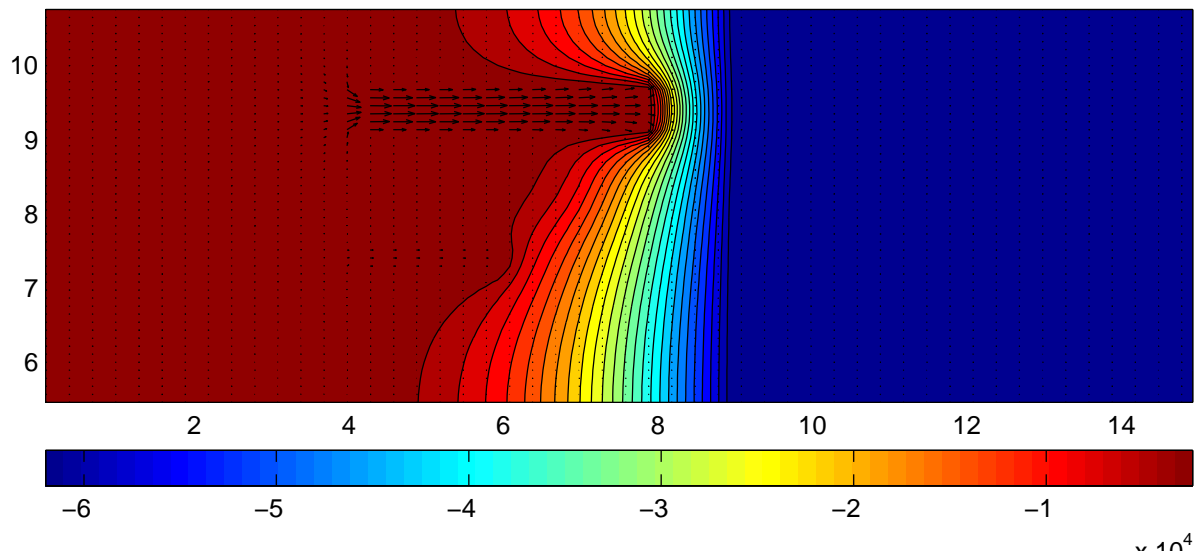Figure 5.9: Geometry of the 3D ceramic porous medium with holes

Figure 5.10: OZY plane at $x = 5.4$, (only the part $y \geq 5.4$). Pressure (colors) and velocity vectors (arrows) for the coupled flow (top) and the geometry of the computational domain (bottom)
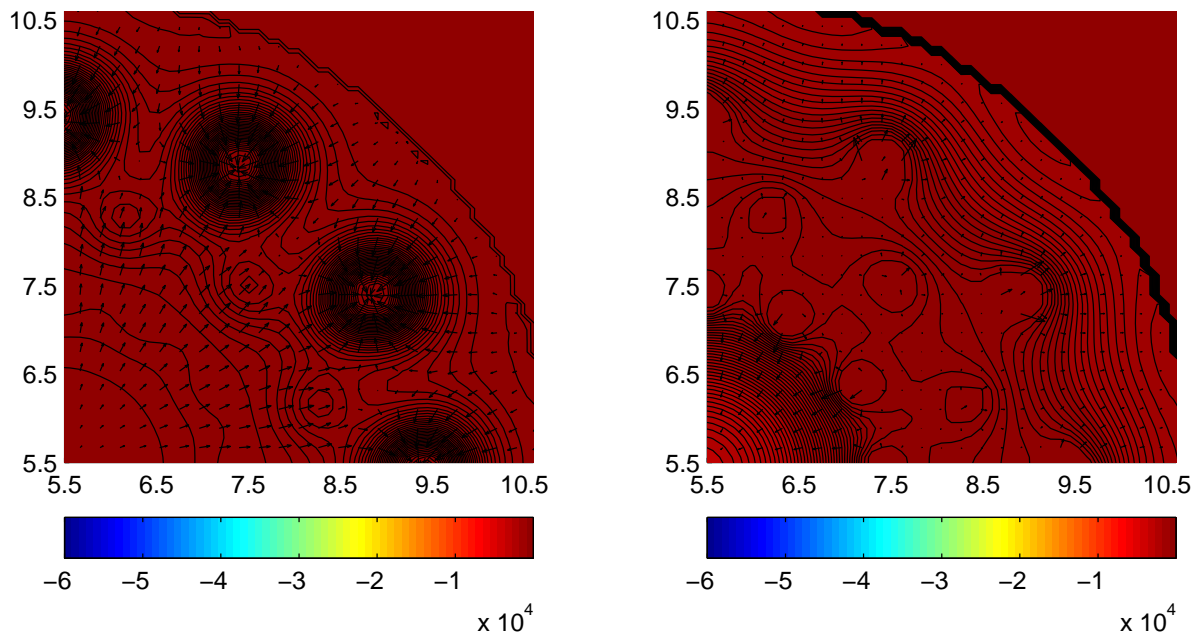
Figure 5.11: Quarters of the OXY planes ($x > 5.4$, $y > 5.4$) at $z = 3.45$ (left), $z = 4.95$ (right). Pressure (colors) and velocity vectors (arrows) for the flow in the ceramic filter with holes.
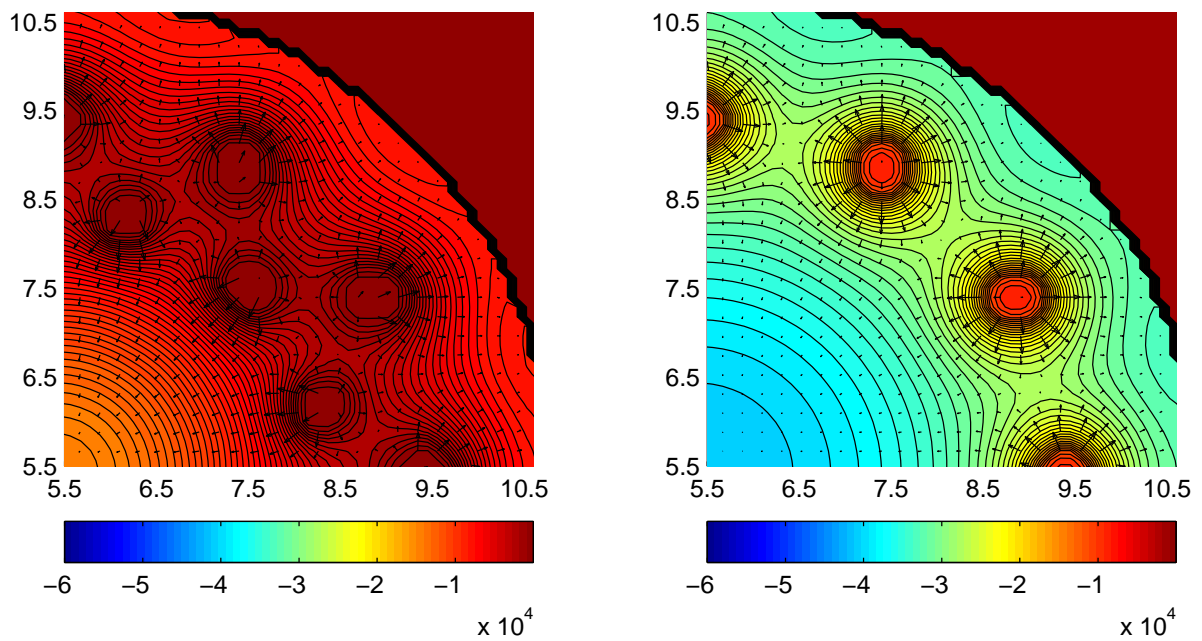

Figure 5.12: Quarters of the OXY planes ($x > 5.4$, $y > 5.4$) at $z = 6.45$ (left), 7.95 (right). Pressure (colors) and velocity vectors (arrows) for the flow in the ceramic filter with holes.

Chapter 6

Summary

6.1 Scientific Achievements

The present thesis deals with coupled steady state laminar flows of isothermal incompressible viscous Newtonian fluids in plain and in porous media. Several aspects of the numerical simulations of such flows are considered:

- the choice of proper interface conditions between the plain and porous media
- analysis of the well-posedness of the arising systems of partial differential equations;
- developing numerical algorithm for the stress tensor jump interface conditions, coupling Navier–Stokes equations in the pure liquid media with the Navier–Stokes–Brinkman equations describing the flow in the porous media;
- validation of the macroscale mathematical models on the base of a comparison with the results from a direct numerical simulation of model representative problems, allowing for grid resolution of the pore level geometry;
- developing software and performing numerical simulation of 3-D industrial flows, namely of oil flows through car filters.

The flow in the pure fluid region is usually described by the (Navier–)Stokes system of equations. The most popular models for the flow in the porous media are those suggested by Darcy and by Brinkman. Interface conditions, proposed in the literature for coupling Darcy and Navier-Stokes equations (these two being different order systems of PDEs), are shortly reviewed in the thesis. The coupling of Navier–Stokes and of Brinkman equations (these two being the same order systems of PDEs) in the mathematical literature is based on the so called continuous stress tensor interface conditions. One of the main tasks of this thesis is to investigate another type of interface conditions, namely, the recently suggested stress tensor jump interface conditions. The mathematical models based on this interface conditions were not carefully investigated from the mathematical point of view, and also their validity was a subject of discussions. The considerations within this thesis are a step toward better understanding of these interface conditions.

The main results of the present thesis are summarized below.

$\Rightarrow$ A numerical algorithm for solving 3-D coupled flow problems, described by Navier–Stokes and Brinkman equations equipped with stress tensor jump interface condition, was developed and validated. The algorithm includes careful treatment of the jumps, as well as an efficient solution procedure for the coupled system.

$\Rightarrow$ The mathematical model based on the stress tensor jump interface conditions was validated for a representative class of model problems: flows which are parallel, perpendicular or inclined with respect to the interface between the plain and porous media. These model

problems include cases of connected, or of multiconnected pure fluid subregions (i.e., when the porous medium separates completely the inlet and the outlet). The validity of the jump stress tensor interface condition for these model problems is concluded on the base of a comparison with the direct numerical simulation of the flows at the microlevel (i.e., when the pore geometry is resolved by the grid).

$\Rightarrow$ An object-oriented software, based on the above algorithm, was developed for numerical simulation of a class of 3-D industrial flows. Results of simulations were validated in comparison with measurements of the pressure drop – flow rate ratio for oil flow through a particular car filter. Numerical simulations of 3-D oil flows through various car filters were performed.

In addition to the above considerations of the macroscale model, in the present thesis we have also shown that:

$\Diamond$ In the case of the benchmark problem for a parallel flow over a porous bed the solution of Navier–Stokes–Brinkman equations, equipped with the stress tensor jump conditions, is able to reproduce the well known results from the Beavers–Joseph experiments;

$\Diamond$ For this benchmark case, the solution of the above model is asymptotically equivalent to the solution of the model based on Darcy equation and pressure jump interface conditions (the last was derived by Jäger and Mikelić on the base of a rigorous asymptotic analysis). Namely, the following representations hold

$$\mathbf{u}(\hat{x},\hat{y}) = \mathbf{u}_{eff}(\hat{x},\hat{y}) + O(\varepsilon^2) \qquad p(\hat{x},\hat{y}) = p_{eff}(\hat{x},\hat{y}) \qquad \text{inside fluid part}$$
$$\mathbf{u}(\hat{x},\hat{y}) = \mathbf{u}_{eff}(\hat{x},\hat{y}) + O(\varepsilon^n) \quad p(\hat{x},\hat{y}) = p_{eff}(\hat{x},\hat{y}) + O(\varepsilon) \quad \text{inside porous part}$$

where $(\hat{x},\hat{y})$ is a fixed point, ε, as usual is the small parameter related to the pore size and $n \in \mathbb{N}$ is arbitrarily large. Here $(\mathbf{u},p)$ denotes the solution of the Stokes–Brinkman model with stress jump interface conditions, while $(\mathbf{u}_{eff}, p_{eff})$ is the solution of Stokes–Darcy model with Beavers–Joseph condition in Saffman from for the liquid subregion and with pressure jump condition for the porous subregion. The above proximity of the two solutions for this benchmark problem is established on the base of analysis of the analytical solutions for the two mathematical models.

$\Diamond$ The free parameter matrix, involved in the stress tensor jump condition, can be uniquely determined for the above benchmark problem through the parameters of the Beavers–Joseph and of the pressure jump interface conditions, rigorously derived by Jäger, Mikelić and Neuss.

$\Diamond$ The mathematical model based on jump stress tensor interface conditions is not always a well posed mathematical problem. For some (probably non–physical) values of the parameters the problem has multiple solutions.

6.2   Further developments

In the preceding section we have formulated several topics for investigating the coupled flows in plain and in porous media, as well as our achievements in this field. Each of the above aspects should be investigated further.

$\bullet$ We have shown that the model with stress tensor jump conditions can be applied for the known problems for coupled flows in plain and in porous media, where other models are applied. It would be reasonable to continue the work in this direction, and for different classes of problems to find the parameters range for which one or another model gives more accurate solution. Also, we have considered here Brinkman model as a perturbation to the Darcy one (i.e., using Darcy permeability), and a rigorous mathematical justification in this case is still an open problem. Another topic of future work is formulation of auxiliary problems for determining the parameters in the stress tensor jump condition. As it is known, for about 30 years the parameters in the Beavers–Joseph interface condition had been experimentally fitted, before

a rigorous mathematical approach for their calculation was suggested in the paper by Jäger, Mikelić and Neuss. Currently, we have been able to show how the parameters of the stress tensor jump interface conditions are related to the parameters computed by Jäger, Mikelić and Neuss. That is, these parameters can be mathematically determined only for a parallel flow over a porous bed. For all other coupled flows the determination of these parameters can be done currently only by fitting the experimental results.

• The well–posedness of the mathematical problem needs further systematic analysis. It would be useful to find the range of parameters for which the problem is a well–posed one, and furthermore to determine the area of applicability of this model.

• The numerical algorithm can be further extended in the direction of accounting for more complicated interface geometries. Currently we require the interface between the plain and the porous media to be aligned with the faces of the (pressure) grid cells. Multigrid and local grid refinement are also proper directions for the future extension of the algorithm.

• The discussion with the industrial partners has shown the needs of developing algorithms for efficient simulation of even more complicated coupled problems, such as i. accounting for the deflection of the porous filtration medium; ii. accounting for the compression of the porous medium; iii. accounting for a possible deflection of the filter housing in the case of car filters; iv. accounting for the transport and capturing of the small particles, filtrated by the porous medium, as well as on their impact on the porosity and permeability of the porous medium; v. coupled multiphase flows in plain and in porous media, etc.

6.3 Conclusions

The mathematical model based on Navier–Stokes and Brinkman equations, equipped with stress tensor jump interface conditions, can be used in numerical simulation of coupled flows through plain and porous media. This model allows to obtain correct results for parallel, perpendicular, or inclined flows for both, connected or multiconnected pure fluid subregion. For the benchmark problem of a parallel flow over a porous bed the solution of this model is asymptotically equivalent to the solution of the pressure jump interface condition for coupling Darcy and Navier–Stokes equations. At the same time, the considered here model has to be carefully used, because for certain (probably non–physical) values of the parameters in the interface condition the mathematical problem might be not a well posed one. The derived numerical algorithm and the developed software can be used successfully in numerical simulation of a class of 3-D industrial flows.

List of notations

d	dimension of the problem $d = 2$ (2D) or $d = 3$ (3D)
$\mathbf{e}_k$, $k \in \mathbb{N}$	a unit vector in k-th direction. For example in 3D: $\mathbf{e}_1 = (1, 0, 0)$, $\mathbf{e}_2 = (0, 1, 0)$, $\mathbf{e}_3 = (0, 0, 1)$.
μ	dynamical viscosity of the fluid. $[kg/ms]$
ρ	density of the fluid $[kg/m^3]$
$\mathbf{u}$, p	velocity, pressure respectively – are the main unknowns in the problems we consider. In the porous media they may have different meaning depending on whether microscopic or macroscopic model is used.
U	characteristic macroscopic velocity. $[m/s]$
L	characteristic macroscopic length. $[m]$.
$\bar{\varepsilon}$	typical pore size (or the smallest period in the case of periodic porous media) in the porous medium. Used for the "real" problem $\mathcal{P}$. $[m]$
ε	"running" parameter for the sequence of imaginary problems $\mathcal{P}^{\varepsilon}$. $[m]$
K, $\mathbf{K}$	scalar and tensor permeabilities. $[m^2]$
$\mathbf{I}$	the unit $d \times d$ matrix
$\mathbf{i}$	a multi-index $\mathbf{i} = (i^1, \ldots, i^d) \in \mathbb{Z}^d$

$$[\phi]|_\Sigma := \phi|_{\Sigma_f} - \phi|_{\Sigma_p}$$

$$\mathbf{K}^{-1} = \left[\begin{array}{c} \mathbf{k}_1 \\ \ldots \\ \mathbf{k}_d \end{array} \right] = \left[\begin{array}{ccc} \kappa_{11} & \ldots & \kappa_{1d} \\ \ldots & \ldots & \ldots \\ \kappa_{d1} & \ldots & \kappa_{dd} \end{array} \right] = \bar{\varepsilon}^{-2} \left[\begin{array}{ccc} \varkappa_{11} & \ldots & \varkappa_{1d} \\ \ldots & \ldots & \ldots \\ \varkappa_{d1} & \ldots & \varkappa_{dd} \end{array} \right]$$

$$\mathbf{M} = \left[\begin{array}{ccc} M_{11} & \ldots & M_{1d} \\ \ldots & \ldots & \ldots \\ M_{d1} & \ldots & M_{dd} \end{array} \right] = \mu \overline{\mathcal{M}} = \frac{\mu}{\varepsilon} \mathcal{M}.$$

$$\nabla \mathbf{u} = \left[\begin{array}{c} \nabla u^1 \\ \ldots \\ \nabla u^d \end{array} \right] = \left[\begin{array}{ccc} \frac{\partial u^1}{\partial x^1} & \ldots & \frac{\partial u^1}{\partial x^d} \\ \ldots & \ldots & \ldots \\ \frac{\partial u^d}{\partial x^1} & \ldots & \frac{\partial u^d}{\partial x^d} \end{array} \right], \quad \triangle \mathbf{u} = \left[\begin{array}{c} \triangle u^1 \\ \ldots \\ \triangle u^d \end{array} \right], \quad (\mathbf{u} \cdot \nabla) \mathbf{u} = \left[\begin{array}{c} u^1 \frac{\partial u^1}{\partial x^1} + \ldots + u^d \frac{\partial u^1}{\partial x^d} \\ \ldots \\ u^1 \frac{\partial u^d}{\partial x^1} + \ldots + u^d \frac{\partial u^d}{\partial x^d} \end{array} \right]$$

$$\mathbf{a} \cdot \mathbf{b} = \sum_{i=1}^{d} a^i b^i, \quad \mathbf{a} \cdot \mathbf{B} = \mathbf{B}\mathbf{a} = \left[\begin{array}{c} \mathbf{a} \cdot \mathbf{b}_1 \\ \ldots \\ \mathbf{a} \cdot \mathbf{b}_d \end{array} \right] = \left[\begin{array}{c} b_{11} a_1 + b_{1d} a_d \\ \ldots \\ b_{d1} a_1 + b_{dd} a_d \end{array} \right]$$

$$\nabla \mathbf{v} : \nabla \mathbf{u} = \sum_{k} \nabla v^k \cdot \nabla u^k = \sum_{k} \sum_{i} \frac{\partial v^k}{\partial x^i} \frac{\partial u^k}{\partial x^i}.$$

$$\|\phi\|_{L^2(\Omega)}^2 = \int_\Omega \phi^2(\mathbf{x}) \, d\mathbf{x}, \quad \|\phi\|_{H^1(\Omega)}^2 = \|\phi\|_{L^2(\Omega)}^2 + \sum_{i=1}^{d} \left\| \frac{\partial \phi}{\partial x^i} \right\|_{L^2(\Omega)}^2, \quad \|\mathbf{v}\|_{H^d}^2 = \sum_{i=1}^{d} \|v^i\|_H^2.$$

Bibliography

[1] G. Allaire : Homogenization of the Stokes flow in a connected porous medium. Asymptotic Anal. **2**,No.3,(1989) 203-222.

[2] G. Allaire : Homogenization of the Navier-Stokes Equations in Open Sets Perforated with Tiny Holes. I. Abstract Framework, a Volume Distribution of Holes. II Non-Critical Sizes of the Holes for a Volume Distribution and a Surface Distribution of Holes. Arch.Rational Mech. Anal. **113** (1991) 209-298.

[3] Ph. Angot : Analysis of singular perturbations on the Brinkman problem for fictitious domain models of viscous flows. Math. Meth. Appl. Sci. **22** (1999) 1395–1412.

[4] Ph. Angot, Ch.-H. Bruneau, P. Fabrie : A penalization method to take into account obstacles in incompressible viscous flows. Numer. Math. **81**, No.4, (1999) 497-520.

[5] J. Bear, Y. Bachmat: *Introduction to modeling of transport phenomena in porous media.* Kluwer Academic Publishers, Dordrecht etc., 1990.

[6] G.S. Beavers, D.D. Joseph : Boundary conditions at a naturally permeable wall. J. Fluid Mech. **30** (1967) 197–207.

[7] G.S. Beavers,E.M. Sparrow,R.A. Magnuson : Experiments on Coupled Parallel Flows in a Channel and a Bounding Porous Medium. Trans. ASME, J. Basic Eng., **92D**,(1970) 843–848.

[8] G.S. Beavers, E.M. Sparrow, B.A. Masha : Boundary Condition at a Porous Surface Which Bounds a Fluid Flow. AIChE J. **20**, No. 3 (1974) 596–597.

[9] A. Bensoussan, J.L. Lions, G. Papanicolaou :*Asymptotic Analysis for Periodic Structures.* North Holland, Amsterdam, 1978.

[10] M. Discacciati, E. Miglio and A. Quarteroni : Mathematical and numerical models for coupling surface and groundwater flows. Appl. Num. Math. 43, (2002) 57-74

[11] M. Discacciati and A. Quarteroni : Convergence analysis of a subdomain iterative method for the finite element approximation of the coupling of Stokes and Darcy Equations. To appear on Comput. Vis. Sci..

[12] H.I Ene, E. Sanchez-Palencia : Equation et phenomene de surface pour l'écoulement dans un modele de milieu poreux. J. Mecanique, **14**, (1975) 73-107.

[13] M.S. Espedal, A.Fasano, A.Mikelić : *Filtration in Porous Media and Industrial Application. Lecture Notes in Mathematics.* Springer, Berlin etc., 2000.

[14] S. Patankar : *Numerical Heat Transfer and Fluid Flow.* Hemisphere Publishing Corporation. New York. 1980.

[15] J.H. Ferziger, M. Peric : *Computational methods for fluid dynamics.* Springer, Berlin, 1996.

[16] C.A.J. Fletcher :*Computational techniques for fluid dynamics. Vol. 2: Specific techniques for different flow categories.* Springer, Berlin etc., 1991.

[17] G.P. Galdi :*An introduction to the mathematical theory of the Navier-Stokes equations, Vol. I.* Springer, 1994

[18] U. Ghia, K.N. Ghia, C.T. Shin : High-Re solutions for incompressible flow using the Navier-Stokes equations and a multigrid method. J.Comput. Phys. **48** (1982) 387-411.

[19] S. Haber, R. Mauri : Boundary conditions for Darcy's flow through porous media. Int. J. Multiphase Flows, **9**, (1983), 561 − 574.

[20] W. Hackbusch :*Elliptic Differential Equations; Theory and Numerical Treatment.* Springer, Heidelberg, 1992.

[21] U. Hornung ed.:*Homogenization and Porous Media* Springer,New York Inc, 1997.

[22] F.A. Howes, S. Whitaker : The Spatial Averaging Theorems Revisited. Chemical Engineering Science, **40**, No. 8, (1985), 1387–1392.

[23] W. Jäger, A. Mikelić : On the boundary conditions at the contact interface between a porous medium and a free fluid. Ann. Sc. Norm. Super. Pisa, Cl. Sci.,IV.**23**, No.3,(1996), 403-465

[24] W. Jäger, A. Mikelić : On the interface boundary condition of Beavers, Joseph, and Saffman. SIAM J. Appl. Math. **60**,(2000),1111-1127

[25] W. Jäger, A. Mikelić, N. Neuss : Asymptotic analysis of the laminar viscous flow over a porous bed. SIAM J. Sci. Comput. **22** (2001) 2006-2028.

[26] M. Kaviany:*Principles of Heat Transfer in Porous media* Springer, New York etc., 1991.

[27] J. Koplik, H. Levine, A. Zee : Viscosity renormalization in the Brinkman equation. Phys. Fluids **26** (19), (1983), 2864 − 2870

[28] A.V. Kuznetsov : Influence of the stress jump boundary condition at the porous-medium/clear-fluid interface on a flow at a porous wall. Int. Comm. Heat Mass Transfer,**24** (3) (1997),401–410

[29] A.V. Kuznetsov : Analytical investigation of Couette flow in a composite channel partially filled with a porous medium and partially with a clear fluid. Int. J. Heat Mass Transfer. **41** (16), (1998), 2556–2560

[30] O.A. Ladyzhenskaya : *The mathematical theory of viscous incompressible flow.* Gordon and Breach, 1969.

[31] W.J. Layton, F. Schieweck, I. Yotov : Coupling fluid flow with porous media flow. SIAM J. Numer. Anal. **40**, No 6, (2003) 2195-2218.

[32] T. Levy, E. Sanchez-Palencia : On boundary conditions for fluid flow in porous media. Int. J Engng Sci **13**, (1975),923–940.

[33] A. Kufner, O. John, S, Fucik : *Function Spaces.* Nordhoff International Publishing, Leyden, 1977

[34] L.D. Landau,E.M. Lifschitz : *Hydrodynamik.* Akademie Verlag, Berlin, 1971.

[35] J.L. Lions : *Some methods in the mathematical analysis of systems and their control,* Science Press, Beijing, 1981.

[36] T.S. Lungren : Slow flow through stationary random beds and suspensions of spheres. J. Fluid Mech. **52** (1972) 273–299.

[37] G.I. Marchuk : *Methods of numerical mathematics. Textbook* (Metody vychislitel'noj matematiki. Uchebnoe posobie) 2nd ed. (Russian), Moskva, "Nauka". 536 p, 1980.

[38] N. Martys, D.P. Bentz, E.J. Garboczi : Computer simulation study of the effective viscosity in Brinkman's equation. Phys. Fluids **6**(4),(1994),1434–1439

[39] N. Massarotti, P.Nithiarasu, O.C. Zienkiewicz : Porous – Fluid Interface Problems. A Characteristic – based –split (CBS) Procedure. ECCOMAS 2000, Barcelona.

[40] A. Mikelić : Homogenization of nonstationary Navier-Stokes equations in a domain with a grained boundary. Ann. Mat. Pura Appl., IV. **158**,(1991), 167–179.

[41] J.Necas : *Les Methodes Directes en Theorie des Equations Elliptiques.* Academia, Editeurs, Prague, 1967.

[42] G. Neale, W. Nader : Practical Significance of of Brinkman's Extension of Darcy's Law: Coupled Parallel Flows within a Channel and a Bounding Porous Medium. Can. J. Chem. Eng.,**52**,(1974), 475-478

[43] D.A. Nield, A.Bejan : *Convection in Porous Media.* Springer, New York etc., 1992.

[44] J.A. Ochoa-Tapia, S. Whitaker : Momentum transfer at the boundary between a porous medium and a homogeneous fluid. I. Theoretical development. Int.J.Heat Mass Transfer, **38**, (1995) 2635–2646.

[45] J.A. Ochoa-Tapia, S. Whitaker : Momentum transfer at the boundary between a porous medium and a homogeneous fluid. II. Comparison with experiment. Int.J.Heat Mass Transfer, **38**, (1995) 2647–2655.

[46] J.A. Ochoa-Tapia, S. Whitaker : Momentum jump condition at the boundary between a porous medium and a homogeneous fluid. Inertia effects. J. Porous Media **1**, No.3, (1998) 201-217

[47] S. Rief : private communication.

[48] E. Sanchez–Palencia : *Non-homogeneous media and vibration theory* Lecture Notes in Physics, 127, Springer- Verlag, Berlin, etc, 1980.

[49] P.G. Saffman : On the boundary condition at the surface of a porous medium Studies appl. Math. **50**, (1971) 93-101.

[50] M. Sahraoui, M. Kaviany : Slip and no-slip velocity boundary conditions at interface of porous, plain media. Int. J. Heat Mass Transport, **35**, (1992) 927-943.

[51] C.W. Somerton,I. Catton : On the thermal instability of superposed porous and fluid layers. ASME J. Heat Transfer. **104**,(1982),160 − 165

[52] D. Stoyanov : private communication.

[53] R. Temam: *Navier-Stokes equations - theory and numerical analysis.* North-Holland, Amsterdam, 1977.

[54] H.K. Versteeg, W. Malalasekera: *An Introduction to Computational Fluid Dynamics* Longman Scientific & Technical, Malaysia, 1995.

[55] P.Wesseling: *Principles of Computational Fluid Dynamics* Springer, Berlin, Heidelberg, 2001.

[56] J. Wloka: *Partielle Differentialgleichungen* B.G.Teubner, Stuttgart, 1982.

[57] A. Ženišek, *Nonlinear elliptic and evolution problems and their finite element approximation* Academic Press, London, 1990.

[58] Fraunhofer Institut für Techno und Wirtschaftsmathematik, Kaiserslautern, Germany. Jahresbericht 2002, http://www.itwm.fhg.de.

[59] http://www.itwm.fhg.de Menu:Abteilungen ⇒ Strömungen und komplexe Strukturen ⇒ Micro Structure Simulation and Virtual Material Design

Curriculum Vitae

28.01.1975	born in Ufa, Russia.
1982 – 1990	School No. 39, Ufa, Russia.
1990 – 1992	School No. 18, Moscow, Russia.
1992 – 1997	Moscow Lomonosov University, Faculty of Computational Mathematics and Cybernetics, Moscow, Russia
1997 – 1999	University Kaiserslautern, Master Program "Industrial Mathematics", Kaiserslautern, Germany
1999 – 2003	Doctoral candidate at the Mathematical Department of the University Kaiserslautern/Fraunhofer Institut für Techno und Wirtschaftsmathematik (ITWM), Germany.